NASA Contractor Report 172507

Nonlinear Potential Analysis Techniques for Supersonic Aerodynamic Design

IN-02

58120

P-149

V. Shankar and K.Y. Szema

ROCKWELL INTERNATIONAL SCIENCE CENTER
Thousand Oaks, California 91360

CONTRACT NAS1-15820
1 MARCH 1985

National Aeronautics and
Space Administration

Langley Research Center
Hampton, Virginia 23665

Review for general release (2 years from report date)

NASA Contractor Report 172507

NONLINEAR POTENTIAL ANALYSIS TECHNIQUES FOR SUPERSONIC AERODYNAMIC DESIGN

V. Shankar and K.Y. Szema

ROCKWELL INTERNATIONAL SCIENCE CENTER

Thousand Oaks, California 91360

CONTRACT NAS1-15820

March 1, 1985

FOREWORD

This final report was prepared by the Science Center of Rockwell International, Thousand Oaks, California, for the Langley Research Center, National Aeronautics and Space Administration, Hampton, Virginia. The work was performed under Contract No. NAS1-15820, "Development of Full Potential Analysis Aero Prediction Technology for Hypersonic Configuration Design." Mr. Noel Talcott and Mr. Kenneth Jones were the Project Monitors of this contract.

Mr. E. Bonner of the Los Angeles Division, Rockwell International, was the Program Manager; Drs. V. Shankar and K.Y. Szema of the Rockwell International Science Center were the Principal Investigators.

SUMMARY

A numerical method based on the conservation form of the full potential equation has been applied to the problem of three-dimensional supersonic flows with embedded subsonic regions. The governing equation is cast in a nonorthogonal coordinate system, and the theory of characteristics is used to accurately monitor the type-dependent flow field. A conservative switching scheme is employed to transition from the supersonic marching procedure to a subsonic relaxation algorithm and vice versa. The newly developed computer program can handle arbitrary geometries with fuselage, canard, wing, flow through nacelle, vertical tail and wake components at combined angles of attack and sideslip. Results are obtained for a variety of configurations that include a Langley advanced fighter concept with fuselage centerline nacelle, Rockwell's Advanced Tactical Fighter (ATF) with wing mounted nacelles, and the Shuttle Orbiter configuration.

CONTENTS

1. INTRODUCTION

An examination of the literature for supersonic/hypersonic aircraft provides an indication of the flexibility and generality required for a prediction technique. Typical configuration development variables include wing section, incidence, height, dihedral, planform, effectiveness of longitudinal control surfaces for trim, effectiveness of empennage for directional stability, and propulsion system–airframe interactions.

State–of–the–art response to these prediction requirements is provided by hypersonic impact methods as well as linearized analysis and design algorithms. These approaches can treat complex geometries with minimum response time and cost, with efficient predicted data coverage in terms of Mach number, angle of attack, trim deflection, yaw angle, etc. Shortcomings are present, however, in both the impact and linearized methods. For the former, interference between surface elements is totally ignored in implementations such as classical Newtonian, tangent wedge, and cone theories. Crossflow interactions and stagnation point singularities are also implicitly disregarded. In the latter, shocks, vorticity, and entropy wakes and layers are excluded. Furthermore, superposition of elementary solutions such as those for thickness and angle of attack freely used in linear models are, strictly speaking, invalid at hypersonic speeds.

A need exists for new aerodynamic prediction techniques to optimize vehicles designed to travel at supersonic/hypersonic speeds. One requirement of a new aerodynamic prediction technique is that it be more accurate than simple noninterfering panel methods. Another specification is that it be more computationally efficient than currently available explicit finite–difference methods so that it can be incorporated into a practical design procedure. The new approach should include enough of the physics of the flow to allow realistic optimization and should permit consideration of appropriate interactions between components of promising arrangements, since this has been found to be the key to increasing aerodynamic efficiency using linear methodology. Nonlinear potential theoretical formulations hold the promise of meeting this objective and providing economic design codes which are responsive to conceptual vehicle definition efforts.

A nonlinear aerodynamic prediction technique based on the full potential equation in conservation form has been developed for the treatment of supersonic flows. References 1 and 2 contain the details of the theoretical development of the full potential analysis method. Detailed description of the method can be found in the publications in Appendix A. The second and third papers of the Appendix constitute a user's manual for the full potential analysis code. Contained therein is a brief description of the code organization, main program and subroutines, flow variables, input data format, and sample test cases.

The computer program entitled, "Nonlinear Supersonic Full Potential Analysis Program" can be obtained for a fee from:

Computer Software Management and Information Center (COSMIC)
112 Barrow Hall
University of Georgia
Athens, GA 30602
(404) 542-3265

Request the program package by the designation LAR–13413. The program is written in FORTRAN IV for use on the Control Data 6600 and the CYBER series of computers.

2. FULL POTENTIAL METHOD

The full potential equation in conservative or nonconservative form is frequently used for transonic flow analysis, where the local Mach number does not exceed approximately 1.4. If the assumptions of irrotationality and isentropicity are reasonably valid, then the full potential equation is expected to yield results comparable to Euler equations, even for supersonic/hypersonic flow fields. For conceptual design studies, where short response time is desired, the full potential methods can be an attractive substitute for expensive Euler methods and less accurate linear theory methods.

A nonlinear aerodynamic prediction technique based on the full potential equation in conservation form has been developed for the treatment of supersonic flows. A detailed description of the method has been presented in several published papers[1–6]. The most recent publications are enclosed in Appendix A for convenience. The first three papers[6–8] describe the method for the treatment of predominantly supersonic flows with regions of subsonic flow that usually occur at low supersonic Mach numberswith the 2nd and 3rd papers constituting a user's manual for the full potential analysis code. The final two papers[9,10] in the Appendix describe the method to treat the unsteady form of the full potential equation. Additional information on the unsteady treatment may be found in References 11 and 12. For blunt nosed configurations with a detached bow shock, the unsteady method is used to generate the starting solution for the marching code. Since the Appendix describes the full potential method, only the results not included in the published articles are presented here.

The following summarizes the salient features of the subject full potential code. Details can be found in the noted references.

- Equation in conservation form (see Refs. 1–6)
- Flux linearized upwind differencing in the marching direction (see Refs. 2–6)
- Conservative switch operators to treat embedded subsonic zones (see Refs. 2 and 3)
- Treatment of wakes (see Refs. 2–6)
- Yaw and angle of attack (see Refs. 2, 5, and 6)
- Complex geometry treatment (fuselage, canopy, wing, canard, nacelle, tail, multibody, etc.) (see Refs. 2, 5, and 6)
- Treatment of blunt nose using unsteady full potential methods (see Refs. 9–12)
- Numerical grid generation with constraints (see Refs. 2, 4, 5, and 6–8)
- Use of GEMPAK[13] or CDS[14] to generate geometry input files (fully automated) (see Refs. 2–8)

3. RESULTS

The full potential analysis code can handle complex aircraft geometries as well as multibody configurations. The following set of four different configuration studies clearly demonstrate the versatility and robustness of the code in handling a wide variety of non-linear flows.

The results to be presented here are

1) Langley's canard–wing fighter configuration, Figures 1 through 21.

Figures 1–2 indicate the complexity of the fighter geometry. Figure 3 schematically shows the variation of the cross plane geometry from the nose to the back end. Figures 4–11 show the cross–sectional geometry and the corresponding grid setup at various axial stations. Figure 12 shows the circumferential pressure distribution at an axial station where only the canard is present. Figure 13 shows the pressure contours, cross flow velocity vectors, and the cross flow streamlines at this axial station. The cross flow velocity vectors and cross flow streamlines are obtained by projecting the total velocity vector on a unit sphere whose center is at the nose of the geometry. Figures 14–19 show similar results at other axial stations. The formation of a shock around the inlet is clearly seen in Fig. 19. Figure 20 shows the computational geometry and the surface grid points for this Langley fighter. Figure 21 shows the pressure contours in the plane of symmetry.

2) Rockwell's Advanced Tactical Fighter with a flow through nacelle, Figures 22 through 24.

Figure 22 shows the geometry of an advanced tactical fighter with a nacelle mounted on the undersurface of the wing. The figure also shows the surface grid setup. Figure 23 shows the grid at an axial station where the nacelle is present. Figure 24 shows the pressure contours at this axial station and the corresponding crossflow velocity vectors.

3) Isolated Shuttle Orbiter flow, Figures 25 through 27,

Figure 25 shows the geometry of the Shuttle Orbiter. Figure 26 shows the upper surface chordwise pressure distribution at various span stations at $M_\infty = 1.4$ and $\alpha = -1.94°$. The agreement with experimental data is very good. Figure 27 shows the OMS pod shock formation and its impingement on the upper wing surface.

4) Shuttle Orbiter — External Tank mated configuration, Figures 28 through 31.

Figure 28 shows the multibody problem of the Shuttle mated configuration with the External Tank and the Solid Rocket Boosters present. Figure 29 shows a typical gridding for this multibody problem at an axial station where the OMS pod, External Tank/SRB, and the blockage are all present. Figure 29 shows the pressure contours at this axial station indicating the OMS pod shock and the detached shock in front of the blockage. Figure 30 shows the Orbiter lower surface chordwise pressure with and without the blockage effect. The comparison with experimental data is good when the blockage effect is accounted for. Figure 31 shows the computational geometry and surface gridding for the mated configuration. More results on this multibody problem can be found in Ref. 15.

The Shuttle Orbiter and the Orbiter/External Tank studies were performed as part of another contract from the Space Division of Rockwell International and funded by NASA–MSFC, Contract No. NAS9–14000. They are included in this contract report only for completeness in illustrating the overall capability of the full potential code.

4. CONCLUSIONS

The full potential analysis code has developed into a powerful nonlinear tool for the analysis of complex aerodynamic configurations: Modifications and enhancements allow analysis of complete configurations including fuselage, canard, wing, vertical and/or horizontal tail, nacelle (body or wing mounted), wake interference effects and multibody flows. Comparisons with available experimental data are in good agreement.

The code is operational on several computer systems, such as the CRAY–XMP, CYBER 203, CDC 7600, CYBER 176 and 175. A vectorized version of the code for the VPS–32 (modified CYBER 205) is currently in development. When fully developed and optimized, the vectorized code is expected to be able to analyze a complete fighter–like configuration in 20–30 seconds using the VPS–32 or CRAY–XMP class machine.

5. REFERENCES

1. Clever, W.C. and Shankar, V., "Nonlinear Potential Analysis Techniques for Supersonic/Hypersonic Configuration Design," NASA CR-166078, March 1983.

2. Shankar, V. and Clever, W.C., "Nonlinear Potential Analysis Techniques for Supersonic/Hypersonic Aerodynamic Design," NASA CR-172299, March 1984.

3. Shankar, V., Szema, K.Y., and Osher, S., "A Conservative Type-Dependent Full Potential Method for the Treatment of Supersonic Flows with Embedded Subsonic Regions," AIAA Paper No. 83-1887, July 1983.

4. Shankar, V., Rudy, S., and Szema, K.Y., "Application of a Two-Dimensional Grid Solver for Three-Dimensional Problems," ASME Paper Vol. No. G00222, June 1983.

5. Jones, K.M., Talcott, N.A., Jr., and Shankar, V., "Application of a Full Potential Method for Computation of Three-Dimensional Supersonic Flows," AIAA Paper No. 84-0139, January 1984.

6. Szema, K.Y. and Shankar, V., "Nonlinear Computation of Wing-Body-Vertical Tail-Wake Flows at Low Supersonic Speed," AIAA Paper No. 84-0427, January 1984.

7. Shankar, V. and Szema, K.Y., "Conservative Full Potential Implicit Marching Scheme for Supersonic Flows," Presented at the University of Tennessee Space Institute Work-

shop on Computational Fluid Dynamics, Article 6.1, UTSI Publication No. E01–4005–023–84, March 1984.

8. Bonner, E., "Supersonic Full Potential Analysis Program Operating Instructions," Rockwell International Report TFD 84–1654, July 1984.

9. Shankar, V., "Implicit Treatment of the Unsteady Full Potential Equation in Conservation Form," AIAA Paper No. 84–0262, January 1984.

10. Shankar, V., Ide, Hiroshi, and Gorski, Joseph, "Relaxation and Approximate Factorization Methods for the Unsteady Full Potential Equation," Presented at the 14th Congress of the International Council of the Aeronautical Sciences (ICAS), Toulouse, France, September 1984.

11. Shankar, V., Szema, K.Y., Gorski, J., and Ide, Hiroshi, "Nonlinear Steady and Unsteady Aerodynamic Prediction Methods Based on the Full Potential Equation," Presented at the Third International Conference on Boundary Interior Layers — Computational and Asymptotic Methods (BAIL III), Dublin, Ireland, June 1984.

12. Shankar, V., Szema, K.Y., Gorski, J., and Ide, Hiroshi, "Steady and Unsteady Nonlinear Flow Treatment Using the Full Potential Equation," Presented at the Ninth International Conference on Numerical Methods in Fluid Dynamics (IC9NMFD), Saclay, France, June 1984.

13. Stack, S.H., Edwards, C.L.W., and Small, W.J., "GEMPAK: An Arbitrary Aircraft Geometry Generator," NASA TP–1022, December 1977.

14. Raymer, D.P., "Configuration Development System," Rockwell International Report TFD–78–755–4, April 1983.

15. Szema, K.Y., Reba, W., Shankar, V., and Gorski, J., "Full Potential Treatment of Flows over Three–Dimensional Geometries Including Multibody Configurations," AIAA Paper No. 85–0272, 23rd Aerospace Sciences Meeting, Reno, Nevada, January 1985.

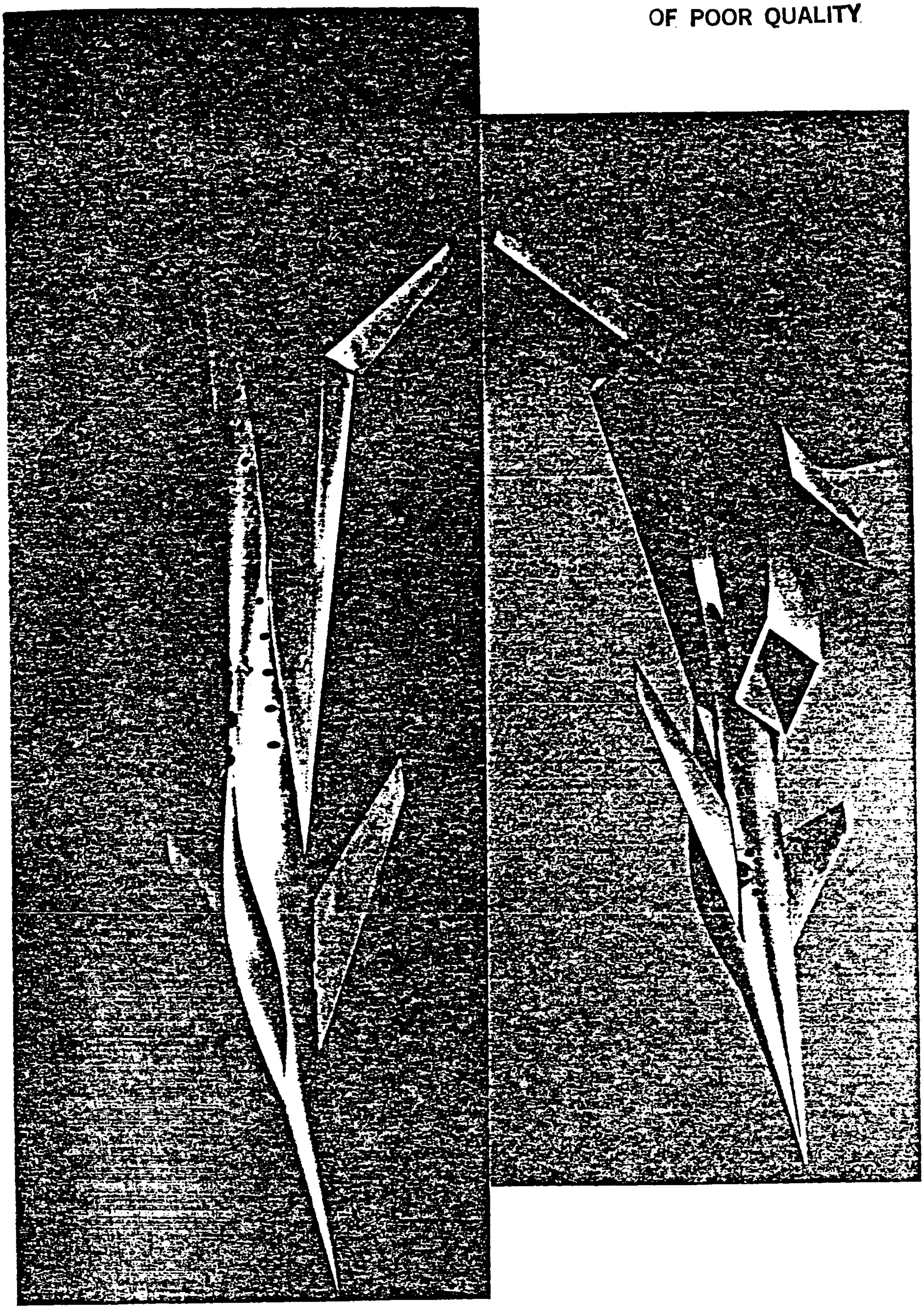

Fig. 1. Canard–wing fighter configuration.

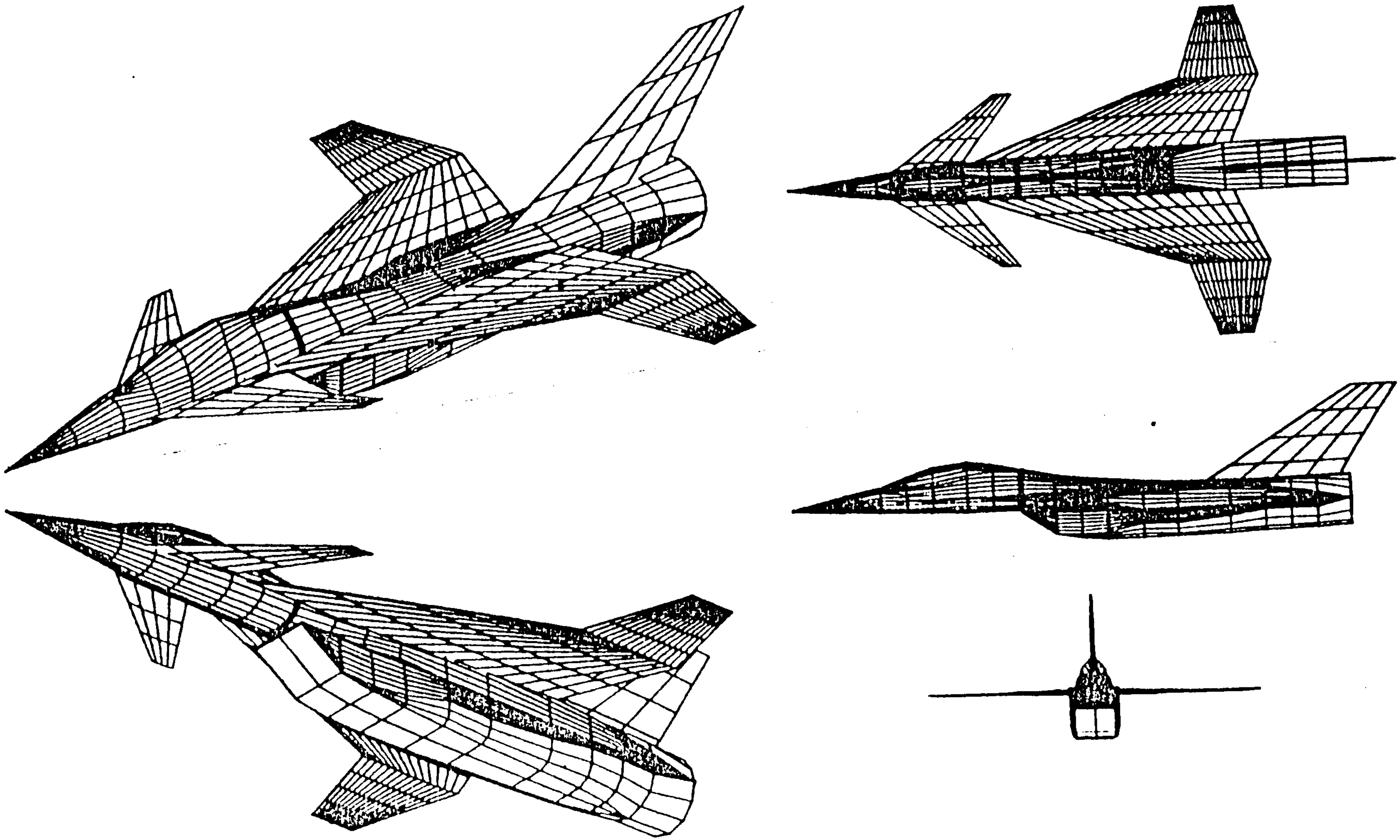

Fig. 2. Treatment of complex aerodynamic configurations.

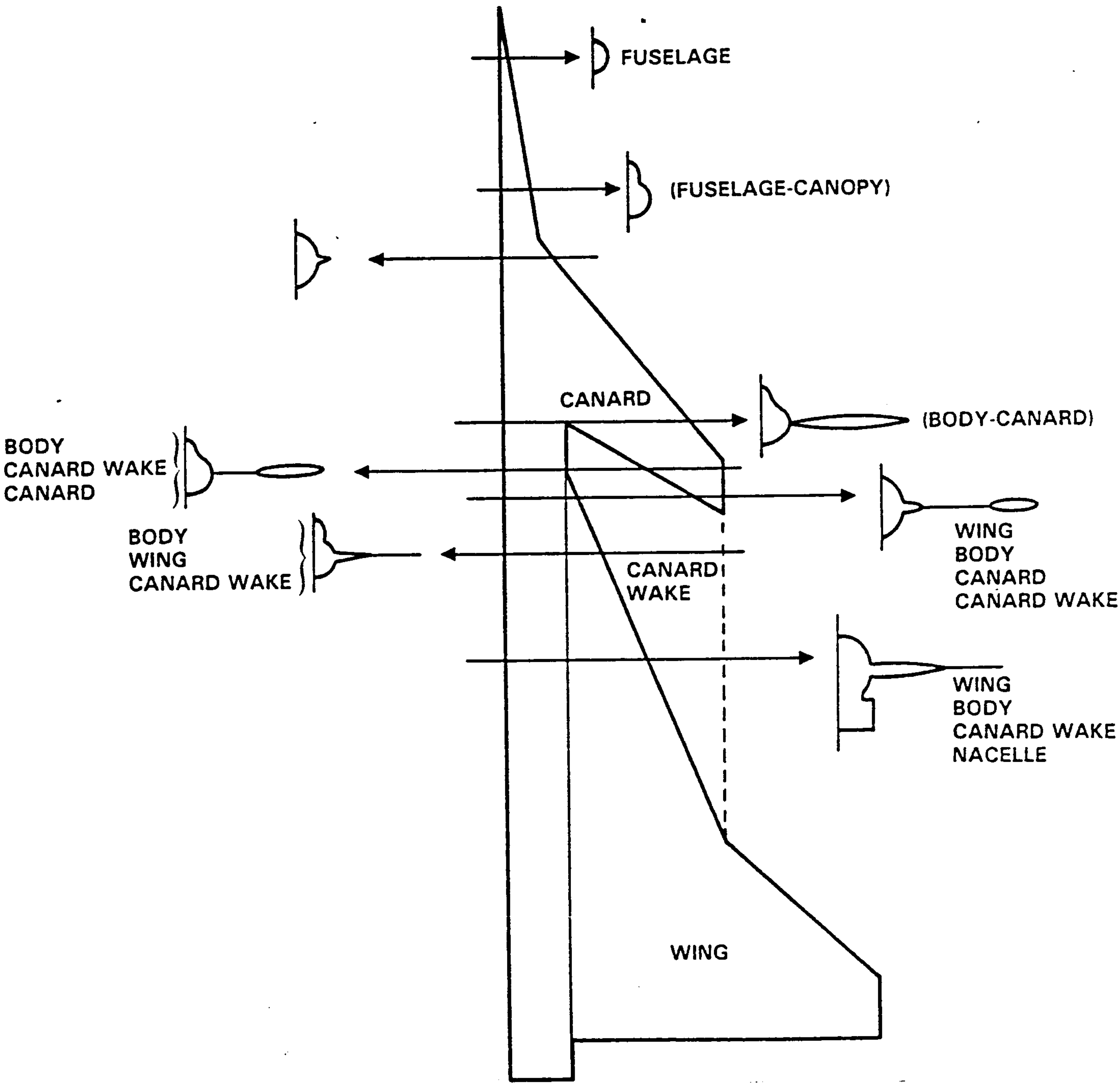

Fig. 3. Variation in cross-sectional shape.

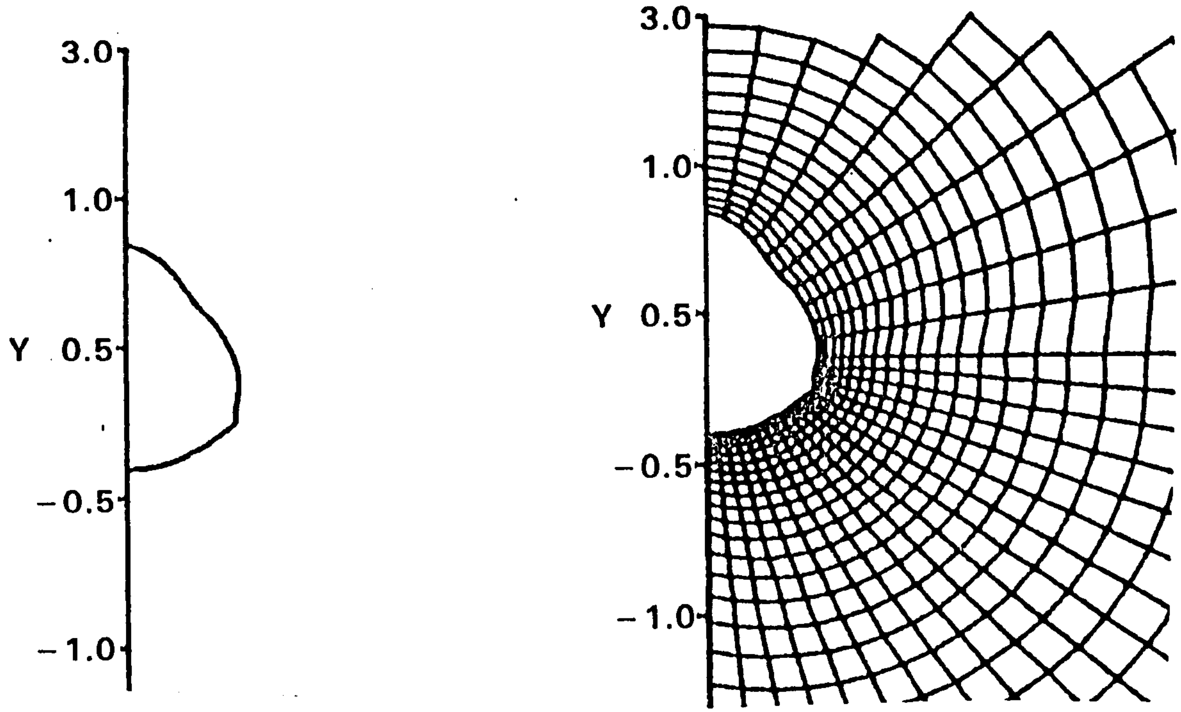

Fig. 4. Cross-section and grid at $x = 5$ (fuselage/canopy/beginning of canard).

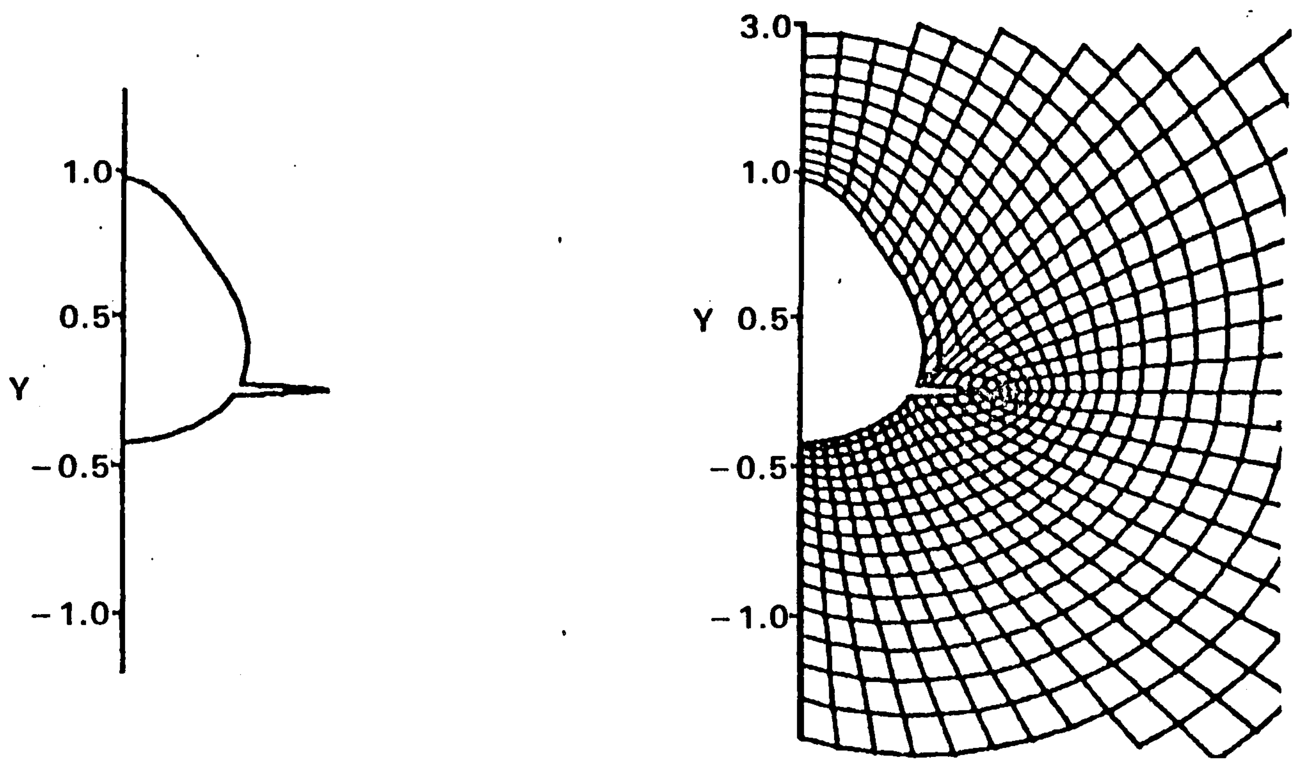

Fig. 5. Cross-section and grid at $x = 7$ (fuselage/canopy/canard).

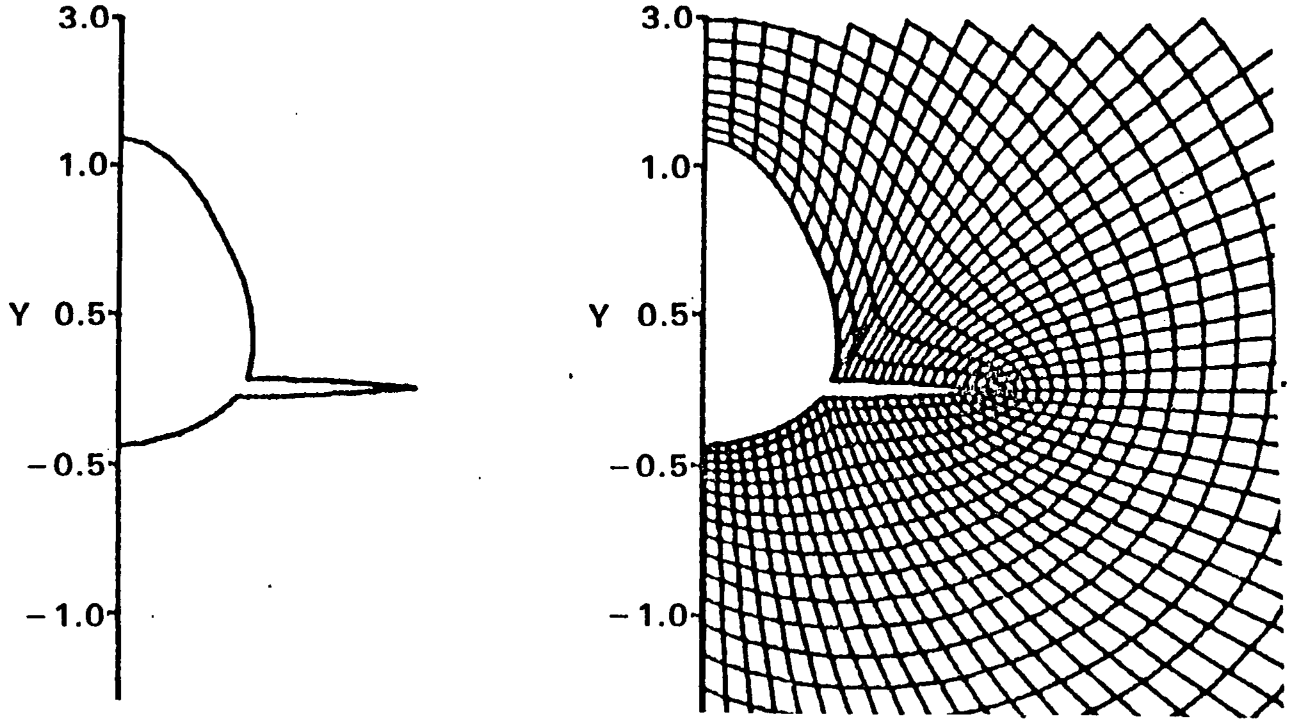

Fig. 6. Cross-section and grid at $x = 8$ (fuselage/canard).

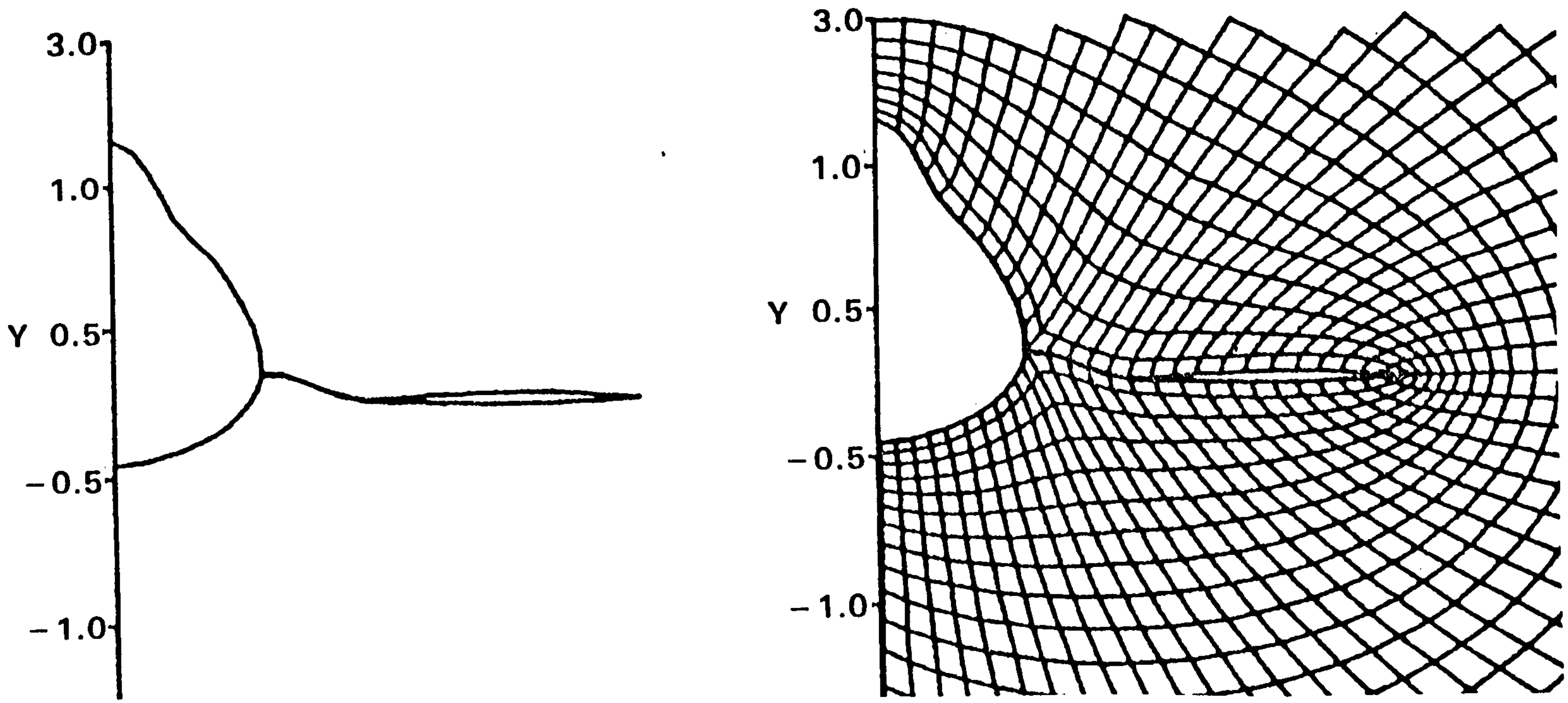

Fig. 7. Cross-section and grid at $x = 10.5$ (fuselage/canopy/canard/canard wake).

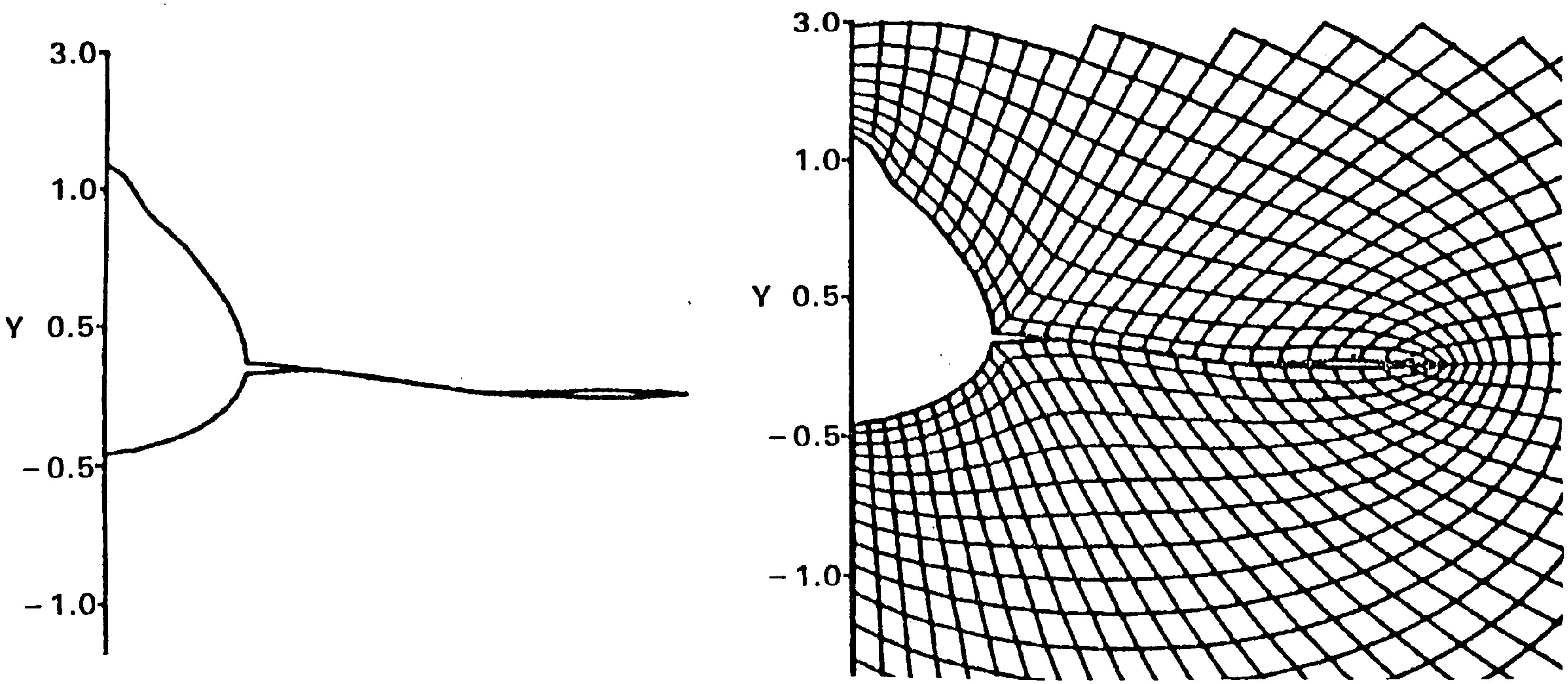

Fig. 8. Cross-section and grid at $x = 11.5$ (fuselage/canopy/wing/canard wake/canard).

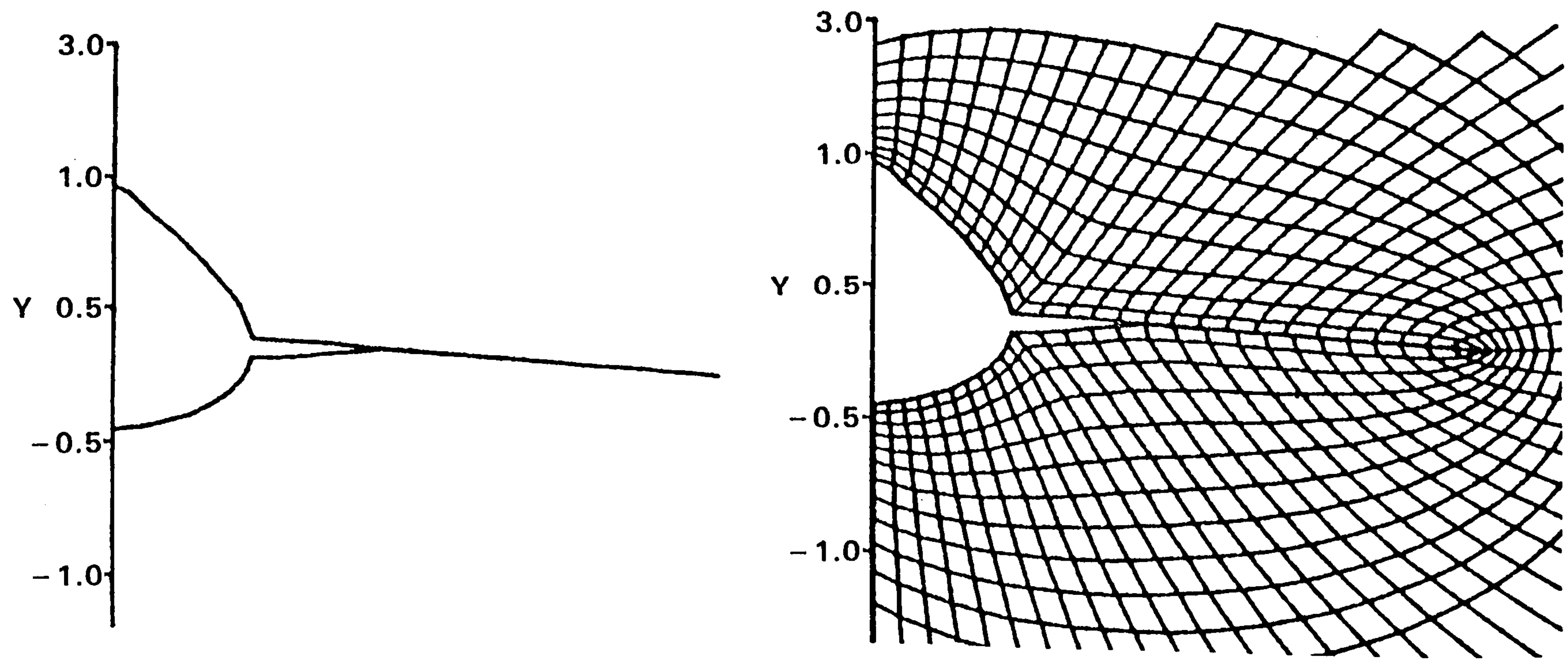

Fig. 9. Cross-section and grid at $x = 13.05$ (fuselage/wing/canard wake).

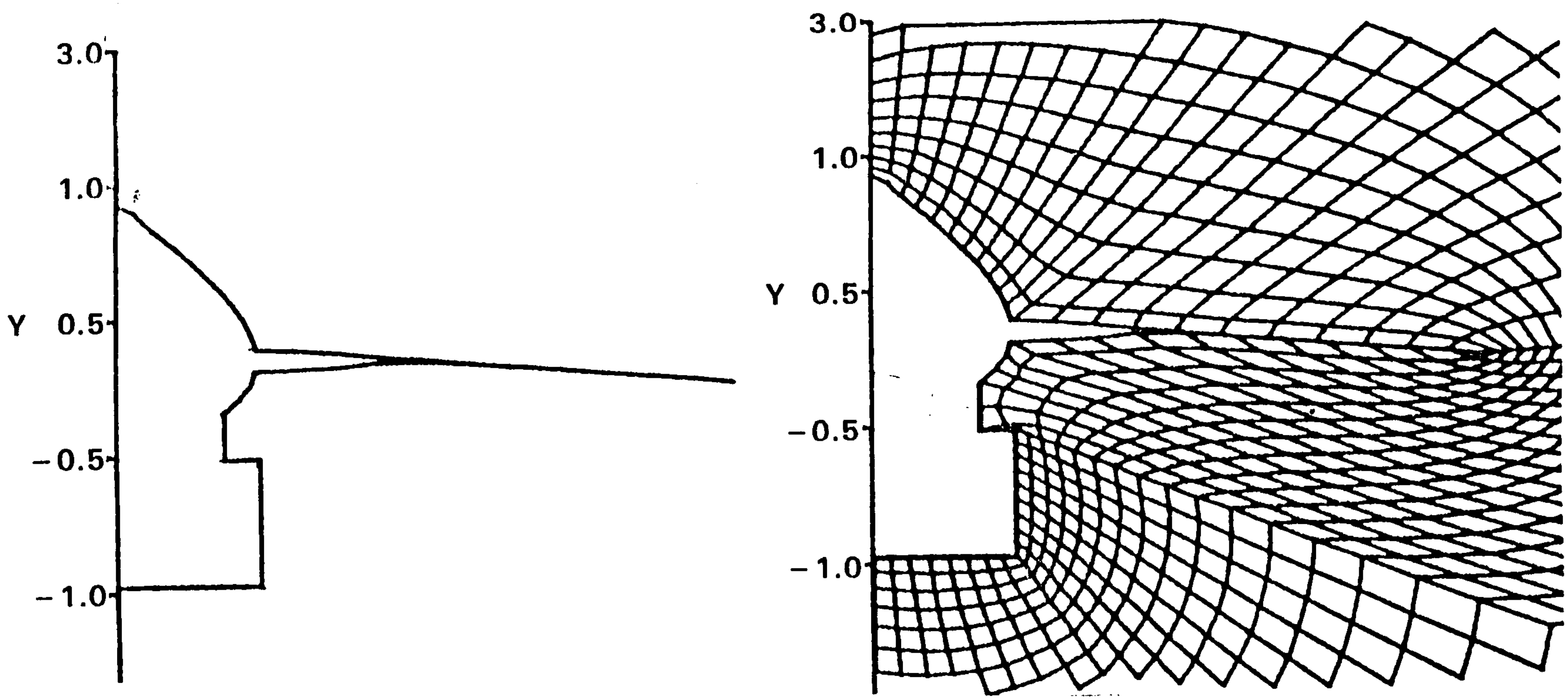

Fig. 10. Cross–section and grid at $x = 13.51$ (fuselage/wing/canard wake/nacelle).

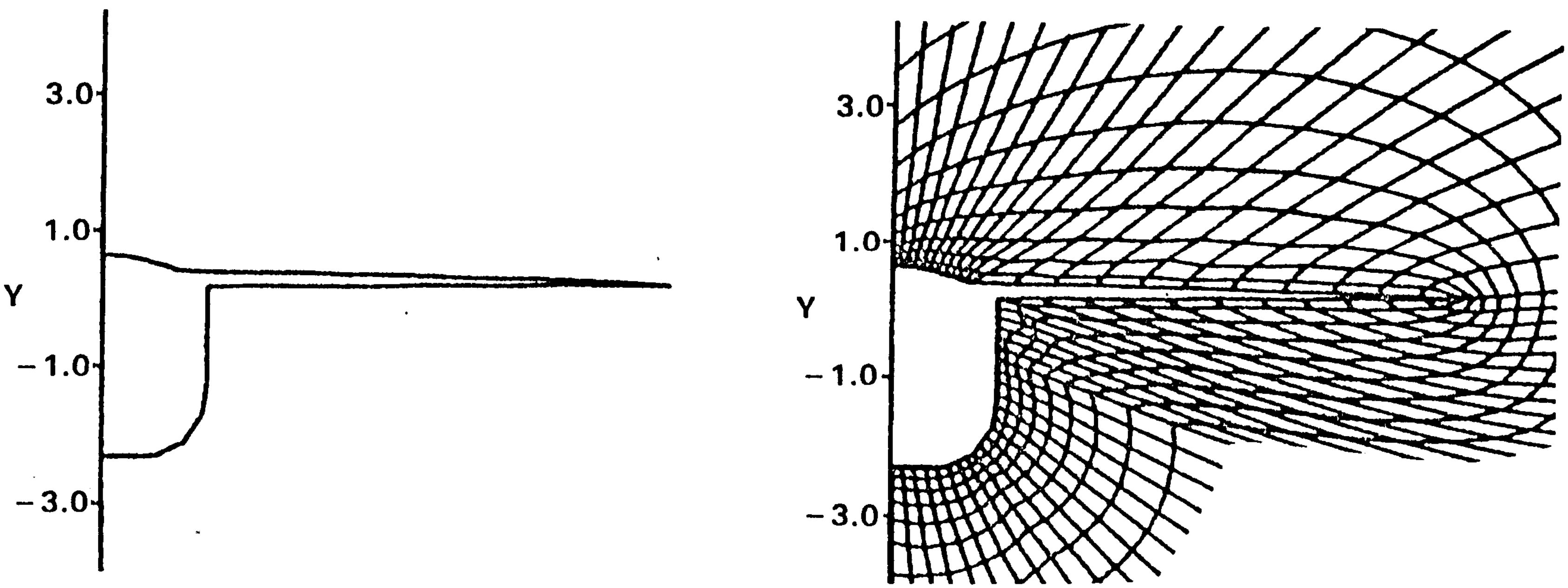

Fig. 11. Cross-section and grid at $x = 26$ (wing/nacelle).

$M_\infty = 2;\ \alpha = 4\,\text{deg};\ x/l = 0.22$

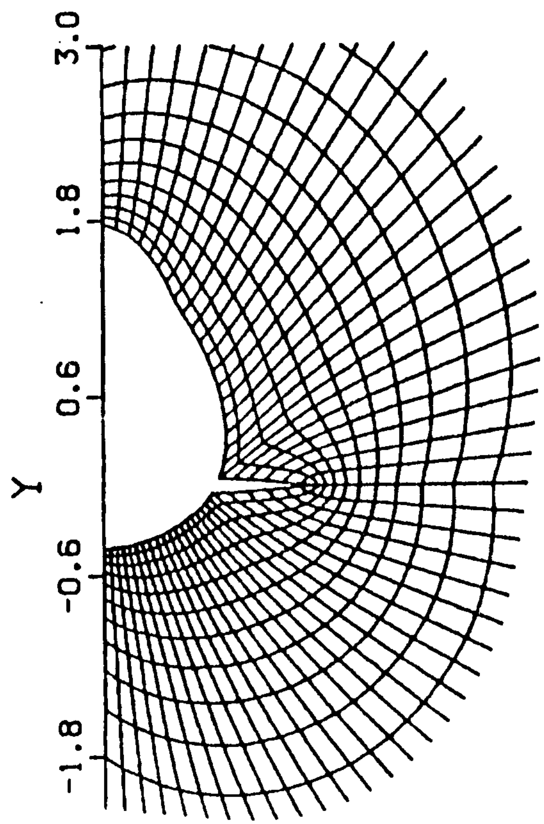

CROSS-SECTIONAL SHAPE

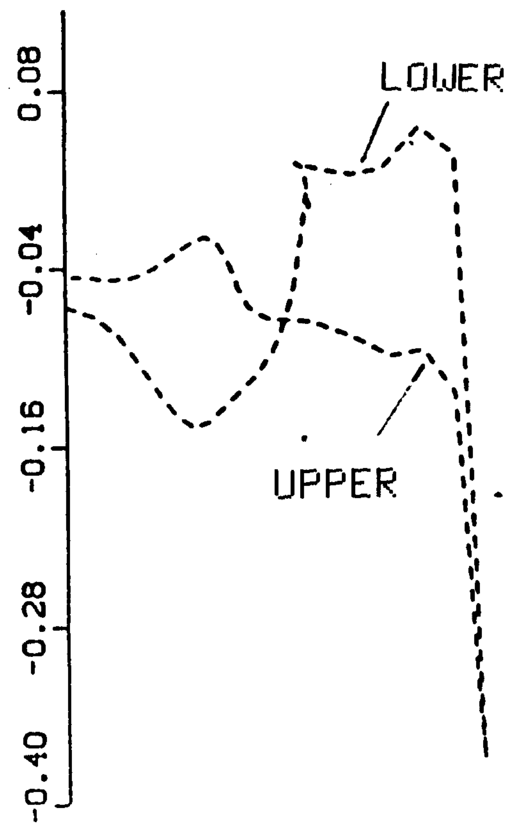

PRESSURE PROFILE

Fig. 12. Solution for Langley fighter configuration.

$M_\infty = 2;\ \alpha = 4\,\text{deg};\ x/l = 0.22$

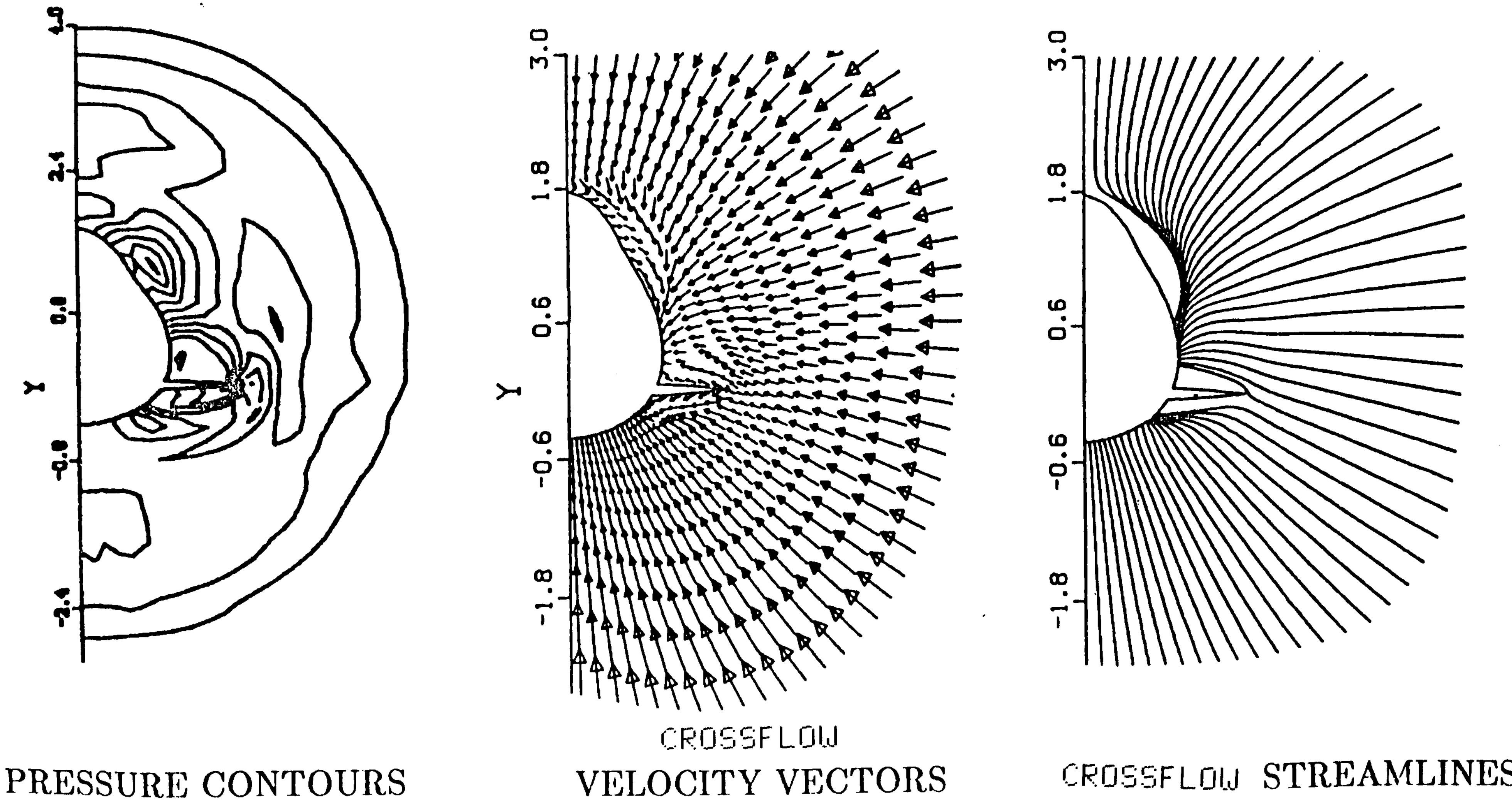

Fig. 13. Solution for Langley fighter configuration.

$M_\infty = 2;\ \alpha = 4\,\mathrm{deg};\ x/l = 0.38$

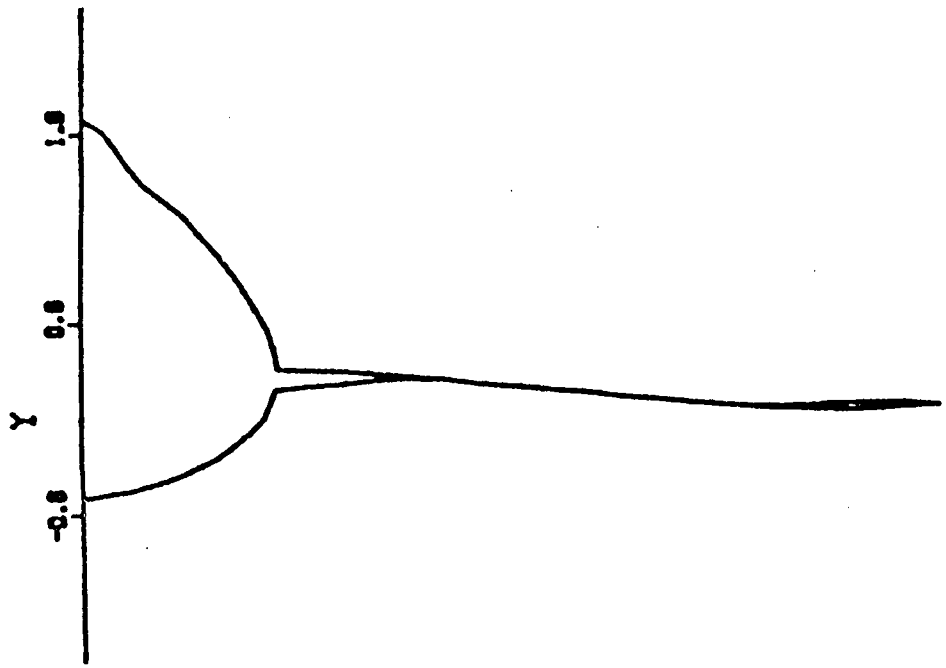

CROSS-SECTIONAL SHAPE

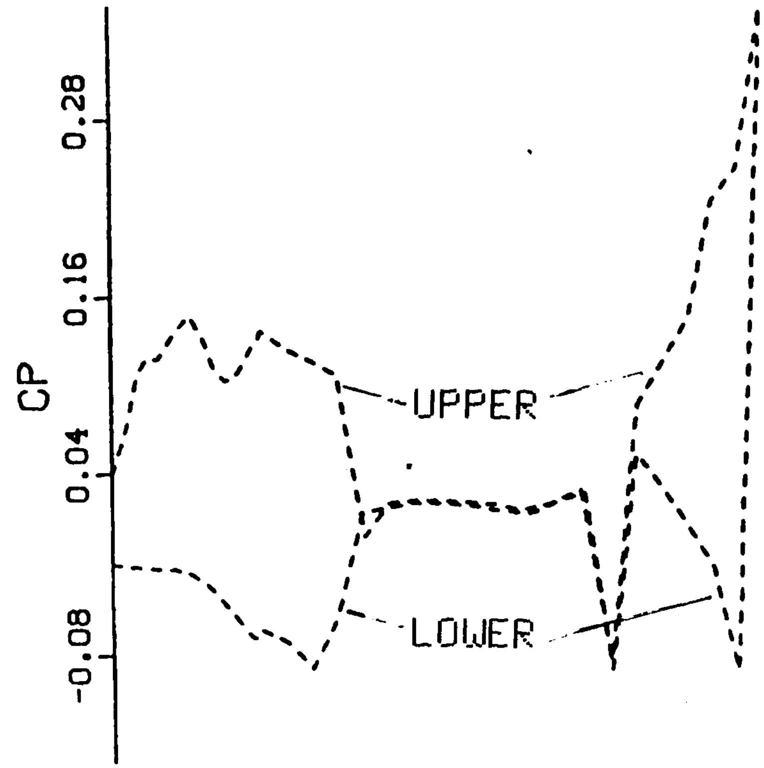

PRESSURE PROFILE

Fig. 14. Solution for Langley fighter configuration.

$M_\infty = 2;\ \alpha = 4\,\text{deg};\ x/l = 0.38$

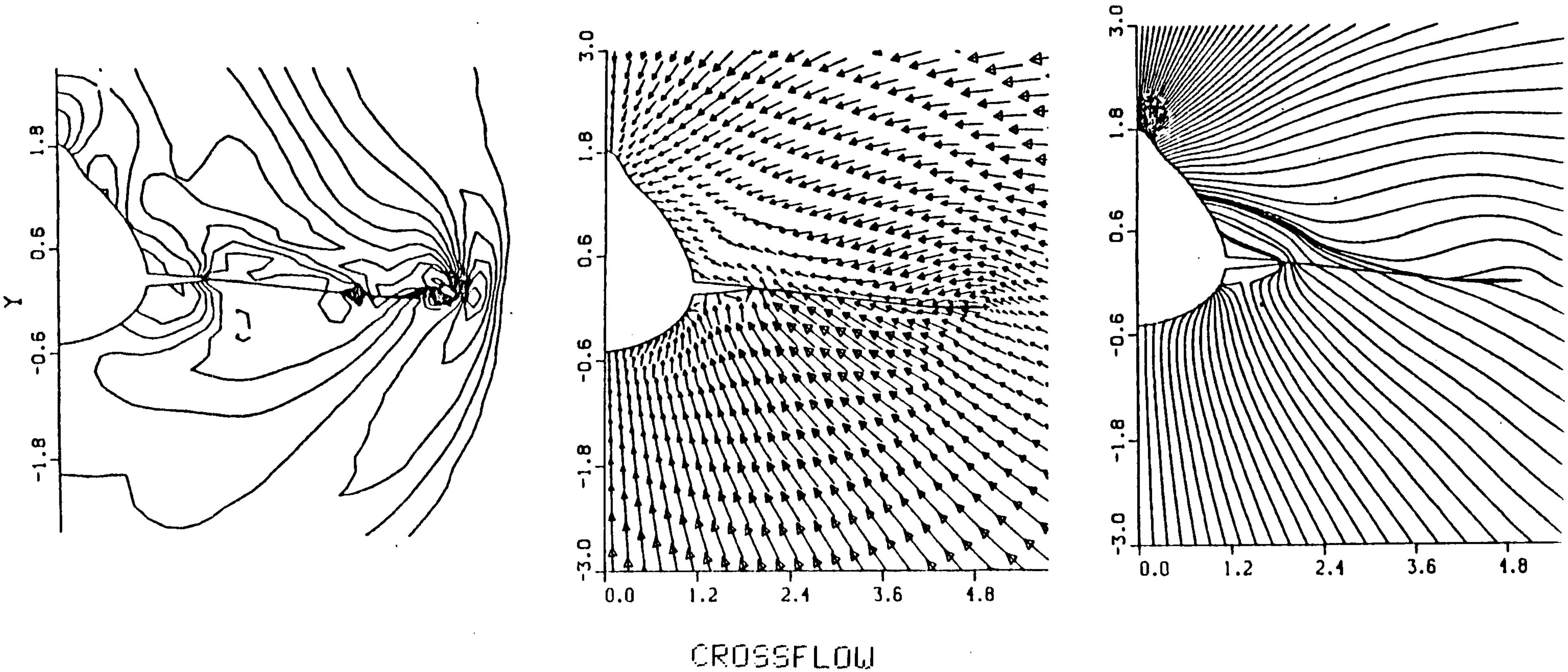

PRESSURE CONTOURS

VELOCITY VECTORS

STREAMLINE

Fig. 15. Solution for Langley fighter configuration.

$M_\infty = 2;\ \alpha = 4\,\mathrm{deg};\ x/l =\ 0.41$

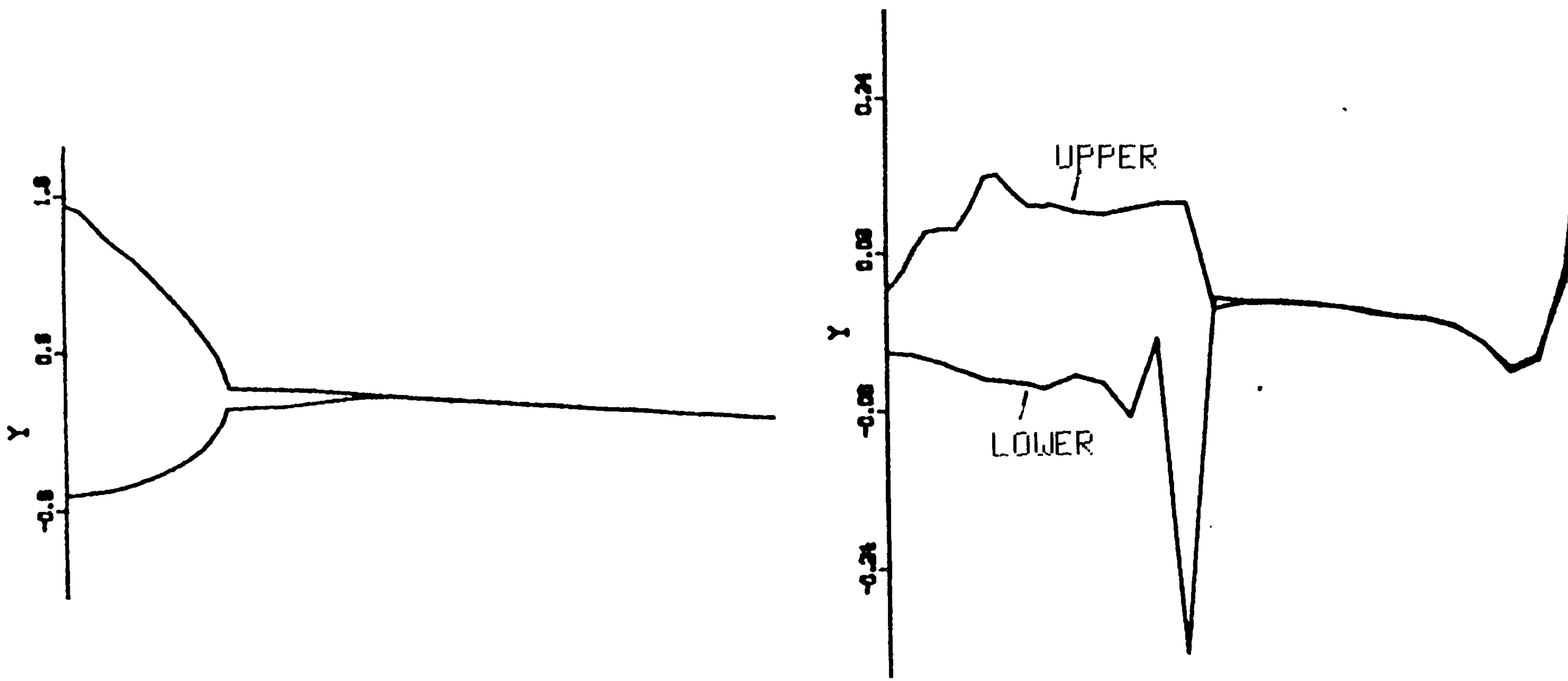

CROSS-SECTIONAL SHAPE

PRESSURE PROFILE

Fig. 16. Solution for Langley fighter configuration.

$$M_\infty = 2;\ \alpha = 4\,\text{deg};\ x/l = 0.41$$

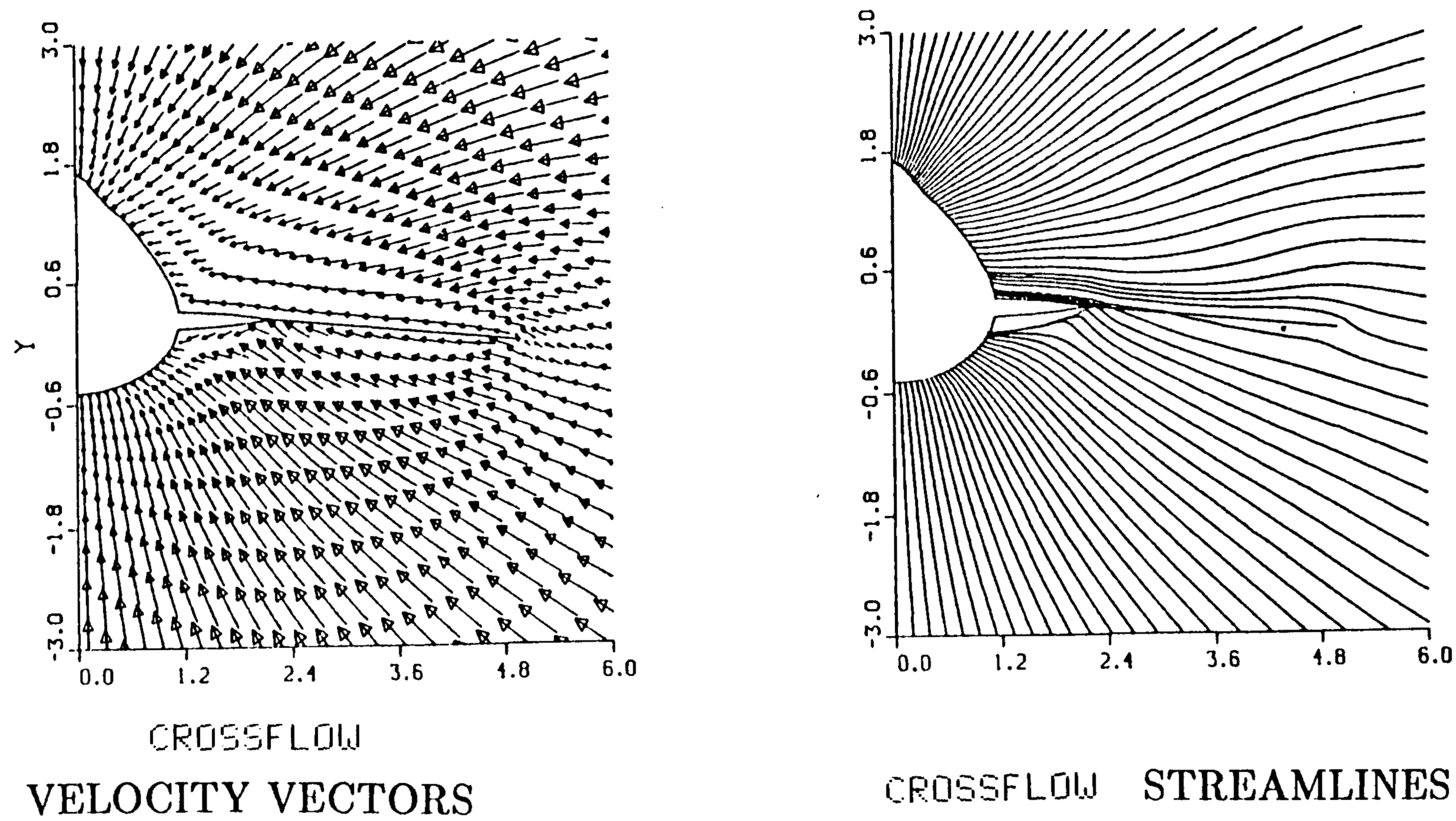

Fig. 17. Solution for Langley fighter configuration.

$M_\infty = 2$; $\alpha = 4$ deg; $x/l = 0.47$

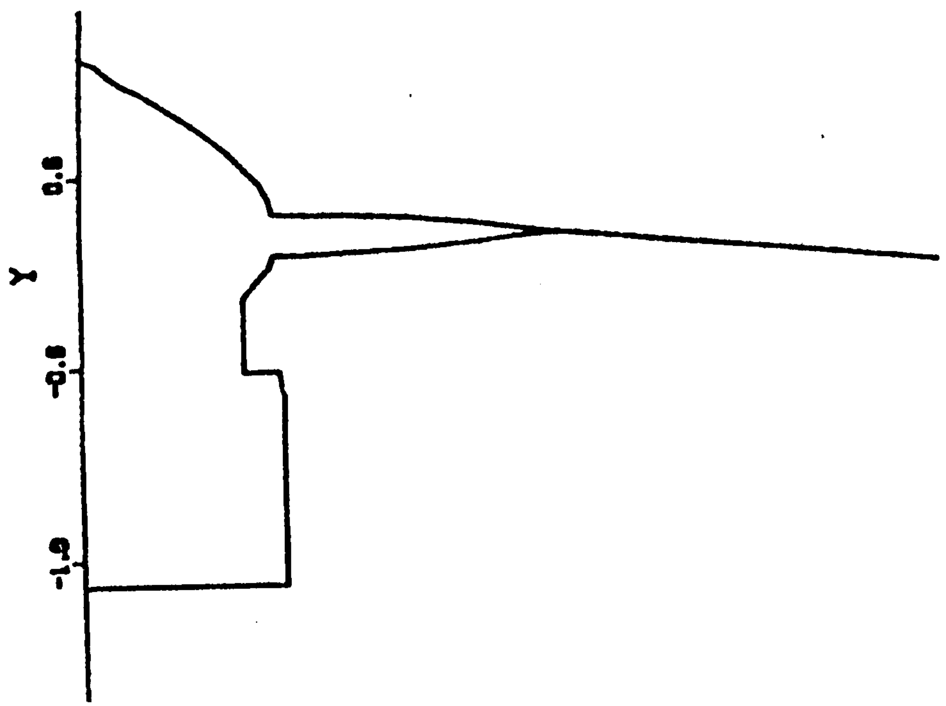

CROSS-SECTIONAL SHAPE

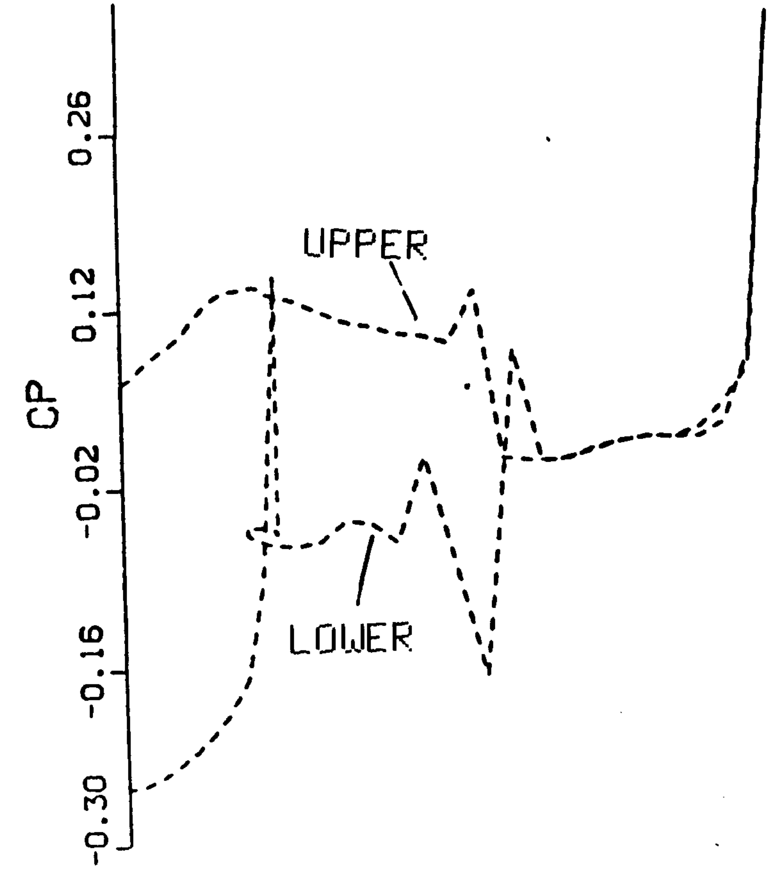

PRESSURE PROFILE

Fig. 18. Solution for Langley fighter configuration.

$M_\infty = 2;\ \alpha = 4\,\text{deg};\ x/l = 0.47$

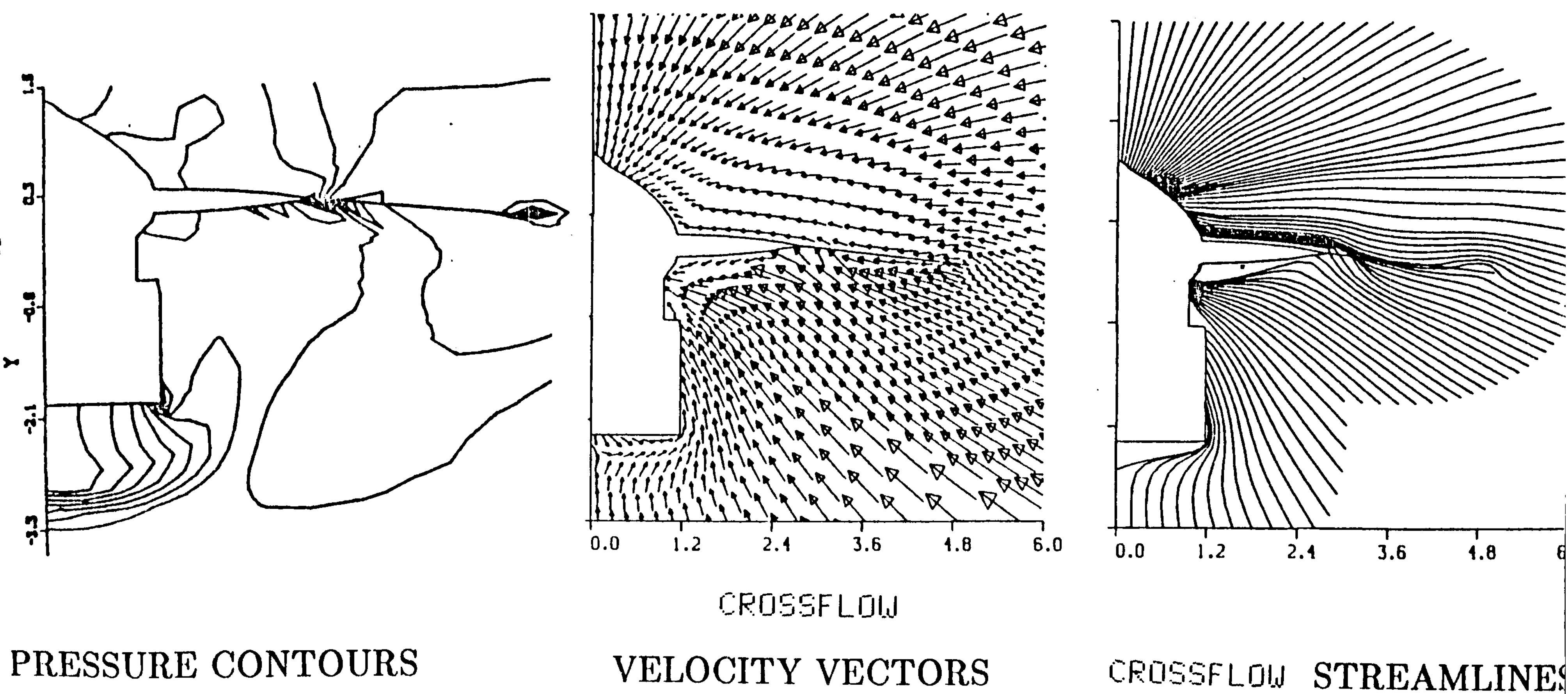

Fig. 19. Solution for Langley fighter configuration.

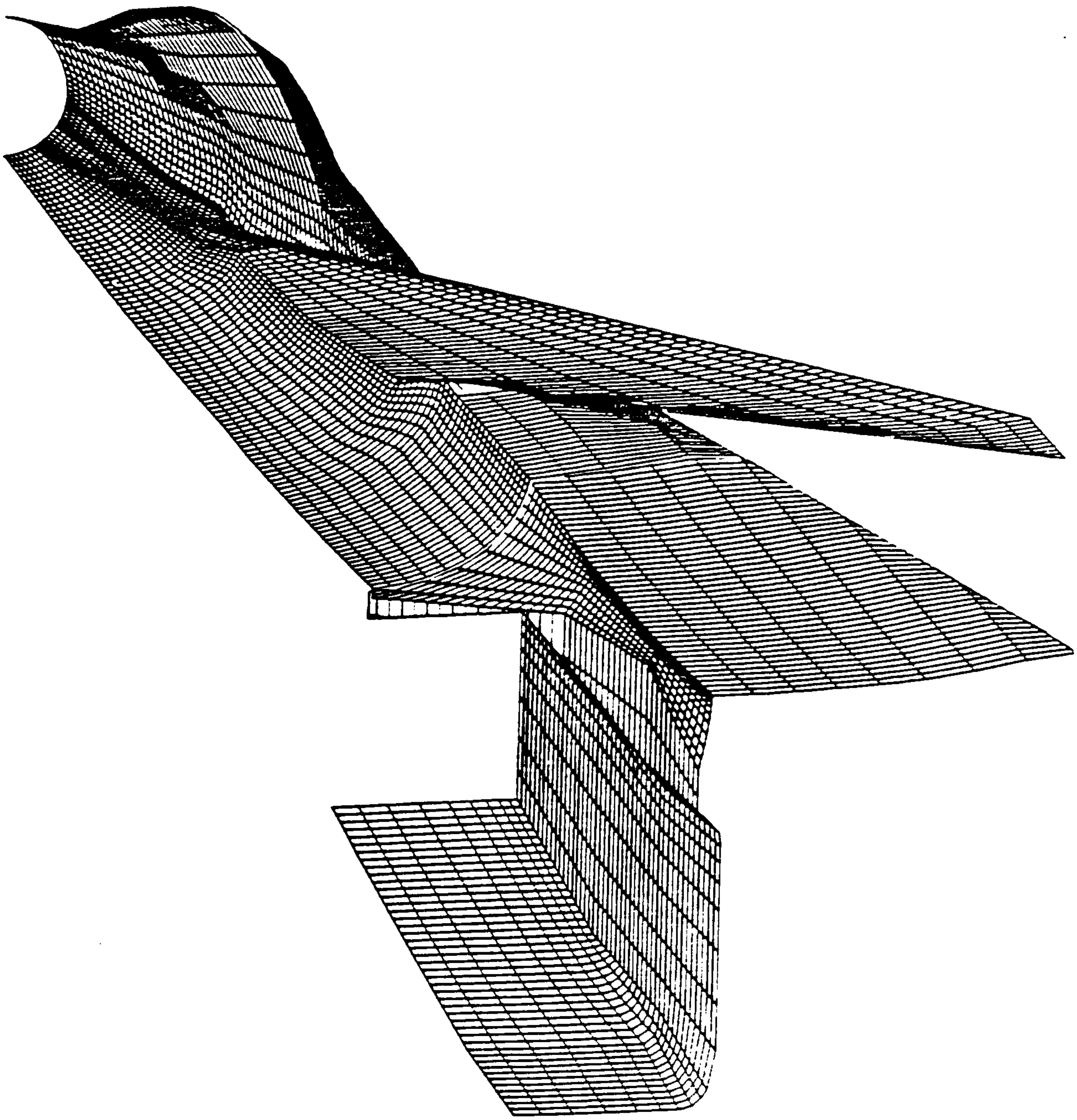

Fig. 20. Computational geometry and surface grid points.

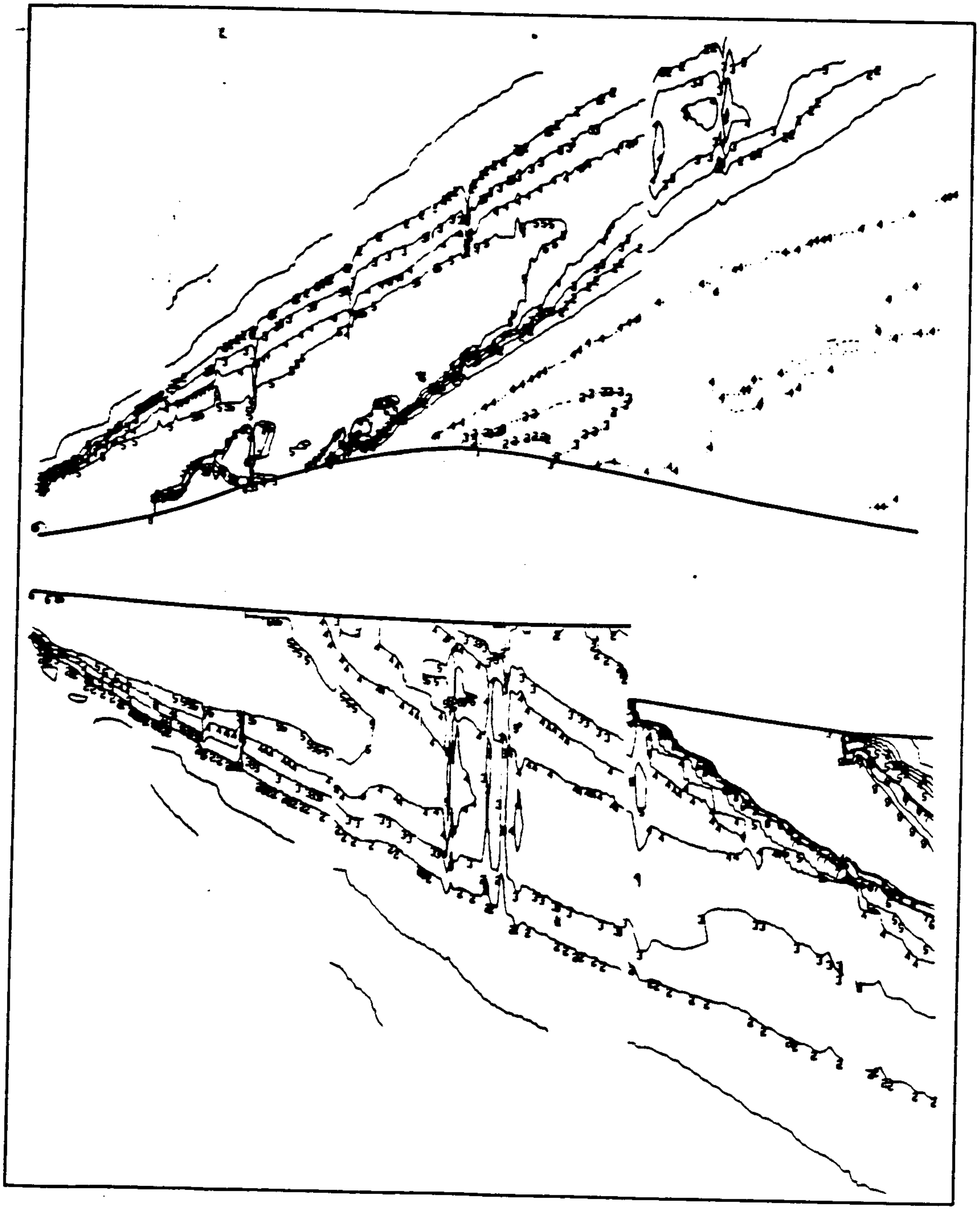

Fig. 21. Pressure contours in the plane of symmetry.

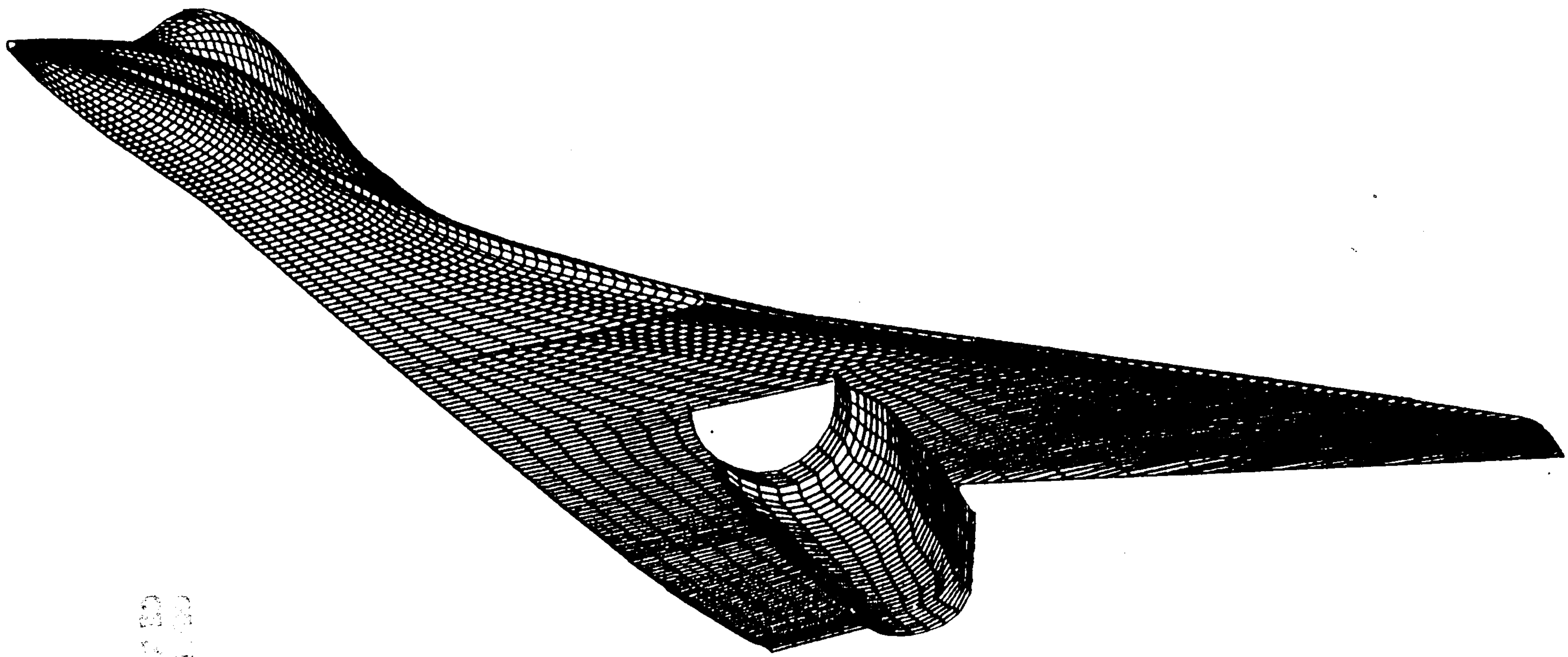

Fig. 22. Geometry of an advanced fighter with a nacelle.

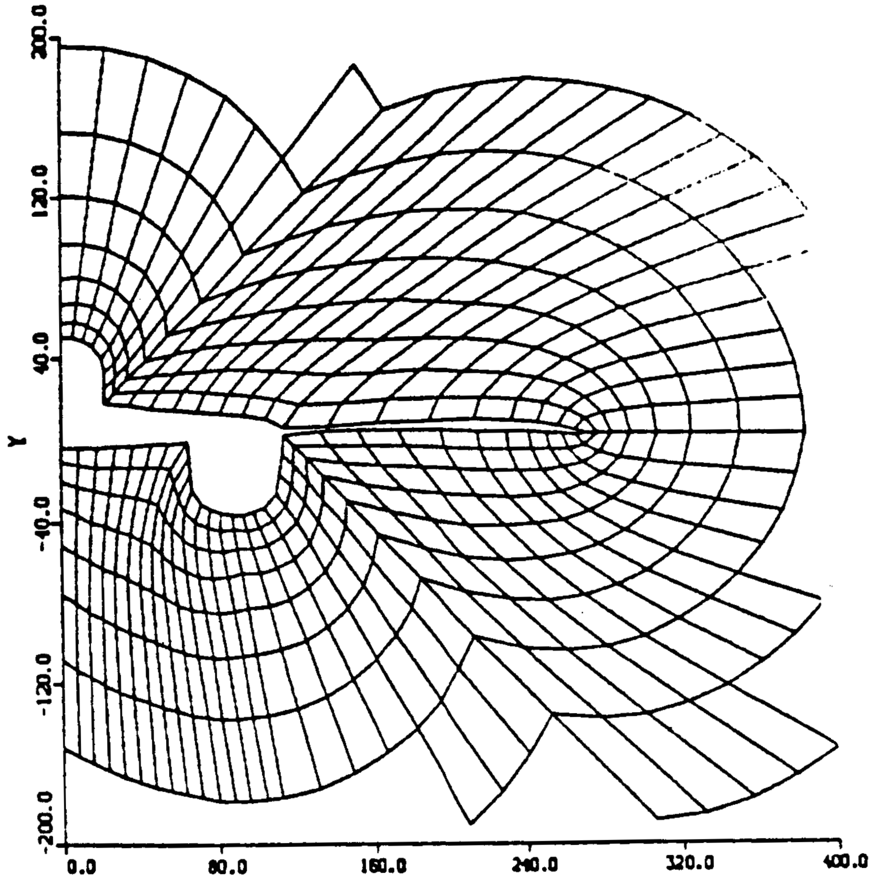

Fig. 23. Grid setup for a wing mounted nacelle.

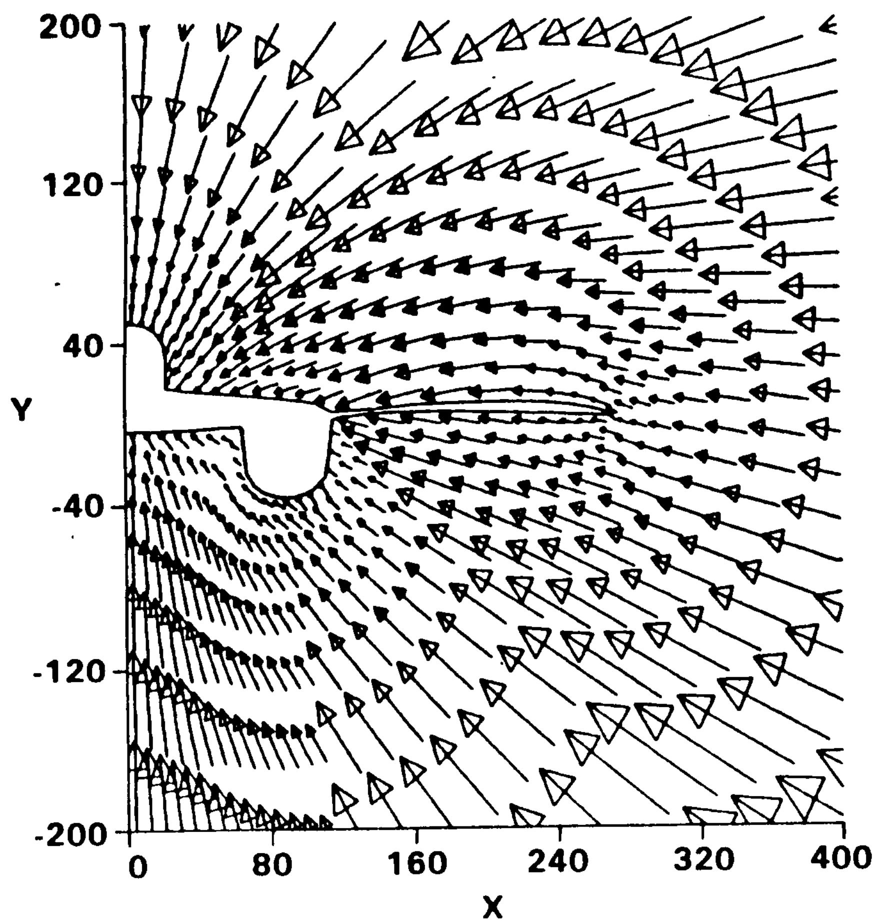

a) Cross flow velocity

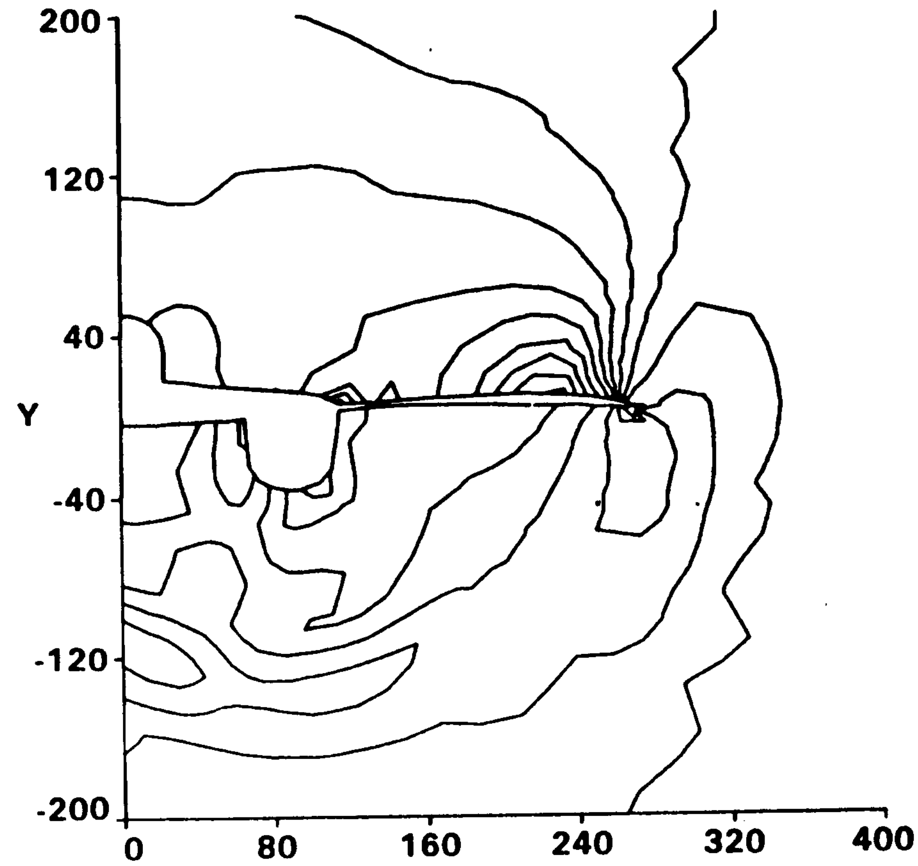

b) Pressure contours

Fig. 24. Tactical fighter results at $M_\infty = 1.6$, $\alpha = 5°$, $\frac{X}{L} = 0.65$

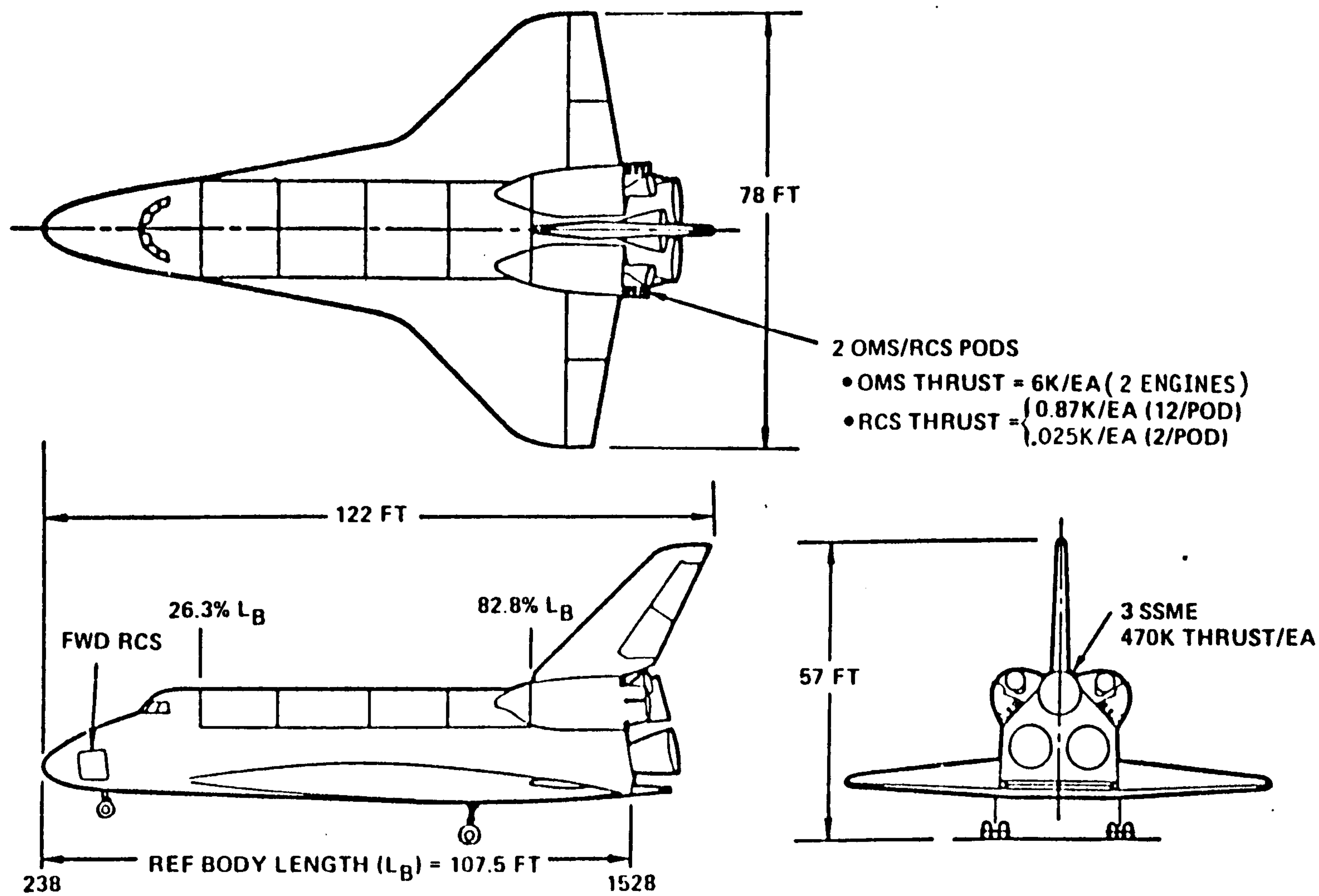

Fig. 25. Space Shuttle Orbiter.

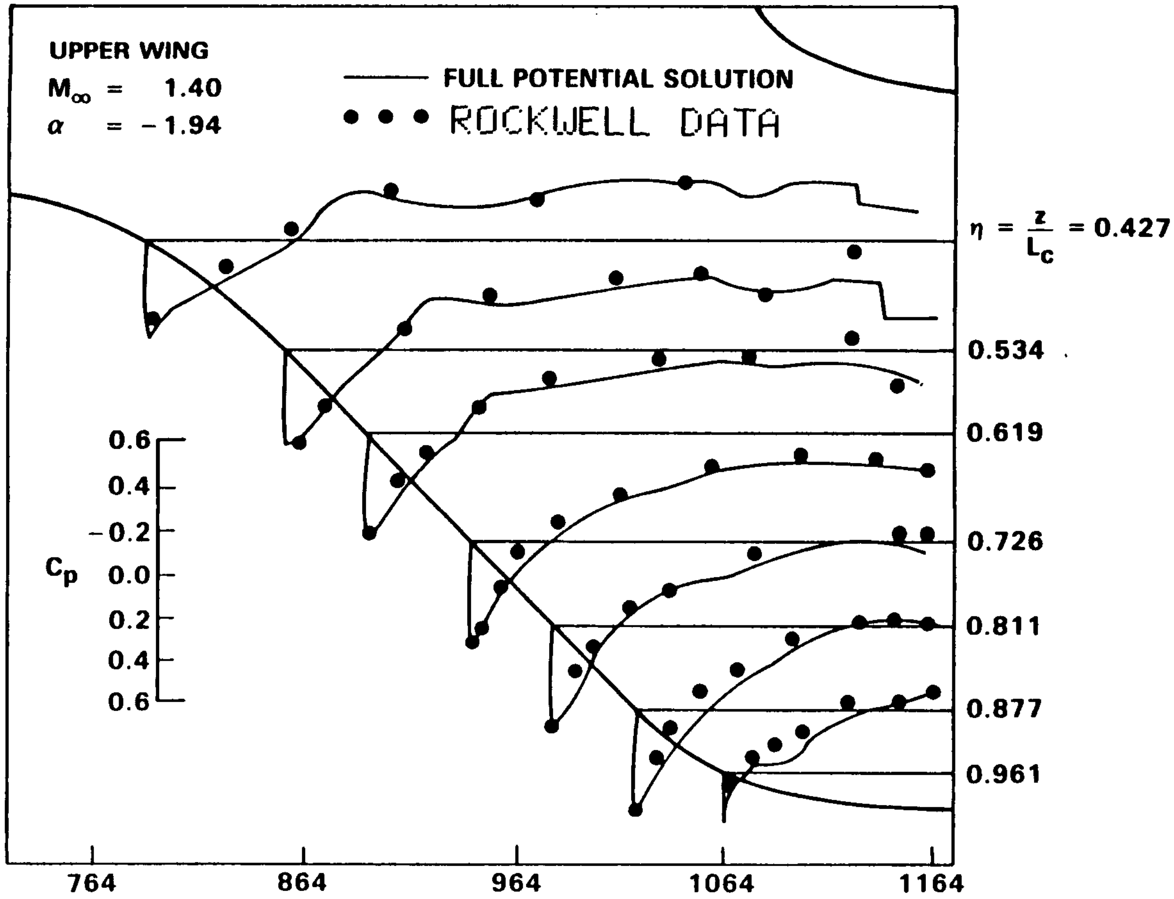

Fig. 26. Shuttle Orbiter upper surface pressure distribution; $M_\infty = 1.4$, $\alpha = 1.94$.

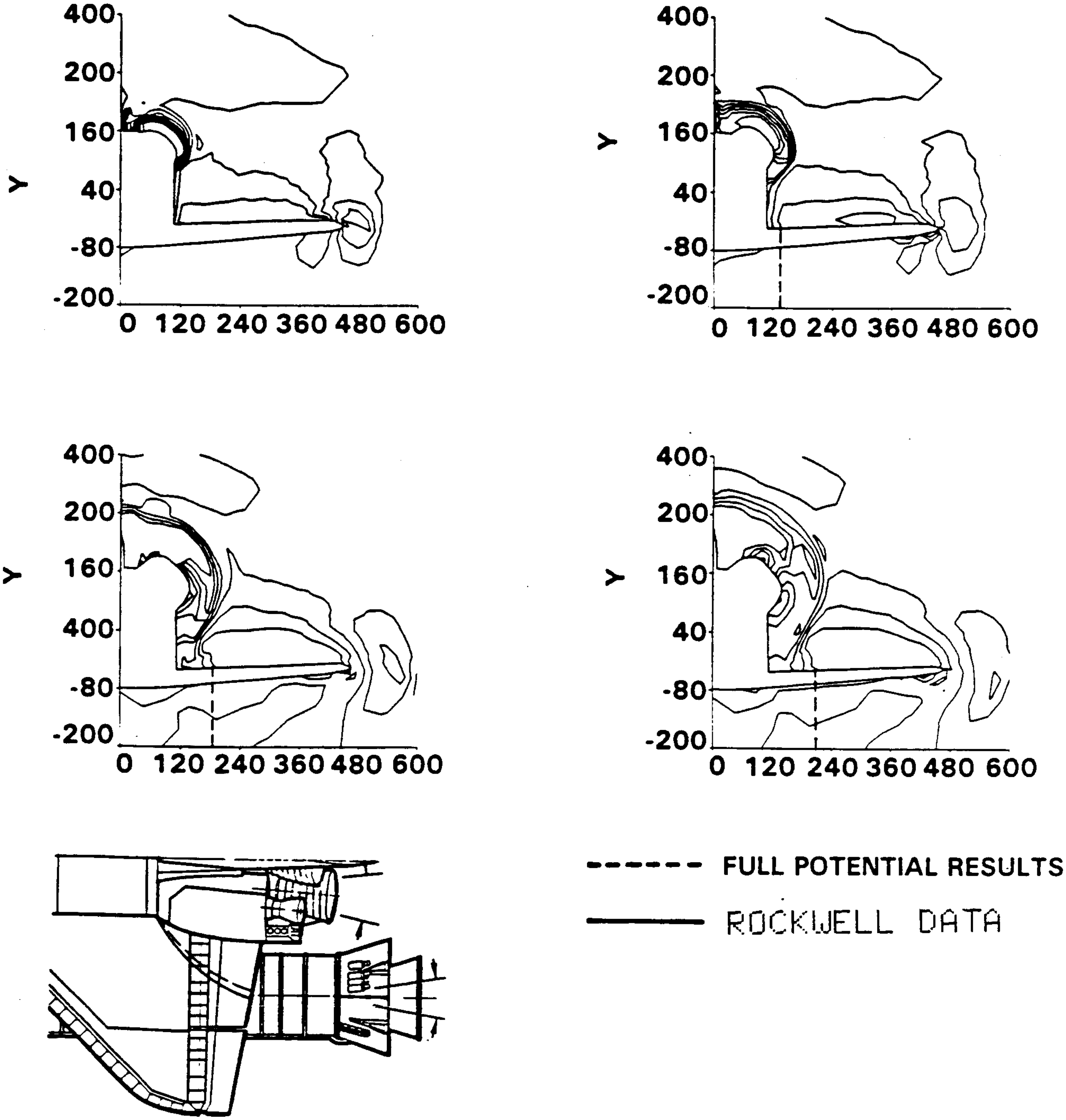

Fig. 27. The trace of OMS pod shock on the upper surface; $M_\infty = 1.4$, $\alpha = 1.94$.

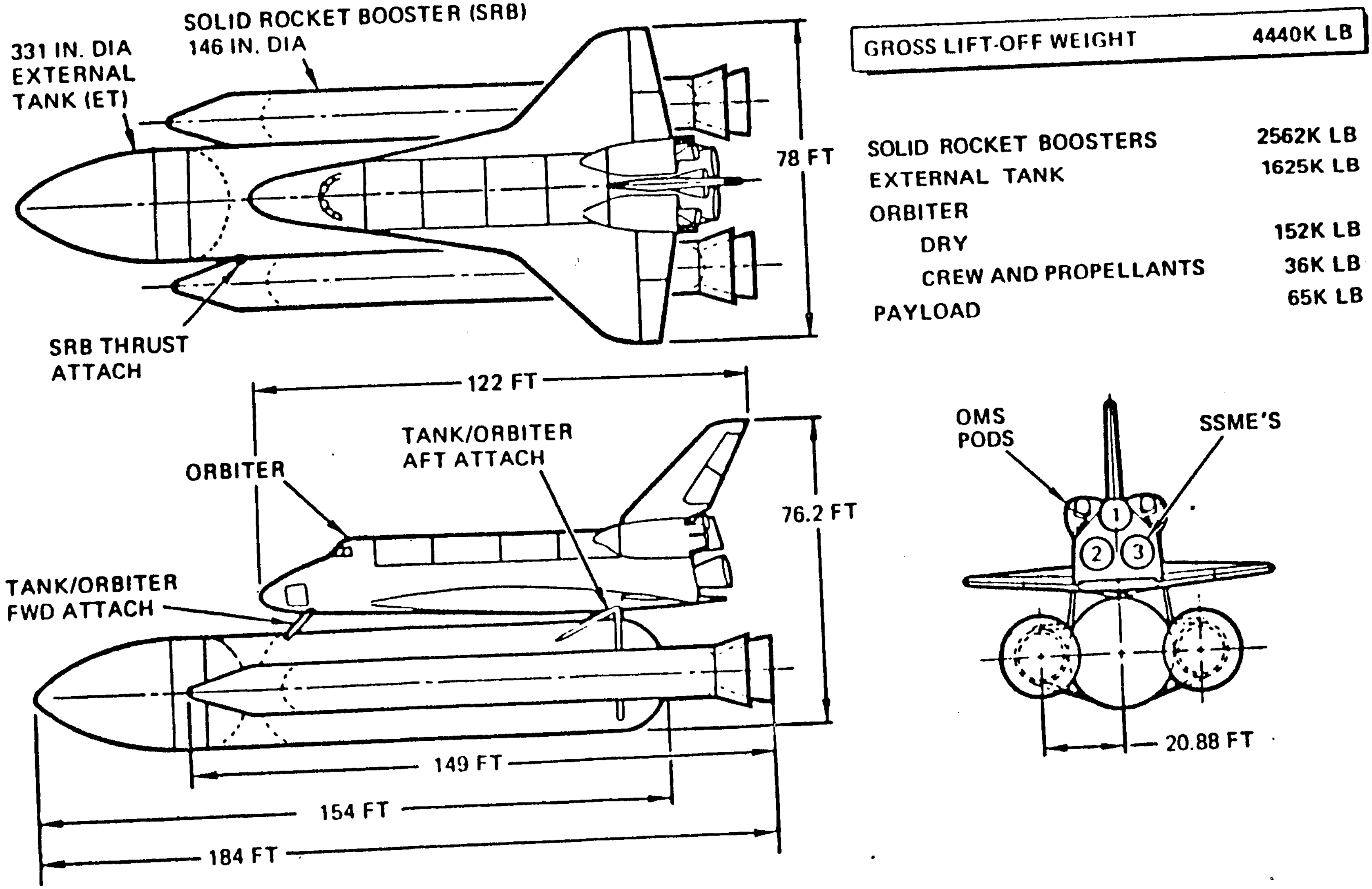

Fig. 28. Space Shuttle Vehicle — mated configuration.

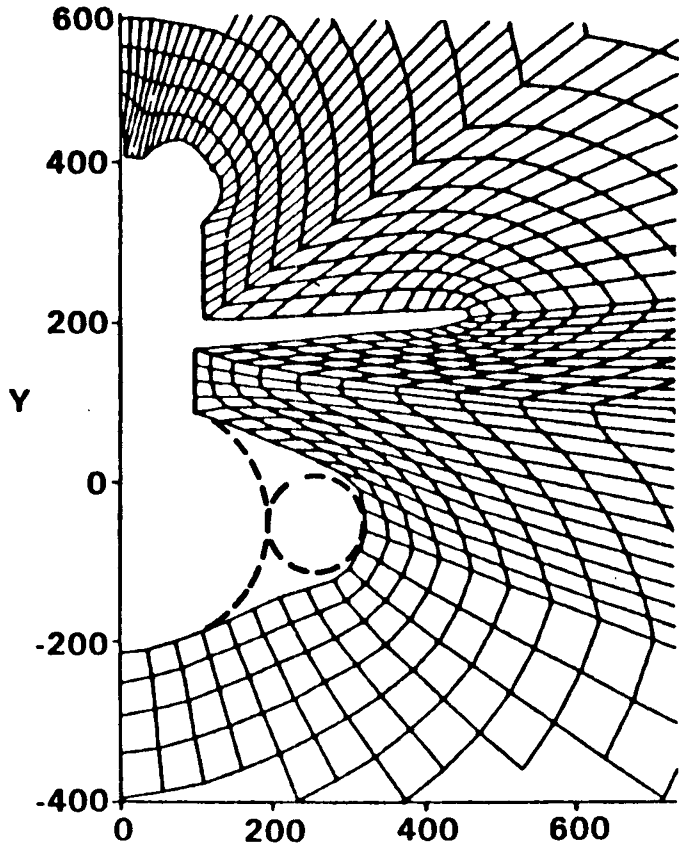

a) Computational grid

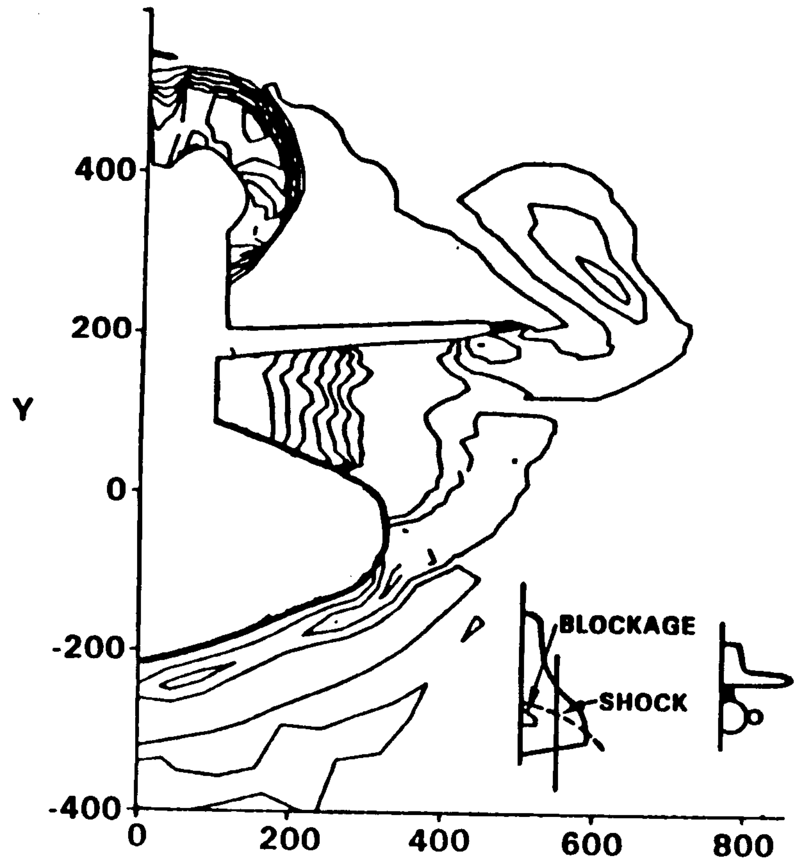

b) Pressure contours

Fig. 29. Multibody problem analysis at M = 1.6, $\alpha = -1.96°$, $\frac{X}{L} = .65$

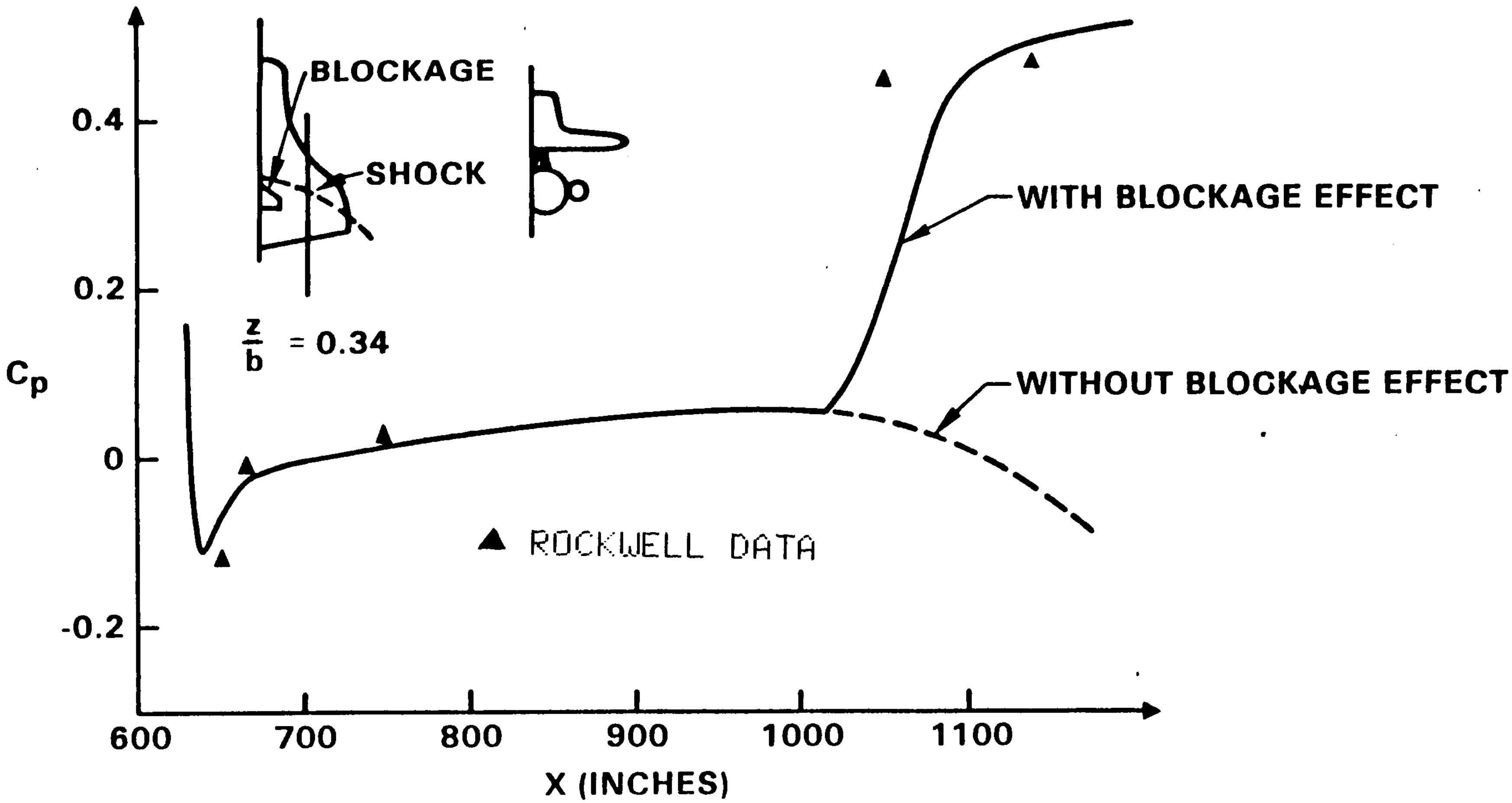

Fig. 30. Orbiter lower surface chordwise pressure distribution.

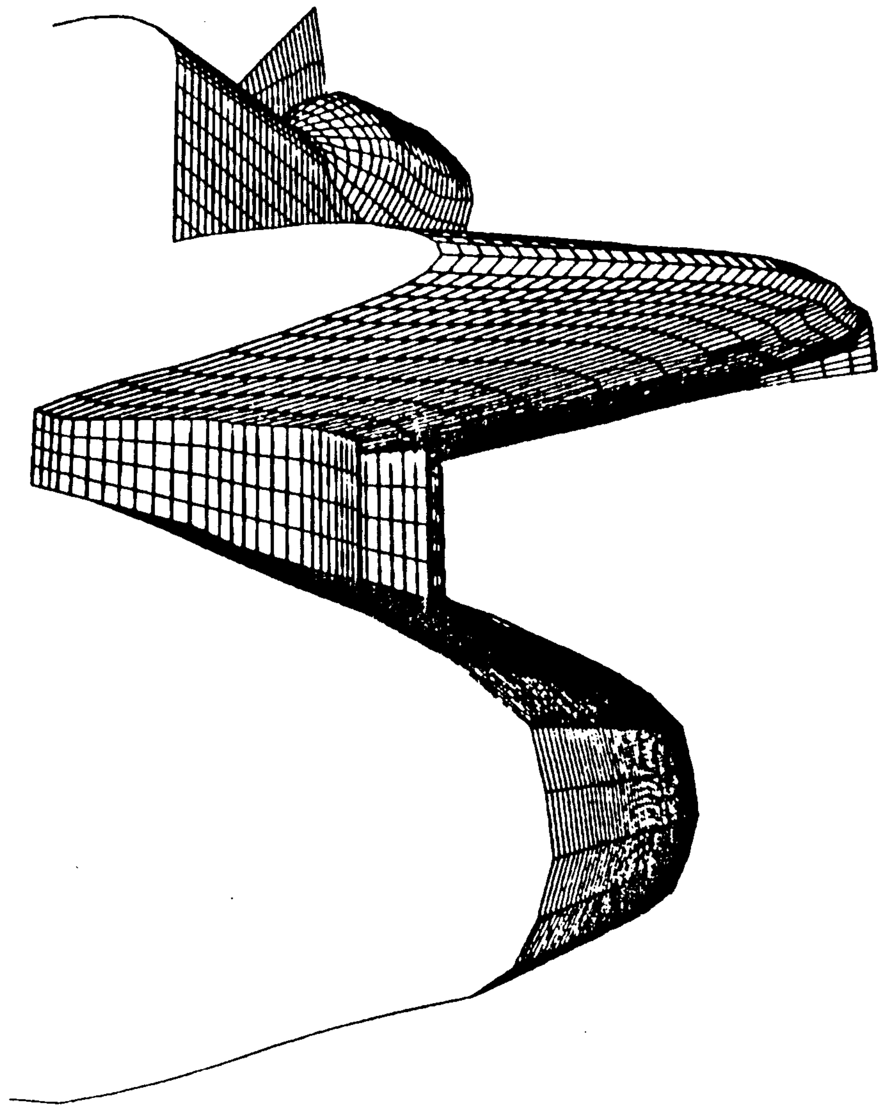

Fig. 31. Computational geometry and surface gridding for mated configuration.

APPENDIX A

CONTRACT PUBLICATIONS

1. AIAA Paper No. 84–0427.*

2. University of Tennessee Space Institute Workshop on Computational Fluid Dynamics — Article 6.1, UTSI Publication No. E02–4005–023–84.

3. Rockwell International Report, TFD 84–1654.

4. AIAA Paper No. 84–0262.*

5. ICAS–84–1.6.2, International Council of the Aeronautical Sciences Meeting, Toulouse, France, September 1984.*

*Permission to reprint these Papers was granted by AIAA, March 6, 1985

AIAA'84

AIAA-84-0427

Nonlinear Computation of Wing-Body-Vertical Tail-Wake Flows at Low Supersonic Speed

K.Y. Szema and V. Shankar, Rockwell International Science Center, Thousand Oaks, CA

AIAA 22nd Aerospace Sciences Meeting

January 9-12, 1984/Reno, Nevada

NONLINEAR COMPUTATION OF WING-BODY-VERTICAL TAIL-WAKE FLOWS AT LOW SUPERSONIC SPEEDS

Kuo-Yen Szema* and Vijaya Shankar**
Rockwell International Science Center
Thousand Oaks, California

Abstract

A numerical method based on the conservation form of the full potential equation has been applied to the problem of three-dimensional supersonic flows with embedded subsonic regions. The governing equation is cast in a nonorthogonal coordinate system, and the theory of characteristics is used to accurately monitor the type-dependent flow field. A conservative switching scheme is employed to transition from the supersonic marching procedure to a subsonic relaxation algorithm and vice versa. The newly developed computer program can handle arbitrary geometries with fuselage, wing, vertical tail and wake components at combined angle of attack and sideslip. Results are presented for a low supersonic mach numbers flow over the Shuttle orbiter (including the OMS pods and vertical tail), and for flows over a realistic fighter type configuration. Comparisons with experimental data are shown to be in good agreement for various cases.

I. Introduction

Currently available numerical algorithms to compute the low supersonic, inviscid flow about complex configurations are frequently either inadequate[1] or too costly to use for routine analysis.[2,3] For treatment of low supersonic flows, the full potential method[4] is an ideal substitute for the Euler methods to avoid the requirements of excessive computer time and memory.

Recently, Shakar et al[4] have developed a numerical method based on the characteristic theory to solve the problem of supersonic flow with embedded subsonic regions. Reference 4 describes the characteristic theory involved in determining the condition for a marching direction to exist. Once that condition is violated, the marching scheme is transitioned to a relaxation scheme through a conservative switching operator. For the marching condition violation, the total velocity q does not have to be subsonic. Even for a supersonic total velocity q, if the component in the marching direction is subsonic, a relaxation scheme is required. In order to properly produce the necessary artificial viscosity through density biasing, Reference 4 defines two situations: (1) the total velocity q is supersonic, but the marching direction component is subsonic (defined as Marching Subsonic Region (MSR)), and (2) the total velocity q is subsonic (termed as Total Subsonic Region (TSR)). The method of Reference 4 uses a numerical mapping technique to generate the body fitted, nonorthogonal curvilinear coordinates system. The key advantage is that it has no restrictions on its applicability to complex geometries and intricate shocked flow fields.

The main purpose of this study is to extend the methodology of Reference 4 to investigate supersonic flows with large embedded subsonic regions over complex configurations, and as well as extend the treatment to combined angle of attack and yaw cases. All the calculations reported in this paper were performed using the CDC CYBER 176 computer. A typical calculation over a complete configuration requires 15 minutes of CPU time on the CYBER system or 3 minutes on the CRAY 1.

II. Basic Formulation

The steady, conservative full potential equation cast in an arbitrary coordinate system defined by $\zeta = \zeta(x,y,z)$, $\eta = \eta(x,y,z)$ and $\xi = \xi(x,y,z)$ can be written as

$$\left(\rho \frac{U}{J}\right)_\xi + \left(\rho \frac{V}{J}\right)_\eta + \left(\rho \frac{W}{J}\right)_\zeta = 0 \qquad (1)$$

where the density ρ is given by

$$\rho = \left[1 - \left(\frac{\gamma-1}{2}\right) M_\infty^2 \left(U\phi_\zeta + V\phi_\eta + W\phi_\xi - 1\right)\right]^{1/(\gamma-1)} \qquad (2)$$

and M_∞ is the free stream mach number, a is the local speed of sound and U,V,W are the contravariant velocity components. Introducing the following notation for convenience.

$$\begin{array}{lll} U_1 = U & U_2 = V & U_3 = W \\ x = x_1 & y = x_2 & z = x_3 \\ \zeta = X_1 & \eta = X_2 & \xi = X_3 \end{array},$$

the contravariant velocity can be expressed as

$$U_i = \sum_{j=1}^{3} a_{ij}\phi_{X_j} \qquad i = 1,2,3$$

$$a_{ij} = \sum_{k=1}^{3} \frac{\partial X_i}{\partial x_k}\frac{\partial X_j}{\partial x_k} \qquad \begin{array}{l} i = 1,2,3 \text{ (transforma-} \\ j = 1,2,3 \text{ tion metrics)} \end{array} \qquad (3)$$

The Jacobian of the transformation J is represented by

$$J = \frac{\partial(\zeta,\eta,\xi)}{\partial(x,y,z)} = \begin{bmatrix} \zeta_x & \zeta_y & \zeta_z \\ \eta_x & \eta_y & \eta_z \\ \xi_z & \xi_y & \xi_z \end{bmatrix} \qquad (4)$$

*Member Technical Staff, Member AIAA
**Manager, CFD Group, Associate Fellow AIAA

The nature of Eq. (1) can be analyzed by studying the eigenvalue system of Eq. (1) combined with the irrotationality condition in the (ζ,η) and (ζ,ξ) planes. A detailed discussion on this can be found in Reference 4. Therefore, only the final results are presented here.

1. At a grid point, the marching direction ζ is <u>hyperbolic</u> and the total velocity q is supersonic, $\left(a_{11} - \frac{U^2}{a^2}\right) < 0$, $q > a$. This point will use the algorithm of Reference 5.

2. At a grid point, the marching direction ζ is <u>elliptic</u>, $\left(a_{11} - \frac{U^2}{a^2}\right) > 0$, but the total velocity q is supersonic, $q > a$. This point will be treated by a transonic operator with a built-in density biasing based on the magnitude of $\left(1 - \frac{a^2}{q^2}\right)$.

3. At a grid point, the direction ζ is <u>elliptic</u> and the total velocity q is <u>subsonic</u>, $q < a$. This point will be treated by a subsonic central differenced operator.

III. Method of Solution

Figure 1 shows the schematic of a fuselage-canopy forebody geometry with an embedded MSR and TSR present in a supersonic flow. To solve this problem, the marching scheme of Reference 5 is used when $\left(a_{11} - \frac{U^2}{a^2}\right)$ is negative, and a relaxation scheme is used when $\left(a_{11} - \frac{U^2}{a^2}\right)$ is positive. First, march from the nose up to the plane denoted by (A-B) in Fig. 1, using the method of Reference 5. Then, between (A-B) and (C-D), which embed the subsonic bubble (MSR and TSR), use a relaxation scheme and iterate until the subsonic bubble is fully captured. Then, resume the marching scheme from the plane (C-D), downstream of the body.

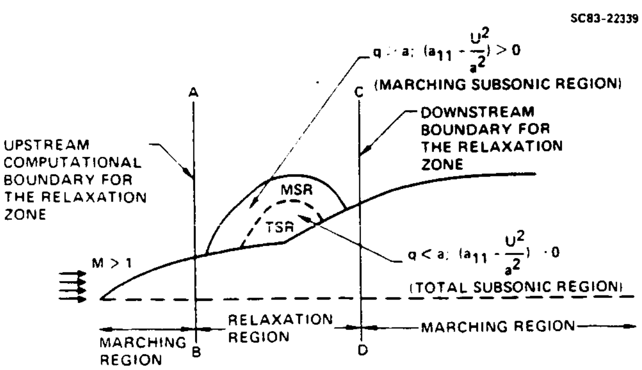

Fig. 1 Embedded subsonic bubble in a supersonic flow.

1. Treatment of $\partial/\partial\zeta\ (\rho\ U/J)$ Term

The finite-difference operator at point $(i+1, \overleftarrow{\partial}, k)$ for the first term in Eq. (1) may be written as

$$\frac{\partial}{\partial\zeta}\left(\rho\,\frac{U}{J}\right) = \theta_i\,\underbrace{\frac{\overleftarrow{\partial}}{\partial\zeta}\left(\rho\,\frac{U}{J}\right)_{i+1}}_{\text{supersonic}} + (1-\theta_{i+1})\,\underbrace{\frac{\overrightarrow{\partial}}{\partial\zeta}\left(\tilde{\rho}\,\frac{U}{J}\right)_{i+1}}_{\text{marching subsonic}} \qquad (5)$$

where

$\overleftarrow{\partial}$ refers to backward differencing

$\overrightarrow{\partial}$ refers to forward differencing

$$\theta_i = 1 \text{ if } \left(a_{11} - \frac{U^2}{a^2}\right) < 0$$

$$= 0 \text{ if } \left(a_{11} - \frac{U^2}{a^2}\right) > 0 \quad .$$

The first term in Eq. (4) corresponds to the supersonic marching operator and the second term is the subsonic operator. By using a local linerization procedure, Eq. (5) can be expressed in term of ϕ only. Details of the procedure are given in Refs. 4 and 5.

2. Treatment of $\partial/\partial\eta\ (\rho\ V/J)$ Term

The finite difference operator for the second term in Eq. (1) is given as

$$\frac{\partial}{\partial\eta}\left(\rho\,\frac{V}{J}\right) = \theta_{i+1}\,\underbrace{\frac{\overleftarrow{\partial}}{\partial\eta}\left(\bar{\rho}\,\frac{V}{J}\right)_{j+1/2}}_{\text{supersonic}} + (1-\theta_{i+1})\,\underbrace{\frac{\overleftarrow{\partial}}{\partial\eta}\left(\bar{\bar{\rho}}\,\frac{V}{J}\right)_{j+1/2}}_{\text{marching subsonic}} \qquad (6)$$

where

$$\theta_{i+1} = 1 \quad \text{if } \left(a_{11} - \frac{U^2}{a^2}\right)_{i+1} < 0 \quad \text{(supersonic point)}$$

$$\theta_{i+1} = 0 \quad \text{if } \left(a_{11} - \frac{U^2}{a^2}\right)_{i+1} > 0 \quad \text{(MSR)} \quad .$$

When $\theta_{i+1} = 1$, that is, the point is <u>supersonic</u> with respect to ζ, only the first term in Eq. (6) is used and the biased density $\bar{\rho}$ is defined by (for $V > 0$)

$$\bar{\rho}_{j+1/2} = (1 - \bar{\nu}_{j+1/2})\rho^*_{j+1/2} + \frac{1}{2}\,\bar{\nu}_{j+1/2}(\rho^*_j + \rho^*_{j-1}) \qquad (7)$$

where

$$\bar{\nu} = \max\left(0,\ 1 - a_{22}\,\frac{a^2}{V^2}\right) \quad .$$

In Eq. (7), the evaluation of ρ^* depends on whether the flow is conical or nonconical. For conical flows, all ρ^* quantities are evaluated at the i^{th} plane. For nonconical flows, at each nonconical marching plane, initially ρ^* is seen to be the value at the i^{th} plane and then subsequently iterated to convergence by setting ρ^* to the previous iterated value of ρ at the current i+1 plane.

When the point is <u>elliptic</u>, the density biasing is defined by

$$\tilde{\tilde{\rho}}^{n+1}_{j+1/2} = (1 - \tilde{\tilde{\nu}}_{J+1/2})\rho^n_{j+1/2} + \frac{1}{2}\tilde{\tilde{\nu}}_{j+1/2}(\rho^n_j + \rho^n_{j-1}) \quad (8)$$

where $\tilde{\tilde{\nu}} = \max(0, 1 - \frac{a^2}{q^2})$. As before, the superscript n+1 denotes the current relaxation cycle for a subsonic bubble calculation. Note the difference in the definition of $\bar{\nu}$ and $\tilde{\tilde{\nu}}$. The density biasing in the cross flow direction η is turned off when the total velocity q is less than the speed of sound $\bar{a}$. The implicit treatment of V in the marching subsonic operator of Eq (6) is the same as that of the supersonic part, explained in Reference 5.

A similar procedure is implemented for $(\rho \frac{W}{J})_\xi$ term in Eq. (1).

3. Implicit Factorization Algorithm

Combining the various terms of Eq. (1) as represented by Eqs. (5)-(8) together with the terms arising from $(\rho \frac{W}{J})_\xi$ will result in a fully implicit model. This is solved using an approximate factorization implicit scheme. After some rearrangement of the terms, the factored implicit scheme becomes

$$\left[1 + \frac{A_3}{\beta\Delta\zeta}\frac{\partial}{\partial\xi} + \frac{1}{\beta}\frac{\partial}{\partial\xi}(\frac{\hat{\rho}}{J}\frac{a_{31}}{\Delta\zeta}) + \frac{1}{\beta}\frac{\partial}{\partial\xi}\frac{\hat{\rho}a_{33}}{J}\frac{\partial}{\partial\xi}\right] \times \left[1 + \frac{A_2}{\beta\Delta\zeta}\frac{\partial}{\partial\eta} + \frac{1}{\beta}\frac{\partial}{\partial\eta}(\frac{\hat{\rho}a_{21}}{J\Delta\zeta}) + \frac{1}{\beta}\frac{\partial}{\partial\eta}\frac{\hat{\rho}a_{22}}{J}\frac{\partial}{\partial\eta}\right]\Delta\phi = R \quad . \quad (9)$$

$$\begin{aligned} R = \theta_i &\left\{\frac{1}{\Delta\zeta}\left[\frac{A_{1i}}{\Delta\zeta_2}\Delta\phi_i + A_{1i-1}(\frac{\Delta\phi_i}{\Delta\zeta_2} - \frac{\Delta\phi_{i-1}}{\Delta\zeta_3}) + A_{2i-1}\frac{\partial\Delta\phi}{\partial\eta} + A_{3i-1}\frac{\partial\Delta\phi_i}{\partial\xi}\right] + \frac{\partial}{\partial\zeta}(\frac{\rho_i U_i}{J})\right\} \\ &+ (1 - \theta_{i+1})\left\{\frac{1}{\beta\Delta\zeta_o}\left[\frac{\tilde{\tilde{\rho}}}{J}(a_{11}\frac{\Delta\phi}{\Delta\zeta_o} + a_{12}\phi_\eta + a_{13}\phi_\xi)\right]_{i+2} + \frac{1}{\beta\Delta\zeta_o}\left[(\frac{\tilde{\tilde{\rho}}a_{12}}{J})_{i+1}\frac{\partial\phi_i}{\partial\eta} + (\frac{\tilde{\tilde{\rho}}a_{13}}{J})_{i+1}\frac{\partial\phi_i}{\partial\xi}\right]\right\} \\ &- \frac{1}{\beta}\frac{\partial}{\partial\eta}\left[(\frac{\hat{\rho}a_{22}}{J}\frac{\partial\phi_i}{\partial\eta}) + (\frac{\hat{\rho}a_{23}}{J}\frac{\partial\phi_i}{\partial\xi})\right] \\ &- \frac{1}{\beta}\frac{\partial}{\partial\xi}\left[(\frac{\hat{\rho}a_{32}}{J}\frac{\partial}{\partial\eta}\phi_i) + \frac{\hat{\rho}a_{33}}{J}\frac{\partial}{\partial\xi}\phi_i\right] \\ &- \frac{1}{\beta}\frac{\partial}{\partial\eta}(\frac{\hat{\rho}a_{23}}{J}\frac{\partial}{\partial\xi})_{i+1}\Delta\phi_{i+1} - \frac{1}{\beta}\frac{\partial}{\partial\xi}(\frac{\hat{\rho}a_{32}}{J}\frac{\partial}{\partial\eta})_{i+1}\Delta\phi_{i+1} \end{aligned} \quad (10)$$

The density $\hat{\rho}$ appearing in Eq. (9) and Eq. (10) can be either $\bar{\rho}$ or ρ depending on the sign of $(a_{11} - \frac{U^2}{a^2})$ as illustrated in Eq. (6).

Equation (9) has the form $L_\xi L_\eta(\Delta\phi) = R$ and it is implemented as follows:

$$L_\xi(\Delta\phi)^* = R \quad L_\eta(\Delta\phi) = (\Delta\phi)^* \quad \phi_{i+1} = \phi_i + \Delta\phi \quad .$$

The various quantities appearing in Eq. (9) are given by

$$R = \frac{1}{\Delta\zeta}\left[\theta_i A_1 - (1 - \theta_{i+1})\frac{\Delta\zeta}{\Delta\zeta_0}(\frac{\tilde{\rho}a_{11}}{J})_{i+1}\right]$$

$$A_1 = \frac{\rho_i}{J_{i+1}}(a_{11} - \frac{U^2}{a^2})$$

$$A_2 = \theta_i\left[\frac{\rho_i}{J_{i+1}}(a_{12} - \frac{UV}{a^2})\right] - (1 - \theta_{i+1})\frac{\Delta\zeta}{\Delta\zeta_0}(\frac{\tilde{\rho}a_{12}}{J})_{i+1}$$

$$A_3 = \theta_i\frac{\rho_i}{J_{i+1}}(a_{13} - \frac{UW}{a^2}) - (1 - \theta_{i+1})\frac{\Delta\zeta}{\Delta\zeta_0}(\frac{\tilde{\rho}a_{13}}{J})_{i+1}$$

$$\Delta\zeta_0 = \zeta_{i+2} - \zeta_{i+1}$$

$$\Delta\zeta = \zeta_{i+1} - \zeta_i \quad (11)$$

If the flow field does not contain an embedded MSR or TSR, the implicit factored algorithm of Eq. (9) performs a pure marching procedure starting from an initial known data plane. In this situation, there is no need to go back to the upstream starting plane and iterate the solution. However, if a subsonic bubble is presnt (between planes AB and CD in Fig. 1, then the solution procedure of Eq. (9) performs a relaxation method, and iterates for the elliptic subsonic bubble to converge.

IV. Initial Conditions

For a pure supersonic flow, initial conditions are required at the starting plane. Usually, the starting plane is set close to the nose region of the configuration. For a sharp nosed configuration, conical solutions are prescribed, and for a blunt nose, the axisymmetric unsteady full potential solver of Reference 6 is used to obtain flow field in the transonic forbody region.

In the embedded subsonic region, when Eq. (5) is applied at an i+1 grid point, information on the flux ρU at i+2 is required. For the first relaxation pass, sonic conditions are assumed at i+2.

$$\rho_{i+2} = \rho^* = \left(\frac{2}{\gamma+1} + \frac{\gamma-1}{\gamma+1} M_\infty^2\right)^{1/\gamma-1}$$

$$U_{i+2} = q^* \, (a_{11})_{i+2}^{1/2} \qquad (12)$$

where

$$q^* = [\rho^{*\gamma-1}/M_\infty^2]^{1/2}$$

The sonic values ρ^* and q^* are purely a function of the free-stream Mach number M_∞. For the second relaxation cycle and onwards, the conditions from the previous relaxation cycle is used.

V. Boundary Conditions

In order to solve the full potential equation, it is essential to specify appropriate boundary conditions of the body surface and outer boundary.

1. Body Surface

At a solid boundary, the contravariant velocity V is set to zero. Exact implementation of V = 0 in the implicit treatment of Eq. (9) is described in Reference 4.

2. Outer Boundary

The outer boundary is set away from the bow shock and the freestream velocity potential ϕ_∞ is imposed along that boundary. All discontinuities in the flow field are captured. The precise density biasing activator ν, based on the characteristic theory, allows for sharp capturing of shocks in the flow.

3. Symmetric Boundary Conditions

For yaw angle $\beta = 0$, only the half plane problem needs to be solved with the plane of symmetry boundary conditions imposed along K = 2 and (Kmax - 1), as shown in Fig. 2a. Imposing that the flow conditions along K = 1 are to be the same as the ones along K = 3, the L_ζ operator results in a tridiagonal system that can be easily solved.

SC83-24987

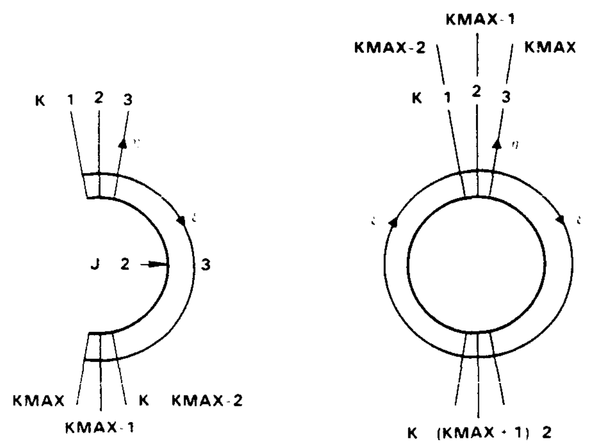

a) PLANE OF SYMMETRY (YAW ANGLE 0)

$\phi_{j,1} = \phi_{j,3}$

$\phi_{j,KMAX} = \phi_{j,KMAX-2}$

b) PERIODIC CONDITION FOR YAW TREATMENT

$\phi_{j,1} = \phi_{j,KMAX-2}$

$\phi_{j,KMAX} = \phi_{j,3}$

Fig. 2 Symmetry and periodic conditions.

4. Combined Yaw and Angle of Attack

Even for a symmetric configuration, when yaw angle is present the entire cross-flow plane needs to be solved as shown in Fig. 2b. In this case the flow conditons along K = 1 are set to be the same as the ones along K = (KMAX - 2). This destroys the tridiagonal nature of the L_ζ operator. A special routine has been developed to invert a matrix of the following type.

$$L_\zeta = \begin{bmatrix} X & X & & X & 0 \\ X & X & X & 0 & 0 \\ & X & X & X & 0 \\ & & & & \\ 0 & 0 & X & X & X \\ 0 & X & & X & X \end{bmatrix} \qquad (13)$$

In the current formulation, positive angle of attack α represents a positive cartesian velocity v in the freestream and similarly positive yaw β produces a positive w in the free stream. When both angle of attack and yaw are present, first the freestream is turned by an angle β and then by α.

Let (x,y,z) be the inertial Cartesian system. After an initial yaw turn β let the wind axis system be (x',y',z'), and after a subsequent α turn let it become $(\tilde{x},\tilde{y},\tilde{z})$.

$$\begin{pmatrix}\tilde{x}\\ \tilde{y}\\ \tilde{z}\end{pmatrix} = \begin{bmatrix} \cos\alpha & \sin\alpha & 0 \\ -\sin\alpha & \cos\alpha & 0 \\ 0 & 0 & 1 \end{bmatrix} \begin{bmatrix} \cos\beta & 0 & \sin\beta \\ 0 & 1 & 0 \\ -\sin\beta & 0 & \cos\beta \end{bmatrix} \begin{pmatrix} x \\ y \\ z \end{pmatrix} \qquad (14)$$

$$= \begin{bmatrix} \cos\alpha\cos\beta & \sin\alpha & \cos\alpha\sin\beta \\ -\sin\alpha\cos\beta & \cos\alpha & 0 \\ -\sin\beta & 0 & \cos\beta \end{bmatrix} \begin{pmatrix} x \\ y \\ z \end{pmatrix}$$

The free stream is now along $\tilde{x}$. The normalized free stream velocity potential is given by

$$\phi_\infty = X\cos\alpha\cos\beta + y\sin\alpha + z\cos\alpha\sin\beta \qquad (15)$$

Using Eq. (14), the lift, drag and side forces are easily represented.

$$D = F_x\cos\alpha\cos\beta + F_y\sin\alpha + F_z\cos\alpha\sin\beta$$

$$L = -F_x\sin\alpha\cos\beta + F_y\cos\alpha \qquad (16)$$

5. Swept Trailing Edge Wake Treatment

Figure 3 shows a schematic of a swept trailing edge wake system. In order to treat the region behind the trailing edge, an artificial cut is created and the pressure jump [P] across this cut is imposed to be zero as a boundary condition. This is achieved by maintaining the jump in the velocity potential ϕ along a k = constant line (see Fig. 3) for j = 2 to be the same as the value $[\phi]$ at the trailing edge. The full potential equation is not solved at grid points on the wake cut. Instead, $\phi_{hh} = 0$ is solved to provide $[\phi_\eta] = 0$ across the wake cut. Maintaining $[\phi]$ constant along a k line provides $[\phi_\zeta] = 0$. The combination

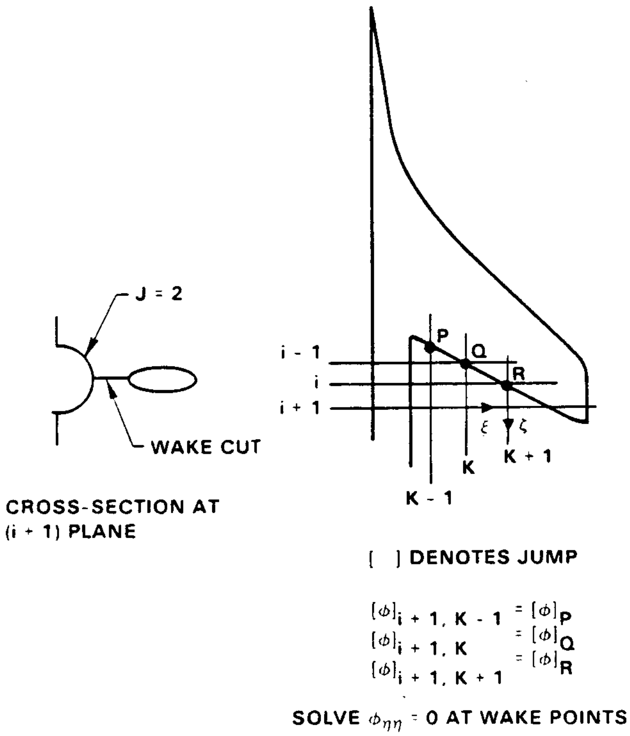

Fig. 3 Wake boundary condition.

of $[\phi_\zeta] = 0$ and $[\phi_\eta] = 0$ across the cut satisfies $[P] = 0$ approximately.

6. Geometry and Grid System

The geometry of a configuration is prescribed at discrete points in a crossplane (usually x = constant plane) at various axial locations. These geometry input points are usually obtained from a geometry package such as GEMPACK or CDS. The input points are then divided into several patches, and at each patch a key-point system is established as shown in Fig. 4. The geometry at a marching plane is then obtained by joining the appropriate key-point for each patch. Using a cubic spline passing through the key points, a desired grid point distribution (clustering) is set up on the body surface. Then, using an appropriate outer boundary, the grid for the flowfield calculation is generated by using an elliptic grid generator.

VI. Results and Discussion

Four cases are presented to substantiate the recently developed code.

1. Flow over an arrow-wing body at M_∞ = 2.96, α = 10.01°.
2. Flow over a forebody configuration at M_∞ = 2.5, β = 5° and at M_∞ = 1.7, α = 10°, β = 5°.
3. Flow over the entire shuttle orbiter geometry at M_∞ = 1.4, α = 0°.
4. Flow over a realistic fighter configuration at different angles of attack and freestream mach numbers.

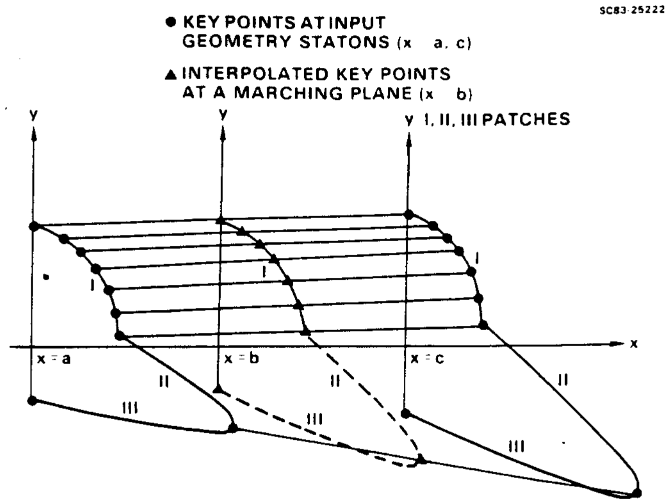

Fig. 4 Geometry setup.

Figure 5 shows the pressure distribution on the surface of an arrow-wing configuration at location x/ℓ = 0.8 for M_∞ = 2.9, and α = 10°. The improvement in the prediction capability achieved using the wake treatment is illustrated. The dashed line represents the result from "no wake" treatment (assumes a flat plate behind the trailing edge) and the solid line represents the modifications to the pressure distribution once a zero jump in pressure across the wake cut is imposed. The solid line pressures on the body agree very well with experiments. Without a proper wake cut treatment, the overall lift and drag forces and the pitching moment can be off by a considerable margin.

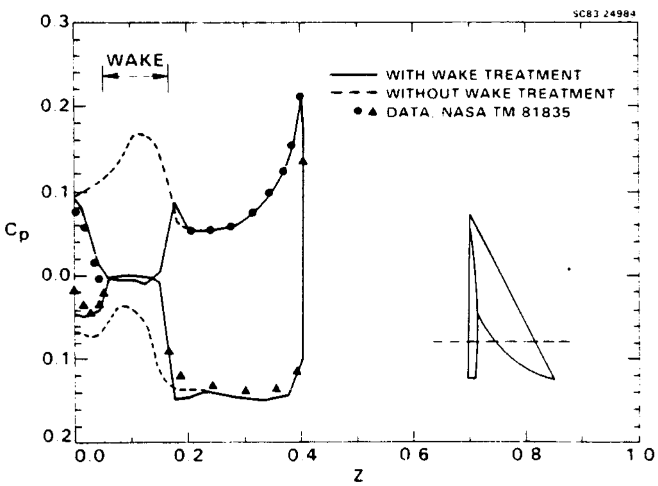

Fig. 5 Circumferential pressure distribution for the arrow-wing at x/ℓ = 0.81, M_∞ = 2.96, α = 10°.

Figure 6 presents the pressure distribution on a fully developed forebody[6] for M_∞ = 2.5 and yaw angle β = 5°. Figure 7 shows the circumferential pressure distribution for the same body at x/ℓ = 0.68 for M_∞ = 1.7, α = 10° and β = 5°. The experimental data[7] are also given in these two figures. The results show that the present prediction is in excellent agreement with the experimental data.

ORIGINAL PAGE IS
OF POOR QUALITY

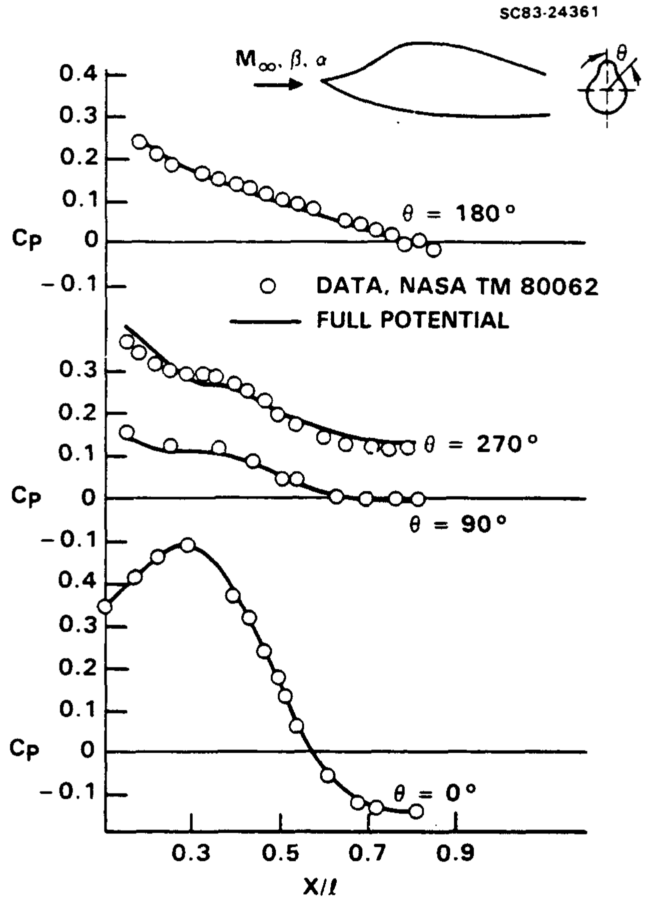

Fig. 6 Pressure distribution on a forebody in sideslip $M_\infty = 2.5$, $\beta = 5.02°$, $\alpha = 0°$.

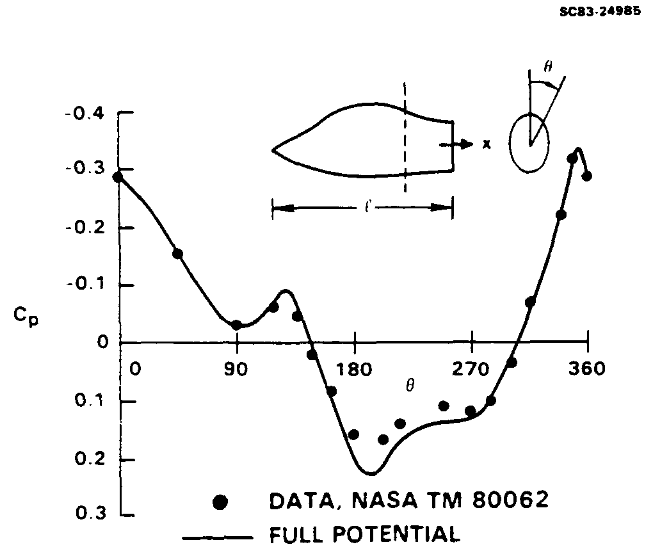

Fig. 7 Circumferential pressure distribution on a forebody at $x/\ell = 5.02°$, $\alpha = 0°$.

Figures 8 to 18 give the geometry and the corresponding flow field solutions for the shuttle orbiter. The side view, cross section and grid in the nose region are given in Fig. 8. The top views, cross-section, grid and chordwise cross-section are presented in Fig. 9. It should be mentioned here that for most of the previous space

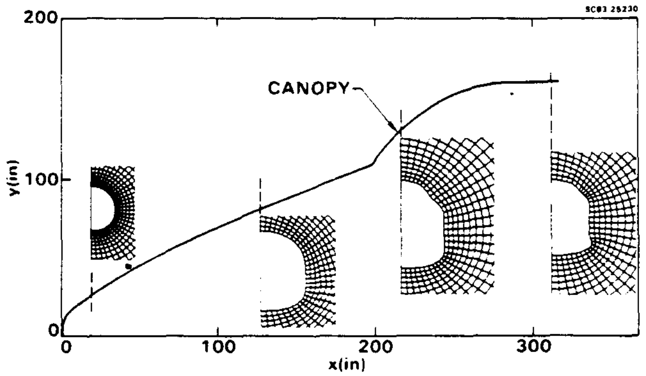

Fig. 8 Nose region geometry for Space Shuttle.

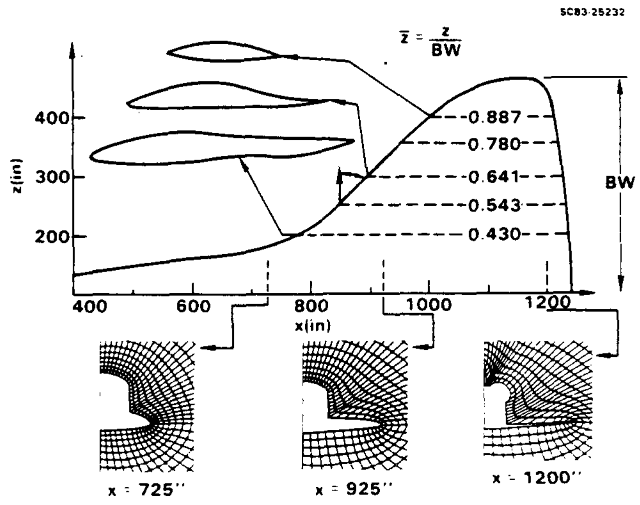

Fig. 9 Geometry and grid generation for Shuttle orbiter at axial cuts.

shuttle calculations[9,10] the geometry has been modified by smoothing out the canopy and increasing the wing sweep angle from 45 to 55 degrees in order to avoid the subsonic bubble. Since the present method is valid for supersonic flow with embedded subsonic region, the realistic shuttle orbiter geometry was used without any modification.

Figure 10 shows the surface pressure distribution along the leeward plane of symmetry. At $x \cong 170$ in. which is the beginning of the canopy, the pressure increases rapidly from $C_p \cong 0.3$ to 1.0, approximately. In the canopy region an MSR/TSR is formed and required three relaxation cycles to develop the solution. The circumferential surface pressure distribution at $x = 240$ in. is shown in Fig. 11. The experimental data is also given in these figures and the agreement is very good. The surface pressure distribution along the wing leading edge is given in Fig. 12. It is seen that the present calculation agrees with the experiment data quite well along the entire wing leading edge except in the vicinity of the wing-fuselage junction, where a vortex flow may exist.

Figure 13 to Figure 17 present the orbiter chordwise pressure distribution on the upper and lower wing surface at $\bar{z} = z/bw = 0.471$, 0.530, 0.641, 0.780 and 0.887, respectively where bw is a semispan defined in Fig. 8. The results show that

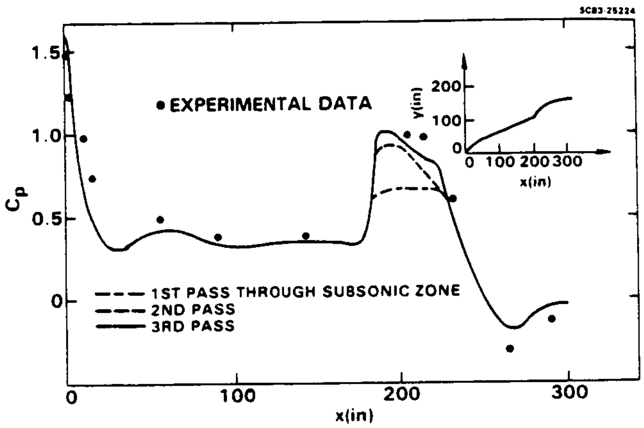

Fig. 10 Surface pressure distribution at leeward plane of symmetry.

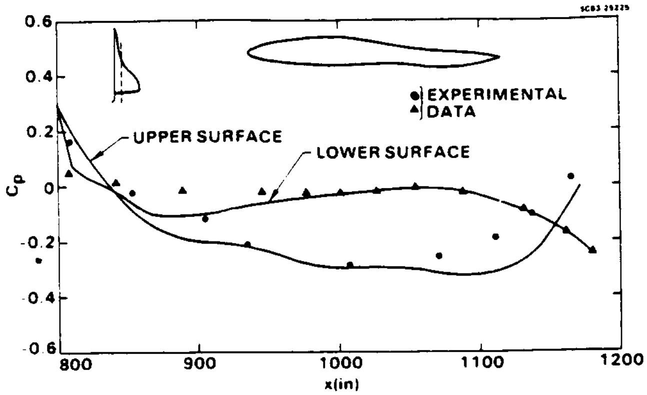

Fig. 13 Shuttle orbiter chordwise pressure distribution; $M_\infty = 1.4$, $\alpha = 0.0°$, $\bar{z} = 0.471$.

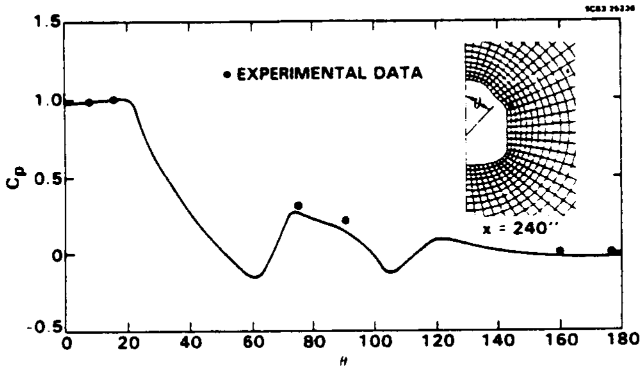

Fig. 11 Surface pressure distribution around the body.

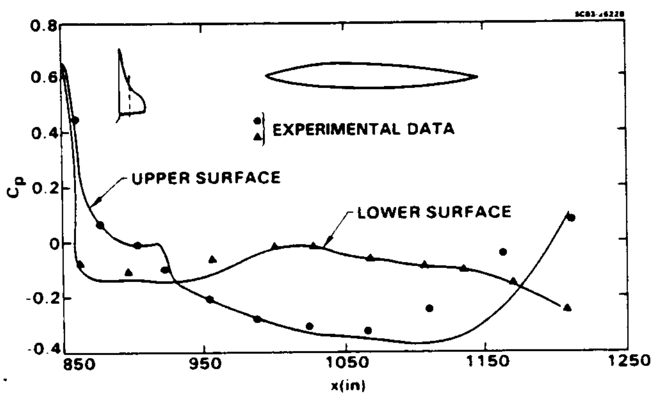

Fig. 14 Shuttle orbiter chordwise pressure distribution; $M_\infty = 1.4$, $\alpha = 0.0°$, $\bar{z} = 0.53$.

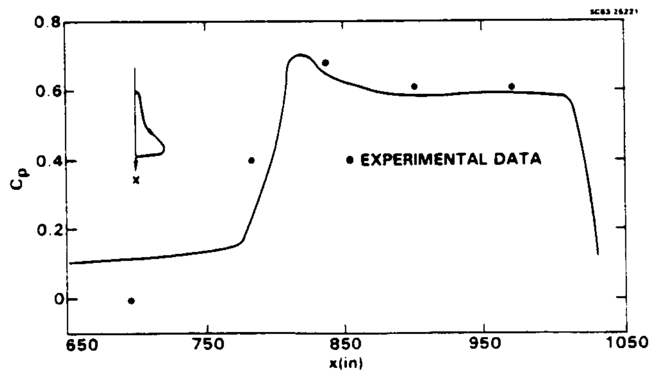

Fig. 12 Surface pressure distribution along the wing leading edge.

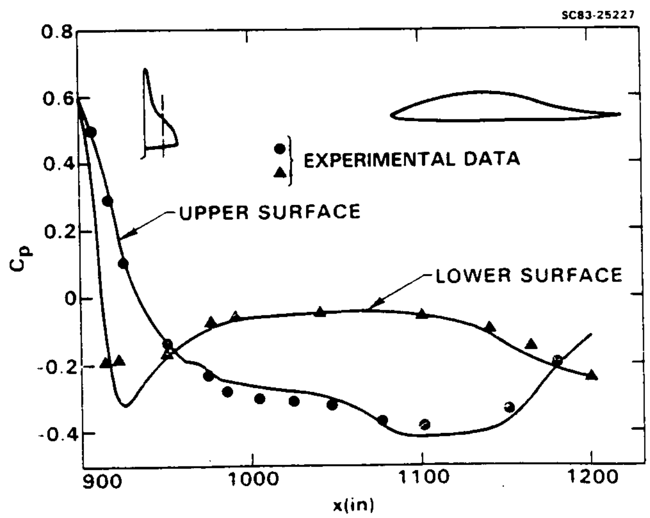

Fig. 15 Shuttle orbiter chordwise pressure distribution; $M_\infty = 1.4$, $\alpha = 0.0°$, $\bar{z} = 0.641$.

the present predictions are in very good agreement with the experimental data, except in the region near the trailing edge of the upper surface at $\bar{z} = 0.471$ and 0.53 span stations. Here again, a vortex flow or separation may be causing the discrepancies. Figure 18 shows the circumferential pressure distribution for the orbiter at x = 1120 in. It is noted that the pressure at the vertical tail and OMS pods are well predicted.

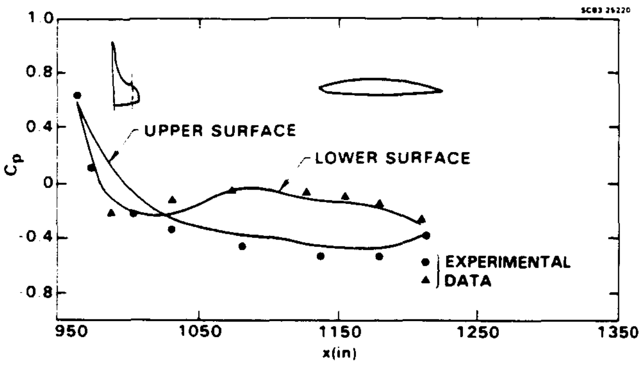

Fig. 16 Shuttle orbiter chordwise pressure distribution; $M_\infty = 1.4$, $\alpha = 0.0°$, $z = 0.78$.

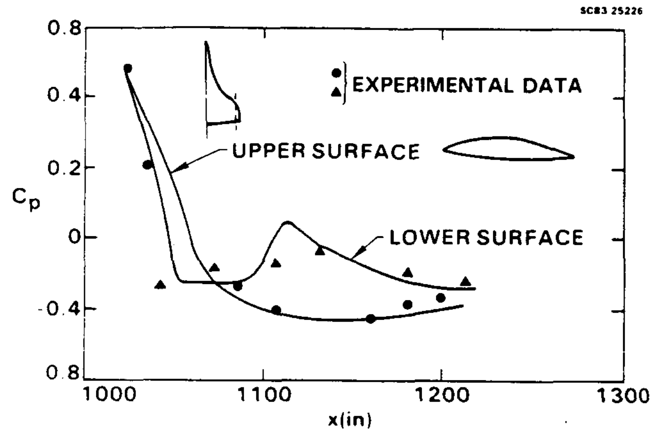

Fig. 17 Shuttle orbiter chordwise pressure distribution; $M_\infty = 1.4$, $\alpha = 0.0°$, $z = 0.887$.

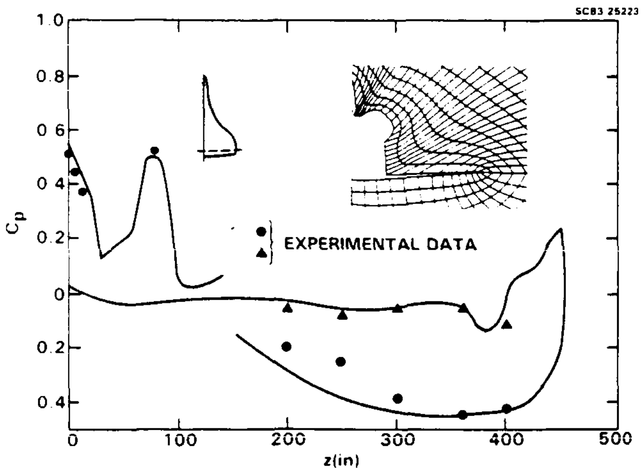

Fig. 18 Circumferential pressure distribution for the orbiter at $x = 1120$ in; $M_\infty = 1.4$, $\alpha = 0.0°$.

Figure 19 shows a supersonic fighter configuration with vertical tails. The free stream mach number, angle of attack and wing sweep angle for the calculation are summarized in Table 1.

Figure 20 presents the surface pressure at various axial stations and the corresponding grid distribution for the wing body geometry. For this case, the MSR/TSR starts around $x = 0.4$ at the leading edge, and remains subsonic all the way to the end of the wing. Figure 21 and 22 show the circumferential pressure distribution in the vertical tail and wake region of the fighter-like configuration. The pressure on the vertical tail surface is given separately along y-direction. The results clearly show that the present wake tretment provides the correct zero pressure jump condition across the wake. The chordwise pressure distributions from the center of the body to the top of the wing are given in Fig. 23. Figure 24 presents the pressure contour on the upper and lower surface of the fighter configuration.

The lift and drag coefficients from the present calculations for this fighter model are also given in Table 1. The comparison with experimental data show excellent agreement.

VII. Conclusions

A nonlinear full potential method has been applied to investigate the supersonic flows with embedded sobsonic regions over some very complex configurations. A conservative switching scheme is employed to transition from the supersonic marching algorithm to a subsonic relaxation procedure. The present predictions are in very good agreement with experiment data.

Work is now progressing to simulate the multibody interaction between the shuttle orbiter and the external tank. The present methodology will also be extended to treat all mach number flows (fully subsonic flow as well as subsonic flow with pockets of supersonic region (transonic case)).

Acknowledgment

This work was partially supported by NASA-Langley Research Center under Contract NAS1-15820.

References

1. Woodward, F.A., Tinoco, E.N., and Larsen, J.W., "Analysis and Design of Supersonic Wing-Body Combinations, Including Flow Properties in the Near Field. Part I - Theory and Application," NASA CR 73106, 1967.

2. Kutler, P., "Computation of Three-Dimensional Inviscid Supersonic Flows," in Lecture Notes in Physics 41, Springer-Verlag, New York, 1975.

3. Marconi, F., Salas, M., and Yeager, L., "Development of a Computer Code for Calculating the Steady Super/Hypersonic Inviscid Flow Around Real Configurations, Vol. I - Computational Techniques," NASA CR 2675, April 1976.

4. Shankar, V., Szema, K.Y., and Osher S., "A Conservative Type-Dependent Full Potential Method for the Treatment of Supersonic Flow with Imbedded Supersonic Region," AIAA Paper No. 83-1887, July 1983.

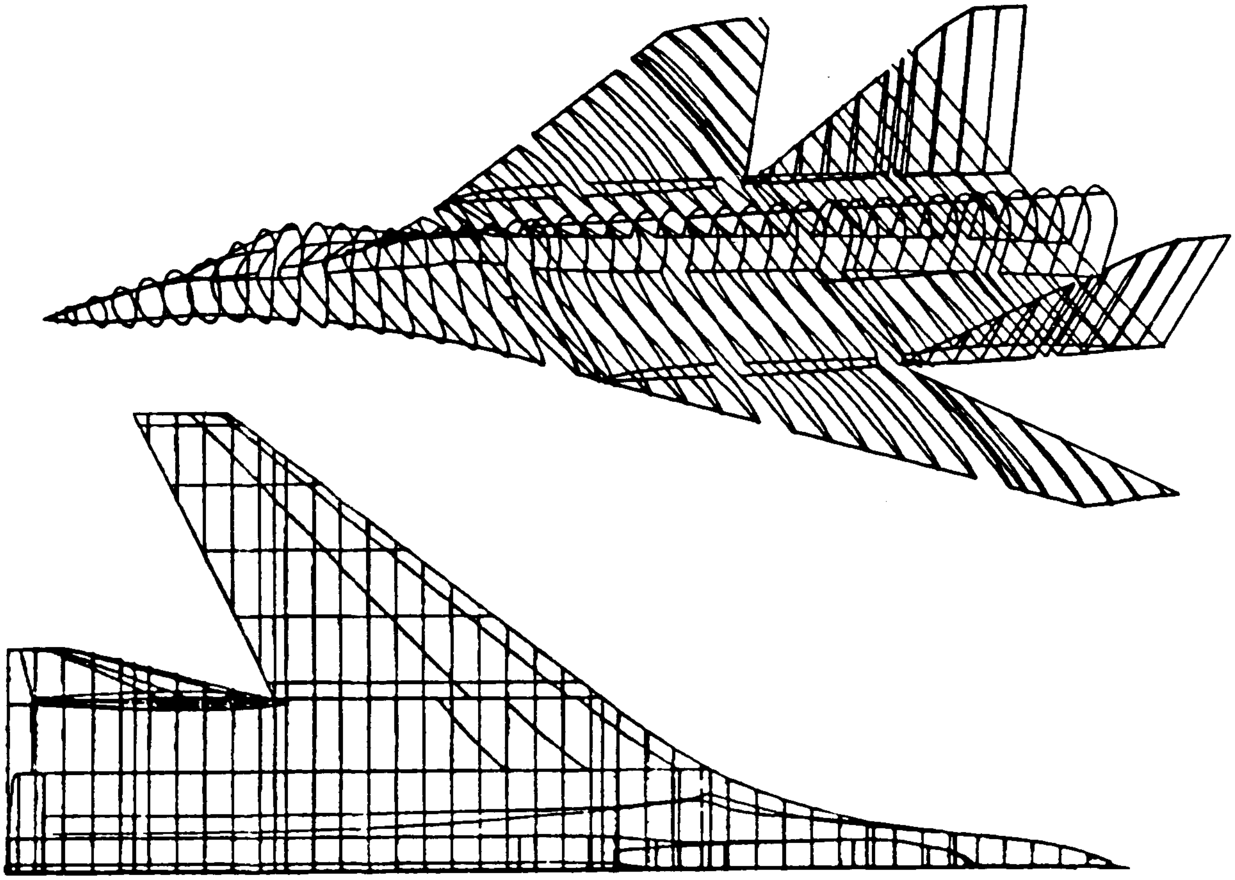

Fig. 19 Fighter-like configuration.

Table 1 Test cases for fighter-like configurations.

α		5°	5°	5°	5°
M_∞		1.6*	1.6†	1.4†	1.6†
Λ		48°	48°	48°	55°
C_L	CODE	0.298	0.3016	0.3561	0.29186
	DATA	0.277	0.295	0.342	0.3
C_D	CODE	0.0462	0.04916	0.04117	0.028129
	DATA	0.0457	0.0493	0.0425	0.0301

Λ = Wing sweep angle
*Without vertical tail
†With vertical tail

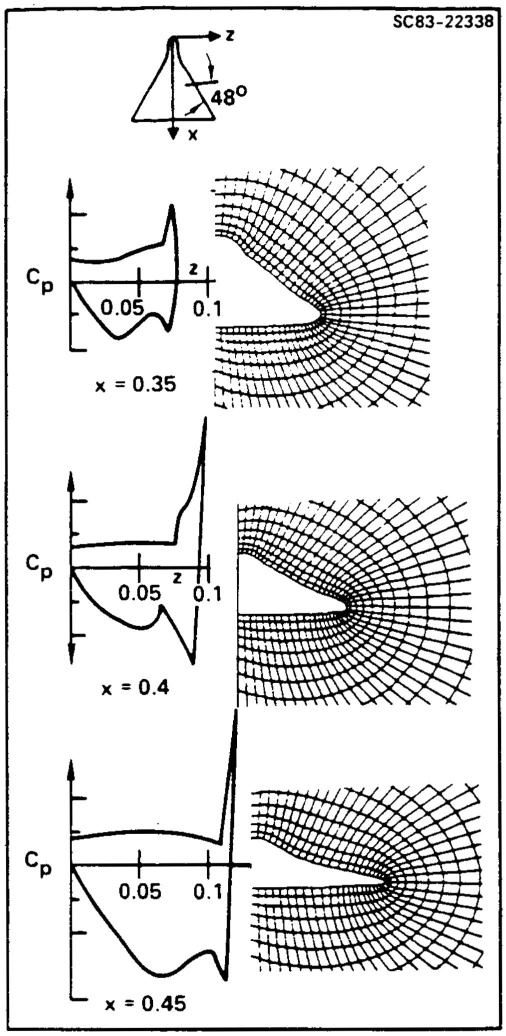

Fig. 20 Pressure distribution on a fighter-like configuration, M_∞ = 1.6, α = 5°.

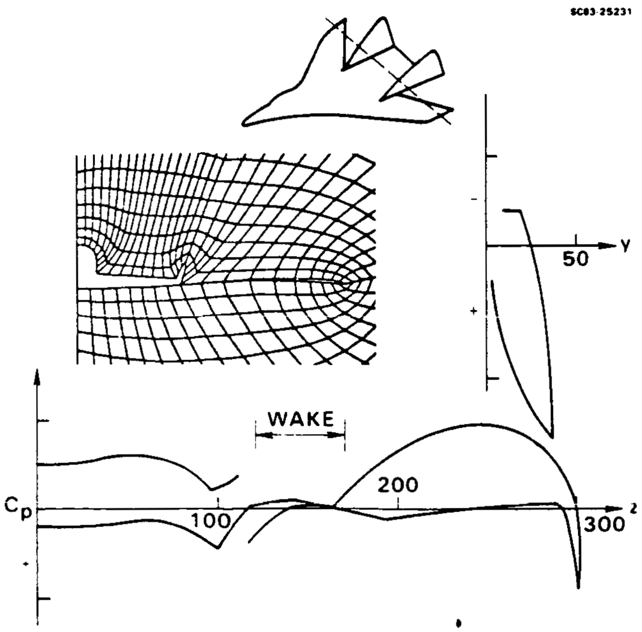

Fig. 21 Circumferential pressure distribution in the vertical tail and wing region of a fighter-like configuration, M_∞ 1.6, α = 4.46, x/ℓ = 0.82.

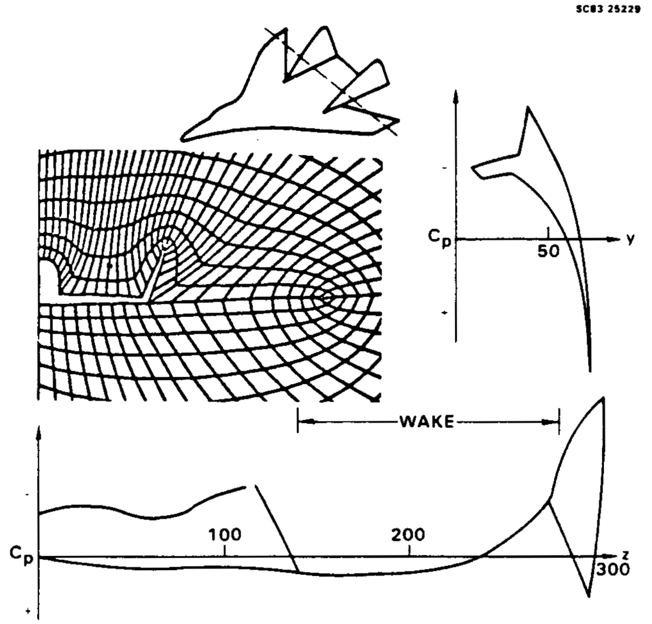

Fig. 22 Circumferential pressure distribution in the vertical tail and wing region of a fighter-like configuration, M_∞ 1.6, α = 4.46, x/ℓ = 0.90.

5. Shankar, V., and Osher, S., "An Efficient Full Potential Implicit Method Based on Characteristics for Analysis of Supersonic Flows," AIAA Paper No. 82-0974, June 1982.

6. Shankar, V., "Implicit Treatment of the Unsteady Full Potential Equation in Conservation Form," AIAA Paper No. 84-0262, January 1984.

7. Townsend, J.C., "Pressure Data for Four Analytically Defined Arrow Wings in Supersonic Flow," NASA TM 81835, September 1980.

8. Townsend, J.C., Howell, D.T., Collins, I.K., and Hayes, C., "Surface Pressure Data on a Series of Analytic Forebodies at Mach Numbers from 1.7 to 4.50 and Combined Angles of Attack and Sideslip," NASA TM 80062, June 1979.

9. Maus, J.R., Griffith, B.J., Szema, K.Y., and Best, J.T., "Hypersonic Mach Number and Real Gas Effects on Space Shuttle Orbiter Aerodynamics," AIAA Paper No. 83-0343, January 1983.

10. Venkatapathy, E., Rakich, J.V., and Tannehill, J.C., "Numerical Solution of Space Shuttle Orbiter Flow Field," AIAA Paper No. 82-0028, January 1982.

11. Rockwell International Space Division Data.

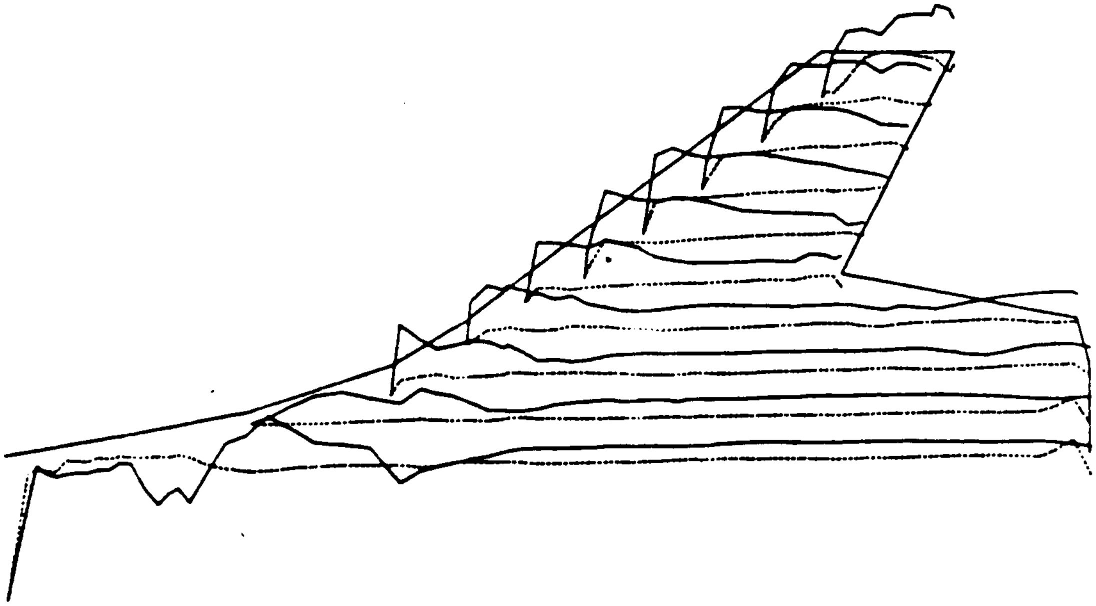

Fig. 23 Chordwise pressure distribution for a fighter-like configuration. M_∞ 1.6, α = 4.46.

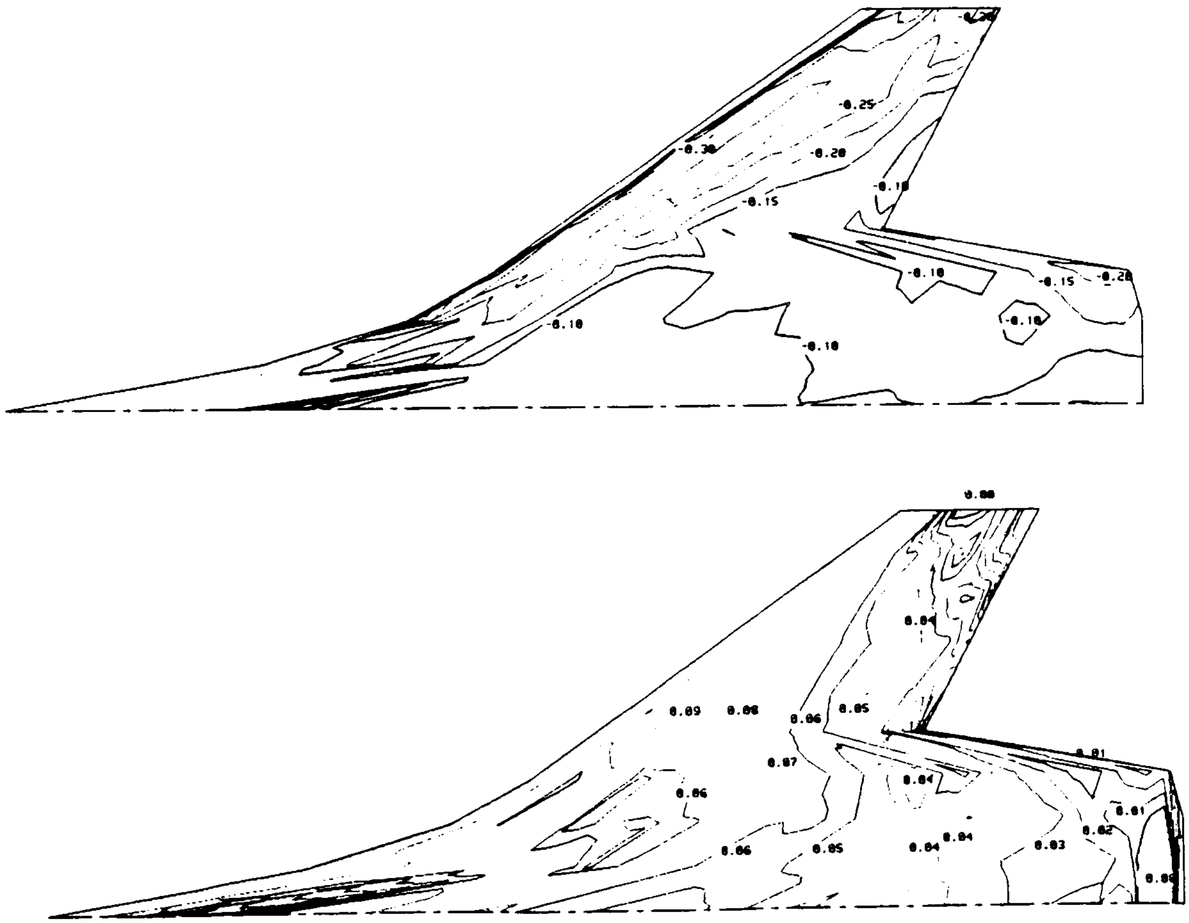

Fig. 24 Pressure contour on the upper and lower surface of the fighter-like configuration. M_∞ = 1.6, α = 4.46°.

CONSERVATIVE FULL POTENTIAL, IMPLICIT MARCHING SCHEME FOR SUPERSONIC FLOWS

VIJAYA SHANKAR and KUO-YEN SZEMA

Rockwell International Science Center
Thousand Oaks, California 91360

I. THEORY

ABSTRACT

A numerical method based on the conservation form of the full potential equation has been applied to three-dimensional supersonic flows with embedded subsonic regions. The governing equation is cast in a nonorthogonal coordinate system, and the theory of characteristics is used to accurately monitor the type-dependent flow field. A conservative switching scheme is employed to transition from the supersonic marching procedure to a subsonic relaxation algorithm and vice versa. The newly developed computer program can handle arbitrary geometries with fuselage, wing, vertical tail and wake components at combined angles of attack and sideslip. Example results in this report include the Shuttle Orbiter flow at a low supersonic Mach number, flow over a realistic fighter-type configuration, wake simulations for an arrow wing, and a forebody in sideslip. Comparisons with experimental data are shown to be in good agreement for various cases.

INTRODUCTION

Nonlinear aerodynamic prediction methods based on the full potential equation are used regularly for treating transonic[1,2] and supersonic[3-5] flows over realistic wing-body configurations. The transonic algorithms[1,2] are designed to treat predominantly subsonic flows with pockets of supersonic regions bounded by sonic lines and shocks. The supersonic methods[3-5] are based on a marching concept, and require the flow to remain supersonic in a given marching direction. Once the marching direction velocity becomes subsonic, the domain of dependence changes and a pure marching scheme[3-5] will violate the rules of characteristics signal propagation. The possibility of a marching velocity becoming subsonic in a supersonic flow is great, especially for low supersonic freestream Mach number flows ($M_\infty = 1.3 \sim 1.7$) over moderately swept fighter-like configurations (sweep angle Λ 45 ~ 50°) and over forebody shapes having a sizeable fuselage-canopy junction region. The methodology of

Refs. 6 and 7 is an extension to the marching scheme of Ref. 5 and is designed to treat embedded subsonic regions in a supersonic flow. In order to properly produce the necessary artificial viscosity through density biasing, Ref. 6 defines two situations: 1) the total velocity, q, is supersonic, but the marching direction component is subsonic (defined as Marching Subsonic Region (MRS)), and 2) the total velocity, q, is subaonic (termed as Total Subsonic Region (TSR).

The method of Refs. 4-7 is based on the characteristic theory of signal propagation and uses a generalized, nonorthogonal, curvilinear coordinate system. It has no restrictions (limitations of the full potential theory hold) on its applicability to complex geometries and intricate shocked flow fields. It is a conservative formulation and uses numerical mapping techniques to generate the body-fitted system.

This report presents a brief description of the overall methodology[4-7] along with some user information on code organization, input and output data, and sample results. A typical calculation over a complete configuration (wing-body-vertical tail-wake) requires fifteen minutes of CPU time on the Cyber 176 machine or three minutes on the Cray-1.

BASIC FORMULATION

The steady, conservative full potential equation cast in an arbitrary coordinate system defined by $\zeta = \zeta(x,y,z)$, $\eta = \eta(x,y,z)$ and $\xi = \xi(x,y,z)$ can be written as

$$\left(\rho \frac{U}{J}\right)_\zeta + \left(\rho \frac{V}{J}\right)_\eta + \left(\rho \frac{W}{J}\right)_\xi = 0 \tag{1}$$

where the density ρ is given by

$$\rho = \left[1 - \left(\frac{\gamma-1}{2}\right) M_\infty^2 \{U\phi_\zeta + V\phi_\eta + W\phi_\xi - 1\}\right]^{1/(\gamma-1)} \tag{2}$$

and M_∞ is the free stream Mach number, a is the local speed of sound and U,V,W are the contravariant velocity components. Introducing the following notation for convenience

$$
\begin{array}{lll}
U_1 = U & U_2 = V & U_3 = W \\
x = x_1 & y = x_2 & z = x_3 \quad . \\
\zeta = X_1 & \eta = X_2 & \xi = X_3 \quad ,
\end{array}
$$

the contravariant velocity can be expressed as

$$U_i = \sum_{j=1}^{3} a_{ij} \phi_{X_j} \qquad i = 1,2,3$$

$$a_{ij} = \sum_{k=1}^{3} \frac{\partial X_i}{\partial x_k} \frac{\partial X_j}{\partial x_k} \qquad \begin{array}{l} i = 1,2,3 \text{ (transforma-} \\ j = 1,2,3 \text{ tion metrics)} \end{array} \tag{3}$$

The Jacobian of the transformation J is represented by

$$J = \frac{\partial(\zeta,\eta,\xi)}{\partial(x,y,z)} = \begin{vmatrix} \zeta_x & \zeta_y & \zeta_z \\ \eta_x & \eta_y & \eta_z \\ \xi_z & \xi_y & \xi_z \end{vmatrix} \tag{4}$$

The nature of Eq. (1) can be analyzed by studying the eigenvalue system of Eq. (1) combined with the irrotationality condition in the (ζ,η) and (ζ,ξ) planes. A detailed discussion on this can be found in Reference 6. Therefore, only the final results are presented here.

1. At a grid point, the marching direction ζ is hyperbolic and the total velocity q is supersonic, $\left(a_{11} - \frac{U^2}{a^2}\right) < 0$, $q > a$. This point will use the algorithm of Reference 5.

2. At a grid point, the marching direction ζ is elliptic, $\left(a_{11} - \frac{U^2}{a^2}\right) > 0$, but the total velocity q is supersonic, $q > a$. This point will be treated by a transonic operator with a built-in density biasing based on the magnitude of $\left(1 - \frac{a^2}{q^2}\right)$.

3. At a grid point, the direction ζ is elliptic and the total velocity q is subsonic, $q < a$. This point will be treated by a subsonic central differenced operator.

METHOD OF SOLUTION

Figure 1 shows the schematic of a fuselage-canopy forebody geometry with an embedded MSR and TSR present in a supersonic flow. To solve this problem, the marching scheme of Reference 5 is used when $\left(a_{11} - \frac{U^2}{a^2}\right)$ is negative, and a relaxation scheme is used when $\left(a_{11} - \frac{U^2}{a^2}\right)$ is positive. First, march from the nose up to the plane denoted by (A-B) in Fig. 1, using the method of Reference 5. Then, between (A-B) and (C-D), which embed the subsonic bubble (MSR and TSR), use a relaxation scheme and iterate until the subsonic bubble is fully captured. Then, resume the marching scheme from the plane (C-D), downstream of the body.

Treatment of $\partial/\partial\zeta\ (\rho\ U/J)$ Term

At a grid point $(i + 1, j,k)$, the derivative in the marching direction ζ is given by

$$\frac{\partial}{\partial\zeta}\left(\rho \frac{U}{J}\right) = \theta_i \underbrace{\frac{\overleftarrow{\partial}}{\partial\zeta}\left(\rho \frac{U}{J}\right)_{i+1}}_{\text{supersonic}} + (1 - \theta_{i+1}) \underbrace{\frac{\overrightarrow{\partial}}{\partial\zeta}\left(\tilde{\rho} \frac{U}{J}\right)_{i+1}}_{\substack{\text{marching} \\ \text{subsonic}}} \qquad (5)$$

where

$\overleftarrow{\partial}$ refers to backward differencing

$\vec{\partial}$ refers to forward differencing

$$\theta_i = 1 \text{ if } \left(a_{11} - \frac{U^2}{a^2}\right) < 0$$

$$= 0 \text{ if } \left(a_{11} - \frac{U^2}{a^2}\right) > 0 \quad .$$

The first term in Eq. (5) corresponds to the supersonic marching operator and the second term is the subsonic operator. By using a local linearization procedure, Eq. (5) can be expressed in terms of ϕ only. Details of the procedure are given in Refs. 4 and 5.

Treatment of $\partial/\partial\eta$ $(\rho\ V/J)$ Term

$$\frac{\partial}{\partial\eta}\left(\rho \frac{V}{J}\right) = \underbrace{\theta_{i+1} \frac{\overleftarrow{\partial}}{\partial\eta}\left(\bar{\rho} \frac{V}{J}\right)_{j+1/2}}_{\text{supersonic}}$$

$$+ \underbrace{(1 - \theta_{i+1}) \frac{\overleftarrow{\partial}}{\partial\eta}\left(\bar{\bar{\rho}} \frac{V}{J}\right)_{j+1/2}}_{\substack{\text{marching}\\ \text{subsonic}}} \tag{6}$$

When $\theta_{i+1} = 1$, that is, the point is supersonic with respect to ξ, only the first term in Eq. (6) is used and the biased density $\bar{\rho}$ is defined by (for $V > 0$)

$$\bar{\rho}_{j+1/2} = (1 - \bar{\nu}_{j+1/2})\rho^*_{j+1/2} + \frac{1}{2}\bar{\nu}_{j+1/2}(\rho^*_j + \rho^*_{j-1}) \tag{7}$$

where $\bar{\nu} = \max\left(0, 1 - a_{22}\dfrac{a^2}{V^2}\right)$.

In Eq. (7), the evaluation of ρ^* depends on whether the flow is conical or nonconical. For conical flows, all ρ^* quantities are evaluated at the i^{th} plane. For nonconical flows, at each nonconical marching plane, initially ρ^* is set to be the value at the i^{th} plane and then subsequently iterated to convergence by setting ρ^* to the previous iterated value of ρ at the current $i+1$ plane.

When the point is elliptic in the marching direction, the density biasing is defined by

$$\bar{\bar{\rho}}^{n+1}_{j+1/2} = (1 - \bar{\bar{\nu}}_{j+1/2})\rho^{n}_{j+1/2} + \frac{1}{2}\bar{\bar{\nu}}_{j+1/2}(\rho^{n}_{j} + \rho^{n}_{j-1}) \tag{8}$$

where $\bar{\bar{\nu}} = \max(0, 1 - \frac{a^2}{q^2})$. As before, the superscript n+1 denotes the current relaxation cycle for a subsonic bubble calculation. Note the difference in the definition of $\bar{\nu}$ and $\bar{\bar{\nu}}$. The density biasing in the cross-flow direction η is turned off when the total velocity, q, is less than the speed of sound a. The implicit treatment of V in the marching subsonic operator of Eq. (6) is the same as that of the supersonic part, explained in Reference 5.

A similar procedure is implemented for $(\rho \frac{W}{J})_\xi$ term in Eq. (1).

Implicit Factorization Algorithm

Combining the various terms of Eq. (1) as represented by Eqs. (5)-(8) together with the terms arising from $(\rho \frac{W}{J})_\xi$ will result in a fully implicit model. This is solved using an approximate factorization implicit scheme. After some rearrangement of the terms, the factored implicit scheme becomes

$$\begin{aligned}&[1 + \frac{A_3}{\beta\Delta\zeta}\frac{\partial}{\partial\xi} + \frac{1}{\beta}\frac{\partial}{\partial\xi}(\frac{\hat{\rho}}{J}\frac{a_{31}}{\Delta\zeta}) + \frac{1}{\beta}\frac{\partial}{\partial\xi}\frac{\hat{\rho}a_{33}}{J}\frac{\partial}{\partial\xi}]\\ &\quad\times [1 + \frac{A_2}{\beta\Delta\zeta}\frac{\partial}{\partial\eta} + \frac{1}{\beta}\frac{\partial}{\partial\eta}(\frac{\hat{\rho}a_{21}}{J\Delta\zeta})\\ &\quad + \frac{1}{\beta}\frac{\partial}{\partial\eta}\frac{\hat{\rho}a_{22}}{J}\frac{\partial}{\partial\eta}]\,\Delta\phi = R \quad .\end{aligned} \tag{9}$$

The density $\hat{\rho}$ appearing in Eq. (9) can be either $\bar{\rho}$ or $\bar{\bar{\rho}}$ depending on the sign of $(a_{11} - \frac{U^2}{a^2})$ as illustrated in Eq. (6).

Equation (9) has the form $L_\xi L_\eta(\Delta\phi) = R$ and it is implemented as follows:

$$L_\xi(\Delta\phi)^* = R,\ L_\eta(\Delta\phi) = (\Delta\phi)^*,\ \phi_{i+1} = \phi_i + \Delta\phi \quad .$$

INITIAL CONDITIONS

For a pure supersonic flow, initial conditions are required at the starting plane. Usually, the starting plane is set close to the nose region of the configuration. For a sharp nosed configuration, conical solutions are prescribed, and for a blunt nose, the axisymmetric unsteady full potential solver of Reference 8 is used to obtain flow field in the transonic forebody region.

In the embedded subsonic region, when Eq. (5) is applied at an i+1 grid point, information on the flux ρU at i+2 is required. For the first relaxation pass, sonic conditions are assumed at i+2.

$$\rho_{i+2} = \rho^* = \left(\frac{2}{\gamma+1} + \frac{\gamma-1}{\gamma+1} M_\infty^2\right)^{1/\gamma-1}$$

$$U_{i+2} = q^* \, (a_{11})_{i+2}^{1/2} \tag{10}$$

where

$$q^* = [\rho^{*\gamma-1}/M_\infty^2]^{1/2}$$

The sonic values ρ^* and q^* are purely a function of the free-stream Mach number M_∞. For the second relaxation cycle and onwards, the conditions from the previous relaxation cycle is used.

BOUNDARY CONDITIONS

In order to solve the full potential equation, it is essential to specify appropriate boundary conditions on the body surface and at the outer boundary.

1. Body Surface

At a solid boundary, the contravariant velocity V is set to zero. Exact implementation of V = 0 in the implicit treatment of Eq. (9) is described in Reference 4.

2. Outer Boundary

The outer boundary is set away from the bow shock and the free-stream velocity potential ϕ_∞ is imposed along that boundary. All discontinuities in the flow field are captured. The precise density biasing activator, ν, based on the characteristic theory, allows for sharp capturing of shocks in the flow.

3. Symmetric Boundary Conditions

For yaw angle $\beta = 0$, only the half plane problem needs to be solved with the plane of symmetry boundary conditions imposed along K = 2 and (KMAX - 1), as shown in Fig. 2a. Imposing that the flow conditions along K = 1 are to be the same as the ones along K = 3, the L_ξ operator results in a tridiagonal system that can be easily solved.

4. Combined Yaw and Angle of Attack

Even for a symmetric configuration, when yaw angle is present the entire cross-flow plane needs to be solved as shown in Fig. 2b. In this case the flow conditions along K = 1 are set to be the same as the ones along K = (KMAX - 2). This destroys the tridiagonal nature of the L_ξ operator. A special routine has been developed to invert a matrix of the following type.

$$L_\xi = \begin{vmatrix} X & X & & & X & 0 \\ X & X & X & & 0 & 0 \\ & X & X & X & & 0 \\ & & & & & \\ 0 & 0 & & X & X & X \\ 0 & X & & & X & X \end{vmatrix} \qquad (11)$$

In the current formulation, positive angle of attack α represents a positive Cartesian velocity v in the free-stream and similarly positive yaw β produces a positive w in the free-stream. When both angle of attack and yaw are present, first the free-stream is turned by an angle β and then by α.

The normalized free stream velocity potential is given by

$$\phi_\infty = x \cos\alpha \cos\beta + y \sin\alpha + z \cos\alpha \sin\beta \tag{12}$$

The lift and drag forces are represented by

$$D = F_x \cos\alpha \cos\beta + F_y \sin\alpha + F_z \cos\alpha \sin\beta$$

$$L = -F_x \sin\alpha \cos\beta + F_y \cos\alpha \tag{13}$$

5. Swept Trailing Edge Wake Treatment

Figure 3 shows a schematic of a swept trailing edge wake system. In order to treat the region behind the trailing edge, an artificial cut is created and the pressure jump [p] across this cut is imposed to be zero as a boundary condition. This is achieved by maintaining the jump in the velocity potential ϕ along a k = constant line (see Fig. 3) for j = 2 to be the same as the value $[\phi]$ at the trailing edge. The full potential equation is not solved at grid points on the wake cut. Instead, $\phi_{\eta\eta} = 0$ is solved to provide $[\phi_\eta] = 0$ across the wake cut. Maintaining $[\phi]$ constant along a k line provides $[\phi_\zeta] = 0$. The combination of $[\phi_\zeta] = 0$ and $[\phi_\eta] = 0$ across the cut satisfies [p] = 0 approximately.

6. Geometry and Grid System

The geometry of a configuration is prescribed at discrete points in a crossplane (usually x = constant plane) at various axial locations. These geometry input points are usually obtained from a geometry package such as the GEMPACK or CDS. The input points are then divided into several patches, and at each patch a key-point system is established as shown in Fig. 4. The geometry at a marching plane is then obtained by joining the appropriate key-point for each patch, as shown in Fig. 5. Using a cubic spline passing through the key points, a desired grid point distribution (clustering) is set up on the body surface. Then, using an appropriate outer boundary, the grid for the flow-field calculation is generated by using an elliptic grid generator.[9]

II. CODE ORGANIZATION

The program is written in FORTRAN language. It can be executed on any CDC machine (Cyber 176, CDC 7600), as well as on the Cray 1. At present, the code is not optimized for a vector machine like the Cray or Cyber 205. for a cross-plane (η,ξ) grid of 30 x 60, the program requires a storage of 230,000 words octal. The program consists of a main routine and several subroutines. A brief description of the main program and other pertinent subroutines are given in this section.

Program Main

Program Main coordinates the entire operation. A flowchart describing the various operations performed by the Main program is given in Fig. 6. The Main program sets up the initial (known) data plane and the body-fitted grid system, and performs the L_ξ and L_η operators to advance the solution. The marching step size $\Delta\zeta$ can either be prescribed or computed at each marching plane from a given Courant number and the maximum eigenvalue. The various read and write tapes used in the calculation are listed below.

Program Main (Tape 1, Tape 2, Tape 3, Tape 4, Tape 5, Tape 7,
Tape 8, Output, Tape 6 = Output)

Tape 1: Output solutions for plot.
Tape 2: Output solutions for restart.
Tape 4: Output solutions for restart.
Tape 3: Read in starting solutions.
Tape 5: Input data.

Tape 6: Solution output.

Tape 7: Read tape containing solutions for subsonic region.

Tape 8: Write tape for subsonic bubble calculation.

Subroutine EIGEN (EIGENY, EIGENZ)

This subroutine computes the maximum eigenvalue EIEGNY in the (ζ,η) plane and the maximum eigen value EIGENZ in the (ζ,ξ) plane. The expression used for calculating the eigenvalue is given in Ref. 5. The maximum eigenvalue information is then used to compute a marching step-size $\Delta\zeta$ for a specified Courant number.

Subroutine NFORCE (PX, PY, PM, AREA, KG)

At the end of each marching plane calculation, this subroutine computes the axial force, PX, vertical force, PY, and the side force, PM, by integrating the pressure force acting on an elemental area, dA. The elemental area, dA, is computed from the transformation matrice using the formula (at a body point j = 2)

$$dA = \{[y_\zeta z_\xi - z_\zeta y_\xi]^2 + [x_\xi z_\zeta - x_\zeta z_\xi]^2 + [y_\xi x_\zeta - y_\zeta x_\xi]^2\}^{1/2}\, d\zeta d\xi \ .$$

KG = 0, conical or blunt body nose force calculation
   = 1, rest of the body force calculation.

The program also prints the C_L and C_D information based on a prescribed reference area, and C_M about a given reference point (X_o, Y_o).

Subroutine GEOM (N9, NRP)

N9 = 0, geometry data at X_1 are read in
   = 1, geometry data at X_1 are updated

NRP = 0, X-plane geometry calculation
    = 1, spherical plane geometry calculation.

Subroutine GEOM sets up the body grid points from a prescribed geometry shape. As illustrated in Fig. 4, the geometry is input in different patches (the number of patches to be used is left to the discretion of the user). From the input geometry points, a key point system is established using cubic splines. These key points are then joined from one prescribed geometry station to the other to provide the geometry at any intermediate marching plane. A flowchart describing GEOM is given in Fig. 7.

Subroutine Grid

Once the body points are obtained at a marching plane from GEOM, subroutine GRID sets up the entire crossflow plane grid using an elliptic grid solver that satisfies certain grid constraints. Figure 8 gives the flowchart for GRID.

Subroutine Metric

This subroutine computes all the necessary transformation metrics and Jacobians at various node and half node locations as required by the solution algorithm (L_ξ and L_η operators).

Subroutine UVW

This subroutine computes all the contravariant velocities U, V and W, and the density ρ.

Subroutine RHOBIAS

This subroutine performs the density biasing in the (η,ξ) plane based on a characteristic theory. This operation is essential to treat crossflow supersonic regions and to capture shock waves.

III. INPUT DATA

Input data includes specifications of flow parameters, grid parameters, read and write tape parameters, and geometry data in patches at various axial stations. A sample inut is presented here.

Input cards 1 through 45 are self-explained. The rest of the input cards are explained below.

	Format	Symbol	Description
Card 46			
Col. 1-80	10F8.4	ZTAPT(10)	Location of detail flow field printout
Card 47			
Col. 1-5	I5	ISC	Number of patch (geometry)
Card 48			
Col. 1-50	10I5	NPT (10)	Number of output points in each patch
Card 49			
Col. 1-15	F15.6	X1	x location at which the geometry cross-section is given.
Col. 16-20	I5	ISC1	Number of input patch at this location
Card 50			
Col. 1-5	I5	ITH	Patch number
Col. 6-10	I5	IPT	Number of input points
Col. 11-15	I5	ND	Clustering control parameter 0: equal space 1: clustering at the beginning of the patch 2: clustering at the end of patch
Card 51			
Col. 1-15	F15.6	y	y-value
Col. 16-30	F15.6	z	z-value

SAMPLE INPUT

```
100-  120       NMAX    I5      NO. OF STREAMWISE STEP.
110-   20       JMAX            NO. OF POINT IN NORMAL DIR.
120-   26       KMAX            NO. OF POINT IN CIRCUM. DIR.
130-   20       JMAXO           OLD JMAX FOR RESTARTING.
140-   26       KMAXO           OLD KMAX FOR RESTARTING.
150-   17       KTEMP           K AT MAX Z
160-    2       NRM             NO.DOFEGRIDNSECTION.
170-   10       NU0             K FOR FIRST SECTION GRID IF NRM>2
180-   05       NP              OUTPUT FOR EVERY NP STEPS.
190-    1       KWKCTR          1:WAKE IS CONTROL BY K; 2:BY Z
200-   18       KWKST           WAKE START PT.
210-   36       KWKED           WAKE END PT.
220-   30       NCON            INITIAL CONICAL DATA ITERATIONS,
230-   30       NITER           NO. OF ITERATION FOR GRID.
240-    2       NSPTI           NO. OF PTS FOR ENTIRE FLOW FIELD OUTPUT.
250-    2       ITERGN          NEW THT USED AFTER NO. OF GLOB ITERATION.
260-    1       ITERGE          NO. OF GLOB ITERATION.
270-  999       KLE             NOT USED
280-  1.4       FSM     F10.5   FREE STREAM MACH NO.
290- -1.94      ALFA            ANGLE OF ATTACK.
300-   70.      THTO            OUTER BOUNDARY. (DEGREE)
310-  0.1       DETA            STEP SIZE IN ETA DIR.
320-  0.1       DXI             STEP SIZE IN XI DIR.
330-  3.00      DZTA            STEP SIZE IN ZTA DIR. (STREAM)
340-  400.000   ZTA1            STARTING X LOCATION.
350- 1200.0     XEND            LAST X LOCATION.
360-   1.75     SWEEP           NOT USED.
370-   1.       AMU1            1:1ST ORDER,2:2ND ORDER ACCURATE.
380-   0.       AMU2            0:1ST ORDER,1:2ND ORDER ACCURATAXE.
390-  1500.0    XWAKE           WAKE START LOCATION.(X)
400-   0.188    ZWAKE           WAKE START LOCATION.(Z)
410-   001.     CHL             CHARACTERISTIC LENGTH
420-   -26.8    PTNOSE          NOSE LOCATION.(X)
430-   0.627    XM0             REF. X POINT FOR PITCH MOMENT.
440-   0.0      YM0             .....Y .....  ...............
450-   0.186    AAA             REF. AREA.
```

```
460-   0.291    ALL                REF. LENGTH FOR PITCH MOMENT.
470-   1.75     OMEGA              RELAXIATION FACTOR.
480-    T       PLANEOS            NOT USED.
490-    T       NUGRID    L3       NUMERICAL GRID GENERATION?
500-    T       IREAD              T:INPUT BODY GEOM;F:ANALYTIC GEOM.
510-    F       RPLANE             R-MARCHING
520-    T       TAPER              RESTART DATA FROM TAPE?
530-    T       TAPEW              WRITE RESTART DATA ON UNIT 2 & 4
540-    T       FORCE              DO FORCE CALCULATION
550-100.     200.0    300.0    400.0    500.0    600.0
560-    5       ISC                NO. OF PATCH. (GEOMETRY)
570-   04    05    05    06    08
580- 338.81               5
590-    1     4     0
600-  100.34                0.00  }
610-   95.99               30.83  }  PATCH I
620-   87.52               58.14  }
630-   74.35               74.08  }
640-    2     5     0
650-   74.35               74.08  }
660-   63.18               84.63  }
670-   52.29               95.44  }  PATCH II
680-   44.26              101.59  }
690-   36.22              105.18  }
700-    3     5     0
710-   36.22              105.18  }
720-   11.73              105.62  }
730-   -9.88              105.62  }  PATCH III
740-  -35.18              105.62  }
750-  -65.87              103.07  }
760-    4     3     2
770-  -65.87              103.07  }
780-  -78.54              109.55  }  PATCH IV
790-  -90.72              112.20  }
800-    5     7     1
810-  -90.72              112.20  }
820-  -99.15              110.39  }  PATCH V
```

INPUT CROSS-SECTION AT X=388.81

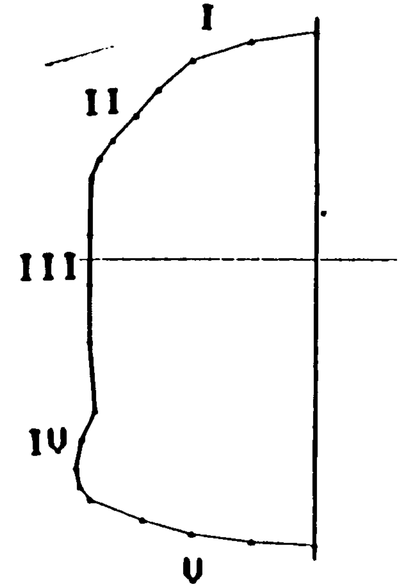

```
 830-  -104.90                    105.46
 840-  -113.79                     80.81
 850-  -119.75                     57.81
 860-  -123.31                     30.04
 870-  -124.64                      0.00
 880-  387.41                  5
 890-     1      3     0
 900-    99.47                      0.00
 910-    95.81                     29.21
 920-    89.47                     53.41
 930-     2      5     0
 940-    89.47                     53.41
 950-    79.11                     75.76
 960-    61.71                     98.21
 970-    52.94                    103.83
 980-    44.11                    105.70
 990-     3      4     0
1000-    44.11                    105.70
1010-    -8.94                    106.05
1020-   -36.99                    106.40
1030-   -63.82                    108.84
1040-     4      5     2
1050-   -63.82                    108.84
1060-   -76.69                    116.04
1070-   -87.81                    119.41
1080-   -96.76                    119.20
1090-  -106.24                    112.73
1100-     5      6     1
1110-  -106.24                    112.73
1120-  -109.89                    105.76
1130-  -112.21                     92.84
1140-  -121.50                     63.21
1150-  -125.54                     30.98
1160-  -126.72                      0.00
1170-  454.23                  5
1180-     1      3     0
1190-    99.47                      0.00
```

OUTPUT CROSS-SECTION AND GRID AT X=400

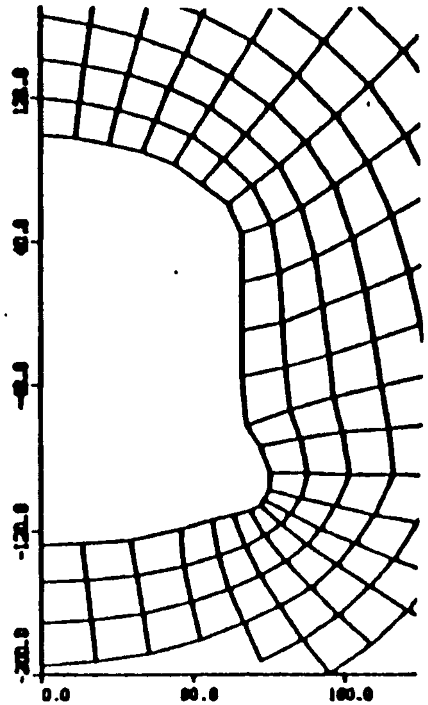

SAMPLE OUTPUT

ITER= 1 DZTA= 3.00000 ZTA1= 410.41814

J	K	RHO	CP	PHI	U	V	W	X	Y	Z
2	1	1.082483	.085533	368.148453	0.000000	0.000000	0.000000	410.418140	157.548064	-11.436041
2	2	1.091121	.094845	368.052851	.953648	0.000000	0.000000	410.418140	168.981000	0.000000
2	3	1.082483	.085533	368.148463	.957929	0.000000	.000123	410.418140	157.548064	11.436041
2	4	1.065946	.068168	368.380630	.966106	0.000000	.000219	410.418140	156.111538	22.871964
2	5	1.044297	.045598	368.727952	.976818	0.000000	.000303	410.418140	154.017090	34.187025
2	6	1.023306	.023802	369.182420	.986914	0.000000	.000424	410.418140	151.097415	45.337222
2	7	1.000144	.000147	369.852573	.997365	0.000000	.000621	410.418140	147.823567	56.373895
2	8	.955520	-.044871	370.828713	1.010527	0.000000	.000939	410.418140	143.631000	67.110000
2	9	.915739	-.084507	371.684815	1.037524	0.000000	.001311	410.418140	139.491203	74.289388
2	10	.883153	-.116377	372.629158	1.053169	0.000000	.001455	410.418140	135.167265	81.359857
2	11	.861980	-.136827	373.881636	1.062300	0.000000	.001651	410.418140	130.465393	88.182320
2	12	.847983	-.150250	374.888474	1.066793	0.000000	.001906	410.418140	125.122754	94.507390
2	13	.845543	-.152680	376.282041	1.065180	0.000000	.002147	410.418140	118.962726	100.037776
2	14	.850199	-.148133	377.772114	1.061968	0.000000	.002207	410.418140	111.716041	103.934170
2	15	.860942	-.129165	379.232960	1.058410	0.000000	.001088	410.418140	103.621000	105.700000
2	16	.874617	-.124649	381.091440	1.058399	0.000000	.000731	410.418140	87.084271	105.847319
2	17	.900271	-.099692	382.989192	1.045774	0.000000	.000732	410.418140	70.547191	105.994642
2	18	.923190	-.077147	384.613520	1.036304	0.000000	.000612	410.418140	54.010129	106.141958
2	19	.950344	-.050161	385.620213	1.024012	0.000000	.000495	410.418140	37.473086	106.289545
2	20	.946284	-.054207	388.377658	1.026787	0.000000	.000444	410.418140	20.935999	106.425505
2	21	.941654	-.068833	388.866847	1.029816	0.000000	.000319	410.418140	4.390613	106.230860
2	22	.946094	-.064407	386.694503	1.027286	0.000000	.000349	410.418140	-12.136424	106.000000
2	23	.959595	-.040894	386.974480	1.017431	0.000000	.000124	410.418140	-18.592232	119.448326
2	24	.979304	-.021031	388.196697	.991049	0.000000	.000089	410.418140	-30.633516	129.977876
2	25	.985104	-.015155	389.715170	.996016	0.000000	.001287	410.418140	-43.400110	122.912745
2	26	.995027	-.005069	390.759384	.998154	0.000000	.000837	410.418140	-58.448659	109.238657
2	27	.987780	-.012439	391.425802	1.003557	0.000000	.000403	410.418140	-65.358901	94.662599
2	28	.998556	-.001473	391.899897	.999084	0.000000	.000337	410.418140	-58.924438	81.433841
2	29	1.024813	.025444	392.221493	.986532	0.000000	.000230	410.418140	-62.490417	68.204936
2	30	1.026163	.026836	392.339406	.986365	0.000000	.000130	410.418140	-64.291899	54.632023
2	31	1.014509	.014848	392.328706	.992385	0.000000	.000070	410.418140	-65.838708	41.018623
2	32	1.019308	.019778	392.350656	.990019	0.000000	.000065	410.418140	-66.985900	27.373132
2	33	1.024350	.024977	392.386412	.987408	0.000000	.000039	410.418140	-67.619499	13.686654
2	34	1.028849	.029606	392.413489	.985085	0.000000	0.000000	410.418140	-68.247628	0.000000
2	35	1.024359	.024977	392.386412	0.000000	0.000000	0.000000	410.418140	-67.619499	-13.686654

J	K	RHO	CP	PHI	U	V	W	X	Y	Z
1	2	1.100731	.104817	367.909457	0.000000	0.000000	0.000000	410.418140	147.455536	0.000000
2	2	1.091121	.094845	368.052851	.953648	0.000000	0.000000	410.418140	168.981000	0.000000
3	2	1.100731	.104817	367.909457	.948370	-.000226	0.000000	410.418140	170.506465	0.000000
4	2	1.099524	.103638	367.383143	.948279	-.000355	0.000000	410.418140	183.330164	0.000000
5	2	1.077825	.080631	366.670006	.969093	-.000384	0.000000	410.418140	197.598332	0.000000
6	2	1.025877	.026541	365.873568	.985685	-.000384	0.000000	410.418140	213.473674	0.000000
7	2	.996633	-.003434	365.088734	1.001008	-.000371	0.000000	410.418140	231.137222	0.000000
8	2	.987749	-.012471	364.466279	1.006007	-.000354	0.000000	410.418140	250.790402	0.000000
9	2	.977198	-.023161	364.162812	1.011639	-.000353	0.000000	410.418140	272.657327	0.000000
10	2	.967420	-.033027	364.285392	1.016640	-.000420	0.000000	410.418140	296.987354	0.000000
11	2	1.014720	.015064	364.379894	.992492	-.000523	0.000000	410.418140	324.057927	0.000000
12	2	1.057717	.059567	364.410100	.970455	-.000573	0.000000	410.418140	354.177745	0.000000
13	2	1.083725	.086841	365.505553	.956238	-.000602	0.000000	410.418140	387.690275	0.000000
14	2	1.104822	.109159	367.752940	.944226	-.000672	0.000000	410.418140	424.977674	0.000000
15	2	1.107506	.112010	370.884531	.941858	-.000784	0.000000	410.418140	466.465145	0.000000
16	2	1.078436	.079171	374.847869	.958455	-.000971	0.000000	410.418140	512.625787	0.000000

IV. OUTPUT DATA

The program provides an output of the flowfield after every NP marching steps (NP is user specified). A small portion of the output is presented here. It provides the flow variable information (density, C_p, ϕ, contravariant velocities, U, V and W, and the grid point location x, y and z) along the body surface (J = 2) and along the planes of symmetry (K = 2 and KMAX-1). Besides this printout for every NP marching steps, the code also prints the Courant number and maximum eigenvalues in the η and ξ crossflow directions, and the rms change in density. A detailed output of the entire flowfield in the crossplane (η,ξ) for all J and K can also be obtained at selected marching plane locations prescribed by the user in the input at card number 46 (see Section III).

The code also stores the results for plotting purposes in Tape 1, and a separate plotting package is used to plot contours and other forms of visual output.

V. RESULTS

Four cases are presented to illustrate the capability of the code.

1. Flow over an arrow-wing body at M_∞ = 2.96. α = 10.01°.
2. Flow over a forebody configuration at M_∞ = 2.5, β = 5° and at M_∞ = 1.7, α = 10°, β = 5°.
3. Flow over the entire Shuttle Orbiter geometry at M_∞ = 1.4, α = 0°.
4. Flow over a realistic fighter configuration at different angles of attack and free-stream Mach numbers.

For an attached shock at the nose (pointed nose configurations), a conical solution is generatd and used as an initial data plane for the non-conical marching calculation. If the nose is blunt and has a detached shock, then an unsteady full potential code[8] is used to generate the initial blunt body solution (free-stream Mach number less than 1.5 is recommended). This initial flow calculation usually takes 40 to 60 iterations. At the beginning of each marching plane calculation, the grid is generated using an elliptic grid solver. Usually, the grid solver requires 30 relaxation cycles to provide an acceptable grid distribution.

Figure 9 shows the pressure distribution on the surface of an arrow-wing configuration at location $x/\ell = 0.8$ for $M_\infty = 2.9$, and $\alpha = 10°$. The improvement in the prediction capability achieved using the wake treatment is illustrated. The dashed line represents the result from "no wake" treatment (assumes a flat plate behind the trailing edge) and the solid line represents the modifications to the pressure distribution once a zero jump in pressure across the wake cut is imposed. The solid line pressures on the body agree very well with experiments.[10] Without a proper wake cut treatment, the overall lift and drag forces and the pitching moment can be off by a considerable margin.

Figure 10 presents the pressure distribution on a fully developed forebody[11] for $M_\infty = 2.5$ and yaw angle $\beta = 5°$. Figure 11 shows the circumferential pressure distribution for the same body at $x/\ell = 0.68$ for $M_\infty = 1.7$, $\alpha = 10°$ and $\beta = 5°$. The experimental data[11] are also given in these two figures. The results show that the present prediction is in excellent agreement with the experimental data.

Figures 12 to 22 give the geometry and the corresponding flow field solutions for the Shuttle Orbiter. The side view, cross-section and grid in the nose region are given in Fig. 12. The top view, cross-section, grid and chordwise cross-sections are presented in Fig. 13. It should be mentioned here that for most of the previous Space Shuttle calculations[12,13] the geometry has been modified by smoothing out the canopy and increasing the wing sweep angle from 45 to 55 degrees in order to avoid the subsonic bubble. Since the present method is valid for supersonic flow with embedded subsonic region, the realistic Shuttle Orbiter geometry was used without any modification.

Figure 14 shows the surface pressure distribution along the leeward plane of symmetry. At $x \cong 170$ in. which is the beginning of the canopy, the pressure increases rapidly from $C_p \cong 0.3$ to 1.0, approximately. In the canopy region an MSR/TSR is formed and required three relaxation cycles to develop the solution. The circumferential surface pressure distribution at $x = 240$ in. is shown in Fig. 15. The experimental data is also given in these figures and the agreement is very good. The surface pressure distribution along the wing leading edge is given in Fig. 16. It is seen that the present calculation agrees with the experimental data quite well along the entire wing leading edge except in the vicinity of the wing-fuselage junction, where a vortex flow may exist.

Figure 17 to Figure 21 present the Orbiter chordwise pressure distribution on the upper and lower wing surface at $\overline{z} = z/bw = 0.471$, 0.530, 0.641, 0.780 and 0.887, respectively where bw is a semispan defined in Fig. 12. The results show that the present predictions are in very good agreement with the experimental data, except in the region near the trailing edge of the upper surface at $\overline{z} = 0.471$ and 0.53 span stations. Here again, a vortex flow or separation may be causing the discrepancies. Figure 22 shows the circumferential pressure distribution for the Orbiter at $x = 1120$ in. It is noted that the pressure at the vertical tail and OMS pods are well predicted.

Figure 23 shows a supersonic fighter configuration with vertical tails. The free-stream Mach number, angle of attack and wing sweep angle for the calculation are summarized in Table 1.

Figure 24 presents the surface pressure at various axial stations and the corresponding grid distribution for the wing body geometry. For this case, the MSR/TSR starts around $x = 0.4$ at the leading edge, and remains subsonic all the way to the end of the wing. Figure 25 and 26 show the circumferential pressure distribution in the vertical tail and wake region of the fighter-like configuration. The pressure on the vertical tail surface is given separately along the y-direction. The results clearly show that the present wake tretment provides the correct zero pressure jump condition across the wake. The chordwise pressure distributions from the center of the body to the tip of the wing are given in Fig. 27. Figure 28 presents the pressure contour on the upper and lower surface of the fighter configuration.

The lift and drag coefficients from the present calculations for this fighter model are also given in Table 1. The comparison with experimental data show excellent agreement.

VI. CONCLUSIONS

A nonlinear full potential method has been developed to analyze supersonic flows with embedded subsonic regions over some very complex configurations. A conservative switching scheme is employed to transition from the supersonic marching algorithm to a subsonic relaxation procedure. The predictions are in very good agreement with experiment data.

Work is now progressing to simulate the multibody interaction between the Shuttle Orbiter and the external tank, and canard-wing fighter geometries. The present methodology will also be extended to treat all Mach number flows (fully subsonic flow, as well as subsonic flow with pockets of supersonic region (transonic case)).

ACKNOWLEDGMENT

This work was partially supported by NASA-Langley Research Center under Contract NAS1-15820. The authors express their appreciation to Prof. Stanley Osher of UCLA for many valuable discussions.

REFERENCES

1. Jameson, A., "Transonic Potential Flow Calculations using Conservation Form," AIAA 2nd Computational Fluid Dynamics Conf. Proc., 1975, pp. 148-155.

2. Holst, T.L., "Fast, Conservative Algorithm for Solving the Transonic Full Potential Equation," AIAA Journal, Vol. 18, No. 12, December, 1980, pp. 1431-1439.

3. Siclari, M.J., "Computation of Nonlinear Supersonic Potential Flow over Three-Dimensional Surfaces," AIAA Paper No. 82-0167, presented at the AIAA 20th Aerospace Sciences Mtg., Orlando, Florida, January 1982.

4. Shankar, V., "A Conservative Full Potential, Implicit Marching Scheme for Supersonic Flows," AIAA Journal, Vol. 20, No. 11, November, 1982, pp. 1508-1514.

5. Shankar, V. and Osher, S., "An Efficient Full Potential Implicit Method Based on Characteristics for Analysis of Supersonic Flows," AIAA Journal, Vol. 21, No. 9, p. 1262, September, 1983.

6. Shankar, V., Szema, K.Y. and Osher S., "A Conservative Type-Dependent Full Potential Method for the Treatment of Supersonic Flow with Embedded Subsonic Regions," AIAA Paper No. 83-1887, July 1983.

7. Szema, K.Y. and Shankar, V., "Nonlinear Computation of Wing-Body-Vertical Tail-Wake Flows at Low Supersonic Speeds," AIAA Paper No. 84-0427, January, 1984.

8. Shankar, V., "Implicit Treatment of the Unsteady Full Potential Equation in Conservation Form," AIAA Paper No. 84-0262, January 1984.

9. Shankar, V., Rudy, S., and Szema, K.-Y., "Application of a Two-Dimensional Grid Solver for Three-Dimensional Problems," ASME Applied Mechanics, Bioengineering and Fluids Eng. Conf., Vol. No. G00222, June 20-22, 1983.

10. Townsend, J.C., "Pressure Data for Four Analytically Defined Arrow Wings in Supersonic Flow," NASA TM 81835, September 1980.

11. Townsend, J.C., Howell, D.T., Collins, I.K., and Hayes, C., "Surface Pressure Data on a Series of Analytic Forebodies at Mach Numbers from 1.7 to 4.50 and Combined Angles of Attack and Sideslip," NASA TM 80062, June 1979.

12. Maus, J.R., Griffith, B.J., Szema, K.Y., and Best, J.T., "Hypersonic Mach Number and Real Gas Effects on Space Shuttle Orbiter Aerodynamics," AIAA Paper No. 83-0343, January 1983.

13. Venkatapathy, E., Rakich, J.V., and Tannehill, J.C., "Numerical Solution of Space Shuttle Orbiter Flow Field," AIAA Paper No. 82-0028, January 1982.

14. Rockwell International Space Division Data.

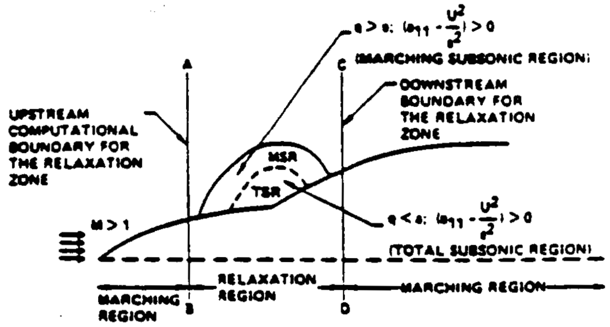

Fig. 1 Embedded subsonic bubble in a supersonic flow.

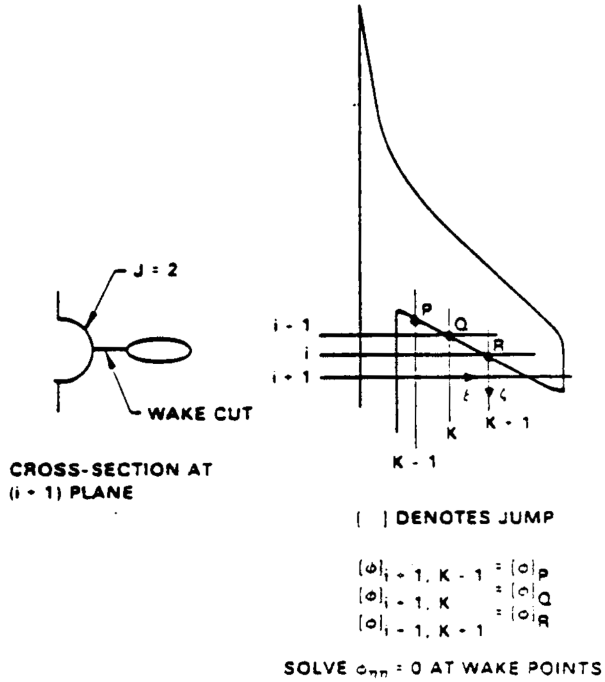

Fig. 3 Wake boundary condition.

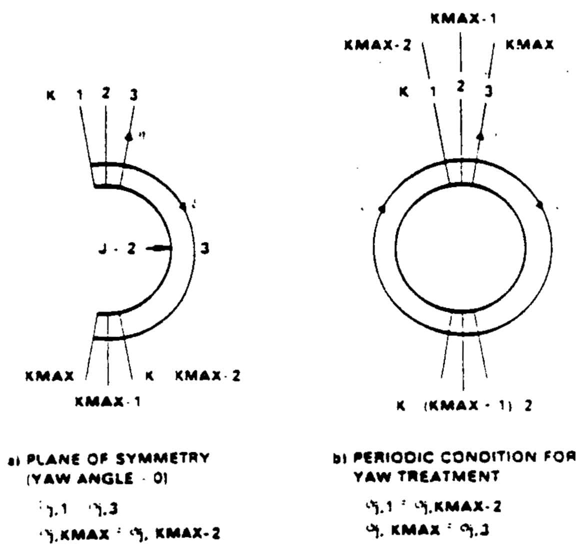

Fig. 2 Symmetry and periodic conditions.

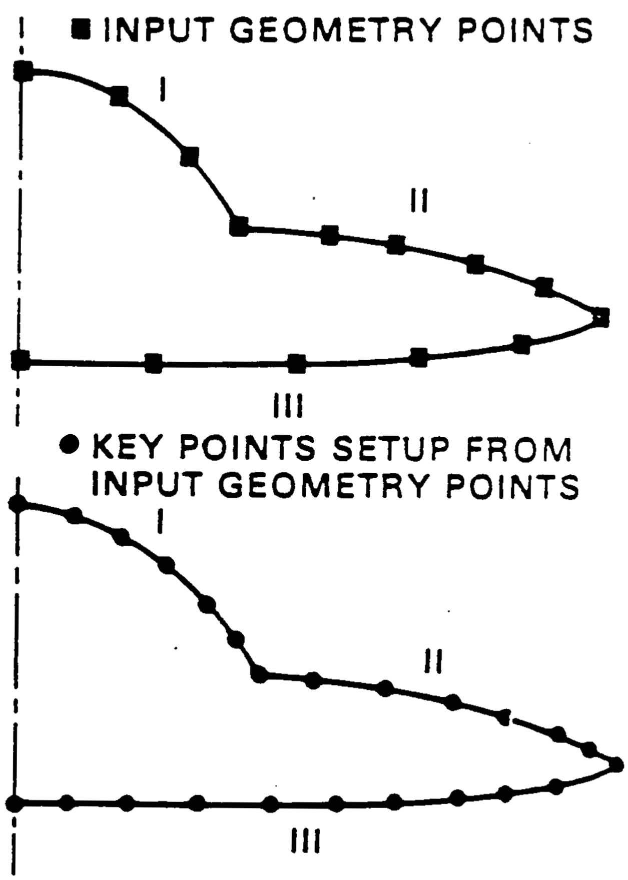

Fig. 4 Input geometry points and setup of key points.

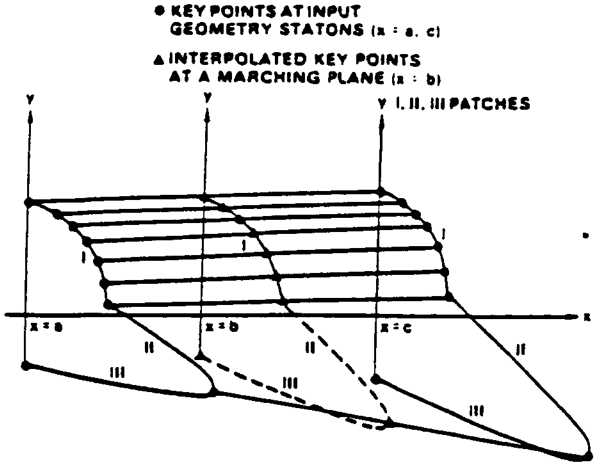

Fig. 5 Geometry setup.

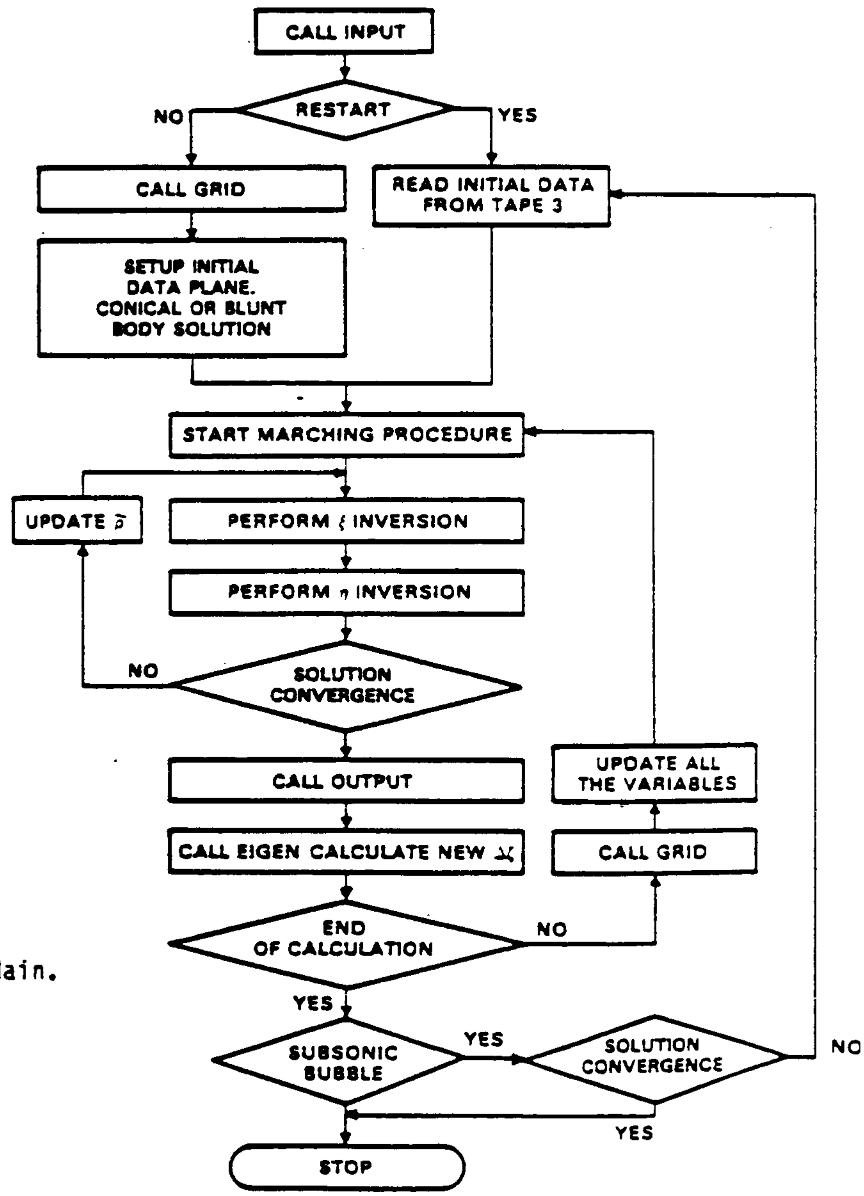

Fig. 6 Flowchart of program Main.

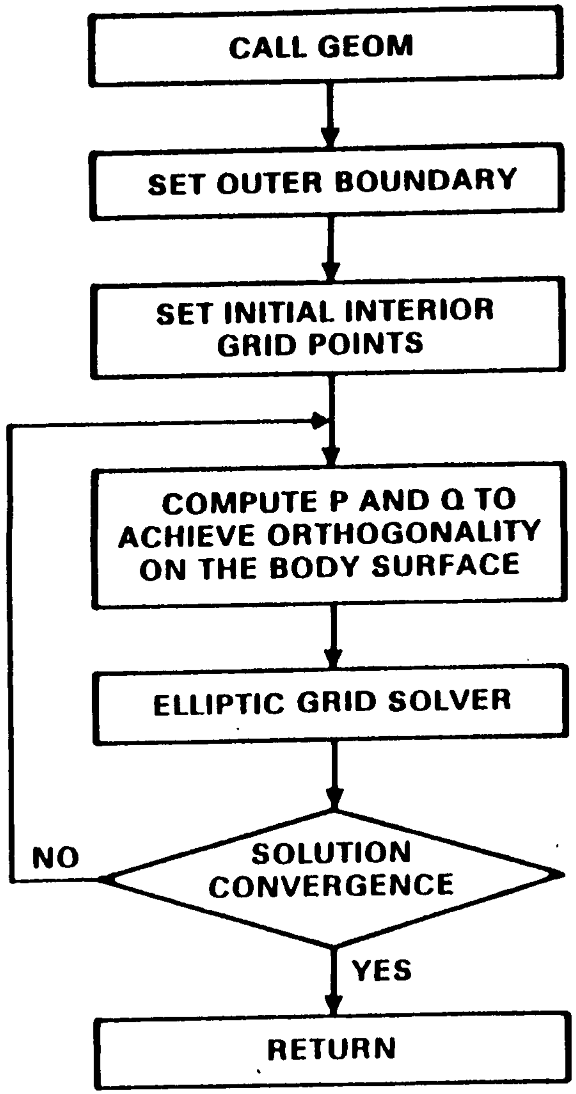

Fig. 7 Flowchart of subroutine GEOM.

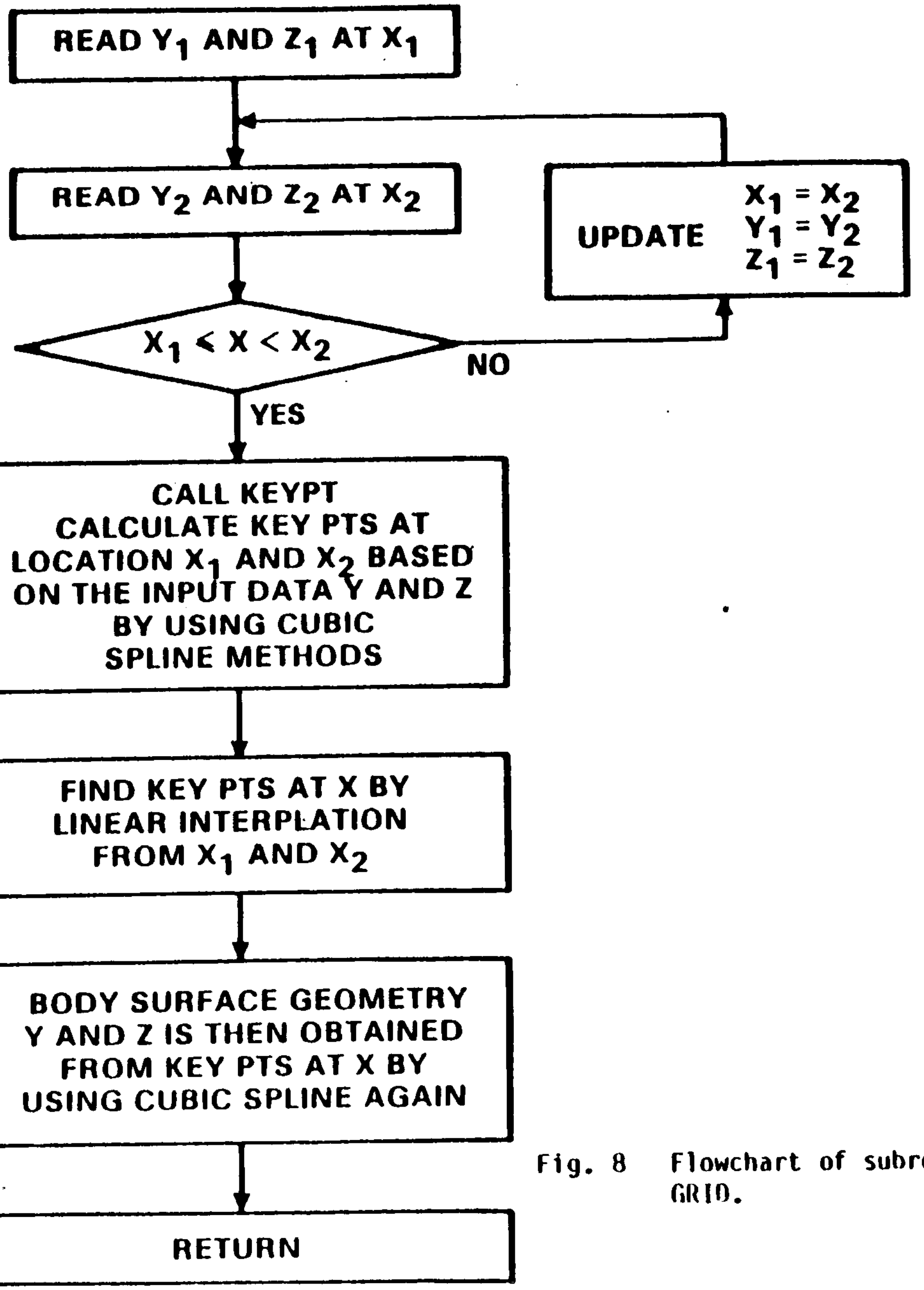

Fig. 8 Flowchart of subroutine GRID.

ORIGINAL PAGE IS
OF POOR QUALITY

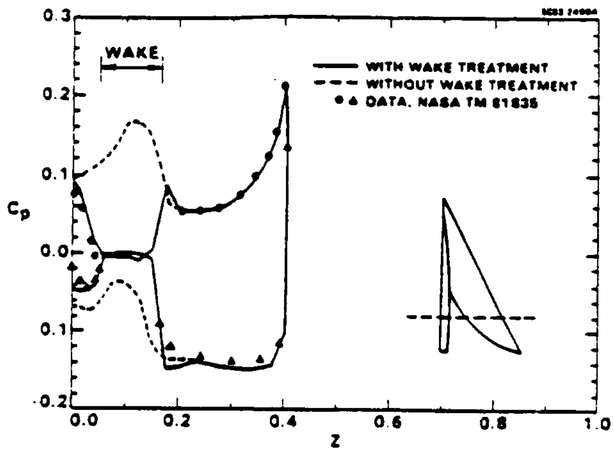

Fig. 9 Circumferential pressure distribution for the arrow-wing at $x/\ell = 0.81$, $M_\infty = 2.96$, $\alpha = 10°$.

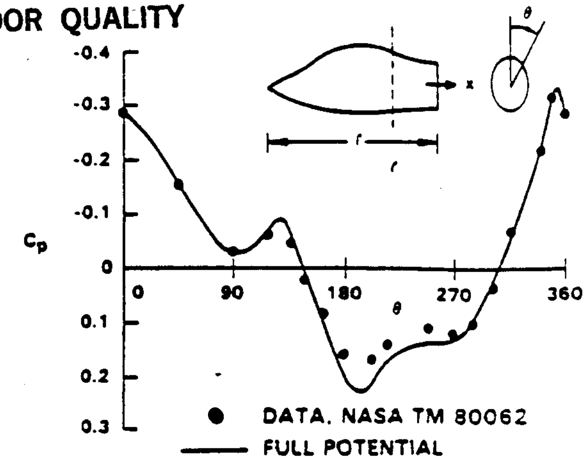

Fig. 11 Circumferential pressure distribution on a forebody at $x/\ell = 5.02°$, $\alpha = 0°$.

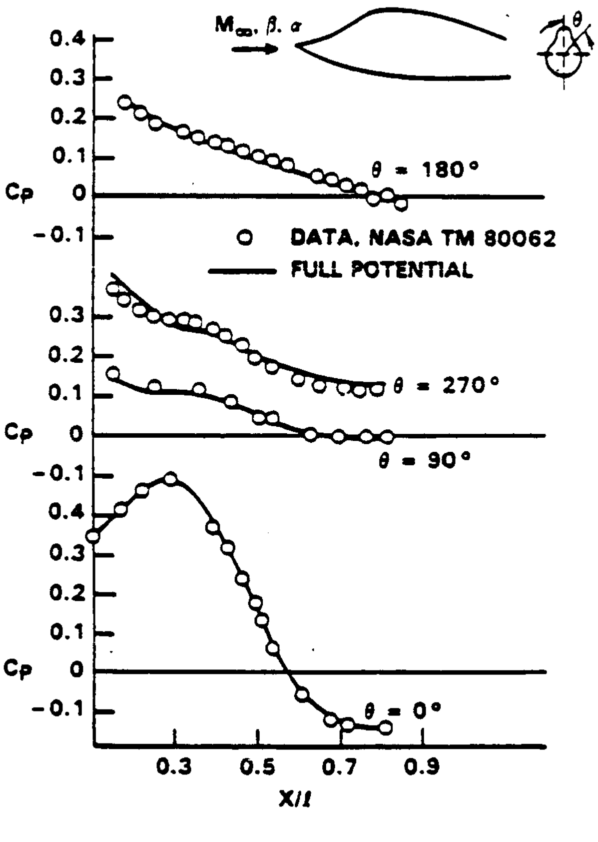

Fig. 10 Pressure distribution on a forebody in slideslip $M_\infty = 2.5$, $\beta = 5.02°$, $\alpha = 0°$.

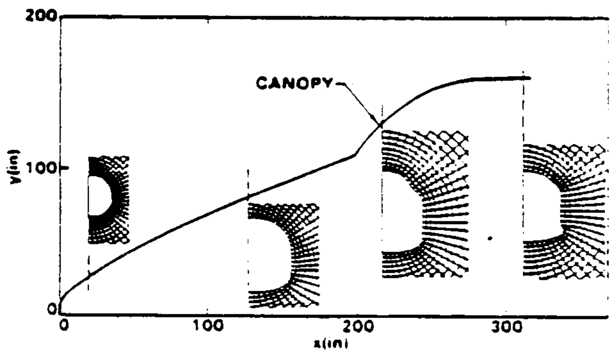

Fig. 12 Nose region geometry for Space Shuttle.

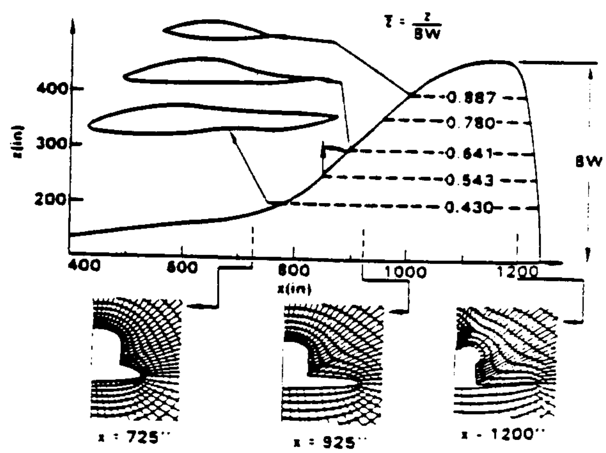

Fig. 13 Geometry and grid generation for Shuttle Orbiter at axial cuts.

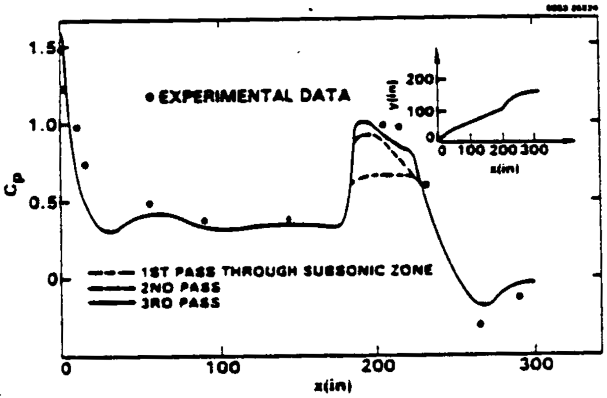

Fig. 14 Surface pressure distribution at leeward plane of symmetry.

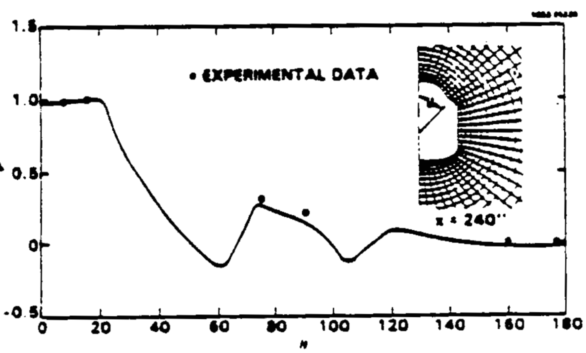

Fig. 15 Surface pressure distribution around the body.

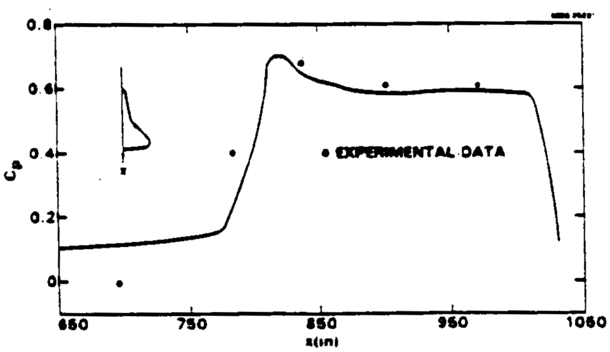

Fig. 16 Surface pressure distribution along the wing leading edge.

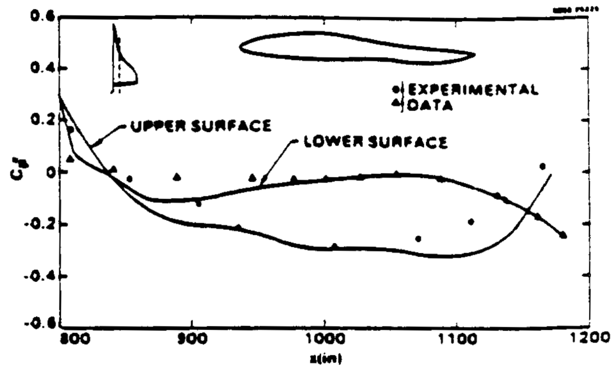

Fig. 17 Shuttle Orbiter chordwise pressure distribution; M_∞ = 1.4, α = 0.0°, $\overline{z}$ = 0.471.

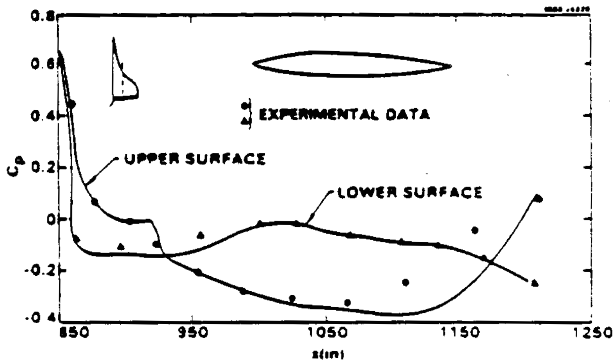

Fig. 18 Shuttle Orbiter chordwise pressure distribution; M_∞ = 1.4, α = 0.0°, $\overline{z}$ = 0.53.

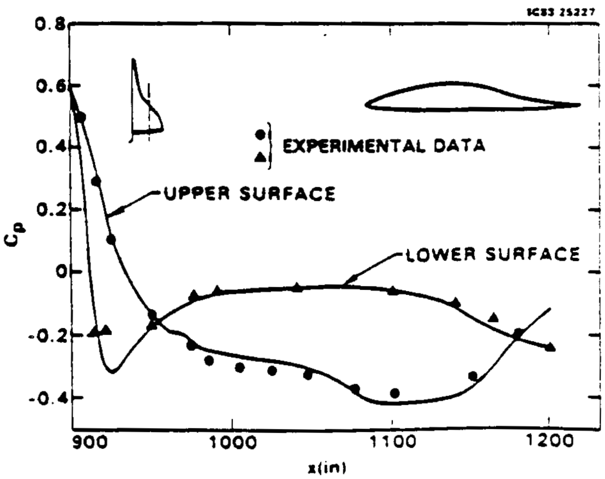

Fig. 19 Shuttle Orbiter chordwise pressure distribution; M_∞ = 1.4, α = 0.0°, $\overline{z}$ = 0.641.

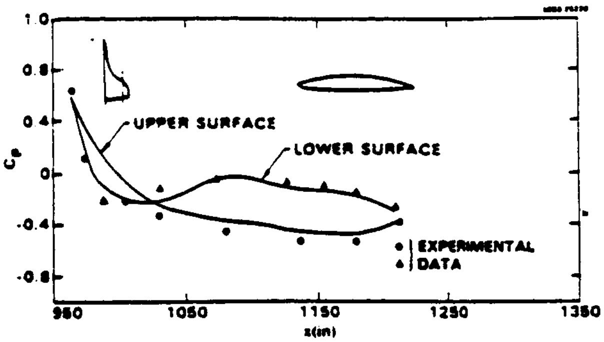

Fig. 20 Shuttle Orbiter chordwise pressure distribution; M_∞ = 1.4, α = 0.0°, $\bar{z}$ = 0.78.

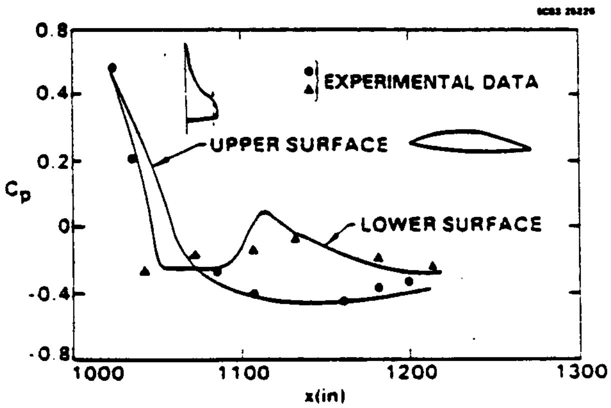

Fig. 21 Shuttle Orbiter chordwise pressure distribution; M_∞ = 1.4, α = 0.0°, $\bar{z}$ = 0.887.

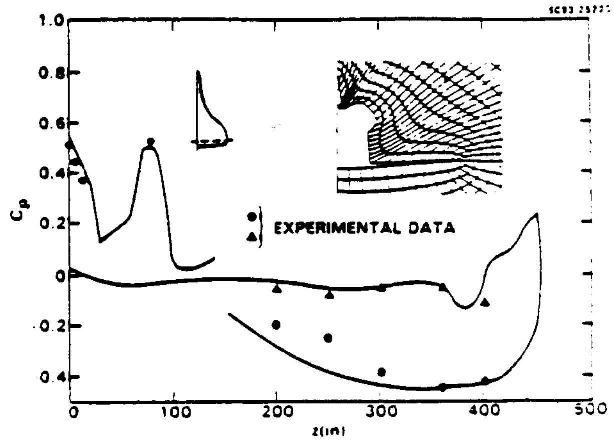

Fig. 22 Circumferential pressure distribution for the Orbiter at x = 1120 in; M_∞ = 1.4, α = 0.0°.

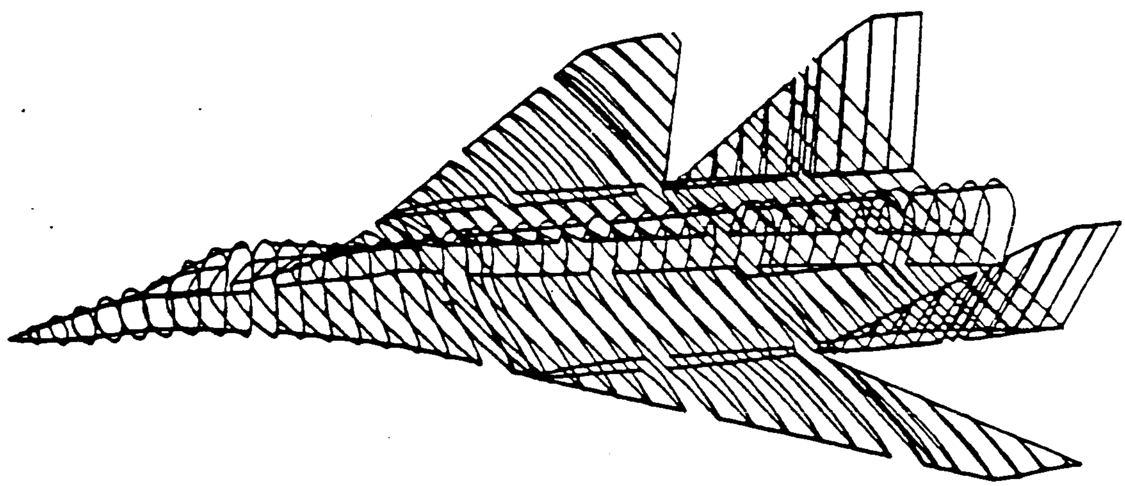

Fig. 23 Fighter-like configuration.

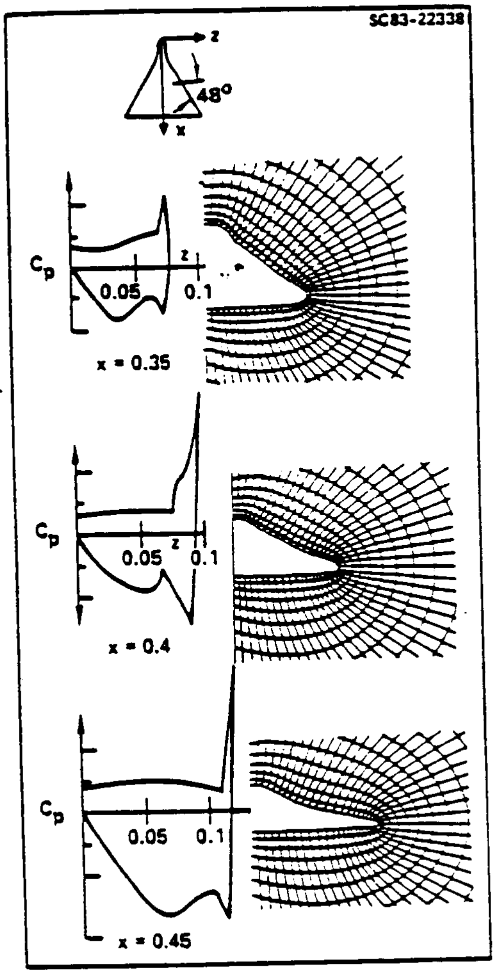

Fig. 24 Pressure distribution on a fighter-like configuration, $M_\infty = 1.6$, $\alpha = 5°$.

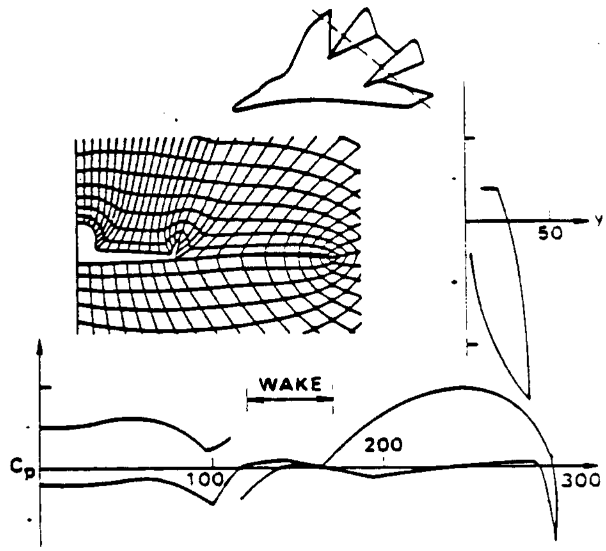

Fig. 25 Circumferential pressure distribution in the vertical tail and wing region of a fighter-like configuration, M_∞ 1.6, α = 4.46, x/ℓ = 0.82.

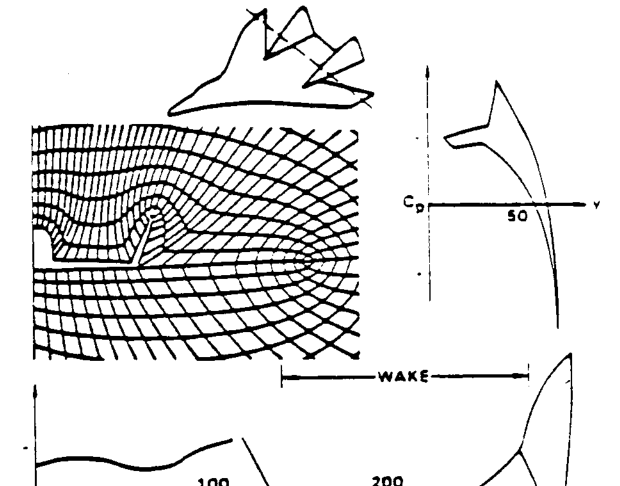

Fig. 26 Circumferential pressure distribution in the vertical tail and wing region of a fighter-like configuration, M_∞ 1.6, α = 4.46, x/ℓ = 0.90.

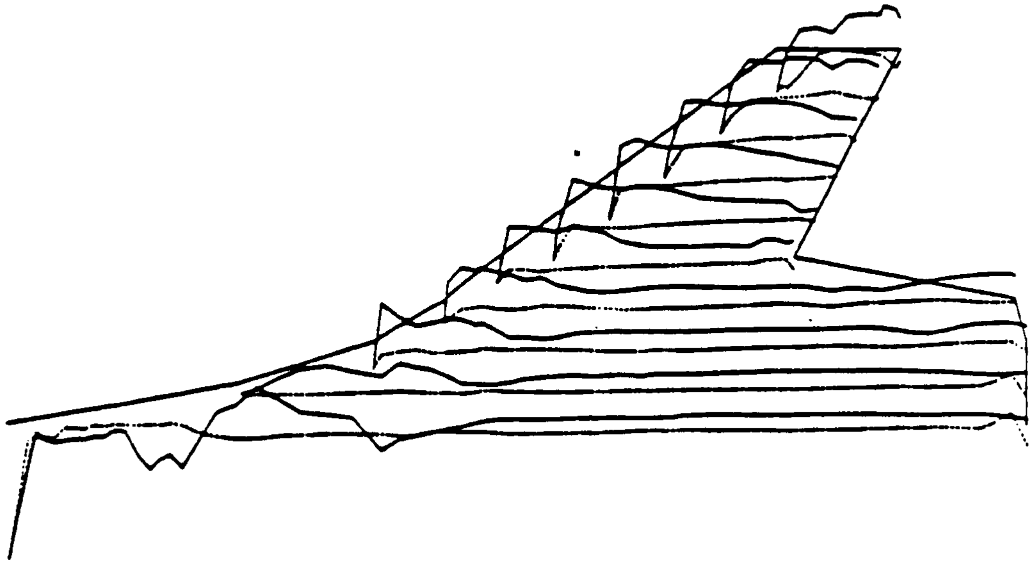

Fig. 27 Chordwise pressure distribution for a fighter-like configuration. M_∞ 1.6, α = 4.46.

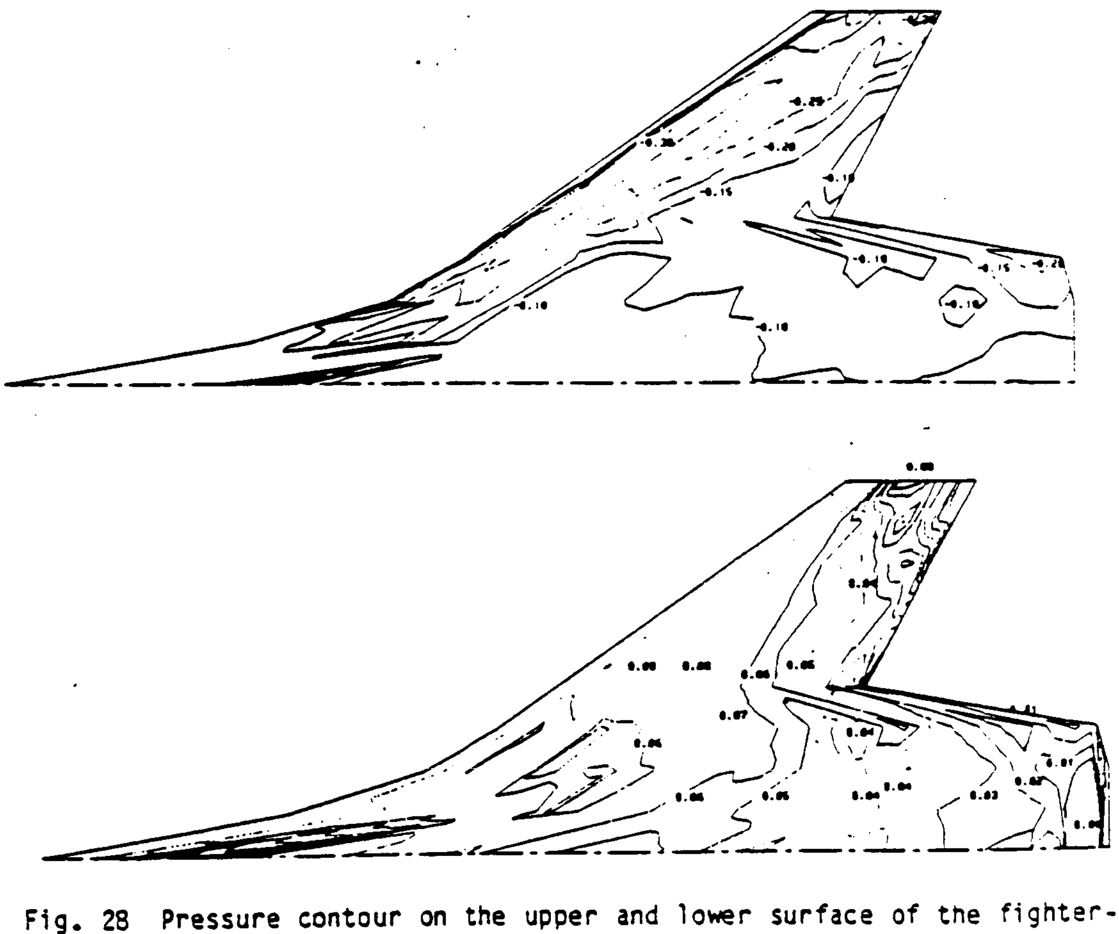

Fig. 28 Pressure contour on the upper and lower surface of the fighter-like configuration. M_∞ = 1.6, α = 4.46°.

α		5°	5°	5°	5°
M_∞		1.6*	1.6†	1.4†	1.6†
Λ		48°	48°	48°	55°
C_L	CODE	0.298	0.3016	0.3561	0.29186
	DATA	0.277	0.295	0.342	0.3
C_D	CODE	0.0462	0.04916	0.04117	0.028129
	DATA	0.0457	0.0493	0.0425	0.0301

Λ = Wing sweep angle
*Without vertical tail
†With vertical tail

Table 1 Test cases for fighter-like configurations.

SUPERSONIC FULL POTENTIAL ANALYSIS PROGRAM OPERATING INSTRUCTIONS

E. BONNER

Rockwell International Corporation
North American Aircraft Operations
Los Angeles, California 90009

ABSTRACT

Description of input/output data and operating instructions are presented for a recently developed supersonic full potential analysis program. Solution pre and post processors are also discussed for completeness. The latter includes a three dimensional finite difference boundary layer program interface

TABLE OF CONTENTS

INTRODUCTION

The supersonic full potential analysis method,[1-3] in conjuction with three dimensional boundary layer analysis[4] is currently being used to derive nonlinear supersonic cruise and maneuver designs to support aerodynamic advance configuration studies. The fundamental advance of full potential methodology relative to linear solutions is the ability to shock capture. The analysis consequently provides the means to achieve necessary conditions of shock weakening and separation elimination /management through appropriate re-design. In this regard, it provides a capability similar to relaxation solvers that are routinely used to develop efficient transonic flows.

Supersonic full potential analysis also provides the ability to accurately assess the impact of sweep, thickness, and lift for a range of design space for which linear theory is unsatisfactory.

DISCUSSION

The supersonic full potential (SFP) analysis code of Shankar[1-3] is applicable to arbitrary wing-body-nacelle-tail arrangements from moderate supersonic Mach number to values of the hypersonic similarity parameter $M\delta \sim O(1)$. The lower code limit is governed by the extent of embedded subsonic flow while the upper limit results from a breakdown in the isentropic assumption for strong shock waves. Also, since potential theory is irrotional, the modeling of vortices is not treated.

The current version of the pilot code is operational on the CDC 875 and is stored as program library FPF7PL.

CASE DESCRIPTION

Four types of data are required to define a problem: a) header data describing mesh information, Mach number, angle of attack, aerodynamic coefficient reference quanities, center of gravity location, etc.; b) detailed geometric coordinates defining configuration cross plane contours; c) program update file directives defining code modifications, wake data, etc.; and d) job control directives defining program and input/output file allocations.

GEOMETRY DATA

A configuration is defined by several regions* of crossplane sections as indicated in figure 1. The number of patches (segments) defining a section is constant for a given region and typically increases from one region to the next.

For the wing-body-vertical case under discussion, a three (3) patch initial region, a six (6) patch center region, and and eight (8) patch final region as indicated on figure 2. Zero length patches are not permissable. Since the analysis is marching in nature, a complete geometry data set is not required to begin and partially process a problem. Appropriate use of restart solutions allows continuation of the analysis as new or modified geometry becomes available.

*The overlap must be sufficient to encompass at least the final three (3) marching data planes of the prior region.

C-2

The format for a typical station is shown below. The group of cards is repeated for each station of a region. The last point of each patch (except for the last patch of a station) should have the same coordinates as the first point of the next patch.

Card#	Format	Field	Name	Description
A1	F15.6,I5	1	X1	The x value (longitudinal) of this station.
		2	ISC1	The number of patches for this section. $1 \leq$ ISC1 ≤ 15

The group of cards A2 thru A3 are repeated ISC1 times.

Card#	Format	Field	Name	Description
A2	3I5	1	ITH	Patch number ≤ 15
		2	IPT1	Number of points in this patch. $2 \leq$ IPT1 ≤ 30
		3	ND	Mesh spacing parameter*. Typically the same for all stations of a region

The A3 card is repeated IPT1 times.

Card#	Format	Field	Name	Description
A3	2F15.6	1	Y1	Vertical location of point (positive upwards). Points start at top centerline.
		2	Z1	Spanwise location of point.

Cubic spline interpolation is performed on input patch data to derive the boundary at the mesh points. Linear interpolation is performed to define the boundary at a marching plane between input stations.

Sample geometry data for the problem of figure 1 is presented on Table I and was developed using CDS[5].

---

*FOR SEGMENT $\overline{AB}$

0 Equal space
1 Bunch near A
2 Bunch near B

TABLE I GEOMETRY DATA

ORIGINAL PAGE IS
OF POOR QUALITY

570=	-84.995010	3	
580=	1 5 0		First Station
590=	1.546702	0.000000	First Patch
600=	1.546643	0.000323	
610=	1.545103	0.018315	
620=	1.540437	0.035744	
630=	1.532935	0.051886	
640=	2 7 2		
650=	1.532935	0.051886	Second Patch
660=	1.522891	0.066404	
670=	1.510559	0.078912	
680=	1.496288	0.089136	
690=	1.480402	0.096745	
700=	1.463288	0.101503	
710=	1.445334	0.103129	
720=	3 10 1		
730=	1.445334	0.103129	Third Patch
740=	1.427338	0.101529	
750=	1.410231	0.096822	
760=	1.394392	0.089222	
770=	1.380169	0.079030	
780=	1.367900	0.066469	
790=	1.357885	0.051917	
800=	1.350419	0.035707	
810=	1.345759	0.018258	
820=	1.344157	0.000000	
830=	-64.838013	3	Second Station
840=	1 5 0		
850=	7.912023	0.000000	
860=	7.907942	0.035226	
870=	7.809140	1.704391	
880=	7.543938	3.104908	
890=	7.167485	4.292385	
900=	2 7 2		
910=	7.167485	4.292385	
920=	6.712801	5.329372	
930=	6.194769	6.250120	
940=	5.610175	7.060595	
950=	4.937719	7.738470	
960=	4.138007	8.233154	
970=	3.153522	8.465744	
980=	3 10 1		
990=	3.153522	8.465744	
1000=	1.927852	8.274061	
1010=	1.149799	7.897685	
1020=	0.640312	7.314930	
1030=	0.265738	6.517867	
1040=	-0.062191	5.512252	
1050=	-0.386351	4.317566	
1060=	-0.704225	2.967078	
1070=	-0.967907	1.507670	
1080=	-1.084095	0.000000	
1090=	-44.675003	3	
1100=	1 5 0		
1110=	13.575716	0.000000	
1120=	13.572840	0.035637	
1130=	13.380495	2.761196	

8380=	289.670959	3	← End of Region 1
8390=	1 13 0		
8400=	49.958420	0.000000	
8410=	49.958382	1.937543	
8420=	49.958420	4.388307	
8430=	49.680511	7.428109	
8440=	48.879784	10.266657	
8450=	47.604164	12.876749	
8460=	45.899948	15.224077	
8470=	43.811752	17.267170	
8480=	41.382515	18.957489	
8490=	38.653473	20.239323	
8500=	35.664185	21.049873	
8510=	32.452553	21.319206	
8520=	30.713291	21.295483	
8530=	2 30 2		
8540=	30.713291	21.295483	
8550=	29.147690	23.898067	
8560=	26.650154	28.498608	
8570=	24.242348	33.629456	
8580=	22.121189	38.922287	
8590=	20.874866	42.500359	
8600=	19.281048	47.515938	
8610=	17.635311	53.495407	
8620=	16.076260	61.088318	
8630=	15.763639	65.987915	
8640=	15.355867	68.569077	
8650=	14.472219	73.730820	
8660=	13.499191	78.891434	
8670=	12.402630	84.404892	
8680=	11.482655	88.847702	
8690=	10.837719	91.789429	
8700=	10.246025	94.368530	
8710=	9.555044	97.232849	
8720=	8.931576	99.526596	
8730=	8.207584	102.105499	
8740=	7.425758	104.684341	
8750=	6.573520	107.263199	
8760=	5.626501	109.842041	
8770=	4.722771	112.048233	
8780=	4.134672	113.304123	
8790=	3.615775	114.227844	
8800=	3.348063	114.597412	
8810=	3.147287	114.798508	
8820=	2.910736	114.946838	
8830=	2.698931	114.993576	
8840=	3 29 1		
8850=	2.698931	114.993756	
8860=	2.579846	114.980423	
8870=	2.459620	114.933670	
8880=	2.363239	114.838547	
8890=	2.245280	114.634491	
8900=	2.062772	113.952515	
8910=	1.905408	112.792099	
8920=	1.762813	111.139282	
8930=	1.631411	109.008453	
8940=	1.515947	106.502197	

8950=	1.424684	103.794922	
8960=	1.356829	101.145477	
8970=	1.204987	96.947678	
8980=	1.005896	94.368591	
8990=	0.917631	90.622635	
9000=	0.640761	86.630768	
9010=	0.257428	81.430713	
9020=	-0.130081	76.311234	
9030=	-0.450283	71.150040	
9040=	-0.645550	65.987915	
9050=	-0.994209	61.978348	
9060=	-1.161518	57.469460	
9070=	-1.294488	52.036896	
9080=	-1.417318	45.268186	
9090=	-1.456881	36.659615	
9100=	-1.600638	27.491192	
9110=	-1.781296	18.323032	
9120=	-1.914585	9.163094	Beginning of
9130=	-1.960518	0.000000	
9140=	257.762939	6	← Region 2
9150=	1 6 0		
9160=	50.010979	0.000000	
9170=	50.010979	0.611856	
9180=	49.824493	3.408121	
9190=	49.187645	6.642347	
9200=	48.033119	9.893850	
9210=	46.359802	12.845306	
9220=	2 6 0		
9230=	46.359802	12.845306	
9240=	44.232117	15.282759	
9250=	41.780586	17.095585	
9260=	39.201439	18.276600	
9270=	36.756043	18.921902	
9280=	34.538315	19.328766	
9290=	3 10 0		
9300=	34.538315	19.328766	
9310=	32.809967	21.765694	
9320=	29.693047	26.516281	
9330=	26.462524	31.830555	
9340=	23.469040	37.253181	
9350=	21.147877	42.008942	
9360=	20.279148	43.921326	
9370=	19.470787	46.044807	
9380=	18.717278	48.341698	
9390=	17.326115	53.308514	
9400=	4 18 2		
9410=	17.326115	53.308514	
9420=	15.954689	59.162178	
9430=	14.366322	65.990817	
9440=	13.750040	68.714981	
9450=	13.192150	71.150070	
9460=	12.580235	73.730789	
9470=	11.938618	76.311203	
9480=	11.212303	78.891495	
9490=	10.451151	81.471466	

ORIGINAL PAGE IS
OF POOR QUALITY

End of Region 2

24360=		528.031982	6
24370=	1	7	0
24380=		50.007111	0.000000
24390=		50.007019	2.742154
24400=		50.005111	4.956256
24410=		49.731850	7.991484
24420=		48.936188	10.893526
24430=		47.665405	13.590030
24440=		45.965797	16.014454
24450=	2	8	0
24460=		45.965797	16.014454
24470=		43.864506	18.106064
24480=		41.469543	19.809887
24490=		38.769760	21.076782
24500=		35.834053	21.863373
24510=		32.715767	22.132114
24520=		25.660957	22.127090
24530=		16.874676	22.126163
24540=	3	17	0
24550=		16.874676	22.126163
24560=		16.113280	30.029079
24570=		15.296806	39.139084
24580=		14.629675	48.051239
24590=		14.137501	56.337900
24600=		13.470024	65.090817
24610=		13.080699	71.150040
24620=		12.432905	78.801418
24630=		11.775507	86.630768
24640=		11.325478	91.789383
24650=		10.802713	96.947571
24660=		10.042400	104.684206
24670=		9.567081	109.842010
24680=		9.088606	113.689621
24690=		8.620909	114.515457
24700=		7.802448	114.869385
24710=		4.650239	114.999863
24720=	4	29	2
24730=		4.650239	114.999863
24740=		5.103719	123.433228
24750=		5.596378	130.728241
24760=		6.415631	141.596466
24770=		7.474307	155.155457
24780=		8.102022	164.025568
24790=		8.563284	174.694519
24800=		8.874420	184.462860
24810=		9.115057	194.230164
24820=		9.400442	208.878906
24830=		9.506882	223.523987
24840=		9.463659	233.285553
24850=		9.169333	243.043579
24860=		8.811359	248.582214
24870=		8.440650	262.798920
24880=		7.926655	257.676614
24890=		7.303553	262.513306
24900=		6.501266	267.634949
24910=		5.575104	272.557800
24920=		4.080721	275.272766
24930=		4.621628	276.748108
24940=		4.288194	278.013977
24950=		3.983303	279.084778
24960=		3.708123	279.972534
24970=		3.461858	280.685852
24980=		3.242233	281.231323
24990=		3.045600	281.613525
25000=		2.866371	281.836182
25010=		2.697090	281.901428
25020=	5	30	1
25030=		2.697090	281.901428
25040=		2.555275	281.812378
25050=		2.455352	281.571533
25060=		2.390940	281.174377
25070=		2.356306	280.615479
25080=		2.347210	279.888855
25090=		2.360858	278.988037
25100=		2.395871	277.904968
25110=		2.451631	276.630676
25120=		2.360858	278.988037
25130=		2.451631	276.630676
25140=		2.687582	272.557922
25150=		2.998391	267.635010
25160=		3.301361	262.630127
25170=		3.639046	256.589478
25180=		4.020390	248.358643
25190=		4.345508	240.274780
25200=		4.592886	232.249451
25210=		4.820795	223.524078
25220=		5.055776	213.761658
25230=		5.270200	201.888916
25240=		5.509740	189.346741
25250=		5.704358	179.578674
25260=		5.801357	169.810730
25270=		5.711005	160.040466
25280=		5.460247	150.270203
25290=		5.115679	140.499298
25300=		4.824990	130.728210
25310=		4.676692	123.433243
25320=		2.500000	115.000000
25330=	6	16	0
25340=		2.500000	115.000000
25350=		0.234524	112.900907
25360=		0.205185	109.842010
25370=		0.049130	104.684326
25380=		-0.214051	96.947586
25390=		-0.615489	86.630768
25400=		-0.909250	78.891403
25410=		-1.228700	71.160055
25420=		-1.472983	65.987900
25430=		-1.646140	59.730128
25440=		-1.985137	50.456306
25450=		-2.540106	40.541016
25460=		-3.078060	28.682034
25470=		-3.383093	16.579712
25480=		-3.529747	8.120135
25490=		-3.599054	0.000000
25500=		409.712952	8

Beginning of Region 3

ORIGINAL PAGE IS
OF POOR QUALITY

25510=	1	7	0
25520=		50.007126	0.000000
25530=		50.007095	2.742030
25540=		50.005126	4.956260
25550=		49.737724	7.991527
25560=		48.950752	10.803637
25570=		47.682236	13.590180
25580=		45.974167	16.014576
25590=	2	8	0
25600=		45.974167	16.014576
25610=		43.874229	18.105961
25620=		41.436035	19.809288
25630=		38.718979	21.075272
25640=		35.788315	21.860439
25650=		32.715111	22.127048
25660=		26.350161	22.127010
25670=		18.414383	22.127018
25680=	3	10	0
25690=		18.414383	22.127018
25700=		17.814026	26.774406
25710=		16.923122	34.597984
25720=		16.013092	43.651665
25730=		15.325804	52.031616
25740=		14.666439	60.607819
25750=		13.918823	68.569077
25760=		13.272402	76.311203
25770=		12.510948	84.051117
25780=		11.722996	91.789398
25790=	4	4	2
25800=		11.722996	91.789398
25810=		10.950851	99.526520
25820=		10.160648	107.263123
25830=		9.658892	112.420868
25840=	5	3	1
25850=		9.658892	112.420868
25860=		7.128384	115.000000
25870=		5.126203	117.956802
25880=	6	29	2
25890=		5.126203	117.956802
25900=		5.853479	125.842819
25910=		6.825004	133.837067
25920=		8.132015	145.828949
25930=		8.799452	153.823059
25940=		9.262857	161.816895
25950=		9.645987	173.806427
25960=		9.769035	181.708798
25970=		9.833309	193.786194
25980=		9.785547	201.776581
25990=		9.639191	209.766571
26000=		9.360663	217.755157
26010=		8.956104	226.046539
26020=		8.400652	233.096222
26030=		7.648726	239.093317
26040=		6.849148	245.704193
26050=		5.749837	251.973328
26060=		5.238540	254.410126
26070=		4.662115	256.086719
26080=		4.369453	258.021057
26090=		4.097445	259.004211
26100=		3.846460	259.842285
26110=		3.616040	260.540894
26120=		3.404875	261.104868
26130=		3.210836	261.537364
26140=		3.102296	261.720947
26150=		3.030986	261.841614
26160=		2.861572	262.018860
26170=		2.697999	262.070618
26180=	7	30	1
26190=		2.697999	262.070618
26200=		2.627872	262.051697
26210=		2.560114	262.012207
26220=		2.513620	261.944702
26230=		2.458703	261.845093
26240=		2.418955	261.742126
26250=		2.378328	261.578125
26260=		2.319113	261.204773
26270=		2.278214	260.722534
26280=		2.253218	260.128967
26290=		2.242231	259.419250
26300=		2.243885	258.591797
26310=		2.257326	257.642151
26320=		2.282346	256.567322
26330=		2.368329	254.016083
26340=		2.521813	250.454346
26350=		2.709336	246.293915
26360=		3.116043	235.725586
26370=		3.460886	221.033502
26380=		3.839483	206.437592
26390=		4.086307	195.451019
26400=		4.351102	184.462891
26410=		4.600918	173.473694
26420=		4.703060	166.146942
26430=		4.687814	158.819366
26440=		4.501820	151.102020
26450=		3.955367	140.499268
26460=		3.023705	127.743134
26470=		2.482436	116.711746
26480=		1.313319	114.999817
26490=	8	13	0
26500=		1.313319	114.999817
26510=		0.154916	112.420914
26520=		0.021698	107.263168
26530=		-0.209001	99.526550
26540=		-0.567024	89.210129
26550=		-0.849183	81.471390
26560=		-1.263398	71.150055
26570=		-1.696522	59.699020
26580=		-2.194694	50.229889
26590=		-2.726831	40.469147
26600=		-3.224504	28.843315
26610=		-3.657449	16.538712
26620=		-3.791033	0.000000
26630=		519.784912	8
26640=	1	7	0
26650=		50.007103	0.000000

```
41600=    721.400878    8        <---- End of
41700=   1   7   0                      Region 3
41710=     50.007126     0.000000
41720=     50.007111     2.190936
41730=     50.007126     4.956260
41740=     49.737625     7.991241
41750=     48.950493    10.892822
41760=     47.681923    13.580085
41770=     45.974007    16.013924
41780=   2  15   0
41790=     45.974007    16.013924
41800=     43.874474    18.106983
41810=     41.436966    19.813690
41820=     38.720818    21.085270
41830=     35.781206    21.878693
41840=     32.719025    22.156746
41850=     29.372906    22.153980
41860=     26.042725    22.151508
41870=     22.696865    22.149920
41880=     19.303780    22.149937
41890=     15.831873    22.152140
41900=     12.249571    22.157227
41910=      8.525335    22.165813
41920=      4.627608    22.170566
41930=      0.524876    22.196121
41940=   3   2   0
41950=      0.524876    22.196121
41960=      1.755000   112.214996
41970=   4   2   2
41980=      1.755000   112.214996
41990=    103.760986   148.779999
42000=   5   2   1
42010=    103.760986   148.779999
42020=      1.755000   112.214996
42030=   6   2   2
42040=      1.755000   112.214996
42050=      5.874999   306.528992
42060=   7   2   1
42070=      5.874999   306.528992
42080=      1.755000   112.214996
42090=   8   3   0
42100=      1.755000   112.214996
42110=      0.524876    22.196121
42120=      0.525000     0.000000
42130=*EOF
--
```

HEADER DATA

The present problem requires a minimum of four (4) marching solutions to complete the analysis of the three region sample geometry of figure 1 - one each for region one and two and two solutions for region three. The latter is a consequence of increasing the number of mesh points on the vertical tail as its local span increased with marching distance. It also illustrates the wake restart procedure.

Each solution has a different set of header instructions for describing grid parameters, wake information if pertinent, restart directions, and number of mesh points for each patch of the region. This information precedes the geometric data discussed in the previous section. The header data used for the sample problem and a description of the various parameters is presented on Table II.

The last header data set is coordinated with the wake update file described in the next section. The pertinent nomenclature is depicted below.

KWAK**	RESTART
1	Standard (geometry)
2	Wake

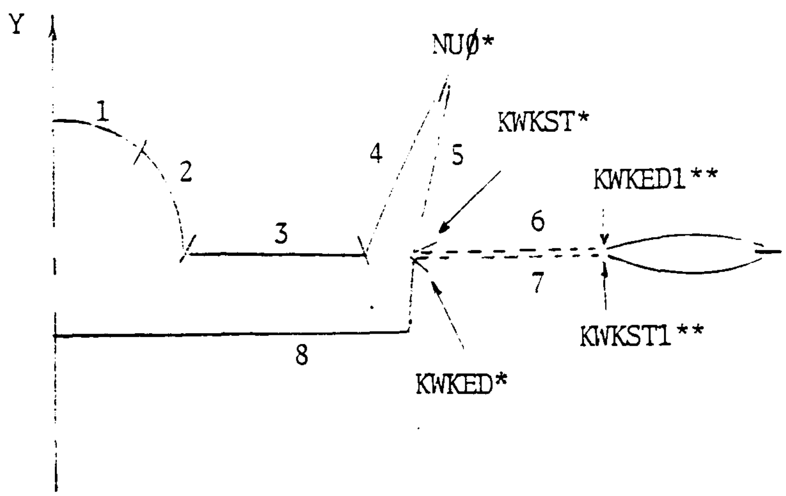

NOTE: Reindex K of VORT (K) to allow for increase of points for patches 4 and 5

---

* TAPE 5
** Update file

TABLE II HEADER DATA


```
100=  175       NMAX    I5      NO. OF AXIAL STEP
110=   15       JMAX            NO. OF PTS IN NORMAL DIR.<26
120=   33       KMAX            NO. OF PTS IN CIRCUM DIR;ISC1+ISC2-1+ISC3+1<81
130=    2       NRM             NO. GRID REGIONS<7;B&WB-2,WBV-3,WBNV-5
140=   13       NU0             SECOND SHARP EDGE K.
150=    2       NP              OUTPUT FOR EVERY NP STEPS
160=   10       KWKST           WAKE START K.
170=   36       KWKED           WAKE END K.
180=   30       NCON            NO. CONE STARTING SOL. STEPS.
190=   30       NITER           NO. OF GRID ITERATIONS.
200=    6       NSPTI           NO. OF ZTA FOR FLOW FIELD OUTPUT.
210=    1       ITERGE          NO. OF GLOB ITERATION.
220=  5.0       CFLIN F10.5     CFL NUMBER
230=  2.5       DZTAIN          IF>0 FIXED STEP SIZE.IF<0 CFL NO.
240=  3.0       DZMAX           MAX. AXIAL STEP SIZE
250=  1.0       DZMIN           MIN. AXIAL STEP SIZE
260=  1.6       FSM             FREE STREAM MACH NO.
270=  4.46      ALFA            ANGLE OF ATTACK-DEG.
280=   60.      THTO            OUTER BOUNDARY-DEG.
290=  0.1       DETA            STEP SIZE IN ETA DIR.
300=  0.1       DXI             STEP SIZE IN XI DIR.
310=    1.5     DZTA            FIRST STEP AFTER CONE START, SOL.
320=  15.00     ZTAI            STARTING ZTA >3*DZTAIN.
330= 371.0      XEND            END ZTA<MAX INPUT ZTA-DZTAIN.
340=    1.      AMU1            1:FIRST ORDER,2:2ND ORDER.
350=   0.       AMU2            0:FIRST ORDER,1:2ND ORDER.
360=  614.      XWAKE           WAKE MINIMUM ZTA.
370=  117.      ZWAKE           WAKE MINIMUM .
380=     1.0    CHL             GEOMETRY SCALE FACTOR
390=    85.0    PTNOSE          AXIAL GEOMETRY SHIFT FOR ZTA>0.
400=    0.      YSHIFT          VERTICAL GEOMETRY SHIFT
410=  500.      XO              AXIAL C.G. ZTA.
420=    0.      YO              VERTICAL C.G.
430=125200.     AAA             REFERENCE AREA.
440=234.627     ALL             REFERENCE LENGTH.
450=   1.75     OMEGA           RELAXATION FACTOR.
460=    T       PLANEOS         PLANE OF SYM.?
470=    T       NUGRID          GENERATE GRID?
480=    T       IREAD           INPUT GEOMETRY?
490=    F       RPLANE          R-MARCHING?
500=    F       TAPER           RESTART DATA FROM TAPE?
510=    T       TAPEW           WRITE RESTART DATA ON UNIT 2 & 4?
520=    F       TAPEBW          WRITE SUBSONIC RESTART DATA ON UNIT 8?
530=    T       FORCE           CALCULATE FORCES?
540=   10                       GRID REGION TERMINAL K,5I5;ISC1+ISC2-1+..+ISCN
550=    0.        00.0       00.0       00.0        POLAR ANGLE-DEG;5F10.4
560=100.      150.     200.     250.     300.     350.     FLOW FIELD OUTPUT ZTA
570=    3        ISC                                NO. GEOM. SEGMENTS
580=    8     10   15                               NO. MESH PTS/SEGMENT
590=    0                       NAJS
```

a) Region 1

```
100=   125      NMAX    I5     NO. OF AXIAL STEPS
110=    15      JMAX           MESH PTS IN NORMAL DIR.<26
120=    57      KMAX           MESH PTS IN CIRCUM DIR;ISC1+ISC2-1+..+ISC6+1<81
130=     2      NRM            NO. GRID REGIONS<7;B&WB-2,WBV-3,WBNV-5
140=    13      NU0            SECOND SHARP EDGE K.
150=     2      NP             OUTPUT FOR EVERY NP STEPS.
160=    28      KWKST          WAKE START K;ISC1+ISC2-1...+ISC5
170=    47      KWKED          WAKE END K;ISC1+ISC2-1+...+ISC7
180=    30      NCON           NO CONE STARTING SOL. STEPS.
190=    30      NITER          NO. OF GRID ITERATIONS.
200=     6      NSPTI          NO. OF ZTA FOR FLOW FIELD OUTPUT.
210=     1      ITERGE         NO. OF GLOB ITERATION.
220=   5.0      CFLIN   F10.5  CFL NUMBER.
230=   2.5      DZTAIN         IF>0 FIXED STEP SIZE.IF<0 CFL NO.
240=   3.0      DZMAX          MAX. AXIAL STEP SIZE
250=   1.0      DZMIN          MIN. AXIAL STEP SIZE
260=   1.6      FSM            FREE STREAM MACH NO.
270=   4.46     ALFA           ANGLE OF ATTACK-DEG.
280=    60.     THTO           OUTER BOUNDARY-DEG.
290=   0.1      DETA           STEP SIZE IN ETA DIR.
300=   0.1      DXI            STEP SIZE IN XI DIR.
310=     1.5    DZTA           FIRST STEP AFTER CONE START. SOL.
320= 371.0      ZTA1           STARTING ZTA.
330= 611.0      XEND           END ZTA<MAX INPUT ZTA-DZTAIN.
340=   1.       AMU1           1:FIRST ORDER,2:2ND ORDER.
350=   0.       AMU2           0:FIRST ORDER,1:2ND ORDER.
360=  614.      XWAKE          WAKE MINIMUM ZTA.
370=  117.      ZWAKE          WAKE MINIMUM Z.
380=     1.0    CHL            GEOMETRY SCALE FACTOR
390=    85.0    PTNOSE         AXIAL GEOMETRY SHIFT FOR ZTA>0.
400=    0.0     YSHIFT         VERTICAL GEOMETRY SHIFT
410=  500.      X0             AXIAL C.G. ZTA.
420=    0.      Y0             VERTICAL C.G.
430=125280.     AAA            REFERENCE AREA.
440=234.627     ALL            REFERENCE LENGTH.
450=    1.75    OMEGA          RELAXIATION FACTOR.
460=     T      PLANEOS        PLANE OF SYM.?
470=     T      NUGRID         GENERATE GRID?
480=     T      IREAD          INPUT GEOMETRY?
490=     F      RPLANE         R-MARCHING?
500=     T      TAPER          RESTART DATA FROM TAPE?
510=     T      TAPEW          WRITE RESTART DATA ON UNIT 2 & 4?
520=     F      TAPE8W         WRITE SUBSONIC RESTART DATA ON UNIT 8?
530=     T      FORCE          CALCULATE FORCES?
540=    32    00    00    00   GRID REGION TERMINAL K,5I5;ISC1+ISC2-1+..+ISCN
550=     0.0      0.00       00.0       00.0     "     POLAR ANGLE;5F10.4
560=400.     450.     500.     550.     575.     600.    FLOW FIELD OUTPUT ZTA
570=     6        ISC                                  NO. GEOM. SEGMENTS
580=    04    05    10    15    15    11               NO. MESH PTS/SEGMENT
590=     0                    NAJS
```

b) Region 2

ORIGINAL PAGE IS
OF POOR QUALITY

TABLE II CONTINUED

ORIGINAL PAGE IS OF POOR QUALITY

```
100=   50       NMAX    I5       NO. OF AXIAL STEPS
110=   15       JMAX             MESH PTS IN NORMAL DIR.<26
120=   63       KMAX             MESH PTS IN CIRCUM DIR;ISC1+ISC2-1+..+ISC8+1<81
130=    3       NRM              NO. GRID REGIONS<7;B&WB-2,WBV-3,WBNV-5
140=   21       NUB              TAIL EDGE K;ISC1+ISC2-1+...+ISC4
150=    2       NP               OUTPUT FOR EVERY NP STEPS
160=   24       KWKST            WAKE START K;ISC1+ISC2-1+...+ISC5
170=   52       KWKED            WAKE END K;ISC1+ISC2-1+...+ISC7
180=   30       NCON             NO. CONE STARTING SOL. STEPS.
190=   30       NITER            NO. OF GRID ITERATIONS.
200=    3       NSPTI            NO. OF ZTA FOR FLOW FIELD OUTPUT.
210=    1       ITERGE           NO. OF GLOB ITERATION.
220=  5.0       CFLIN   F10.5    CFL NUMBER.
230=  2.5       DZTAIN           IF>0 FIXED STEP SIZE.IF<0 CFL NO.
240=  3.0       DZMAX            MAX. AXIAL STEP SIZE
250=  1.0       DZMIN            MIN. AXIAL STEP SIZE
260=  1.6       FSM              FREE STREAM MACH NO.
270=  4.46      ALFA             ANGLE OF ATTACK-DEG.
280=   60.      THTO             OUTER BOUNDARY-DEG.
290=  0.1       DETA             STEP SIZE IN ETA DIR.
300=  0.1       DXI              STEP SIZE IN XI DIR.
310=    1.5     DZTA             FIRST STEP AFTER CONE START. SOL.
320= 611.0      ZTA1             STARTING ZTA.
330= 685.0      XEND             END ZTA<MAX INPUT ZTA-DZTAIN.
340=   1.       AMU1             1:FIRST ORDER,2:2ND ORDER.
350=   0.       AMU2             0:FIRST ORDER,1:2ND ORDER.
360=  614.      XWAKE            WAKE MINIMUM ZTA.
370=  117.      ZWAKE            WAKE MINIMUM Z.
380=     1.0    CHL              GEOMETRY SCALE FACTOR
390=    85.0    PTNOSE           AXIAL GEOMRTRY SHIFT FOR ZTA>0.
400=    0.0     YSHIFT           VERTICAL GEOMETRY SHIFT.
410=  500.      XO               AXIAL C.G. ZTA.
420=    0.      YO               VERTICAL C.G.
430=125280.     AAA              REFERENCE AREA
440=234.627     ALL              REFERENCE LENGTH.
450=   1.75     OMEGA            RELAXATION FACTOR.
460=    T       PLANEOS          PLANE OF SYM.?
470=    T       NUGRID           GENERATE GRID?
480=    T       IREAD            INPUT GEOMETRY?
490=    F       RPLANE           R-MARCHING?
500=    T       TAPER            RESTART DATA FROM TAPE?
510=    T       TAPEW            WRITE RESTART DATA ON UNIT 2 & 4?
520=    F       TAPEBW           WRITE SUBSCNIC RESTART DATA ON UNIT 8?
530=    T       FORCE            CALCULATE FORCES?
540=   21    30    00    00      GRID REGICN TERMINAL K,5I5;ISC1+ISC2-1+..+ISCN
550=   70.0         0.00        00.0       00.0   "       POLAR ANGLE;5F10.4
560=625.        650.     675.                            FLOW FIELD OUTPUT ZTA
570=    8        ISC                                     NO. GEOM. SEGMENTS
580=   04    05    10    04    04   15    15    11       NO. MESH PTS/SEGMENT
590=    0                            NAJS
```

c) Region 3, Solution 1

TABLE II COMPLETED

ORIGINAL PAGE IS
OF POOR QUALITY

```
100=    75        NMAX    I5       NO. OF STEP
110=    15        JMAX             MESH PTS IN.NORMAL DIR.<26
120=    60        KMAX             MESH PTS IN CIRCUM DIR;ISC1+ISC2-1+..+ISC8+1<81
130=     3        NRM              NO. GRID REGIONS<7;B&WB-2,WBV-3,WBNV-5
140=    24        NU0              TAIL EDGE K;ISC1+ISC2-1+...+ISC4
150=     2        NP               OUTPUT FOR EVERY NP STEPS
160=    30        KWKST            WAKE START K;ISC1+ISC2-1+...+ISC5
170=    58        KWKED            WAKE END K;ISC1+ISC2-1+...+ISC7
180=    30        NCON             NO. CONE STARTING SOL. STEPS.
190=    30        NITER            NO. GRID OF ITERATIONS.
200=     5        NSPTI            NO. OF ZTA FOR FLOW FIELD OUTPUT.
210=     1        ITERGE           NO. OF GLOB ITERATION.
220=   5.0        CFLIN   F10.5    CFL NUMBER.
230=   2.5        DZTAIN           IF>0 FIXED STEP SIZE.IF<0 CFL NO.
240=   3.0        DZMAX            MAX. AXIAL STEP SIZE
250=   1.0        DZMIN            MIN. AXIAL STEP SIZE
260=   1.6        FSM              FREE STREAM MACH NO.
270=   4.46       ALFA             ANGLE OF ATTACK-DEG.
280=    60.       THTO             OUTER BOUNDARY-DEG.
290=   0.1        DETA             STEP SIZE IN ETA DIR.
300=   0.1        DXI              STEP SIZE IN XI DIR.
310=    1.5       DZTA             FIRST STEP AFTER CONE START. SOL.
320= 685.0        ZTA1             STARTING ZTA.
330= 804.0        XEND             END ZTA<MAX INPUT ZTA-DZTAIN.
340=    1.        AMU1             1:FIRST ORDER,2:2ND ORDER.
350=    0.        AMU2             0:FIRST ORDER,1:2ND ORDER.
360=  614.        XWAKE            WAKE MINIMUM ZTA.
370=  117.        ZWAKE            WAKE MINIMUM Z.
380=     1.0      CHL              GEOMETRY SCALE FACTOR
390=    85.0      PTNOSE           AXIAL GEOMETRY SHIFT FOR ZTA>0.
400=   0.0        YSHIFT           VERTICAL GEOMETRY SHIFT.
410=  500.        XO               AXIAL C.G. ZTA.
420=    0.        YO               VERTICAL C.G.
430=125280.       AAA              REFERENCE AREA
440=234.627       ALL              REFERENCE LENGTH.
450=    1.75      OMEGA            RELAXATION FACTOR.
460=     T        PLANEOS          PLANE OF SYM.?
470=     T        NUGRID           GENERATE GRID?
480=     T        IREAD            INPUT GEOMETRY?
490=     F        RPLANE           R-MARCHING?
500=     T        TAPER            RESTART DATA FROM TAPE?
510=     T        TAPEW            WRITE RESTART DATA ON UNIT 2 & 4?
520=     F        TAPE8W           WRITE SUBSONIC RESTART DATA ON UNIT 8?
530=     T        FORCE            CALCULATE FORCES?
540=    24   44    00    00        GRID REGION TERMINAL K,5I5:ISC1+ISC2-1+..+ISCN
550=    70.0        0.00       00.0      00.0                POLAR ANGLE;5F10.4
560=700.        725.      750.      775.      800.           FLOW FIELD OUTPUT ZTA
570=     8        ISC                                        NO. GEOM. SEGMENTS
580=    04   05    10     7     7   15    15   11            NO. MESH PTS/SEGMENT
590=     1   04    04    05    04NAJS,NPTCHA,NODPTA,NPTCHB,NODPTB
```

d) Region 3, Solution 2

UPDATE FILE DATA

The purpose of this data is to define specialized information logic which has not been incorporated into the pilot code. It is anticipated that this type of input will be progressively eliminated as a production status evolves.

Two basic update files (see table III) are typically used. One for a standard (i.e. geometry) restart and a second for a wake restart. The former defines certain potential averaging, leading edge mesh, nacelle directives, etc. In addition, the wake restart file describes the vorticity distribution which is output by the prior (for the present case the third) solution.

The update files also contain modifications to the pilot code which have not been incorporated permanently. These directives do not need to be changed (but must be included) for a new problem.

TABLE III UPDATE FILE DIRECTIVES

```
*IDENT HRDWIRE
*I MAIN.14
C        TAPE9: OUTPUT PRESSURE DISTRIBUTIONS AT SPECIFIED Z
*D MAIN.55,MAIN.72
C
C     RESTART DIRECTIVE;KWAK=1-SOLID BOUNDARY,=2-WAKE
C
       KWAK=1
*D INVSETA.175,INVSETA.176
C     AVERAGE PHI AT MAX Z
        IF(ZTA1 .LT. 371.0 ) PHI(1,2,KTEMP)=
      *(PHI(1,2,KTEMP+1)+PHI(1,2,KTEMP-1))/2.0
*D NFORCE.151
   18 FORMAT (2X,'PITCH MOMENT=',E12.4,3X,'CM=',E12.4,
*D INPUT.27
       DO 10 NAA=1,50
*D METRIC.51,METRIC.52
C     CONST.FOR ZTA1 SHOULD BE CHANGE AT VERY THIN,SHARP
C     LEADING EDGE USING METRIC 56-79
*EOF
```

a) Region 1

```
*IDENT HRDWIRE
*I MAIN.14
C        TAPE9: OUTPUT PRESSURE DISTRIBUTIONS AT SPECIFIED Z
*D MAIN.55,MAIN.72
C
C     RESTART DIRECTIVE:KWAK=1-SOLID BOUNDARY,=2-WAKE
C
       KWAK=1
*D NFORCE.151
   18 FORMAT (2X,'PITCH MOMENT=',E12.4,3X,'CM=',E12.4,
*D GEOM.175
C     INCREASE NO. OF MESH POINTS IN WING L.E. REGION
       DS=SSS/(NPT(IS)*3.5)
*D GEOM.186
C     INCREASE NO. OF MESH POINTS IN WING L.E. REGION
       DS=SSS/(AD*3.5)
*D INPUT.27
       DO 10 NAA=1,50
*D METRIC.51,METRIC.52
C     CONST.FOR ZTA1 SHOULD BE CHANGE AT VERY THIN,SHARP
C     LEADING EDGE USING METRIC 56-79
*EOF
```

b) Region 2

```
*IDENT HRDWIRE
*I MAIN.14
C        TAPE9: OUTPUT PRESSURE DISTRIBUTIONS AT SPECIFIED Z
*D MAIN.55,MAIN.72
C**
C**  RESTART DIRECTIVE;KWAK=1-SOLID BOUNDARY,=2-WAKE
C**
       KWAK=1
*D MAIN.308
C     DEFINE WING T.E. EQUATION
       ZWAKE1=1.8622*ZTA1-1026.53
*D MAIN.315,MAIN.316
C     SPECIFY MAXIMUM WAKE Z(I.E. WING HALF SPAN)
       IF (ZWAKE1 .GT. 306.53) KWKST1=KTEMP
       IF (ZWAKE1 .GT. 306.53) GO TO 54
*D MAIN.360,MAIN.361
C     OUTPUT VORTICITY FOR WAKE RESTART
       IF (NI .NE. 29) GO TO 130
*D INVSETA.175,INVSETA.176
C     AVERAGE PHI AT OR NEAR WING TIP
       IF(ZTA1 .GT. 645.0 .AND. ZTA1 .LT. 717.0) PHI(1,2,KTEMP)=
      *(PHI(1,2,KTEMP+1)+PHI(1,2,KTEMP-1))/2.0
       IF(ZTA1 .GT. 645.0 .AND. ZTA1 .LT. 717.0) PHI(1,2,KTEMP+1)=
      *(PHI(1,2,KTEMP)+PHI(1,2,KTEMP+2))/2.0
*D NFORCE.151
   18 FORMAT (2X,'PITCH MOMENT=',E12.4,3X,'CM=',E12.4,
*D GEOM.175
C     INCREASE NO. OF MESH POINTS IN WING L.E. REGION
       DS=SSS/(NPT(IS)*3.5)
*D GEOM.186
C     INCREASE NO. OF MESH POINTS IN WING L.E. REGION
       DS=SSS/(AD*3.5)
*D INPUT.27
       DO 10 NAA=1,50
*D METRIC.51,METRIC.52
C     CONST.FOR ZTA1 SHOULD BE CHANGE AT VERY THIN,SHARP
C     LEADING EDGE USING METRIC 56-79
*EOF
```

ORIGINAL PAGE IS
OF POOR QUALITY

c) Region 3, Solution 1

TABLE III COMPLETED

```
*IDENT HROWIRE
*I MAIN.14
C       TAPE9: OUTPUT PRESSURE DISTRIBUTIONS AT SPECIFIED Z
*D MAIN.55,MAIN.72
C
C    RESTART DIRECTIVE;KWAK=1-SOLID BOUNDARY,=2-WAKE
C    KWED1-MAX U.S. WAKE K; KWKST1-MIN L.S. WAKE K
C    D703-15A 55 DEG W.T. MODEL DESIGN;M=1.6,ALPHA=4.46
C    USE NACELLE OFF FILE 055C,ITER=20 WITH REINDEXED K
C
      KWAK=2
      KWED1=36
      KWKST1=52
      VORT(30)=28.51
      VORT(31)=28.27
      VORT(32)=27.52
      VORT(33)=27.49
      VORT(34)=26.03
      VORT(35)=23.31
      VORT(36)=19.83
      VORT(52)=-19.84
      VORT(53)=-23.31
      VORT(54)=-26.04
      VORT(55)=-27.49
      VORT(56)=-27.52
      VORT(57)=-28.57
      VORT(58)=-28.82
*D MAIN.308
C    DEFINE WING T.E. EQUATION
      ZWAKE1=1.8622*ZTA1-1026.53
*D MAIN.315,MAIN.316
C    SPECIFY MAXIMUM WAKE Z(I.E. WING HALF SPAN)
      IF (ZWAKE1 .GT. 306.53) KWKST1=KTEMP
      IF (ZWAKE1 .GT. 306.53) GO TO 54
*D MAIN.360,MAIN.361
C    OUTPUT VORTICITY FOR WAKE RESTART
      IF (NI .NE. 48) GO TO 138
*D INVSETA.175,INVSETA.176
C    AVERAGE PHI AT OR NEAR WING TIP
      IF(ZTA1 .GT. 648.0 .AND. ZTA1 .LT. 717.0) PHI(1,2,KTEMP)=
     *(PHI(1,2,KTEMP+1)+PHI(1,2,KTEMP-1))/2.0
      IF(ZTA1 .GT. 648.0 .AND. ZTA1 .LT. 717.0) PHI(1,2,KTEMP+1)=
     *(PHI(1,2,KTEMP)+PHI(1,2,KTEMP+2))/2.0
C    AVERAGE PHI AT OR NEAR VERTICAL TIP
      IF(ZTA1 .GT. 760.) PHI(1,2,24)=(PHI(1,2,23)+PHI(1,2,25))/2.
      IF(ZTA1 .GT. 760.) PHI(1,2,25)=PHI(1,2,24)
*D NFORCE.151
   18 FORMAT (2X,'PITCH MOMENT=',E12.4,3X,'CM=',E12.4,
*D GRID.133
C    INCREASE GRID CELL AREA IN VERTICAL/WAKE CORNER
      FAC1=.75
*I GRID.162
C    CONVERGE MORE SLOWLY TO AVOID GRID DIVERGANCE
      IF(NN .EQ. 1) OP=.005
      IF(NN .GE. 2) OP=.01
*D INPUT.27
      DO 18 NAA=1,50
*D METRIC.51,METRIC.52
C    CONST.FOR ZTA1 SHOULD BE CHANGE AT VERY THIN,SHARP
C    LEADING EDGE USING METRIC 56-70
*EOF
```

d) Region 3, Solution 2

JOB CONTROL

The final type of information required to process a problem is program/update and input/output file declarations. These directives change from solution to solution in order to properly process and save data.

The pertinent submit files for the CDC 875 under NOS Operating System 2.1 are presented on table IV for the sample problem. The file functions are:

TAPE 1: Last X Plot Data
TAPE 2: Output Marching Plane Restart Data
TAPE 3: Input Marching Plane Restart Data
TAPE 4: Output Marching Plane Restart Data Backup
TAPE 5: Input Data
TAPE 7: Input Subsonic Region Data: 30 Step Limit
TAPE 8: Output Subsonic Region Data: 30 Step Limit
TAPE 9: Output Pressure Distribution at Specified Z for Post Processor

TABLE IV SAMPLE JOB CONTROL DIRECTIVES

ORIGINAL PAGE IS OF POOR QUALITY

```
100=S55A,EC700,T300,P3.
110=USER,D0236,XXXXXX.
120=CHARGE,*011,XXXX.
130=ACCT(BONNER     ST18422401*011XXXX)
140=RFL,EC=700.
150=ATTACH,OLDPL=SFP7PL/UN=D0835.
160=GET,INP=U55A.
170=UPDATE,I=INP.
180=FTN5,I,OPT=2,LCM=I,L=0,PL=20000.
190=ATTACH,TAPE5=AT55A.
200=PURGE,PL55A/NA.
210=DEFINE,TAPE1=PL55A.
220=PURGE,R55A1/NA.
230=DEFINE,TAPE2=R55A1.
240=PURGE,R55A2/NA.
250=DEFINE,TAPE4=R55A2.
260=PURGE,P55/NA.
270=DEFINE,TAPE9=P55.
280=ATTACH,LIB1=SFP7LGO/UN=D0835.
290=COPYL,LIB1,LGO,LGO1.
300=LGO1.
310=*EOF
```

a) Region 1

```
100=S55B,EC700,T500,P3.
110=USER,D0236,XXXXXX.
120=CHARGE,*011,XXXX.
130=ACCT(BONNER     ST18422401*011XXXX)
140=RFL,EC=700.
150=ATTACH,OLDPL=SFP7PL/UN=D0835.
160=GET,INP=U55B.
170=UPDATE,I=INP.
180=FTN5,I,OPT=2,LCM=I,L=0,PL=20000.
190=ATTACH,TAPE5=AT55B.
200=ATTACH,TAPE3=R55A1.
210=PURGE,PL55B/NA.
220=DEFINE,TAPE1=PL55B.
230=PURGE,R55B1/NA.
240=DEFINE,TAPE2=R55B1.
250=PURGE,R55B2/NA.
260=DEFINE,TAPE4=R55B2.
270=ATTACH,TAPE9=P55/M=A.
280=SKIPEI,TAPE9.
290=ATTACH,LIB1=SFP7LGO/UN=D0835.
300=COPYL,LIB1,LGO,LGO1.
310=LGO1.
320=*EOF
```

b) Region 2

```
100=S55C,EC700,T200,P3.
110=USER,D0236,XXXXXX.
120=CHARGE,*011,XXXX.
130=ACCT(BONNER     ST18422401*011XXXX)
140=RFL,EC=700.
150=ATTACH,OLDPL=SFP7PL/UN=D0835.
160=GET,INP=U55C.
170=UPDATE,I=INP.
180=FTN5,I,OPT=2,LCM=I,L=0,PL=20000.
190=ATTACH,TAPE5=AT55C.
200=ATTACH,TAPE3=R55B1.
210=PURGE,PL55C/NA.
220=DEFINE,TAPE1=PL55C.
230=PURGE,R55C1/NA.
240=DEFINE,TAPE2=R55C1.
250=PURGE,R55C2/NA.
260=DEFINE,TAPE4=R55C2.
270=ATTACH,TAPE9=P55/M=A.
280=SKIPEI,TAPE9.
290=ATTACH,LIB1=SFP7LGO/UN=D0835.
300=COPYL,LIB1,LGO,LGO1.
310=LGO1.
320=*EOF
```

c) Region 3, Solution 1

```
100=S55D,EC700,T300,P3.
110=USER,D0236,XXXXXX.
120=CHARGE,*011,XXXX.
130=ACCT(BONNER     ST18422401*011XXXX)
140=RFL,EC=700.
150=ATTACH,OLDPL=SFP7PL/UN=D0835.
160=GET,INP=U55D.
170=UPDATE,I=INP.
180=FTN5,I,OPT=2,LCM=I,L=0,PL=20000.
190=ATTACH,TAPE5=AT55D.
200=ATTACH,TAPE3=R55C1.
210=PURGE,PL55D/NA.
220=DEFINE,TAPE1=PL55D.
230=PURGE,R55D1/NA.
240=DEFINE,TAPE2=R55D1.
250=PURGE,R55D2/NA.
260=DEFINE,TAPE4=R55D2.
270=ATTACH,TAPE9=P55/M=A.
280=SKIPEI,TAPE9.
290=ATTACH,LIB1=SFP7LGO/UN=D0835.
300=COPYL,LIB1,LGO,LGO1.
310=LGO1.
320=*EOF
```

d) Region 3, Solution 2

ANALYSIS

It is recommended that a general file nomenclature be developed prior to the analysis in order to achieve a consistent function/code/problem seven character descriptor. The following is provided as an example.

FUNCTION	FILE
Submit	Function Code Solutions SXYYYY A, B, C, D Case
Input	I
Sectional Plot	X
Restart	R
Printed Output	O
Pressure Plot	P

A review of the submit, header input, and update files should be completed before processing each solution. A check list which has been found to be useful in this regard is

SOLUTION	TAPE 5	UPDATES
Region 1	Taper=F NAJS=0	Modify as appropriate
Region 2	Taper=T	———
Region 3 Solution 1	NRM=3, NUØ KWST,KWKED, XWAKE	Main. 360, VORT (k) Output
Region 3 Solution 2	NAJS=1, etc	KWAK= 2, Reindex KWKED1,KWKST1, and VORT (k)

Typical problem (one Mach number and angle of attack) run time on the CDC 875 under OPT = 2 compilation is

SOLUTION	ZTA1	J	K	ITER	CPU-SEC	SEC/STEP
Region 1	0-370	15	33	172	121	.7
Region 2	370-455	15	57	34	60	1.76
Region 3	455-610	15	68	62	111	1.78
Region 4 Solution 1	610-685	15	74	30	79	2.65
Region 4 Solution 2	685-802.5	15	80	47	133	2.82
					504	

PRE-PROCESSOR

A pre-processor is available for evaluating input geometry and grid quality. It may be accessed and executed using

GET,SFPPLTX/UN=D0235

SFPPLTX,XPFN,DOXXX

The file XPFN is generated for ZTA1 by the supersonic full potential analysis as tape 1 when NMAX=0, TAPER=F.

Typical grid program prompt response is

```
get,sfppltx
/sfppltx,p4815c,d0096
   .1600E+01   .1590E+01   .6085E+03   20   51
IPLOT...IS
       =   2 FOR MACH NO. CONTOURS
       =   3 FOR PRESSURE CONTOURS
       =  10 FOR COMPUTATIONAL      GRID
       =  12 FOR MACH NO. PROFILES
       =  13 FOR PRESSURE PROFILES
-----+-----0-----+-----0-----+-----0-----+-----0
?    10
XMIN=  0.                 XMAX=   .94091865E+03
YMIN=  -.90619733E+03YMAX=   .88599023E+03
XMIN,XMAX,YMIN,YMAX...4F10.4
X  IS THE PLOTIS X COORDINATE
Y  IS THE PLOTIS Y COORDINATE
Y  IS THUS  MACH NO. FOR IPLOT=12
Y  IS THUS  PRESSURE FOR IPLOT=13
Y  IS OTHERWISE THE PHYSICAL Y COORDINATE
X IS ALWAYS THE PHYSICAL X COORDINATE
XMIN=  0.                 XMAX=   .94091865E+03
YMIN=  -.90619733E+03YMAX=   .88599023E+03
-----+-----0-----+-----0-----+-----0-----+-----0
XMIN=  0.                 XMAX=   .94091865E+03
YMIN=  -.90619733E+03YMAX=   .88599023E+03
? 0.       400.       -200.        200.
```


Typical output is shown below. The grid is truncated at Z=400 and Y=±200 as specified in the input above

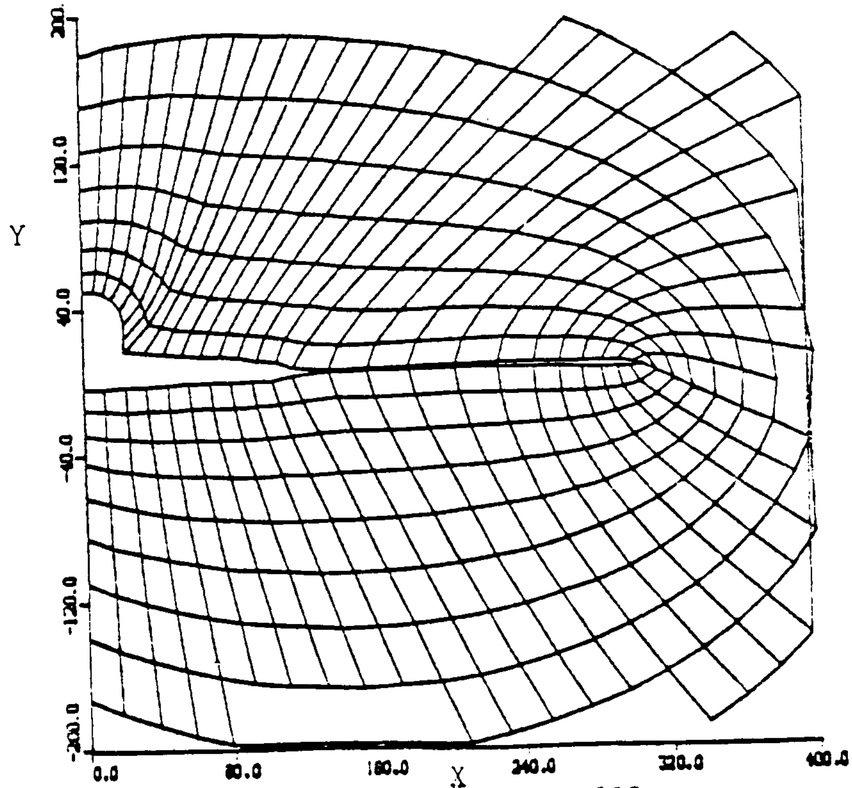

ORIGINAL PAGE IS
OF POOR QUALITY

OUTPUT DATA

Sample printed output data is presented on table V for region 3, solution 2. Standard tabulated data is produced every NP marching steps as defined in the header data. More detailed physical plane data can be output at specified stations using the parameter NSPTI and the tabulated stations following the true/false header data input. Cartesion coordinates, velocities, and mesh indices are indicated in the following sketch. The axial velocity component, U, is positive out of the plane of the paper.

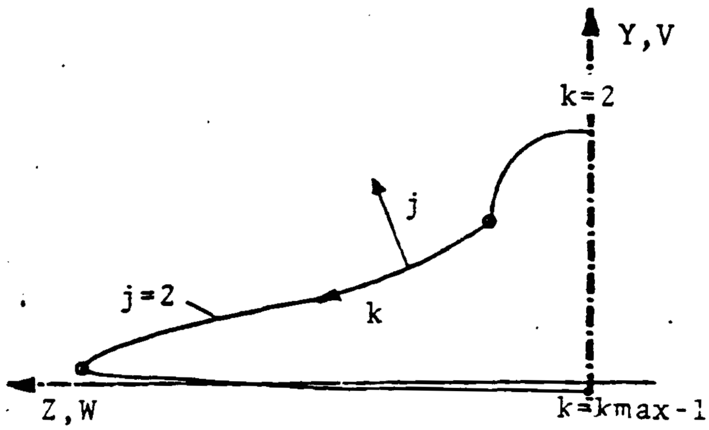

Crossplane data and tabulated surface pressure coefficient data at constant span stations (i.e. z) are output via tapes 1 and 9 respectively. These files are displayed using the pre and post processors described in this document.

TABLE V SAMPLE OUTPUT DATA

ITER= 5 (STEP) DZTA= 2.50000 ZTA1= 696.58838

J	K	RHO ρ/ρ_∞	CP C_p	PHI	U	V	W	X	Y	Z
					Contravariant Velocities					
2	1	.872616	-.096915	714.215315	I	I	I	696.588384	49.946005	-5.649278
2	2	.872623	-.096910	714.204622	1.050623	0.000000	0.000000	696.588384	50.007111	0.000000
2	3	.872616	-.096915	714.215315	1.050518	0.000000	.000071	696.588384	49.946005	5.649278
2	4	.873174	-.096503	714.248745	1.050269	0.000000	.000147	696.588384	48.830548	11.157859
2	5	.874366	-.095620	714.305288	1.049688	0.000000	.000251	696.588384	45.976709	16.013771
2	6	.872136	-.097271	714.504990	1.050287	0.000000	.000103	696.588384	38.523018	21.151141
2	7	.862499	-.104383	714.836467	1.053838	0.000000	-.000019	696.588384	29.496730	22.217937
2	8	.850378	-.113283	715.239224	1.058207	0.000000	-.000116	696.588384	20.360161	22.099892
2	9	.841292	-.119921	715.803286	1.060812	0.000000	-.000339	696.588384	11.222849	22.130118
2	10	.848717	-.114499	715.640282	1.057427	0.000000	-.000116	696.588384	10.635839	34.678301
2	11	.856343	-.108909	715.546134	1.054818	0.000000	-.000163	696.588384	10.167208	47.231016
2	12	.862010	-.104742	715.215639	1.051803	0.000000	-.000364	696.588384	9.980513	59.791822
2	13	.896769	-.078948	714.493998	1.036773	0.000000	-.000598	696.588384	9.546090	72.346230
2	14	.878214	-.092769	713.454512	1.044120	0.000000	-.000634	696.588384	9.033332	84.897888
2	15	.855106	-.109817	712.639572	1.055693	0.000000	-.000403	696.588384	8.453547	97.446525
2	16	.796150	-.152476	712.355240	1.079943	0.000000	-.000323	696.588384	7.656034	109.983178
2	17	.750268	-.184816	711.603647	1.098479	0.000000	-.001455	696.588384	19.543347	114.612843
2	18	.571523	-.303054	710.240655	1.178196	0.000000	-.002982	696.588384	34.426818	120.638436
2	19	.968568	-.024403	709.952537	1.011578	0.000000	-.004748	696.588384	46.562350	125.885400
2	20	1.384285	.321781	710.068083	.851226	0.000000	-.008015	696.588384	53.717897	129.188570
2	21	1.687214	.602611	709.537858	.731483	0.000000	-.009591	696.588384	58.456765	131.626700
2	22	1.203788	.165454	710.328615	.688019	0.000000	-.023466	696.588384	61.448687	133.958279
2	23	1.187687	.151942	708.419447	.856460	0.000000	.004271	696.588384	57.404383	133.773184
2	24	1.211263	.171750	707.036204	.905288	0.000000	.005404	696.588384	51.839495	132.488912
2	25	.938402	-.047523	706.321779	1.021979	0.000000	.003958	696.588384	43.679468	130.254218
2	26	.814356	-.139434	705.713319	1.074143	0.000000	.002269	696.588384	30.141000	126.154023
2	27	.747032	-.187067	706.033838	1.102131	0.000000	.001185	696.588384	13.793620	120.801278
2	28	.778193	-.165224	706.225323	1.088395	0.000000	.000573	696.588384	.867854	116.363281
2	29	1.040903	.032214	707.005377	.983751	.000066	.000109	696.588384	2.142344	140.624250
2	30	1.047007	.037067	707.509698	.981139	.000330	-.000188	696.588384	3.497559	166.660347
2	31	1.020956	.016441	706.811346	.989676	.000578	-.000335	696.588384	4.974130	195.631517
2	32	.997484	-.001964	705.783749	.998770	.000690	-.000321	696.588384	6.431195	224.529098
2	33	.905790	-.072188	705.017271	1.033382	.000656	-.000571	696.588384	7.684317	247.718921
2	34	.851733	-.112290	702.271370	1.052011	.000490	-.000891	696.588384	8.262393	264.931600
2	35	.358500	-.426312	701.901114	1.275561	0.000000	-.001226	696.588384	8.611518	278.402489
2	36	.387657	-.409959	698.161106	1.230990	0.000000	-.002962	696.588384	8.829093	289.487817
2	37	.549374	-.316780	694.830364	1.097994	0.000000	-.005217	696.588384	8.753903	298.793426
2	38	.457297	-.371424	690.329619	1.008294	0.000000	-.014518	696.588384	7.796446	306.528992
2	39	1.008353	.006537	688.484540	.978897	0.000000	-.002028	696.588384	7.459420	298.747500
2	40	1.072089	.057120	687.482653	.962986	0.000000	-.001175	696.588384	7.958001	289.456406
2	41	1.272637	.224039	686.206321	.885956	0.000000	-.001111	696.588384	8.007882	278.373004
2	42	.864753	-.102722	684.305635	1.051430	.000004	-.000468	696.588384	7.946608	264.900973
2	43	.908679	-.070017	684.290840	1.035219	-.000708	-.000280	696.588384	7.716527	247.684786
2	44	.998102	-.001482	683.209029	.998665	-.000577	-.000280	696.588384	6.419563	224.503204
2	45	1.020192	.015838	681.803950	.990154	-.000501	-.000267	696.588384	5.010471	195.610113
2	46	1.042044	.033121	680.575873	.982155	-.000397	-.000253	696.588384	3.548817	166.645427
2	47	1.031691	.024915	679.795940	.984745	-.000376	-.000346	696.588384	2.174109	140.616372
2	48	1.032494	.025550	677.918751	.985072	0.000000	-.000445	696.588384	.867854	116.363281
2	49	1.029608	.023267	677.213594	.987619	0.000000	-.000394	696.588384	.522167	101.820516
2	50	1.028351	.022274	676.758143	.988580	0.000000	-.000264	696.588384	.069392	87.274129
2	51	1.044217	.034847	676.523870	.982598	0.000000	-.000167	696.588384	-.411646	72.728332
2	52	1.047296	.037297	676.410182	.981438	0.000000	-.000115	696.588384	-.962648	58.179577
2	53	1.038723	.030485	676.318889	.984731	0.000000	-.000096	696.588384	-1.203779	43.640848
2	54	1.029345	.023060	676.204160	.988351	0.000000	-.000077	696.588384	-1.889275	29.10[illegible]01
2	55	1.026936	.021157	676.126533	.989269	0.000000	-.000042	696.588384	-2.116542	14.552648
2	56	1.027394	.021518	676.096079	.989098	0.000000	0.000000	696.588384	-2.257743	0.000000
2	57	1.026936	.021157	676.126533	I	I	I	696.588384	-2.116542	-14.552648

15	56	1.006286	.004917	652.950876	.994820	-.000576	0.000000	696.588384	-530.992758	0.000000
16	56	1.000046	.000036	645.388007	.996996	-.000649	0.000000	696.588384	-629.183474	0.000000
17	56	1.001168	.000913	636.587362	.996560	-.000719	0.000000	696.588384	-742.906384	0.000000
18	56	1.000015	.000011	626.447526	.997006	-.000793	0.000000	696.588384	-874.618431	0.000000
19	56	.998826	-.001073	614.629796	.997515	-.000871	0.000000	696.588384	-1027.165207	0.000000
20	56	1.000000	0.000000	600.864805	1	-.000983	1	696.588384	-1203.842432	0.000000

RMS DENSITY= .08857158

+++UPER SURFACE+++

			C_p	P/P_∞	
X=	.69659E+03	Z= 0.	CP= -.86910E-01	RHO= .87262E+00	IU= 1
X=	.69659E+03	Z= .30600E+02	CP= -.11826E+00	RHO= .84630E+00	IU= 2
X=	.69659E+03	Z= .61200E+02	CP= -.10188E+00	RHO= .86591E+00	IU= 3
X=	.69659E+03	Z= .91800E+02	CP= -.10215E+00	RHO= .86550E+00	IU= 4
X=	.69659E+03	Z= .12240E+03	CP= -.20914E+00	RHO= .70533E+00	IU= 5
X=	.69659E+03	Z= .15300E+03	CP= .34521E-01	RHO= .10438E+01	IU= 6
X=	.69659E+03	Z= .18360E+03	CP= .25006E-01	RHO= .10318E+01	IU= 7
X=	.69659E+03	Z= .21420E+03	CP= .46142E-02	RHO= .10059E+01	IU= 8
X=	.69659E+03	Z= .24480E+03	CP= -.63349E-01	RHO= .91733E+00	IU= 9
X=	.69659E+03	Z= .27540E+03	CP= -.35894E+00	RHO= .46844E+00	IU= 10
X=	.69659E+03	Z= .30693E+03	CP= -.37142E+00	RHO= .90433E+00	IU=

LEADING EDGE

SPECIFIED Z SURFACE PRESSURE COEFFICIENT

+++LOWER SURFACE+++

X=	.69659E+03	Z= 0.	CP= .21518E-01	RHO= .10274E+01	IU= 1
X=	.69659E+03	Z= .30600E+02	CP= .23824E-01	RHO= .10303E+01	IU= 2
X=	.69659E+03	Z= .61200E+02	CP= .36788E-01	RHO= .10467E+01	IU= 3
X=	.69659E+03	Z= .91800E+02	CP= .22583E-01	RHO= .10287E+01	IU= 4
X=	.69659E+03	Z= .12240E+03	CP= .25391E-01	RHO= .10323E+01	IU= 5
X=	.69659E+03	Z= .15300E+03	CP= .28819E-01	RHO= .10366E+01	IU= 6
X=	.69659E+03	Z= .18360E+03	CP= .23005E-01	RHO= .10293E+01	IU= 7
X=	.69659E+03	Z= .21420E+03	CP= .46942E-02	RHO= .10060E+01	IU= 8
X=	.69659E+03	Z= .24480E+03	CP= -.61488E-01	RHO= .91981E+00	IU= 9
X=	.69659E+03	Z= .27540E+03	CP= .15193E+00	RHO= .11826E+01	IU= 10

```
RMSR3=   .17218126E-01      NN=  312      NR3ITER=   2
RMSR3=   .16591918E-01      NN=  312      NR3ITER=   3
RMSR3=   .11200030E-04      NN=  312      NR3ITER=   4
 EIGENY=    .92064673E-01   CFLE=    .23016168E+01   EIGENZ=    .78797052E-01   CFLX=     .1970E+01   DZTA=     .2500E+01
KST,KED1,KST1,KED,KS,KE,KIA,KAWK     28    35    41    48    35    35     1     2
VORT,PHM,K        .16133E+02      .68830E+03    35
KST,KED1,KST1,KED,KS,KE,KIA,KAWK     28    35    41    48    41    41     2     2
VORT,PHM,K       -.16136E+02      .70444E+03    41
L= .31948E+06   D= .28019E+04   CL= .25501E+00   CD= .22365E-01   SURFACE A= .36979E+06   REF. A= .12828E+06
PITCH MOMENT=  -.4698E+06   CP=  -.1598E-01   XO=   .5000E+03   YO= 0.          .1545E+03    .1603E+05    .2346E+03
        FLOW FIELD AT ZTA=  699.0884
```

J	K	RHO P/P_∞	P P/P_∞	U-VEL U/V_∞	V-VEL V/V_∞	W-VEL W/V_∞	A T_∞/T_c	M	X	Y	Z
2	2	.8731E+00	.8270E+00	.1050E+01	.7814E-06	0.	.6083E+00	.1727E+01	.6991E+03	.5001E+02	0.
3	2	.8758E+00	.8306E+00	.1049E+01	-.1508E-01	0.	.6086E+00	.1724E+01	.6991E+03	.6383E+02	0.
4	2	.8764E+00	.8314E+00	.1049E+01	-.1420E-01	0.	.6087E+00	.1723E+01	.6991E+03	.7985E+02	0.
5	2	.8801E+00	.8362E+00	.1047E+01	-.9394E-02	0.	.6092E+00	.1719E+01	.6991E+03	.9845E+02	0.
6	2	.8890E+00	.8481E+00	.1044E+01	-.7727E-03	0.	.6106E+00	.1710E+01	.6991E+03	.1200E+03	0.
7	2	.8963E+00	.8579E+00	.1041E+01	.9083E-02	0.	.6115E+00	.1702E+01	.6991E+03	.1450E+03	0.
8	2	.9038E+00	.8679E+00	.1038E+01	.1903E-01	0.	.6125E+00	.1695E+01	.6991E+03	.1740E+03	0.
9	2	.9099E+00	.8762E+00	.1035E+01	.2816E-01	0.	.6133E+00	.1688E+01	.6991E+03	.2077E+03	0.
10	2	.9238E+00	.8950E+00	.1029E+01	.3802E-01	0.	.6152E+00	.1674E+01	.6991E+03	.2467E+03	0.
11	2	.9404E+00	.9175E 00	.1022E+01	.4930E-01	0.	.6174E+00	.1658E+01	.6991E+03	.2919E+03	0.
12	2	.9633E+00	.9490E+00	.1012E+01	.6413E-01	0.	.6203E+00	.1635E+01	.6991E+03	.3444E+03	0.

ORIGINAL PAGE IS OF POOR QUALITY

TABLE V CONCLUDED

```
 7 56  .1065E+01  .1092E+01  .9745E+00  .2535E-01  0.          .6329E+00  .1540E+01  .6991E+03  -.1020E+03  0.
 8 56  .1071E+01  .1101E+01  .9721E+00  .2646E-01  0.          .6336E+00  .1535E+01  .6991E+03  -.1323E+03  0.
 9 56  .1071E+01  .1101E+01  .9718E+00  .3007E-01  0.          .6337E+00  .1534E+01  .6991E+03  -.1675E+03  0.
10 56  .1061E+01  .1086E+01  .9756E+00  .3697E-01  0.          .6324E+00  .1544E+01  .6991E+03  -.2083E+03  0.
11 56  .1052E+01  .1074E+01  .9787E+00  .4351E-01  0.          .6314E+00  .1551E+01  .6991E+03  -.2555E+03  0.
12 56  .1051E+01  .1072E+01  .9790E+00  .4806E-01  0.          .6312E+00  .1553E+01  .6991E+03  -.3102E+03  0.
13 56  .1046E+01  .1065E+01  .9806E+00  .5437E-01  0.          .6307E+00  .1557E+01  .6991E+03  -.3736E+03  0.
14 56  .1028E+01  .1039E+01  .9872E+00  .6436E-01  0.          .6284E+00  .1574E+01  .6991E+03  -.4470E+03  0.
15 56  .1006E+01  .1009E+01  .9948E+00  .7363E-01  0.          .6258E+00  .1594E+01  .6991E+03  -.5321E+03  0.
16 56  .1000E+01  .1000E+01  .9970E+00  .7722E-01  0.          .6250E+00  .1600E+01  .6991E+03  -.6307E+03  0.
17 56  .1001E+01  .1002E+01  .9966E+00  .7717E-01  0.          .6251E+00  .1599E+01  .6991E+03  -.7449E+03  0.
18 56  .1000E+01  .1000E+01  .9970E+00  .7724E-01  0.          .6250E+00  .1600E+01  .6991E+03  -.8773E+03  0.
19 56  .9986E+00  .9980E+00  .9975E+00  .7771E-01  0.          .6248E+00  .1601E+01  .6991E+03  -.1031E+04  0.

    ITER=    6 ZTA1= 699.08838 DZTA1=    2.50000
RMSR3=  .23415121E-01     NN=  313     NR3ITER=    2
RMSR3=  .16881968E-01     NN=  313     NR3ITER=    3
RMSR3=  .92558456E-05     NN=  313     NR3ITER=    4
 EIGENY=   .21338727E+00  CFLE= cL .53346819E+01  EIGENZ=   .63246441E-01  CFLX=      .1581E+01  DZTA=      .2500E+01
 L= .32070E+05   D= .28180E+04   CL= .25599E+00   CD= .22494E-01   SURFACE A= .37196E+06   REF. A= .12528E+06   Sref
 PITCH MOMENT=  -.4946E+06   CP= -.1683E-01   XO= CD .5000E+03   YO= 0           .1578E+03   .1610E+05   .2346E+03
                              CM

    ITER=    7 ZTA1= 701.58838 DZTA1=    2.50000
RMSR3=  .16894983E-01     NN=  314     NR3ITER=    2
RMSR3=  .19344000E-01     NN=  314     NR3ITER=    3
RMSR3=  .17461672E-04     NN=  314     NR3ITER=    4
    COMPLEX EIGEN VALUE  J=    2  K=   22  NN=  314  Q2ETA=   .20812154E-04  Q2XI=  -.32109857E-04
 EIGENY=   .24856313E-01  CFLE=   .62140783E+00  EIGENZ=   .42286298E-01  CFLX=      .1057E+01  DZTA=      .2500E+01
 L= .32201E+05   D= .28350E+04   CL= .25703E+00   CD= .22629E-01   SURFACE A= .37414E+06   REF. A= .12528E+06
 PITCH MOMENT=  -.5214E+06   CP=  -.1774E-01   XO=   .5000E+03   YO= 0.           .1612E+03   .1616E+05   .2346E+03

    ITER=    8 ZTA1= 704.08838 DZTA1=    2.50000
RMSR3=  .19873105E-01     NN=  315     NR3ITER=    2
RMSR3=  .19259946E-01     NN=  315     NR3ITER=    3
RMSR3=  .16920610E-04     NN=  315     NR3ITER=    4
    COMPLEX EIGEN VALUE  J=    2  K=   22  NN=  315  Q2ETA=   .10570612E-04  Q2XI=  -.74477587E-03
 EIGENY=   .18347013E-01  CFLE=   .46867532E+00  EIGENZ=   .29677634E-01  CFLX=      .7419E+00  DZTA=      .2500E+01
 KST,KED1,KST1,KED,KS,KE,KIA,KAWK   28   36   40   48   36   36    1    2
 VORT,PHM,K     .14187E+02     .69610E+03    36
 KST,KED1,KST1,KED,KS,KE,KIA,KAWK   28   36   40   48   40   40    2    2
 VORT,PHM,K    -.14187E+02     .71029E+03    40
 L= .32302E+05   D= .28506E+04   CL= .25784E+00   CD= .22754E-01   SURFACE A= .37624E+06   REF. A= .12528E+06
 PITCH MOMENT=  -.5426E+06   CP=  -.1846E-01   XO=   .5000E+03   YO= 0.           .1650E+03   .1621E+05   .2346E+03

    ITER=    9 ZTA1= 706.58838 DZTA1=    2.50000
RMSR3=  .24927362E-01     NN=  316     NR3ITER=    2
RMSR3=  .19872039E-01     NN=  316     NR3ITER=    3
RMSR3=  .20722912E-04     NN=  316     NR3ITER=    4
    COMPLEX EIGEN VALUE  J=    2  K=   22  NN=  316  Q2ETA=   .10124578E-04  Q2XI=  -.78430692E-03
 EIGENY=   .15843887E-01  CFLE=   .39609718E+00  EIGENZ=   .23966680E-01  CFLX=      .5992E+00  DZTA=      .2500E+01
 L= .32412E+05   D= .28674E+04   CL= .25872E+00   CD= .22888E-01   SURFACE A= .37835E+06   REF. A= .12528E+06
 PITCH MOMENT=  -.5658E+06   CP=  -.1925E-01   XO=   .5000E+03   YO= 0.           .1691E+03   .1627E+05   .2346E+03
        +++++RESTART DATA WRITE ON UNIT  4+++++
```

POST PROCESSOR

A graphics geometry and surface pressure coefficient output processor for the Techtronix 4114 has been recently developed to support advance design effort using the supersonic full potential analysis. It may accessed and executed using

```
GET,SFPPLT/UN=D0235
SFPPLT,FPIN,FPOUT,DOXXX
```

The pertinent files are

NAME	TYPE	DESCRIPTION
SFPPLT	ID	Proc for Post Processor
FPIN	DA	SFP Output Data Set ≤ 5 Characters. UN=DOXXX
FPOUT	DA	Created to Store Post Processor Output for Debug if necessary.

The input file FPIN is generated by supersonic full potential analysis as tape 9 output. This file must be edited as follows:

1. Delete *EOR's and repetitious results.
2. Delete cone starting solution off front end.
3. Add the following data at the beginning.

    (a) Title Card
    (b) Mach Number and Angle of Attack. One card, format 2E12.5.
    (c) Number of trailing edge points. One card, format I3.
    (d) Planform trailing edge data. Input trailing edge X from root to tip, for each section stored in FPIN. Format 5E12.5

4. Check end of data set to make sure the last x-station is fully represented. If it is not, (examine previous x-station to see a fully represented example) delete these incomplete data.

5. If you do not want a particular z-value (3rd column) to be included in the data you will process, delete any reference to such data out of the 3rd column at the very end of the data set.

Sample graphics post processor input data is presented on Table VI.

The following nine post processor options are available to the analyst.

```
0  TO END
1  TO DISPLAY PLANFORM
2  TO DISPLAY 3-D VIEW OF WING Z/C
3  TO DISPLAY 3-D VIEW OF WING CP S
4  TO DISPLAY SECTION      CP S
5  TO DISPLAY SECTION      Z/C
6  TO DISPLAY SPANWISE     CL,CD,XCP
7  TO DISPLAY PLANFORM     ISOBARS
8  TO CREATE  BOUNDARY LAYER DATA FILE
```

The last creates a boundary layer analysis[4] input file FPINBL for the upper and lower surface. This data must be edited to remove the first STOP card, update case identification, static pressure and temperature, and specified transition point location.

TABLE VI POST PROCESSOR INPUT FILE STRUCTURE

ADDED HEADER DATA

```
100= D703-15A 55 DEG SWEEP MAN. POINT DESIGN DERIVATIVE
110=    .1600E+01    .4460E+01
120= 21
130=    .8000E+03    .8000E+03    .8000E+03    .8000E+03    .8000E+03
140=    .8000E+03    .8000E+03    .8000E+03    .6171E+03    .6253E+03
150=    .6336E+03    .6418E+03    .6500E+03    .6582E+03    .6665E+03
160=    .6747E+03    .6829E+03    .6912E+03    .6994E+03    .7076E+03
170=    .7159E+03
180=    .1500E+02    .6292E+01    .0000E+00    .3742E+00
190=    .1502E+02    .2716E+01    .6324E-01    .3653E+00
200=    .1500E+02   -.4622E+00    .0000E+00    .1749E+00
210=    .2000E+02    .7861E+01    .0000E+00    .1507E+00
220=    .2000E+02    .3140E+01    .8300E-01    .1317E+00
230=    .2000E+02   -.1865E+01    .0000E+00    .2620E+00
240=    .2500E+02    .9271E+01    .0000E+00   -.1004E+00
250=    .2500E+02    .3631E+01    .9502E-01   -.5543E-01
260=    .2500E+02   -.1349E+01    .0000E+00    .7038E-01
270=    .3000E+02    .1068E+02    .0000E+00    .4053E-01
280=    .3000E+02    .4124E+01    .1076E+02    .6044E-02
290=    .3000E+02   -.1624E+01    .0000E+00    .7075E-01
300=    .3500E+02    .1200E+02    .0000E+00    .8464E-01
310=    .3500E+02    .4618E+01    .1192E+02    .1335E+00
320=    .3500E+02   -.1898E+01    .0000E+00    .8600E-01
330=    .4000E+02    .1348E+02    .0000E+00    .1205E+00
340=    .4000E+02    .5111E+01    .1300E+02    .2104E+00
350=    .4000E+02   -.2172E+01    .0000E+00    .8487E-01
360=    .4500E+02    .1487E+02    .0000E+00    .1579E+00
370=    .4500E+02    .5694E+01    .1300E+02    .7023E-01
380=    .4500E+02   -.2246E+01    .0000E+00    .6772E-02
390=    .5000E+02    .1625E+02    .0000E+00    .1763E+00
400=    .5000E+02    .6283E+01    .1467E+02    .7004E-01
410=    .5000E+02   -.2306E+01    .0000E+00    .1026E-01
420=    .5500E+02    .1763E+02    .0000E+00    .1664E+00
430=    .5500E+02    .8039E+01    .1533E+02    .8650E-01
440=    .5500E+02    .6872E+01    .1545E+02    .8729E-01
450=    .5500E+02   -.2367E+01    .0000E+00    .1621E-01
460=    .5500E+02    .5044E+01    .1533E+02    .8118E-01
470=    .6000E+02    .1900E+02    .0000E+00    .1563E+00
480=    .6000E+02    .1176E+02    .1533E+02    .1196E+00
490=    .6000E+02    .7462E+01    .1622E+02    .9695E-01
500=    .6000E+02   -.2427E+01    .0000E+00    .2764E-01
510=    .6000E+02    .3186E+01    .1533E+02    .7560E-01
520=    .6500E+02    .2032E+02    .0000E+00    .1271E+00
530=    .6500E+02    .1366E+02    .1533E+02    .7140E-01
540=    .6500E+02    .8044E+01    .1682E+02    .3206E-01
550=    .6500E+02   -.2363E+01    .0000E+00   -.4580E-02
560=    .6500E+02    .2674E+01    .1533E+02    .1547E-01
570=    .7000E+02    .2164E+02    .0000E+00    .1267E+00
580=    .7000E+02    .1548E+02    .1533E+02    .8662E-01
590=    .7000E+02    .8625E+01    .1730E+02    .4700E-01
600=    .7000E+02   -.2285E+01    .0000E+00    .1104E-01
```

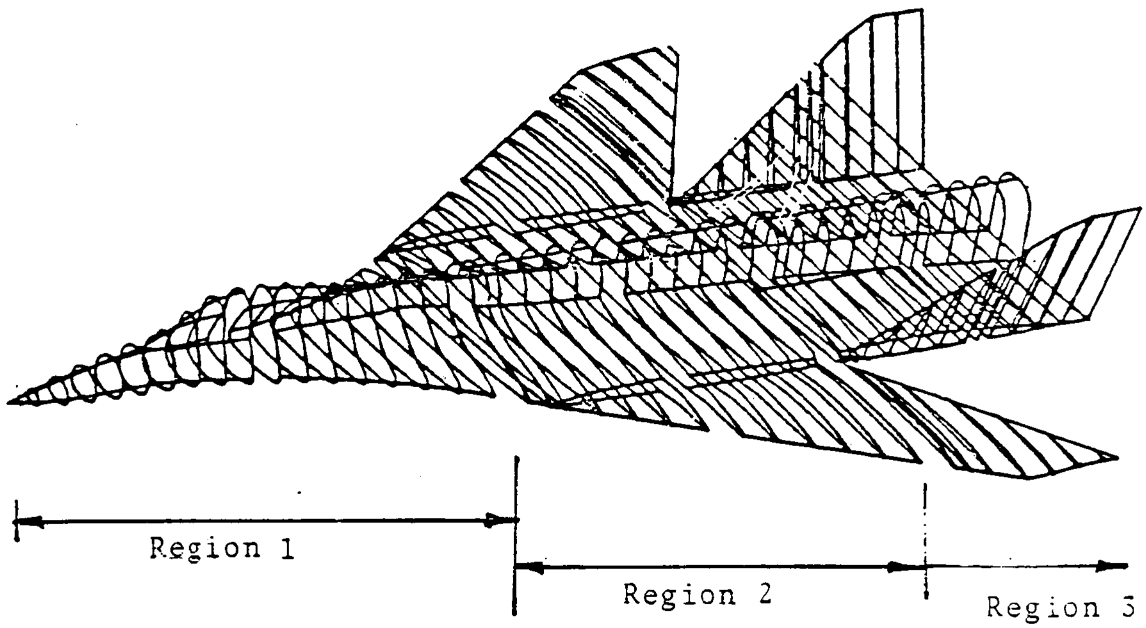

Figure 1. Sample Problem

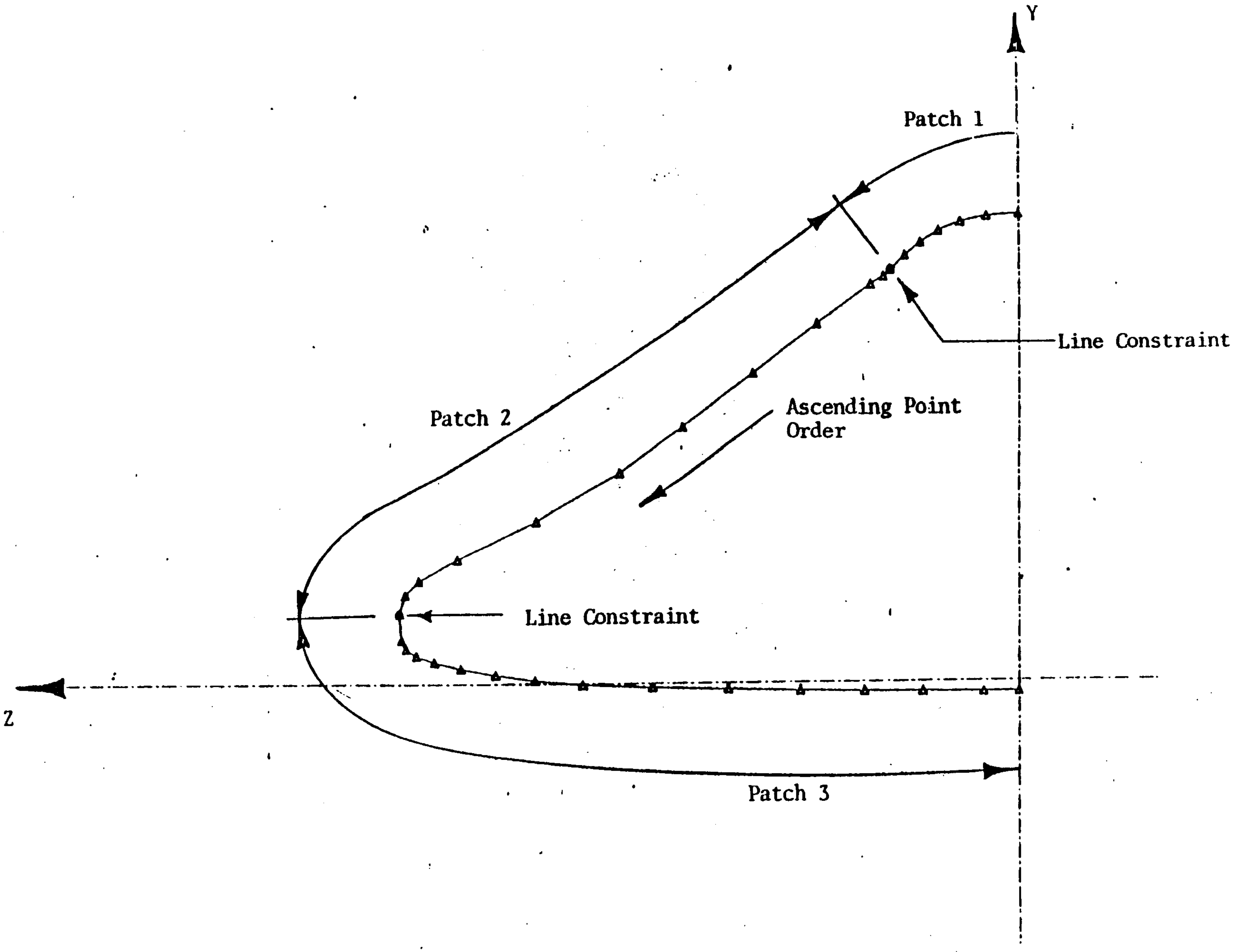

Figure 2. Region 1 Patching

REFERENCES

1. Shankar, V., "A Conservative Full Potential, Implicit, Marching Scheme for Supersonic Flows," AIAA Journal, Vol. 20, No. 11, November, 1982, pp. 1508-1514.

2. Shankar, v. and Osher, S., "An Efficient Full Potential Implicit Method Based on Charateristics for Analysis of Supersonic Flows," AIAA Paper No. 82-0974, June, 1982; also to appear in AIAA Journal, August, 1983.

3. Shankar, V., Szema, K.Y. and Osher, S., "A Conservative Type-Dependent Full Potential Method for the Treatment of Supersonic Flows with Embedded Subsonic Regions," AIAA Paper No. 83-1887. July 1983.

4. Nash, J. and Scrugs, R. "An Implicit Method for Calculation of Three Dimension Boundary Layers on Finite Thick Wings, "AFFD1 TR-77-122 February, 1977.

5. Crehan, M; "Supersonic Full Potential Analysis Modeling Using CDS," to be published.

AIAA'84

AIAA-84-0262

Implicit Treatment of the Unsteady Full Potential Equation in Conservation Form

V. Shankar, Rockwell International Science Center, Thousand Oaks, CA

AIAA 22nd Aerospace Sciences Meeting

January 9-12, 1984/Reno, Nevada

IMPLICIT TREATMENT OF THE UNSTEADY FULL POTENTIAL EQUATION IN CONSERVATION FORM

Vijaya Shankar*

Rockwell International Science Center
Thousand Oaks, California 91360

Abstract

An implicit, conservative treatment for the unsteady full potential equation in two-dimensions is presented. The method employs a local time linearization for density, and introduces flux biasing concepts based on sonic conditions for the generation of artificial viscosity to capture shocks without any overshoots. The boundary condition is treated implicitely using a splitting procedure consistent with the approximate factorization scheme. This allows for extremely large Courant numbers, even for nonorthogonal grid at the body. The method has application not only to unsteady problems, but also to generate the starting blunt body solution for a supersonic full potential marching code. Results are presented for flows over cylinders, spheres and airfoils. Comparisons are made with available Euler and full potential results, and are in excellent agreement.

I. Introduction

Nonlinear aerodynamic prediction methods based on the steady form of the full potential equation are used ragularly for treating transonic[1,2] and supersonic[3-6] flows over realistic wing-body configurations. Numerical algorithms to compute the unsteady form of the full potential equation is still in a developmental stage, and several researchers[7-11] have recently made significant progress in this area. There are several issues involved in the construction of a robust and efficient numerical algorithm for the unsteady full potential equation. They are: 1) proper treatment of boundary conditions in a nonorthogonal grid system, 2) correct formulation for the production of artificial viscosity to capture sharp shocks, and 3) proper time linearization concepts.

The objective of the present paper is to present a numerical treatment of the unsteady full potential equation that properly takes into account the importance of the above three listed items. The paper discusses a local time linearization procedure for treating the time derivative term, a flux biasing concept based on sonic conditions (instead of the usual density biasing procedures) for the treatment of spatial derivative terms, and a split boundary condition procedure for incorporation into an approximately factored implicit algorithm. The resulting unsteady method has application not only to unsteady problems in transonics, but also to generate the starting blunt body solution for a full potential supersonic marching code.[6] The unsteady method of this paper, when combined with the steady methods of Refs. 4-6, provides a complete treatment of the full potential equations.

Results are presented for flows over cylinders, spheres and airfoils at various Mach numbers, and some comparisons are made with Euler solutions. Use of the split boundary condition technique, combined with the flux biasing concepts,[12,13] has produced a very robust method which, even for a difficult case with a fish-tail shock at the trailing edge of an airfoil, did not require any user specified "constants", such as the ones discussed in Ref. 2.

The paper also presents the results from a "hybrid" calculation, wherein the spherical blunt body solution from the unsteady code has been effectively used to provide the initial data plane for a supersonic marching calculating performed over the Shuttle Orbiter geometry.

II. Formulation

The two-dimensional/axisymmetric unsteady full potential equation written in a body-fitted coordinate system represented by $\tau = t$, $\zeta = \zeta(x,y,t)$ and $\eta = \eta(x,y,t)$ takes the form

$$\left(\frac{\rho}{J}\right)_\tau + \left(\rho \frac{U}{J}\right)_\zeta + \left(\rho \frac{V}{J}\right)_\eta + S\rho \frac{v}{yJ} = 0 \qquad (1)$$

where,

$S = 0$ for two dimensions, $= 1$ for axisymmetric

$$\rho = \text{density} = [1 - \frac{\gamma-1}{2} M_\infty^2 (2\phi_\tau + \bar{U}\phi_\zeta + \bar{V}\phi_\eta - 1)]^{1/(\gamma-1)}$$

$$U = \zeta_t + a_{11}\phi_\zeta + a_{12}\phi_\eta; \quad \bar{U} = U + \zeta_t$$

$$V = \eta_t + a_{12}\phi_\zeta + a_{22}\phi_\eta; \quad \bar{V} = V + \eta_t$$

$$a_{11} = \zeta_x^2 + \zeta_y^2; \quad a_{12} = \zeta_x\eta_x + \zeta_y\eta_y;$$

$$a_{22} = \eta_x^2 + \eta_y^2$$

$$J = \text{Jacobian} = \zeta_x\eta_y - \zeta_y\eta_y$$

The density ρ and the fluxes ρU and ρV are complicated nonlinear functions of ϕ, the velocity potential. Hence, to solve for ϕ from Eq. (1) will require a local linearization.

Let 'n' be the running index in the time direction, 'k' in the ζ direction and 'j' in the η direction leading out of the surface. The objective is to solve Eq. (1) for $\phi_{j,k}^{n+1}$ at the current time plane, knowing the information at n, n-1, n-2,... planes.

* Manager, Computational Fluid Dynamics Group, Associate Fellow AIAA.

A. Treatment of $\frac{\partial}{\partial\tau}(\frac{\rho}{J})$ in Eq. (1)

$$\frac{\partial}{\partial\tau}(\frac{\rho}{J})^{n+1} =$$

$$\frac{(a_1-\theta b_1)\{(\frac{\rho}{J})^{n+1} - (\frac{\rho}{J})^n\} - \theta b_1\{(\frac{\rho}{J})^n - (\frac{\rho}{J})^{n-1}\}}{a_1\Delta\tau_1 - \theta b_1(\Delta\tau_1 + \Delta\tau_2)}$$

where

$a_1 = (\Delta\tau_1 + \Delta\tau_2)^2$
$b_1 = \Delta\tau_1^2$
θ = 0 for first order time accuracy
θ = 1 for second order accuracy
$\Delta\tau_1 = \tau^{n+1} - \tau^n$
$\Delta\tau_2 = \tau^n - \tau^{n-1}$

In order to write Eq. (2) in terms of ϕ^{n+1}, a local time linearization procedure is introduced.

$$\rho^{n+1} \doteq \rho^n + (\frac{\partial\rho}{\partial\phi})^n \Delta\phi + \ldots \tag{3}$$

where $\Delta\phi = (\phi^{n+1} - \phi^n)$. The term $(\frac{\partial\rho}{\partial\phi})$ is a differential operator given by

$$(\frac{\partial\rho}{\partial\phi})^n = -\frac{\rho^n}{a^2}(\frac{\partial}{\partial\tau} + U^n\frac{\partial}{\partial\zeta} + V^n\frac{\partial}{\partial\eta}) \tag{4}$$

where 'a' is the local speed of sound.

Combining Eqs. (3) and (4), the nonlinear density function in terms of ϕ has been linearized, and the coefficients multiplying $\Delta\phi$ are evaluated at the known previous time level. To maintain conservation form, both ρ^{n+1} and ρ^n appearing in the first term of Eq. (2) are linearized according to Eq. (3).

B. Treatment of $\frac{\partial}{\partial\zeta}(\rho\frac{U}{J})$ in Eq. (1)

$$(\rho\frac{U}{J})^{n+1}_\zeta = \frac{\overleftarrow{\delta}}{\partial\zeta}(\frac{\tilde{\rho}^*_{j,k+1/2}\,U^{n+1}_{j,k+1/2}}{J_{j,k+1/2}})$$

$$= \frac{\overleftarrow{\delta}}{\partial\zeta}\{\frac{\tilde{\rho}^*}{J}(a_{11}\{\Delta\phi + \phi^n\}_\zeta \tag{5}$$

$$+ a_{12}\{\Delta\phi + \phi^n\}_\eta)\}_{j,k+1/2}$$

where $\rho^{n+1}_{j,k+1/2}$ appearing in the spatial derivative term has been linearized to $\tilde{\rho}^*_{j,k+1/2}$. The symbol ~ appearing over ρ denotes that the density has been modified to produce the necessary artificial viscosity. The modified density is obtained from a flux biasing concept to be described later in this paper. For a genuine unsteady problem (where a time asymptotic steady state does not exist), initially, $\tilde{\rho}^*$ is set to $\tilde{\rho}^n$ and then subsequently iterated to convergence by setting $\tilde{\rho}^*$ to the previously iterated value of ρ at the current n+1 time plane. For problems where the steady state exists and is of interest (steady transonic flow over airfoils or blunt objects), $\tilde{\rho}^*$ is always set to $\tilde{\rho}^n$ and requires no internal iterations at n+1 plane.

The only unknown in Eq. (5) is $\Delta\phi$.

C. Treatment of $\frac{\partial}{\partial\eta}(\rho\frac{V}{J})$ in Eq. (1)

$$(\rho\frac{V}{J})^{n+1}_\eta \doteq \frac{\overleftarrow{\delta}}{\partial\eta}(\tilde{\rho}^*\frac{V^{n+1}}{J^{n+1}})_{j+1/2,k}$$

$$= \frac{\overleftarrow{\delta}}{\partial\eta}\{\frac{\tilde{\rho}^*}{J^{n+1}}(a_{12}\{\Delta\phi + \phi^n\}_\zeta \tag{6}$$

$$+ a_{22}\{\Delta\phi + \phi^n\}_\eta)\}_{j+1/2,k}$$

Similarly, $\tilde{\rho}^*_{j+1/2,k}$ is a modified density based on flux biasing.

D. Flux Biasing Procedure

The density $\tilde{\rho}$ appearing in Eqs. (5) and (6) is modified according to a flux biasing formula given by

$$\left.\begin{aligned}
&\text{for } U > 0 \\
&\tilde{\rho}_{j,k+1/2} = \frac{1}{q_{j,k+1/2}}\{\rho q - \Delta\zeta\frac{\overleftarrow{\delta}}{\partial\zeta}(\rho q)^-\}_{j,k+1/2} \\
&\text{for } U < 0 \\
&\qquad = \frac{1}{q_{j,k+1/2}}\{\rho q + \Delta\zeta\frac{\overrightarrow{\delta}}{\partial\zeta}(\rho q)^-\}_{j,k+1/2} \\
&\text{for } V > 0 \\
&\tilde{\rho}_{j+1/2,k} = \frac{1}{q_{j+1/2,k}}\{\rho q - \Delta\eta\frac{\overleftarrow{\delta}}{\partial\eta}(\rho q)^-\}_{j+1/2,k} \\
&\text{for } V < 0 \\
&\qquad = \frac{1}{q_{j+1/2,k}}\{\rho q + \Delta\eta\frac{\overrightarrow{\delta}}{\partial\eta}(\rho q)^-\}_{j+1/2,k}
\end{aligned}\right\} \tag{7}$$

where

$$(\rho q)^- = (\rho q - \rho^* q^*) \text{ if } q > q^*$$
$$= 0 \quad \text{if } q < q^*$$

$\overleftarrow{\delta}$ = backward difference operator

$\overrightarrow{\delta}$ = forward difference opertor.

The quantities ρ^*q^*, ρ^* and q^* represent sonic values of the flux, density and total velocity, respectively. These sonic conditions are given by (using the density and speed of sound relationships)

$$(q^*)^2 = \frac{1 + \frac{(\gamma-1)}{2}M_\infty^2(1-2\phi_\tau)}{\frac{\gamma+1}{2}M_\infty^2} \tag{8}$$

$$\rho^* = (q^* M_\infty)^{2/(\gamma-1)}\ .$$

Note that for steady flows, the sonic conditions ρ^* and q^* are only a function of the freestream Mach number, and for a given flow they are constants. For unsteady flows, ρ^* and q^* need to be computed everywhere due to the presence of ϕ_τ in Eq. (8).

Now, the following four cases can be defined.

a) Subsonic Flow ($q < q^*$ at $(j,k+1/2)$ and $(j,k-1/2)$) for $U > 0$, the modified density in Eq. (7) becomes

$$\tilde{\rho}_{j,k+1/2} = \frac{1}{q_{j,k+1/2}} \{(\rho q)_{j,k+1/2} - [(\rho q)^-_{j,k+1/2} - (\rho q)^-_{j,k-1/2}]\} \tag{9}$$

$= \rho_{j,k+1/2}$ (since $(\rho q)^-$ at $(j,k+1/2)$ and $(j,k-1/2)$ is zero, according to Eq. (8).

b) Supersonic Flow ($q > q^*$ at $(j,k+1/2)$ and $(j,k-1/2)$ for $U > 0$,

$$\tilde{\rho}_{j,k+1/2} = \frac{1}{q_{j,k+1/2}} \{(\rho q)_{j,k+1/2} - [(\rho q-\rho^* q^*)_{j,k+1/2} - (\rho q-\rho^* q^*)_{j,k-1/2}]\}$$

$$= \frac{(\rho q)_{j,k-1/2}}{q_{j,k+1/2}} + \frac{1}{q_{j,k+1/2}} [\{(\rho^* q^*)_{j,k+1/2} - (\rho^* q^*)_{j,k-1/2}\}] \quad . \tag{10}$$

For steady supersonic flows where $(\rho^* q^*)$ is a constant everywhere, Eq. (10) reduces to

$$\tilde{\rho}_{j,k+1/2} = \rho_{j,k-1/2} \left\{\frac{q_{j,k-1/2}}{q_{j,k+1/2}}\right\} \tag{11}$$

c) Transition Through Sonic Line ($q > q^*$ at $k+1/2$ and $q < q^*$ at $k-1/2$. Refer to Fig. 1a). For $U > 0$,

$$\tilde{\rho}_{j,k+1/2} = \frac{1}{q_{j,k+1/2}} \{(\rho q)_{j,k+1/2} - [(\rho q-\rho^* q^*)_{j,k+1/2} - \overset{0}{\cancel{(\rho q)^-_{j,k-1/2}}}]\}$$

$$= \frac{\rho^* q^*}{q_{j,k+1/2}} \tag{12}$$

d) Transition Through Shock ($q > q^*$ at $k-1/2$ and $q < q^*$ at $k+1/2$. Refer to Fig. 1b). For $U > 0$,

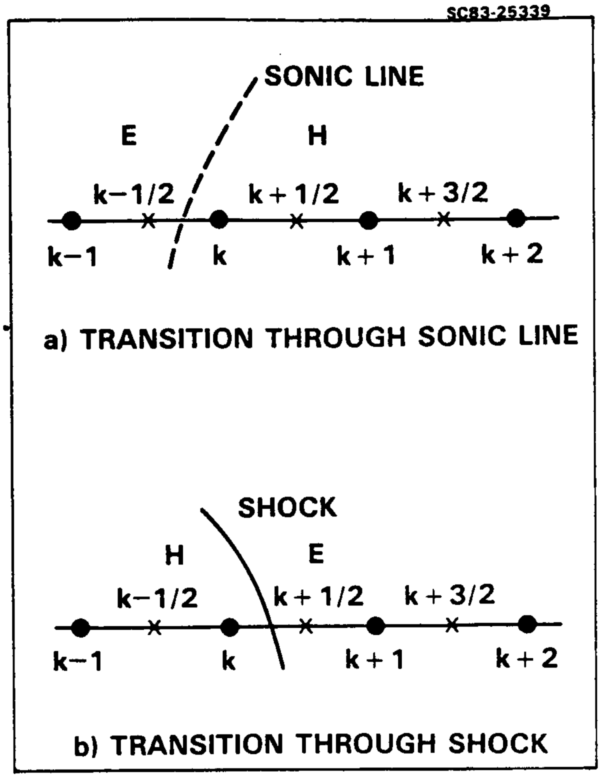

Fig. 1 Notation for flux biasing.

$$\tilde{\rho}_{j,k+1/2} = \frac{1}{q_{j,k+1/2}} \{(\rho q)_{j,k+1/2} - [\overset{0}{\cancel{(\rho q)^-_{j,k+1/2}}} - (\rho q-\rho^* q^*)_{j,k-1/2}]\}$$

$$= \rho_{j,k+1/2} + \frac{1}{q_{j,k+1/2}} \{\rho q-\rho^* q^*\}_{j,k-1/2} \tag{13}$$

For steady flows where $\rho^* q^*$ is a constant, it can be shown that at a pure supersonic point (case b above), the flux biasing procedure and the usual density biasing technique of Ref. 2 are identical. Using the following relationships:

$$\frac{\partial \rho}{\partial q} = -\frac{\rho}{a^2} q \tag{14}$$

$$\frac{\partial \rho}{\partial \zeta} = \frac{\partial \rho}{\partial q}\frac{\partial q}{\partial \zeta} = -\frac{\rho}{a^2} q\, q_\zeta \tag{15}$$

$$\frac{\partial}{\partial \zeta}(\rho q)^- = \frac{\partial}{\partial \zeta}(\rho q-\rho^* q^*)$$

$$= \frac{\partial}{\partial \zeta}(\rho q) \text{ (for steady flows only)}$$

$$= \rho_\zeta q + \rho q_\zeta \tag{16}$$

Using Eq. (15)

$$\frac{\partial}{\partial \zeta}(\rho q)^- = \rho_\zeta q \left\{1 - \frac{a^2}{q^2}\right\} = \rho_\zeta q \left\{1 - \frac{1}{M^2}\right\} \tag{17}$$

Using Eq. (17), thus, for a pure supersonic point, Eq. (7) becomes, for $U > 0$

$$\tilde{\rho}_{j,k+1/2} = \frac{1}{q_{j,k+1/2}} \{\rho q - \Delta\zeta \overset{+}{\rho}_{\zeta} q (1 - \frac{1}{M^2})\}_{j,k+1/2} \tag{18}$$

Using $\nu = (1 - \frac{1}{M^2})$, Eq. (18) can be written as

$$\tilde{\rho}_{j,k+1/2} = \rho_{j,k+1/2} - \nu(\rho_{j,k+1/2} - \rho_{j,k-1/2}) \tag{19}$$

$$= (1-\nu)\,\rho_{j,k+1/2} + \nu\rho_{j,k-1/2} \quad .$$

Equation (19) is the usual density biasing technique of Holst.[2] However, while transitioning through a sonic line (case c) or through a shock (case d), the flux biasing procedure of Eq. (7) accurately monitors the sonic conditions ρ^* and q^*, as given by Eqs. (12) and (13).

The advantages of flux biasing over the density biasing[2] scheme are:

1. Does not require any user specified constants (the parameter 'c' in Ref. 2) that depend on the severity of the flow.

2. Provides a monotone profile through the shock wave (for details, see Refs. 12 and 13).

3. Allows for larger Courant numbers to be taken during the calculation (by not producing undesired pressure overshoots at shocks, which could cause instability during transient calculations).

4. Provides a two point transition through a shock wave.

A detailed mathematical description of the flux biasing procedure can be found in the works of Osher[12] and Hafez.[13]

E. Implicit Approximate Factorization

Combining the various terms of Eq. (1) given by Eqs. (2-6) will result in a fully implicit model. This is solved using an approximate factorization implicit algorithm. After some rearrangement of the terms, the factored implicit scheme becomes

$$L_\zeta L_\eta \Delta\phi = R \tag{20}$$

where

$$L_\zeta = [1 + \Delta\tau_1\, U \frac{\partial}{\partial\zeta} + \frac{\alpha}{\beta}\frac{\partial}{\partial\zeta}\frac{\tilde{\rho}^*}{J}\, a_{11}\frac{\partial}{\partial\zeta}]$$

$$L_\eta = [1 + \Delta\tau_1\, V \frac{\partial}{\partial\eta} + \frac{\alpha}{\beta}\frac{\partial}{\partial\eta}\frac{\tilde{\rho}^*}{J}\, a_{22}\frac{\partial}{\partial\eta}]$$

$$\beta = -\left(\frac{\rho^n}{J^{n+1}(a^n\Delta\tau_1)^2}\right)_{j,k}$$

$$\alpha = (1-\theta) + \theta\,[\{a_1 - b_1(\Delta\tau_1 + \Delta\tau_2)/\Delta\tau_1\}/\{a_1 - b_1\}]$$

and R consists of various known terms at n, n-1 and n-2 levels.

Equation (20) is solved at the (n+1) plane in two steps.

$$L_\zeta\,\overline{\Delta\phi} = R, \quad \text{Step 1}$$

$$L_\eta\,\Delta\phi = \overline{\Delta\phi}, \quad \text{Step 2}$$

$$\phi^{n+1}_{j,k} = \phi^n_{j,k} + \Delta\phi_{j,k}$$

Both L_ζ and L_η result in tridiagonal matrices.

F. Boundary Condition

The direction ζ is along the body surface and η leads out of the surface. The boundary condition for the L_ζ operator usually depends on the problem. It can be a plane of symmetry condition, a periodic condition or a jump in ϕ condition that goes with a lifting airfoil. All these conditions are easily implemented in the L_ζ operator. Special attention needs to be given for the boundary condition that is required in the L_η operator. For inviscid flows, the surface flow tangency condition dictates that the contravariant velocity, V, be zero at the body. Implementation of the condition, $V = 0$, in the L_η operator is a crucial step in achieving a true implicit scheme. Usually, the boundary condition $V = 0$ is set only in the right hand side term R of Eq. (2), and a careless or no boundary condition treatment is imposed in the left hand side L_η operator.[2] In the present method, the condition $V = 0$ is imposed on both sides of the Eq. (20). Let $j = J$ denote the body point. Then,

$$V = (a_{12}\phi_\zeta + a_{22}\phi_\eta)_{J,k} = 0 \tag{21}$$

or

$$(\phi_\eta)_{J,k} = -\left(\frac{a_{12}}{a_{22}}\phi_\zeta\right)_{J,k} \quad . \tag{22}$$

Now, the following adjustments are made for body points (using Eqs. (21) and (22)):

1. Set $V = 0$ in Eq. (4).

2. Replace $a_{12}(\Delta\phi + \phi^n)_\eta$ by $-\frac{a_{12}^2}{a_{22}}(\Delta\phi + \phi^n)_\zeta$ in Eq. (5).

3. Replace $\frac{\partial}{\partial\eta}(\rho\frac{V}{J})$ by $\frac{2}{\Delta\eta}[\frac{\tilde{\rho}^*}{J}\{a_{12}(\Delta\phi + \phi)_\zeta + a_{22}(\Delta\phi + \phi)_\eta\}]_{J+1/2}$ in Eq. (6). This assumes $(\rho\frac{V}{J})_{J-1/2} = -(\rho\frac{V}{J})_{J+1/2}$.

The approximate factorization at a body point, J, is done after the above three boundary condition steps are implemented. This leads to the following approximate factored scheme for a body point, J.

$$\bar{L}_\zeta \bar{L}_\eta\,\Delta\phi = \bar{R} \tag{23}$$

where

$$\bar{L}_\zeta = [1 + \Delta\tau_1 \left(U - \cancelto{0}{V\frac{a_{12}}{a_{22}}}\right) \frac{\partial}{\partial\zeta}$$

$$+ \frac{\alpha}{\beta}\frac{\partial}{\partial\zeta}\frac{\tilde{\rho}^*}{J}\left(a_{11} - \frac{a_{12}^2}{a_{22}}\right)\frac{\partial}{\partial\zeta}]$$

$$\bar{L}_\eta = [1 + \frac{2}{\Delta\eta}\frac{\alpha}{\beta}\left(\frac{\tilde{\rho}^*}{J}a_{22}\frac{\partial}{\partial\zeta}\right)_{J+1/2}]$$

$\tilde{R}$ = modified form of R in Eq. (20) after imposing $V^n = 0$.

In Eq. (23), the boundary condition is split between the two operators, L_ζ and L_η. Even for nonorthogonal mesh at the body ($a_{12}{}^n \neq 0$), the boundary condition is set implicitly. This allows for large time steps, or Courant numbers, to be taken during the calculation. Imposing Eq. (21) directly into the L_η operator in the approximate factorization of Eq. (20) would lead to an explicit treatment for the part $a_{12}\phi_\zeta$ in Eq. (21).

For all calculations to be reported in this paper, the above split boundary condition approach has proved to be an efficient and robust method, even for highly nonorthogonal grid at the body.

III. Results

Results are presented for various steady flows computed using the unsteady code for time-asymptotic steady state solution. The time-step $\Delta\tau_1$ appearing in Eq. (2) is computed from a prescribed Courant number. When impulsively starting the calculation from free-stream, the Courant number is usually set at 30 ~ 50, and as the iteration proceeds, the Courant number is rapidly increased to very large values such as 500 ~ 2000.

Figures 2 and 3 show the results of a flow over a cylinder at $M_\infty = 0.4$ and 0.45. At $M_\infty = 0.4$, the flow is barely critical, and a comparison with an efficient Euler code[14] is excellent. At $M_\infty = 0.45$, a shock is formed on the cylinder surface. The flux biasing procedure of Eq. (7) produces a shock with no overshoots and requires no user specified 'constants'[2] to stabilize the calculation. Calculations of Figs. 2 and 3 required 40 time-step iterations.

Figures 4 to 6 show results for supersonic flows over a sphere at different low Mach numbers 1.08, 1.2 and 1.4. The density distribution for all these cases are compared with a bench mark type Euler calculation.[15] The present full potential calculation required 80 time-steps to converge for all these cases. It is worth noting at this point that the Euler calculations of Ref. 15 for Mach number 1.08 required in excess of 20,000 interations.

Figure 7 shows the flow over NACA 0012 airfoil at Mach 0.75 and $\alpha = 2°$. The pressure distribution compares well with other full potential methods.[2] Since there are no user specified parameters in the dissipation part of the calculation (flux biasing), there is only one flow solution for the shock in the present method, and it has no overshoots. This calculation required 200 iterations to converge (residual 10^{-5}).

Figures 8 and 9 show the flow over NACA 0012 airfoil at $M_\infty = 0.98$ and $\alpha = 0°$ and 2°, respectively. The fish-tail shock pattern reported in Ref. 2 is nicely reproduced for the zero degree case with 250 time-step iterations. At 4° angle of attack, the trailing edge shock pattern is changed, as seen in Fig. 9. The trailing edge shock on the lower surface is weakened, while the one on the upper surface grew in strength compared to $\alpha = 0°$ case. Even these severe flow cases with complex shock shapes required only minimal time-step iterations and produced no unnecessary 'wiggles' near shocks.

Figure 10 shows the schematic of a hybrid calculation where the unsteady code is used to generate the blunt body solution for setting up the initial data plane for the full potential marching code.[16] A hybrid calculation was performed for the flow over the Shuttle Orbiter at $M_\infty = 1.4$, $\alpha = 0°$. The results of Fig. 6 were used as a starting solution for the marching calculation. The nose region geometry and the pressure distribution along the leeside symmetry of the Orbiter are shown in Figs. 11 and 12.

IV. Conclusions

An implicit method for the unsteady full potential equation is presented. The method employs a local time linearization process, a flux biasing technique for generation of artificial viscosity, and a split boundary condition scheme consistent with the approximate factorization algorithm. Results for flows over airfoils, cylinders and spheres are presented, along with a 'hybrid' calculation performed for the Shuttle Orbiter, using the unsteady and steady codes. Extensions of this work into three dimensions is currently in progress. Appropriate relaxaton schemes[14] will replace the approximate factorization procedure in three dimensions.

Acknowledgement

The author expresses his thanks to Prof. Osher of UCLA, and Drs. Chakravarthy and Szema of Rockwell for many valuable discussions. This work was partially funded by NASA Langley Research Center under Contract NAS1-15820.

References

1. Jameson, A., "Transonic Potential Flow Calculations Using conservation Form," AIAA 2nd Computational Fluid Dynamic Conference Proceedings, 1975, pp. 148-155.

2. Holst, T.L., "Fast, Conservative Algorithm for Solving the Transonic Full Potential Equation," AIAA Journal, Vol. 18, No. 12, December, 1980, pp. 1431-1439.

3. Siclari, M.J., "Computation of Nonlinear Supersonic Potential Flow Over Three-Dimensional Surfaces," AIAA Paper No. 82-0167, presented at the AIAA 20th Aerospace Sciences Meeting, Orlando, Florida, January, 1982.

4. Shankar, V., "A Conservative Full Potential, Implicit, Marching Scheme for Supersonic Flows," AIAA Journal, Vol. 20, No. 11, November, 1982, pp. 1508-1514.

5. Shankar, V. and Osher, S., "An Efficient Full Potential Implicit Method Based on Characteristics for Analysis of Supersonic Flows," AIAA Paper No. 82-0974, June, 1982; also to appear in AIAA Journal, August, 1983.

6. Shankar, V., Szema, K.Y. and Osher, S., "A Conservative Type-Dependent Full Potential Method for the Treatment of Supersonic Flows with Embedded Subsonic Regions," AIAA Paper No. 83-1887

7. Chipman, R. and Jameson, A., "An Alternating Direction Implicit Algorithm for Unsteady Potential Flow," Presented at AIAA 19th Aerospace Sciences Meeting, January, 1981.

8. Goorjian, P.M., "Compuations of Unsteady Transonic Flow Governed by the conservative Full Potential Equation Using an Alternating Direction Implicit Algorithm," NASA CR-152274, June, 1979.

9. Sankar, N.L. and Tassa, Y., "An Algorithm for Unsteady Transonic Potential Flow Past Airfoils," paper presented at 7th International Conference on Numerical Methods in Fluid Dynamics, June, 1980.

10. Steger, J. and Caradonna, F., "A Conservative Implicit Finite Difference Algorithm for the Unsteady Transonic Full Potential Equation," AIAA paper No. 80-1368, presented at the 13th Fluid and Plasma Dynamics Conference, July, 1980.

11. Malone, J.B. and Sankar, N.L., "Numerical Simulation of 2-D Unsteady Transonic Flows Using the Full Potential Equation," AIAA Paper No. 83-0233.

12. Osher, S., "Scheme Design for Transonic Unsteady Aerodynamics Based on Riemann Solvers and the Entropy Condition," Transonic Unsteady Aerodynamics and Aeroelasticity Workshop, NASA Langley Research Center, June 22-23, 1983.

13. Hafez, M., "Entropy Inequality for Transonic Flows," Transonic Unsteady Aerodynamics and Aeroelasticity Workshop, NASA Langley Research Center, June 22-23, 1983.

14. Sukamar, C.R., "Implicit Upwind Schemes Without Approximate Factorization," AIAA Paper No. 84-0165.

15. Salas, M.D., "Flow Properties for a Spherical Body at Low Supersonic Speeds," Symposium on Computers in Aerodynamics, 25th Anniversary of Aerodynamics Labs, PINY, Farmingdale, NY, June 4-5, 1979.

16. Szema, K.Y. and Shankar, V., "Nonlinear Computation of Wing-Body-Vertical Tail-Wake Flows at Low Supersonic Speeds," AIAA Paper No. 84-0427.

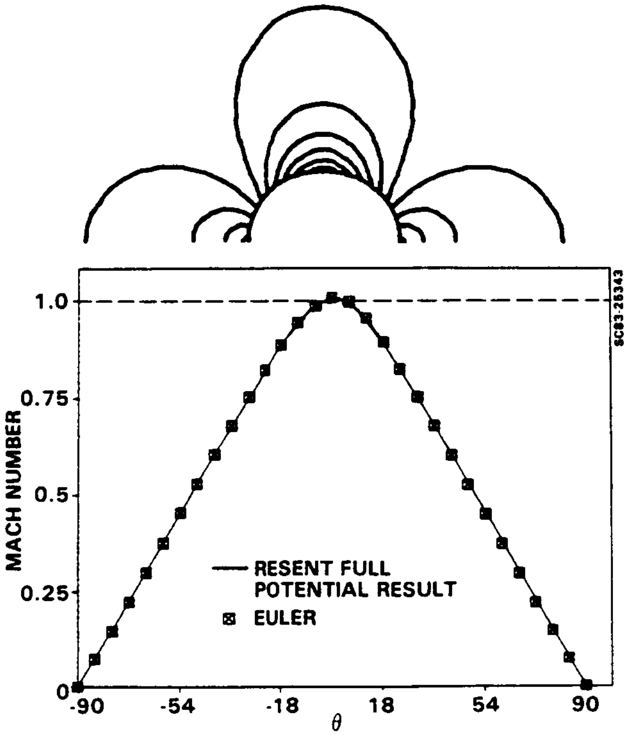

Fig. 2 Mach number distribution for cylinder flow at $M_\infty = 0.4$.

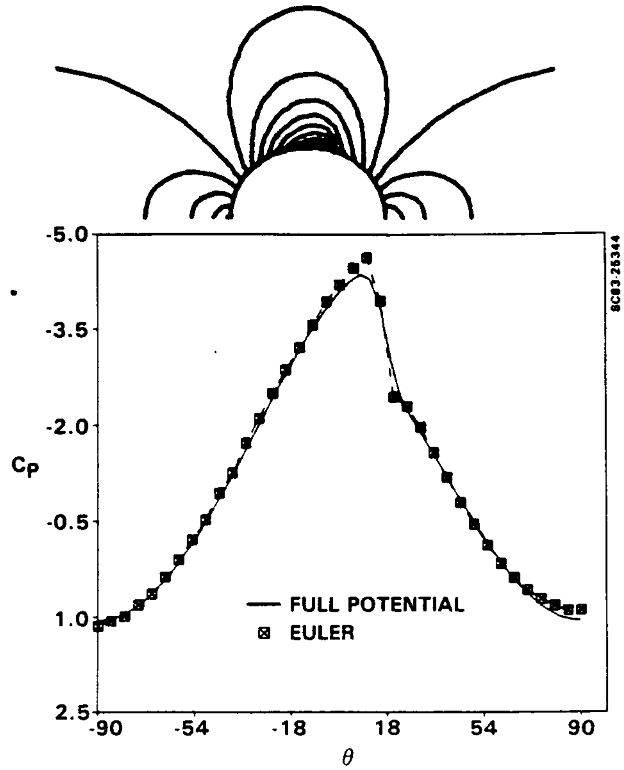

Fig. 3 Mach number distribution and contours for cylinder flow at $M_\infty = 0.45$.

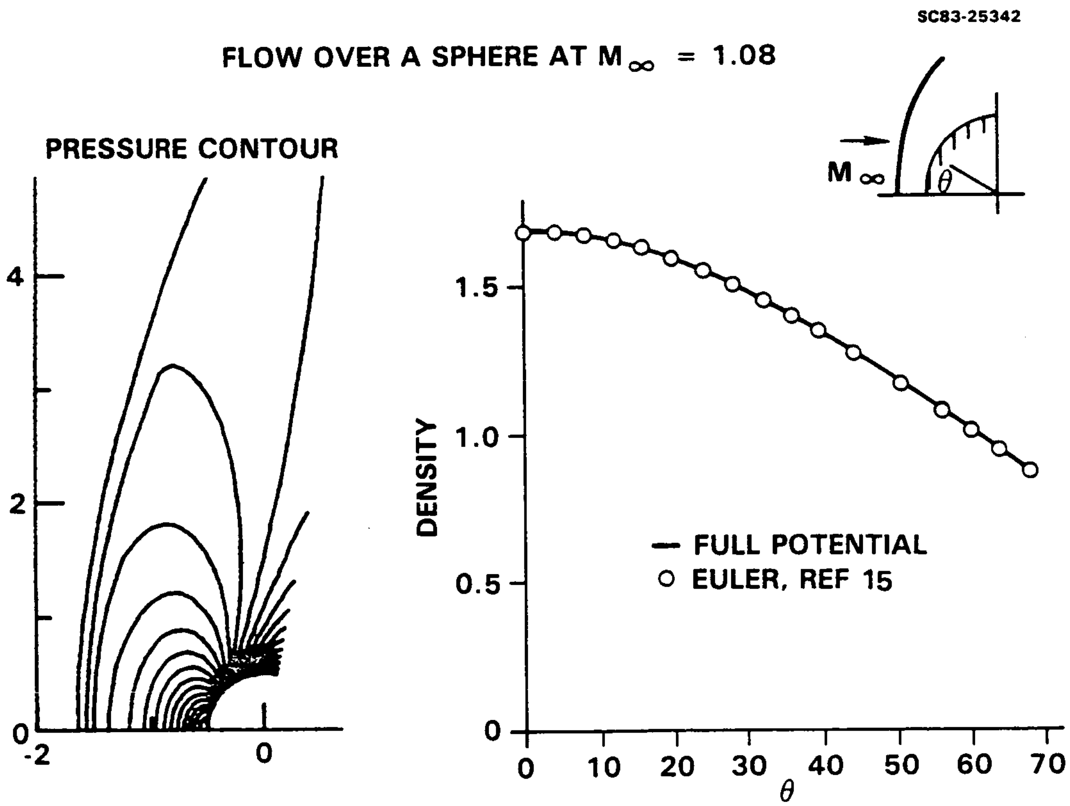

Fig. 4 Density distribution and Mach number contours for flow over a sphere at $M_\infty = 1.08$.

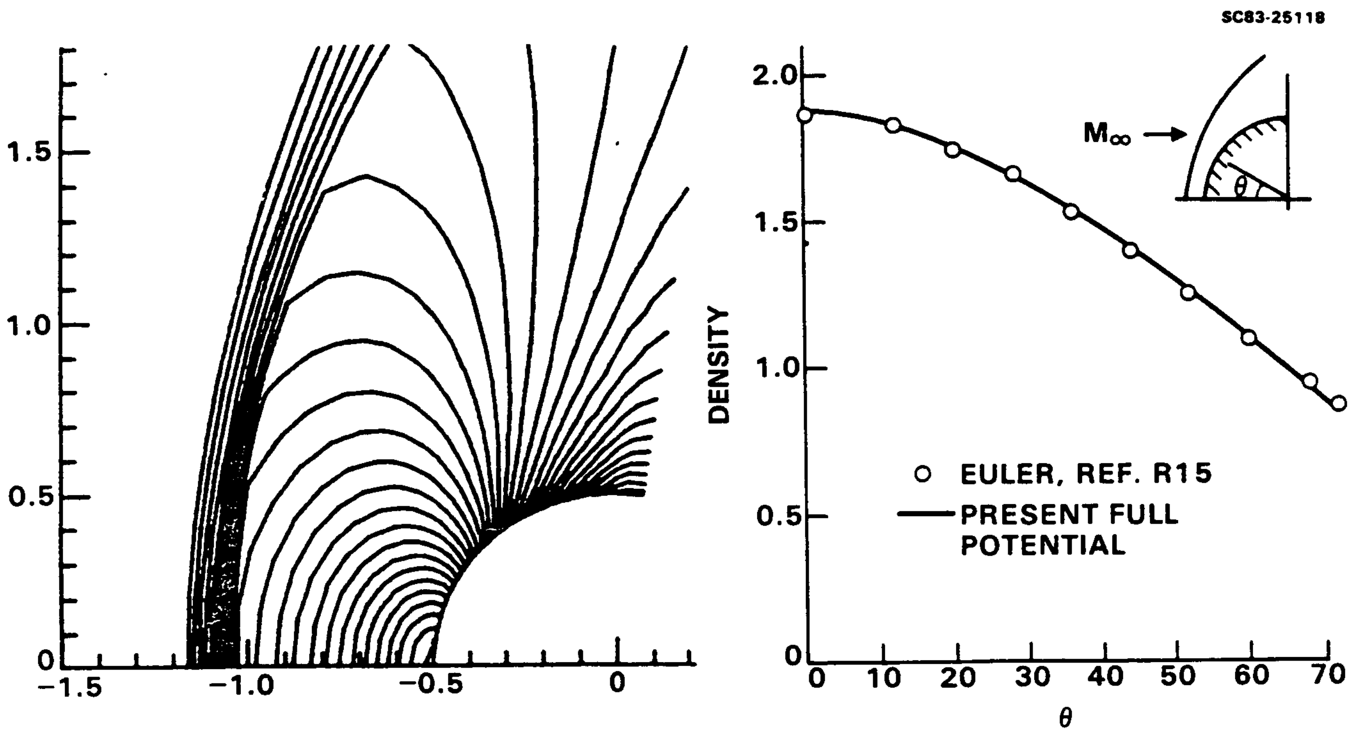

Fig. 5 Density distribution and Mach number contours for flow over a sphere at $M_\infty = 1.2$.

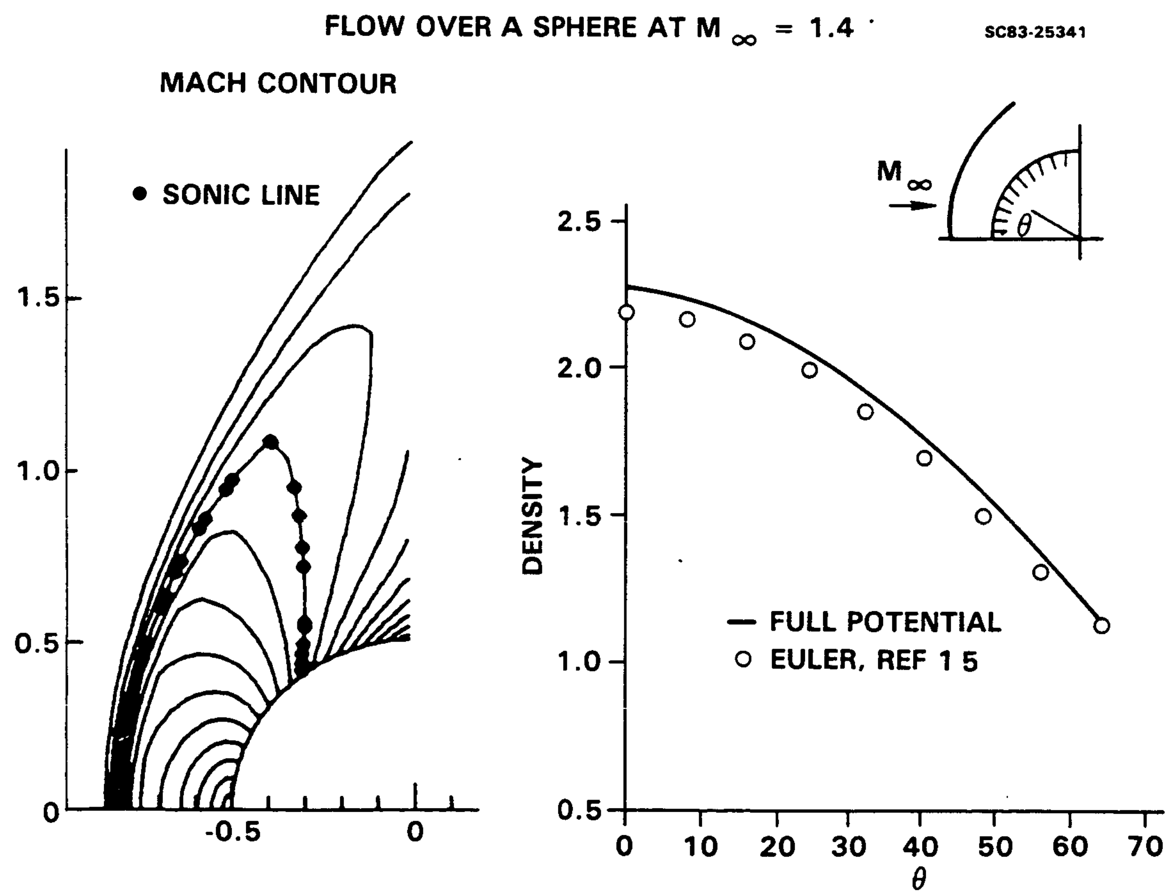

Fig. 6 Density distribution and Mach number contours for flow over a sphere at $M_\infty = 1.4$.

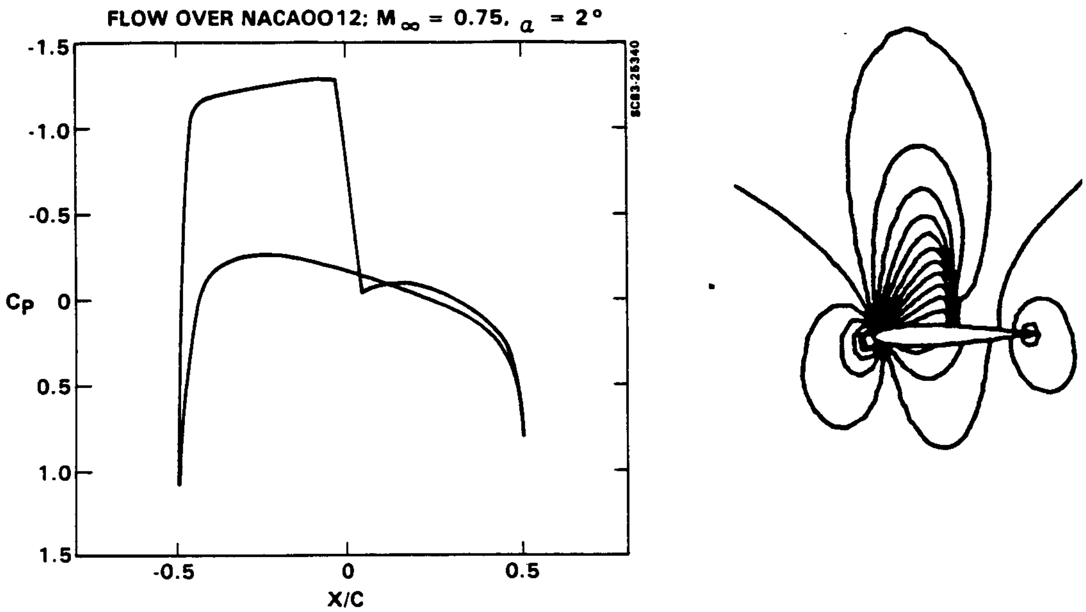

Fig. 7 Pressure distribution and Mach contours for flow over NACA 0012; M_∞ = 0.75, α = 2°.

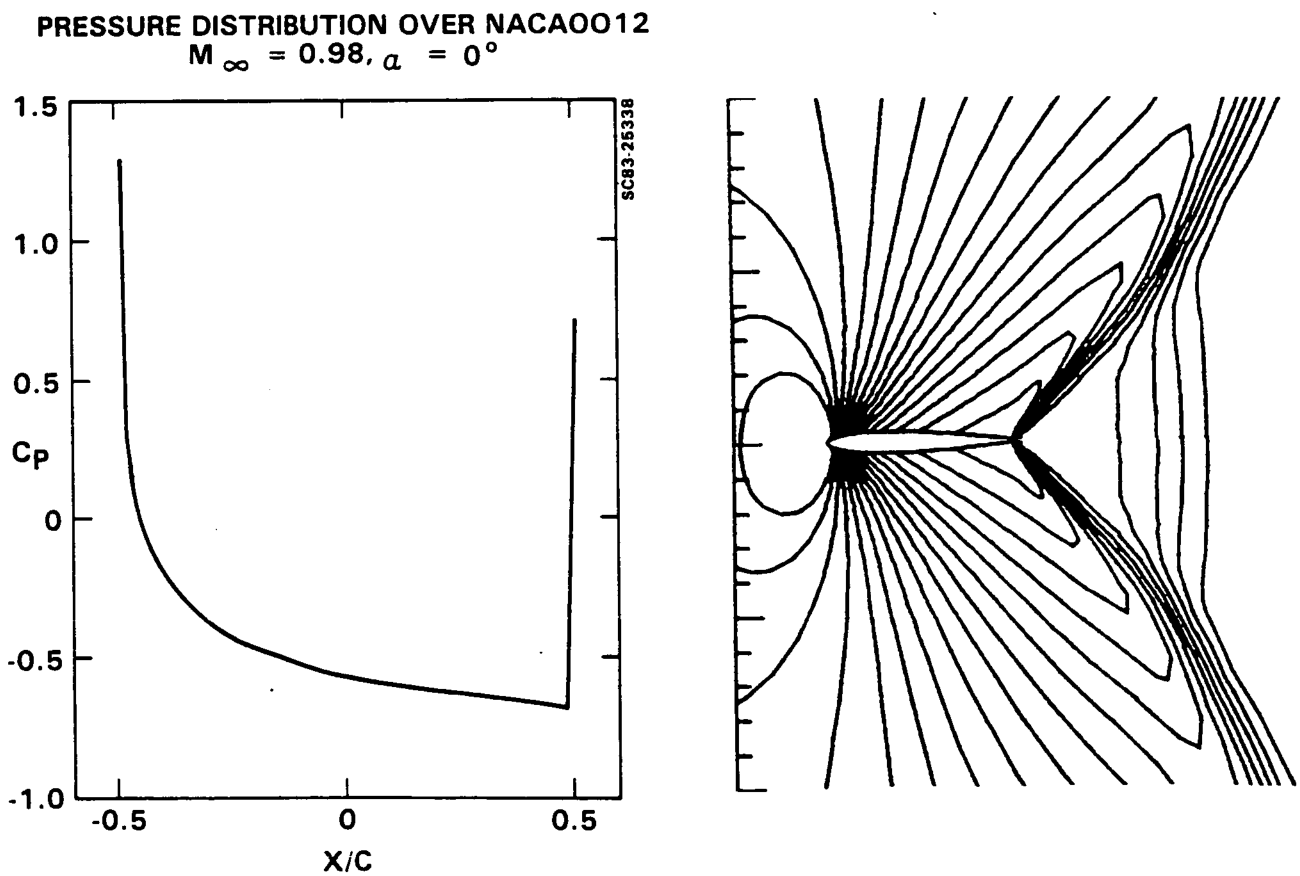

Fig. 8 Pressure distribution and Mach contours for flow over NACA 0012; M_∞ = 0.98, α = 0°.

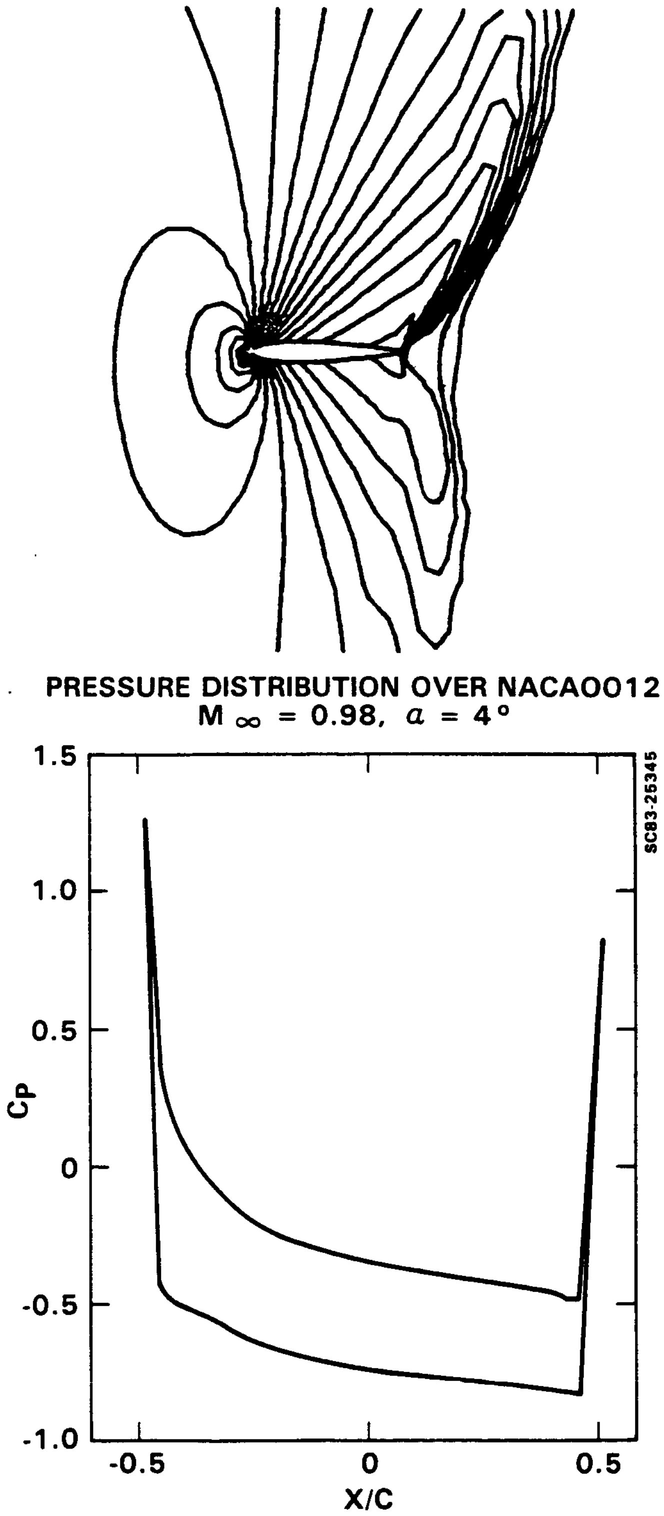

Fig. 9 Pressure distribution and Mach contours for flow over NACA 0012; M_∞ = 0.98, α = 4°.

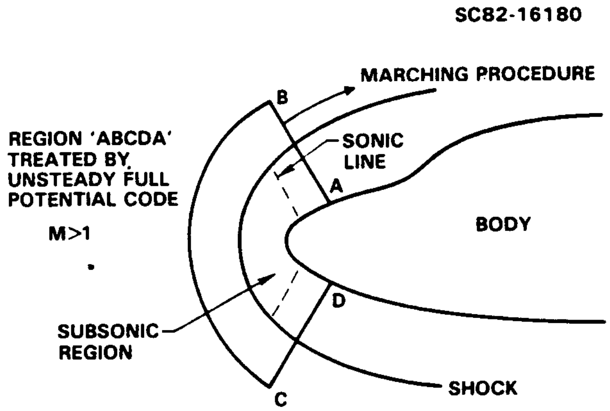

Fig. 10 Blunt body starting solution for a marching code.

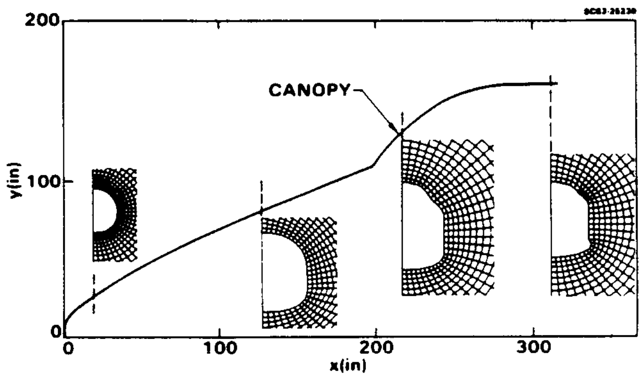

Fig. 11 Nose region geometry of Shuttle Orbiter.

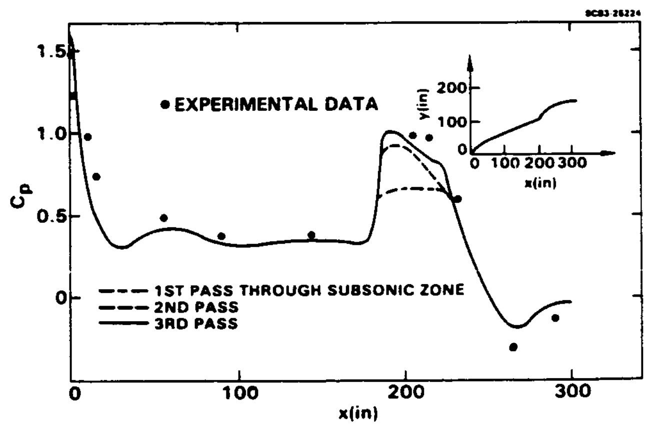

Fig. 12 Hybrid unsteady blunt body/supersonic marching calculation for the Orbiter at M_∞ = 1.4, α = 0°.

ICAS-84-1.6.2

Relaxation and Approximate Factorization Methods for the Unsteady Full Potential Equation

V. Shankar, H. Ide, and J. Gorski

14TH CONGRESS OF THE INTERNATIONAL COUNCIL OF THE AERONAUTICAL SCIENCES

September 9 – 14, 1984 Toulouse, France

ICAS-84-1.6.2

RELAXATION AND APPROXIMATE FACTORIZATION METHODS FOR THE UNSTEADY FULL POTENTIAL EQUATION

Vijaya Shankar*, Hiroshi Ide**, and Joseph Gorski†
Rockwell International Science Center
Thousand Oaks, California 91360

Abstract

The unsteady form of the full potential equation is solved in conservation form using implicit methods based on approximate factorization and relaxation schemes. A local time linearization for density is introduced to enable solution to the equation in terms of ϕ, the velocity potential. A novel flux biasing technique is applied to generate proper forms of the artificial viscosity to treat hyperbolic regions with shocks and sonic lines present. The wake is properly modeled by accounting not only for jumps in ϕ, but also for jumps in higher derivatives of ϕ, obtained from requirements of density continuity. The far field is modeled using the Riemann invariants to simulate nonreflecting boundary conditions. Results are presented for flows over airfoils, cylinders, and spheres. Comparisons are made with available Euler and full potential results.

I. Introduction

Nonlinear aerodynamic prediction methods based on the steady form of the full potential equation are used regularly for treating transonic[1,2] and supersonic[3–6] flows over realistic wing–body configurations. Numerical algorithms to compute the unsteady form of the full potential equation are still in a developmental stage, and several researchers[7–11] have recently made significant progress in this area. There are several issues involved in the construction of a robust and efficient numerical algorithm for the unsteady full potential equation. They are: 1) proper treatment of boundary conditions in a nonorthogonal grid system, 2) correct formulation for the production of artificial viscosity to capture sharp shocks, 3) proper time linearization concepts, 4) unsteady wake treatment, and 5) nonreflecting outer boundary conditions.

The objective of the present paper is to present a numerical treatment of the unsteady full potential equation that properly takes into account the importance of the above listed items. The paper discusses a local time linearization procedure for treating the time derivative term, a flux biasing concept based on sonic conditions (instead of the usual density biasing procedures) for the treatment of spatial derivative terms, split boundary condition procedures consistent with approximate factorization schemes, unsteady wake models with proper jumps in ϕ and higher derivatives of ϕ taken into account from density relationships, and nonreflecting unsteady far field procedures based on Riemann invariants derived from the characteristic theory.

*Manager, Computational Fluid Dynamics Group

**Member Technical Staff, Aircraft Operations Div.

†Senior Technical Associate

Use of unsteady methods has application not only to unsteady problems, but also to time asymptotic steady state solutions. If the unsteady method is constructed properly (robust and efficient), then it can even be made to generate steady state solutions faster than methods based on the steady form of the equation. Also, in the unsteady method, since the time direction is always present, the hyperbolicity of the unsteady full potential equation will allow one to obtain solutions to problems across the Mach number range (subsonic, transonic, and supersonic), whether steady or unsteady. The unsteady method of this paper, when combined with the steady marching method of Refs. 4–6, provides a complete treatment of the full potential equation.

Results are presented for flows over cylinders, spheres, and airfoils at various Mach numbers, and some comparisons are made with Euler solutions. Use of the split boundary condition technique, combined with the flux biasing concepts[12,13], has produced a very robust method which, even for a difficult case with a fishtail shock at the trailing edge of an airfoil, did not require any user–specified "constants", such as the ones discussed in Ref. 2.

The paper also presents the results from a "hybrid" calculation, wherein the spherical blunt body solution from the unsteady code has been effectively used to provide the initial data plane for a supersonic marching calculation performed over the Shuttle Orbiter geometry.

II. Formulation

The two–dimensional/axisymmetric unsteady full potential equation written in a body–fitted coordinate system represented by $\tau = t$, $\varsigma = \varsigma(x,y,t)$ and $\eta = \eta(x,y,t)$ takes the form

$$\left(\frac{\rho}{J}\right)_\tau + \left(\rho\frac{U}{J}\right)_\varsigma + \left(\rho\frac{V}{J}\right)_\eta + S\rho\frac{v}{yJ} = 0 \qquad (1)$$

where

$S = 0$ for two dimensions, $= 1$ for axisymmetric

$$\rho = \text{density} = \left[1 - \tfrac{\gamma-1}{2}M_\infty^2\,(2\phi_\tau + \bar{U}\phi_\varsigma + \bar{V}\phi_\eta - 1\right]^{1/(\gamma-1)}$$

$U = \varsigma_t + a_{11}\phi_\varsigma + a_{12}\phi_\eta$; $\bar{U} = U + \varsigma_t$

$V = \eta_t + a_{12}\phi_\varsigma + a_{22}\phi_\eta$; $\bar{V} = V + \eta_t$

$a_{11} = \varsigma_x^2 + \varsigma_y^2$; $a_{12} = \varsigma_x\eta_x + \varsigma_y\eta_y$

$a_{22} = \eta_x^2 + \eta_y^2$

$J = \text{Jacobian} = \varsigma_x\eta_y - \varsigma_y\eta_y$

The density ρ and the fluxes ρU and ρV are complicated nonlinear functions of ϕ, the velocity potential.

Hence, to solve for ϕ from Eq. (1) will require a local linearization.

Let 'n' be the running index in the time direction, 'k' in the ς direction, and 'j' in the η direction leading out of the surface. The objective is to solve Eq. (1) for $\phi_{j,k}^{n+1}$ at the current time plane, knowing the information at $n, n-1, n-2, \cdots$ planes.

A. Treatment of $\frac{\partial}{\partial\tau}\left(\frac{\rho}{J}\right)$ in Eq. (1)

$$\frac{\partial}{\partial\tau}\left(\frac{\rho}{J}\right)^{n+1} = \frac{(a_1-\theta b_1)\left\{\left(\frac{\rho}{J}\right)^{n+1}-\left(\frac{\rho}{J}\right)^{n}\right\}-\theta b_1\left\{\left(\frac{\rho}{J}\right)^{n}-\left(\frac{\rho}{J}\right)^{n-1}\right\}}{a_1\Delta\tau_1-\theta b_1(\Delta\tau_1+\Delta\tau_2)} \tag{2}$$

where

$a_1 = (\Delta\tau_1+\Delta\tau_2)^2$

$b_1 = \Delta\tau_1^2$

$\theta = 0$ for first order time accuracy

$\theta = 1$ for second order accuracy

$\Delta\tau_1 = \tau^{n+1}-\tau^n$

$\Delta\tau_2 = \tau^n - \tau^{n-1}$

In order to write Eq. 2 in terms of ϕ^{n+1}, a local time linearization procedure is introduced.

$$\rho^{n+1} \doteq \rho^n + \left(\frac{\partial\rho}{\partial\phi}\right)^n \Delta\phi + \cdots \tag{3}$$

where $\Delta\phi = (\phi^{n+1}-\phi^n)$. The term $\left(\frac{\partial\rho}{\partial\phi}\right)$ is a differential operator given by

$$\left(\frac{\partial\rho}{\partial\phi}\right)^n = -\frac{\rho^n}{a^2}\left(\frac{\partial}{\partial\tau}+U^n\frac{\partial}{\partial\varsigma}+V^n\frac{\partial}{\partial\eta}\right) \tag{4}$$

where 'a' is the local speed of sound.

Combining Eqs. (3) and (4), the nonlinear density function in terms of ϕ has been linearized, and the coefficients multiplying $\Delta\phi$ are evaluated at the known previous time level. To maintain conservation form, both ρ^{n+1} and ρ^n appearing in the first term of Eq. (2) are linearized according to Eq. (3).

B. Treatment of $\frac{\partial}{\partial\varsigma}\left(\rho\frac{U}{J}\right)$

$$\begin{aligned}\left(\rho\frac{U}{J}\right)_\varsigma^{n+1} &= \overleftarrow{\frac{\partial}{\partial\varsigma}}\left(\frac{\bar\rho_{j,k+1/2}U_{j,k+1/2}^{n+1}}{J_{j,k+1/2}}\right)\\ &= \overleftarrow{\frac{\partial}{\partial\varsigma}}\left\{\frac{\bar\rho}{J}\left(a_{11}\{\Delta\phi+\phi^n\}_\varsigma\right.\right.\\ &\quad \left.\left.+a_{12}\{\Delta\phi+\phi^n\}_\eta\right)\right\}_{j,k+1/2}\end{aligned} \tag{5}$$

where $\rho_{j,k+1/2}^{n+1}$ appearing in the spatial derivative term has been linearized to $\bar\rho_{j,k+1/2}$. The symbol $\bar{}$ appearing over ρ denotes that the density has been modified to produce the necessary artificial viscosity. The modified density is obtained from a flux biasing concept to be described later in this paper. For a genuine unsteady problem (where a time asymptotic steady state does not exist), initially, $\bar\rho$ is set to $\bar\rho^n$ and then subsequently iterated to convergence by setting $\bar\rho$ to the pre-time plane. For problems where the steady state exists and is of interest (steady transonic flow over airfoils or blunt objects), $\bar\rho$ is always set to $\bar\rho^n$ and requires no internal iterations at the $n+1$ plane.

The only unknown in Eq. (5) is $\Delta\phi$.

C. Treatment of $\frac{\partial}{\partial\eta}\left(\rho\frac{V}{J}\right)$

$$\begin{aligned}\left(\rho\frac{V}{J}\right)_\eta^{n+1} &\doteq \overleftarrow{\frac{\partial}{\partial\eta}}\left(\bar\rho\frac{V^{n+1}}{J^{n+1}}\right)_{j+1/2,k}\\ &= \overleftarrow{\frac{\partial}{\partial\eta}}\left\{\frac{\bar\rho}{J^{n+1}}\left(a_{12}\{\Delta\phi+\phi^n\}_\varsigma\right.\right.\\ &\quad \left.\left.+a_{22}\{\Delta\phi+\phi^n\}_\eta\right)\right\}_{j+1/2,k}\end{aligned} \tag{6}$$

Similarly, $\bar\rho_{j+1/2,k}$ is a modified density based on flux biasing.

D. Biasing Procedure

The spatial derivative terms given by Eqs. (5) and (6) are central differenced expressions about the node point (j,k) and are symmetric operators. For shocked flows and for treatment of hyperbolic regions, these operators are desymmetrized by introducing the biased value of density in the upwind direction. This will create the necessary artificial viscosity to form shocks and exclude the expansion shock. The biased value of density $\bar\rho$ can be obtained in several ways. Some of them are presented here.

a) Density Biasing[2] (in the ς-direction)

$$\begin{aligned}\bar\rho_{k+1/2} &= \rho_{k+1/2}\mp\nu\Delta\varsigma\left(\overleftrightarrow{\frac{\partial\rho}{\partial\varsigma}}\right)_{k+1/2},\\ \nu &= \max\left(0,1-\frac{1}{M^2}\right)_{k+1/2}\end{aligned} \tag{7}$$

where M is the local Mach number. For $U>0$, the $-$ sign and backward differencing ($\leftarrow$) is used in Eq. (7), while for $U<0$, the $+$ sign and ($\rightarrow$) operator is used.

b) Directional Flux Biasing

$$\bar\rho = \frac{1}{q}\left\{\rho q \mp \Delta\varsigma\overleftrightarrow{\frac{\partial}{\partial\varsigma}}(\rho q)^-\right\} \tag{8}$$

c) Streamwise Flux Biasing

$$\tilde{\rho} = \frac{1}{q}\left\{\rho q \mp \Delta S \overleftrightarrow{\frac{\partial}{\partial S}}(\rho q)^{-}\right\} \tag{9}$$

where S is the local streamwise direction. Equation (9) can be rearranged as

$$\tilde{\rho} = \frac{1}{q}\left[\rho q \mp \left\{\frac{U}{Q}\Delta\varsigma\overleftrightarrow{\frac{\partial}{\partial\varsigma}} + \frac{V}{Q}\Delta\eta\overleftrightarrow{\frac{\partial}{\partial\eta}}\right\}(\rho q)^{-}\right] \tag{10}$$

where $Q = \sqrt{U^2 + V^2}$.

In Eqs. (8) and (10), the term $(\rho q)^{-}$ is defined to be

$$\begin{aligned}(\rho q)^{-} &= \rho q - \rho^* q^* \qquad &\text{if } q > q^* \\ &= 0 &\text{if } q \le q^*\end{aligned} \tag{11}$$

The quantities $\rho^* q^*$, ρ^*, and q^* represent sonic values of the flux, density, and total velocity, respectively. These sonic conditions are given by (using the density and speed of sound relationships)

$$(q^*)^2 = \frac{1 + \frac{(\gamma-1)}{2}M_\infty^2\,(1 - 2\phi_\tau - \varsigma_t\phi_\varsigma - \eta_t\phi_\eta)}{\frac{\gamma+1}{2}M_\infty^2} \tag{12}$$

$$\rho^* = (q^* M_\infty)^{2/(\gamma-1)}.$$

Note that for steady flows, the sonic conditions ρ^* and q^* are only a function of the freestream Mach number, and for a given flow they are constants. For unsteady flows, ρ^* and q^* need to be computed everywhere due to the presence of ϕ_τ and other unsteady terms in Eq. (12).

The density biasing based on flux, Eq. (10), is more accurate than the one presented in Eq. (7), since it is based on sonic reference conditions. To illustrate the flux biasing procedure for various situations, Eq. (8) is considered.

1) Subsonic Flow ($q < q^*$ at $(j, k+1/2)$ and $(j, k-1/2)$) for $U > 0$, the modified density in Eq. (8) becomes

$$\begin{aligned}\tilde{\rho}_{j,k+1/2} = \frac{1}{q_{j,k+1/2}}\Big\{&(\rho q)_{j,k+1/2} \\ &- \left[(\rho q)^{-}_{j,k+1/2} - (\rho q)^{-}_{j,k-1/2}\right]\Big\}\end{aligned} \tag{13}$$

$= \rho_{j,k+1/2}$ (since $(\rho q)^{-}$ at $(j, k+1/2)$ and $(j, k-1/2)$ is zero, according to Eq. (11).

2) Supersonic Flow ($q > q^*$ at $(j, k+1/2)$ and $(j, k-1/2)$) for $U > 0$,

$$\begin{aligned}\tilde{\rho}_{j,k+1/2} &= \frac{1}{q_{j,k+1/2}}\{(\rho q)_{j,k+1/2} \\ &\quad -[(\rho q - \rho^* q^*)_{j,k+1/2} - (\rho q - \rho^* q^*)_{j,k-1/2}]\} \\ &= \frac{(\rho q)_{j,k-1/2}}{q_{j,k+1/2}} + \frac{1}{q_{j,k+1/2}}[\{(\rho^* q^*)_{j,k+1/2} \\ &\quad -(\rho^* q^*)_{j,k-1/2}\}].\end{aligned} \tag{14}$$

For steady supersonic flows where $(\rho^* q^*)$ is a constant everywhere, Eq. (14) reduces to

$$\tilde{\rho}_{j,k+1/2} = \rho_{j,k-1/2}\left\{\frac{q_{j,k-1/2}}{q_{j,k+1/2}}\right\}. \tag{15}$$

3) Transition Through Sonic Line ($q > q^*$ at $k + 1/2$ and $q < q^*$ at $k - 1/2$. Refer to Fig. 1a.) For $U > 0$,

$$\begin{aligned}\tilde{\rho}_{j,k+1/2} &= \frac{1}{q_{j,k+1/2}}\{(\rho q)_{j,k+1/2} \\ &\quad - [(\rho q - \rho^* q^*)_{j,k+1/2} - \cancelto{0}{(\rho q)^{-}_{j,k-1/2}}]\} \\ &= \frac{\rho^* q^*}{q_{j,k+1/2}}.\end{aligned} \tag{16}$$

4) Transition Through Shock ($q > q^*$ at $k - 1/2$ and $q < q^*$ at $k + 1/2$. Refer to Fig. 1b.) For $U > 0$,

$$\begin{aligned}\tilde{\rho}_{j,k+1/2} &= \frac{1}{q_{j,k+1/2}}\{(\rho q)_{j,k+1/2} \\ &\quad - [\cancelto{0}{(\rho q)^{-}_{j,k+1/2}} - (\rho q - \rho^* q^*)_{j,k-1/2}]\} \\ &= \rho_{j,k+1/2} + \frac{1}{q_{j,k+1/2}}\{\rho q - \rho^* q^*\}_{j,k-1/2}\end{aligned} \tag{17}$$

For steady flows where $\rho^* q^*$ is a constant, it can be shown that at a pure supersonic point (case 2 above), the

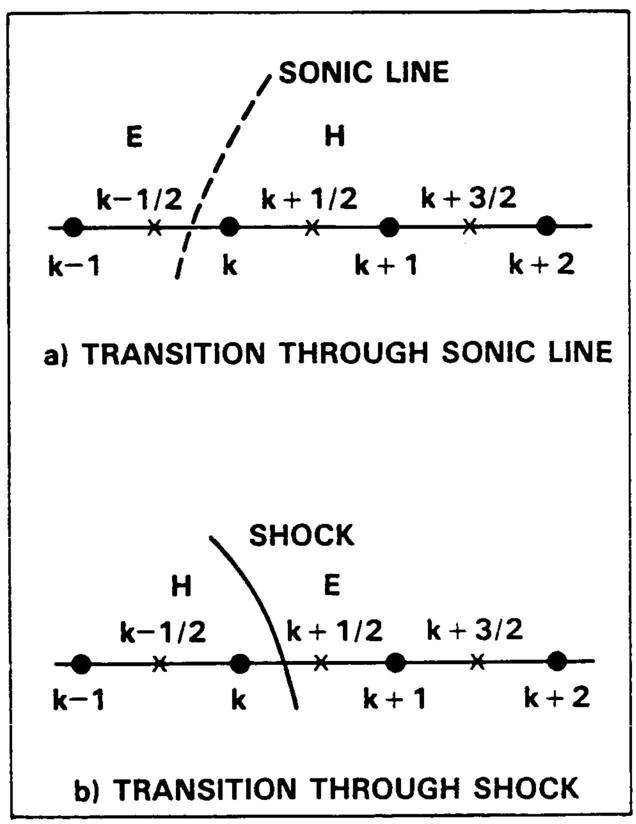

Fig. 1. Notation for flux biasing.

flux biasing procedure, Eq. (8), and the usual density biasing technique of Ref. 2, Eq. (7), are identical.

$$\frac{\partial \rho}{\partial q} = -\frac{\rho}{a^2} q \tag{18}$$

$$\frac{\partial \rho}{\partial \varsigma} = \frac{\partial \rho}{\partial q}\frac{\partial q}{\partial \varsigma} = -\frac{\rho}{a^2} q q_\varsigma \tag{19}$$

$$\begin{aligned}\frac{\partial}{\partial \varsigma}(\rho q)^- &= \frac{\partial}{\partial \varsigma}(\rho q - \rho^* q^*) \\ &= \frac{\partial}{\partial \varsigma}(\rho q) \text{ (for steady flows only)} \\ &= \rho_\varsigma q + \rho q_\varsigma\end{aligned} \tag{20}$$

Using Eq. (20)

$$\begin{aligned}\frac{\partial}{\partial \varsigma}(\rho q)^- &= \rho_\varsigma q \left\{1 - \frac{a^2}{q^2}\right\} \\ &= \rho_\varsigma q \left\{1 - \frac{1}{M^2}\right\}.\end{aligned} \tag{21}$$

Using Eq. (21), thus, for a pure supersonic point, Eq. (8) becomes, for $U > 0$

$$\begin{aligned}\tilde{\rho}_{j,k+1/2} = &\frac{1}{q_{j,k+1/2}} \\ &\left\{\rho q - \Delta\varsigma \overleftarrow{\rho}_\varsigma q \left(1 - \frac{1}{M^2}\right)\right\}_{j,k+1/2}\end{aligned} \tag{22}$$

Using $\nu = \left(1 - \frac{1}{M^2}\right)$, Eq. (22) can be written as

$$\begin{aligned}\tilde{\rho}_{j,k+1/2} &= \rho_{j,k+1/2} - \nu(\rho_{j,k+1/2} - \rho_{j,k-1/2}) \\ &= (1-\nu)\rho_{j,k+1/2} + \nu\rho_{j,k-1/2}.\end{aligned} \tag{23}$$

Equation (23) is the usual density biasing technique of Holst[2]. However, while transitioning through a sonic line (case 3) or through a shock (case 4), the flux biasing procedure of Eq. (8) accurately monitors the sonic conditions ρ^* and q^*, as given by Eqs. (16) and (17).

The advantages of flux biasing over the density biasing[2] scheme are:

1. Does not require any user–specified constants (the parameter 'c' in Ref. 2) that depend on the severity of the flow.
2. Provides a monotone profile through the shock wave (for details, see Refs. 12 and 13).
3. Allows for larger Courant numbers to be taken during the calculation (by not producing undesired pressure overshoots at shocks, which could cause instability during transient calculations).
4. Provides a two point transition through a shock wave.

A detailed mathematical description of the flux biasing procedure can be found in the works of Osher[12] and Hafez[13].

E. Unsteady Wake Treatment

Figure 2 shows the schematic of a wake cut behind the trailing edge of an airfoil. This wake cut has to be properly modeled in the unsteady formulation. An expression for the jump in ϕ across the wake cut can be derived by requiring that the pressure be continuous across the cut. In the full potential framework, this results in the continuity of density. Equating the density $\rho_u = \rho_\ell$ at any point along the wake (refer to Fig. 2), one can write

$$2\Gamma_t + (U_u + U_\ell)(\phi_\varsigma)_u - U_\ell \Gamma_\varsigma = 0 \tag{24}$$

assuming $[V\phi_\eta] \cong 0$, where $[f]$ stands for the jump in the quantity given by $(f_u - f_\ell)$. Equation (24) is integrated from the trailing edge to the downstream boundary (along TE in Fig. 2) to obtain the Γ distribution along the wake cut. To maintain stability, the ς derivatives in Eq. (24) are upwind differenced. For a steady flow, Eq. (24) will result in a constant value for Γ along the wake given by $\Gamma = \phi_T - \phi_{T'}$ in Fig. 2.

Beside the Γ evaluation, solution to the unsteady equation also requires information on (ϕ_η) at a wake point. Referring to Fig. 2 for notation, one can write the following using Taylor's series expansion.

$$\begin{aligned}\phi_2 &= \phi_3 - (\phi_\eta)_u + (\phi_{\eta\eta})_u/2 + \cdots \\ \phi_{\bar{2}} &= \phi_{\bar{3}} - (\phi_\eta)_\ell + (\phi_{\eta\eta})_\ell/2 + \cdots\end{aligned} \tag{25}$$

The subscripts 'u' and 'ℓ' stand for upper and lower, respectively.

For the chosen coordinate system, requiring that $(\phi_\eta)_u = -(\phi_\eta)_\ell$ and defining $\phi_2 - \phi_{\bar{2}} = \Gamma$, using Eqs. (25) one can write

$$(\phi_\eta)_u = \frac{\phi_3 - \{\phi_{\bar{3}} + \Gamma + [\phi_{\eta\eta}]/2\}}{2} \tag{26}$$

Equation (26) requires an estimate for the jump in $\phi_{\eta\eta}$ at the wake cut. This can be obtained by setting the jump in the equation to be zero at a wake point.

$$\left[\left(\frac{\rho}{J}\right)_\tau + \left(\rho\frac{U}{J}\right)_\varsigma + \left(\rho\frac{V}{J}\right)_\eta\right] = 0. \tag{27}$$

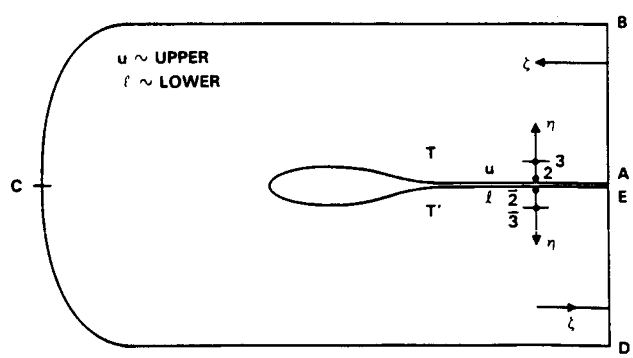

Fig. 2. Wake and outer boundary treatment.

Writing down Eq. (27) in terms of the transformation metrics and requiring that $\rho_u = \rho_\ell$, the following relationship is obtained.

$$[\phi_{\eta\eta}] = -\frac{(\rho a_{11}\Gamma_\varsigma)_\varsigma}{\rho a_{22}}. \tag{28}$$

For steady flows, the jump in $\phi_{\eta\eta}$ along the wake is zero because $\Gamma_\varsigma = 0$. For unsteady flows, to maintain accuracy, Eqs. (24)-(28) have to be employed.

F. Far Field Boundary Condition

Along the outer boundary ABCDE in Fig. 2, appropriate Riemann invariants are prescribed. The concept can be explained by considering the Cartesian form of the full potential equation cast in terms of the Riemann invariants.

$$\begin{aligned}\frac{\partial}{\partial t}\left(u+\frac{2}{\gamma-1}a\right)+(u+a)\frac{\partial}{\partial x}\left(u+\frac{2}{\gamma-1}a\right)&=0\\ \frac{\partial}{\partial t}\left(u-\frac{2}{\gamma-1}a\right)+(u-a)\frac{\partial}{\partial x}\left(u-\frac{2}{\gamma-1}a\right)&=0\end{aligned} \tag{29}$$

Equation (29) implies that along the $(u+a)$ positive characteristics the quantity $\left(u+\frac{2}{\gamma-1}a\right)$ is invariant, and along the $(u-a)$ negative characteristics the quantity $\left(u-\frac{2}{\gamma-1}a\right)$ is invariant, known as the Riemann invariants. Usually, along the outer boundary, the Riemann invariant that corresponds to the positive characteristics with respect to the inward normal can be prescribed as a boundary condition. For an arbitrary coordinate system (τ, ς, η), such as the one in Fig. 2, the following boundary conditions are appropriate.

$$\begin{aligned}\frac{U}{\sqrt{a_{11}}}+\frac{2}{\gamma-1}a &= \text{constant along AB}\\ -\frac{U}{\sqrt{a_{11}}}+\frac{2}{\gamma-1}a &= \text{constant along ED}\\ -\frac{V}{\sqrt{a_{22}}}+\frac{2}{\gamma-1}a &= \text{constant along BCD}\end{aligned} \tag{30}$$

Equation (30) is nonlinear in nature. Hence, to implement the Riemann invariant boundary condition, a linearization technique similar to Eq. (3) is employed. For example, equating the right hand side of Eq. (30) to the freestream value, along BCD one can write

$$\begin{aligned}&-\frac{\left(a_{12}\frac{\partial}{\partial\varsigma}+a_{22}\frac{\partial}{\partial\eta}\right)^n\Delta\phi}{\sqrt{a_{22}}}\\ &-\frac{1}{a^n}\left(\frac{\partial}{\partial\tau}+U\frac{\partial}{\partial\varsigma}+V\frac{\partial}{\partial\eta}\right)^n\Delta\phi\\ &=\left(-\frac{V}{\sqrt{a_{22}}}+\frac{2}{\gamma-1}a\right)_{\text{freestream}}-\left(-\frac{V}{\sqrt{a_{22}}}+\frac{2}{\gamma-1}a\right)^n\end{aligned} \tag{31}$$

The finite differenced form of Eq. (31) will provide an estimate for $(\Delta\phi)$ along the outer boundary. Use of the Riemann invariant boundary conditions is better than prescribing ϕ_∞ from the compressible vortex solution, and will serve as a nonreflecting boundary condition.

G. Relaxation and Approximate Factorization Schemes

When all the terms of Eq. (1) are put together, it will be in terms of the unknown $\Delta\phi$. It can be written as

$$F(\Delta\phi)+R(\phi^n,\phi^{n-1},\cdots)=0 \quad , \quad \Delta\phi=\phi^{n+1}-\phi^n. \tag{32}$$

The Newton iterative procedure for solving Eq. (32) becomes

$$\frac{\partial F}{\partial\Delta\phi}(\Delta\phi^{n+1}-\Delta\phi^i)=-R(\phi^n,\phi^{n-1},\cdots)-F(\Delta\phi^i) \tag{33}$$

The off-diagonal elements of $\frac{\partial F}{\partial\Delta\phi}$, which cannot be accommodated within the tridiagonal setup of SLOR, can be set to zero. In Eq. (33), $\Delta\phi^i$ represents the intermediate iterative value of $\Delta\phi$. For steady state problems, $\Delta\phi^i$ can be set to $\Delta\phi^n$. If all the off-diagonal terms of $\frac{\partial F}{\partial\Delta\phi}$ are set to zero, then the relaxation process becomes the point Jacobi iteration. Results based on the relaxation procedure of Eq. (32) are presented in this paper.

Another procedure to solve Eq. (32) is the approximate factorization technique. This can be written as

$$L_\varsigma L_\eta \Delta\phi = R \tag{34}$$

where

$$\begin{aligned}L_\varsigma &= \left[1+\Delta\tau_1 U\frac{\partial}{\partial\varsigma}+\frac{\alpha}{\beta}\frac{\partial}{\partial\varsigma}\frac{\bar{\rho}^*}{J}a_{11}\frac{\partial}{\partial\varsigma}\right]\\ L_\eta &= \left[1+\Delta\tau_1 V\frac{\partial}{\partial\eta}+\frac{\alpha}{\beta}\frac{\partial}{\partial\eta}\frac{\bar{\rho}^*}{J}a_{22}\frac{\partial}{\partial\eta}\right]\\ \beta &= -\left(\frac{\rho^n}{J^{n+1}(a^n\Delta\tau_1)^2}\right)_{j,k}\\ \alpha &= (1-\theta)+\theta\,[\{a_1-b_1(\Delta\tau_1+\Delta\tau_2)/\Delta\tau_1\}\,/\,\{a_1-b_1\}]\end{aligned}$$

Equation (34) is solved at the $(n+1)$ plane in two steps.

$$\begin{aligned}L_\varsigma\overline{\Delta\phi} &= R \quad , \quad \text{Step 1}\\ L_\eta\Delta\phi &= \overline{\Delta\phi} \quad , \quad \text{Step 2}\\ \phi^{n+1}_{j,k} &= \phi^n_{j,k}+\Delta\phi_{j,k}\end{aligned}$$

Both L_ς and L_η result in tridiagonal matrices.

H. Body Boundary Condition

For inviscid flows, the surface flow tangency condition dictates that the contravariant velocity, V, be zero at the body. Implementation of the condition, $V = 0$, in the L_η operator is a crucial step in achieving a true implicit scheme. Usually, the boundary condition $V = 0$ is set only in the right hand side term R, and a careless or no boundary condition treatment is imposed in the left hand side L_η operator[2]. In the present method, the condition $V = 0$ is imposed on both sides of Eq. (34). Let $j = J$ denote the body point. Then,

$$V=(a_{12}\phi_\varsigma+a_{22}\phi_\eta)_{J,k}=0 \tag{35}$$

or

$$(\phi_\eta)_{J,k} = -\left(\frac{a_{12}}{a_{22}}\phi_\varsigma\right)_{J,k} . \tag{36}$$

Using Eqs. (35) and (36), and the relationship

$$\left(\rho\frac{V}{J}\right)_{J-1/2} = -\left(\rho\frac{V}{J}\right)_{J+1/2}, \tag{37}$$

the L_ς and the L_η operators in Eq. (34) can be modified to the form, for a body point J,

$$\tilde{L}_\varsigma \tilde{L}_\eta \Delta\phi = \tilde{R} \tag{38}$$

where

$$\tilde{L}_\varsigma = \left[1 + \Delta\tau_1 U \frac{\partial}{\partial\varsigma} + \frac{\alpha'\partial}{\beta\,\partial\varsigma}\frac{\bar{\rho}}{J}\left(a_{11} - \frac{a_{12}^2}{a_{22}}\right)\frac{\partial}{\partial\varsigma}\right]$$

$$\tilde{L}_\eta = \left[1 + \frac{2}{\Delta\eta}\frac{\alpha}{\beta}\left(\frac{\bar{\rho}}{J}a_{22}\frac{\partial}{\partial\varsigma}\right)_{J+1/2}\right].$$

In Eq. (38), the boundary condition is split between the two operators, $\tilde{L}_\varsigma$ and $\tilde{L}_\eta$. Even for nonorthogonal mesh at the body ($a_{12} \neq 0$), the boundary condition is set implicitly. This allows for large time steps, or Courant numbers, to be taken during the calculation.

III. Results

Computer codes based on both the relaxation method (Eq. (33)) and the approximate factorization method (Eq. (34)) have been constructed for two-dimensional and axisymmetric problems. The grid around the geometry can be either a C-type (Fig. 2) or an O-type. At present, the relaxation method is somewhat slower (at least 50%) in convergence than the approximate factorization code. However, the future implementation of multigrid techniques[17] and implicit relaxation concepts[14] to the present relaxation code can make it competitive to approximate factorization methods in three-dimensional applications, where the approximate factorization methods with triple factorization can be less flexible to handle complex geometries[14].

The unsteady code has been applied, at present, only to steady state problems. Calculations involving unsteady motions such as plunge, pitch, and oscillating flaps are currently in progress. For steady state problems, the time step $\Delta\tau_1$ appearing in Eq. (34) is computed from a prescribed Courant number, usually set much greater than one (~ 50).

Figure 3 shows the result for a flow over a cylinder at $M_\infty = 0.4$. The flow is barely critical, and a comparison with an efficient Euler code[14] is excellent. Figures 4 and 5 show results for supersonic flows over a sphere at low Mach numbers of 1.08 and 1.4. The density distribution for these cases are compared with benchmark Euler calculations[15]. The present full potential code required approximately 80 time steps to converge (residual $< 10^{-5}$). It is worth noting at this point that the Euler code of Ref. 15 requires in excess of 20,000 iterations to perform the low Mach number calculation of 1.08.

Figure 6 shows the pressure distribution obtained over the NACA 0012 airfoil at $M_\infty = 0.8$ and $\alpha = 0°$ with

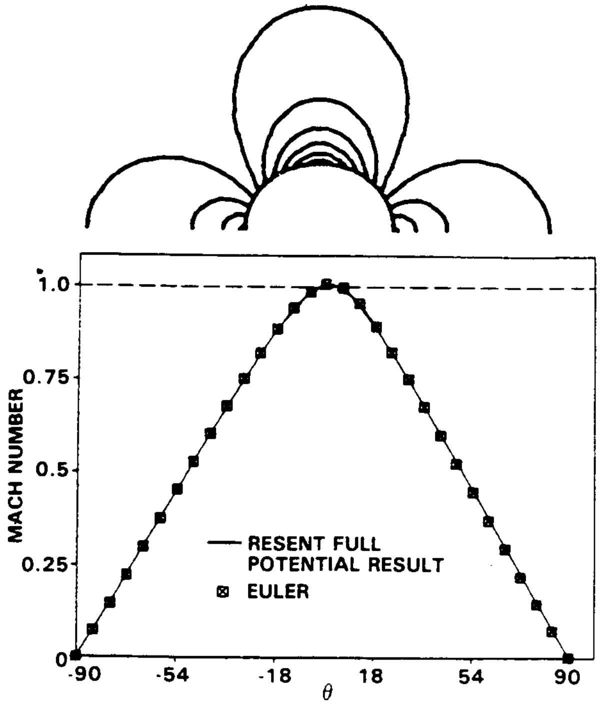

Fig. 3. Mach number distribution for cylinder flow at $M_\infty =$ 0.4.

a grid of 84 points around the airfoil and 18 in the η-direction. The comparison with an Euler code[14] is good. Figure 7 shows the results for $M_\infty = 0.75$ and $\alpha = 2°$ over the same airfoil. Even with a crude grid, the formation of a strong shock without any overshoots is made possible by the use of flux biasing concepts. Calculations of this type require no user-specified "constants" to increase or decrease the amount of dissipation. Depending on the strength of the shock, the flux biasing automatically chooses the right amount of dissipation, since it is based on sonic reference conditions. The perfect matching of pressure contours across the wake cut (Fig. 7) illustrates the correctness of the unsteady wake model described in this paper. Figure 8 shows some difficult cases with fishtail shocks.

The unsteady code can also be effectively used to generate the blunt body solution, the outflow of which is to be prescribed as an initial data plane for a full potential supersonic marching code[6]. Figure 9 shows the schematic of such a hybrid calculation. The flow over the entire Shuttle Orbiter with a blunt nose has been simulated at $M_\infty = 1.4$ and $\alpha = 0°$. The results of Fig. 5 were used as a starting solution for the marching calculation[16]. The nose region geometry and the pressure distribution along the leeside symmetry of the Orbiter are shown in Figs. 10 and 11.

Simulation of unsteady phenomena, such as flutter and control surface oscillations will be presented in the future.

IV. Conclusions

A computational treatment for the unsteady full potential equation is presented. The method employs a local time linearization, flux biasing concepts for generation of

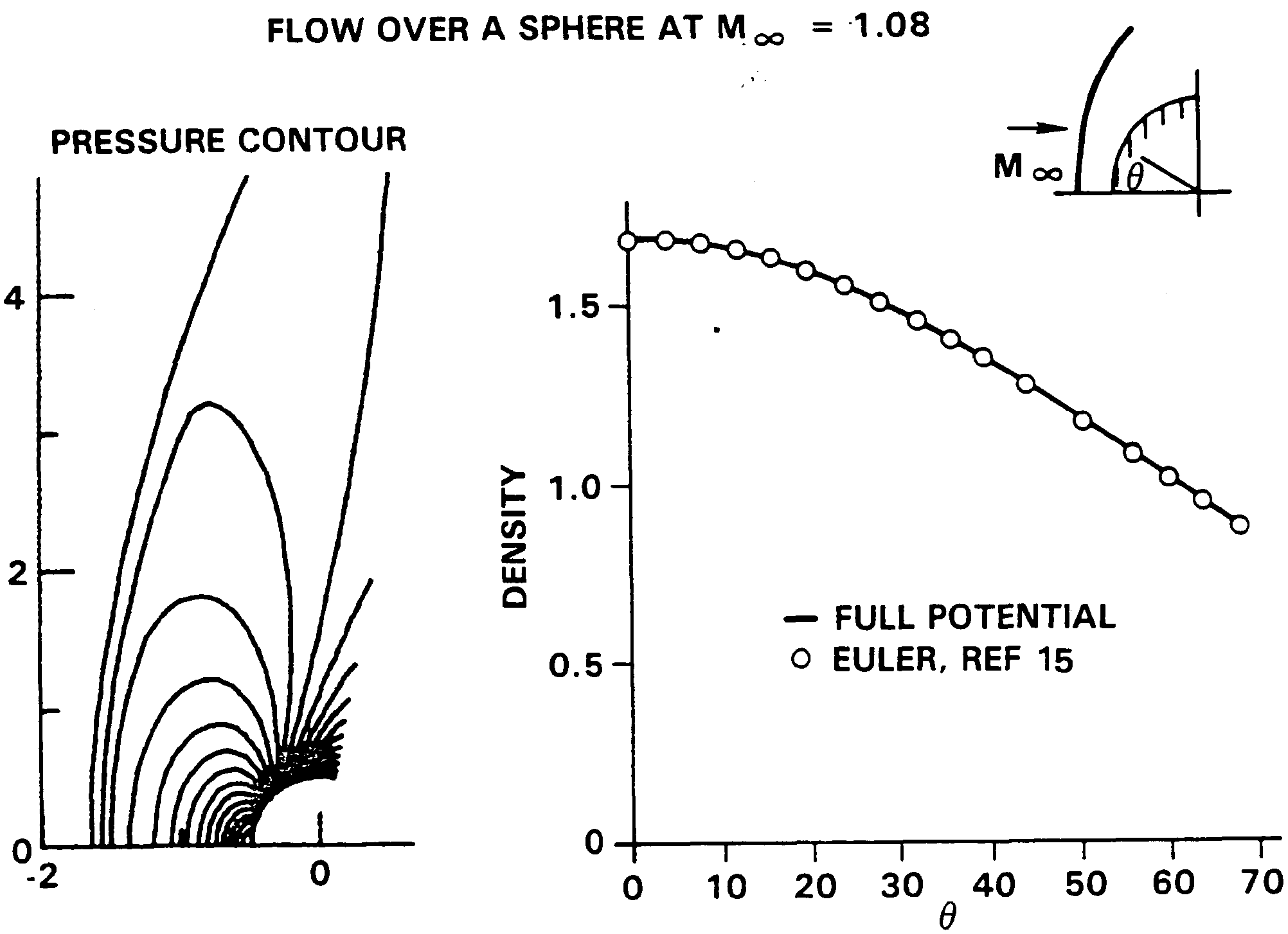

Fig. 4. Density distribution and Mach number contours for flow over a sphere at $M_\infty = 1.08$.

artificial viscosity, unsteady wake treatment, outer boundary conditions based on the Riemann invariants, and relaxation and approximate factorization algorithms. Use of the code for problems with steady state solution has been very effective and computationally fast. Extensions of this work to simulate unsteady phenomena such as flutter, and to three dimensions to treat wings, and wing-body combinations, are currently in progress.

V. Acknowledgement

The authors express their thanks to Prof. Osher of U.C.L.A., and Drs. Chakravarthy and Szema of Rockwell for many valuable discussions. This work was partially funded by NASA-Langley Research Center under Contract NAS1-15820.

VI. References

1. Jameson, A., "Transonic Potential Flow Calculations using Conservation Form," AIAA 2nd Computational Fluid Dynamic Conference Proceedings, 1975, pp. 148–155.
2. Holst, T.L., "Fast, Conservative Algorithm for Solving the Transonic Full Potential Equation," AIAA Journal, Vol. 18, No. 12, December 1980, pp 1431–1439.
3. Siclari, M.J., "Computation of Nonlinear Supersonic Potential Flow over Three-Dimensional Surfaces," AIAA Paper No. 82-0167, presented at the AIAA 20th Aerospace Sciences Meeting, Orlando, Florida, January 1982.
4. Shankar, V., "A Conservative Full Potential, Implicit, Marching Scheme for Supersonic Flows," AIAA Journal, Vol. 20, No. 11, November 1982, pp. 1508–1514.
5. Shankar, V. and Osher, S., "An Efficient Full Potential Implicit Method Based on Characteristics for Analysis of Supersonic Flows," AIAA Paper No. 82-0974, June 1982; AIAA Journal, Vol. 21, No. 9, p. 1262, September 1983.
6. Shankar, V., Szema, K.-Y., and Osher, S., "A Conservative Type-Dependent Full Potential Method for the Treatment of Supersonic Flows with Embedded Subsonic Regions," AIAA Paper No. 83-1887; to appear in the AIAA Journal, November 1984.
7. Chipman, R. and Jameson, A., "An Alternating Direction Implicit Algorithm for Unsteady Potential Flow," presented at the AIAA 19th Aerospace Sciences Meeting, January 1981.

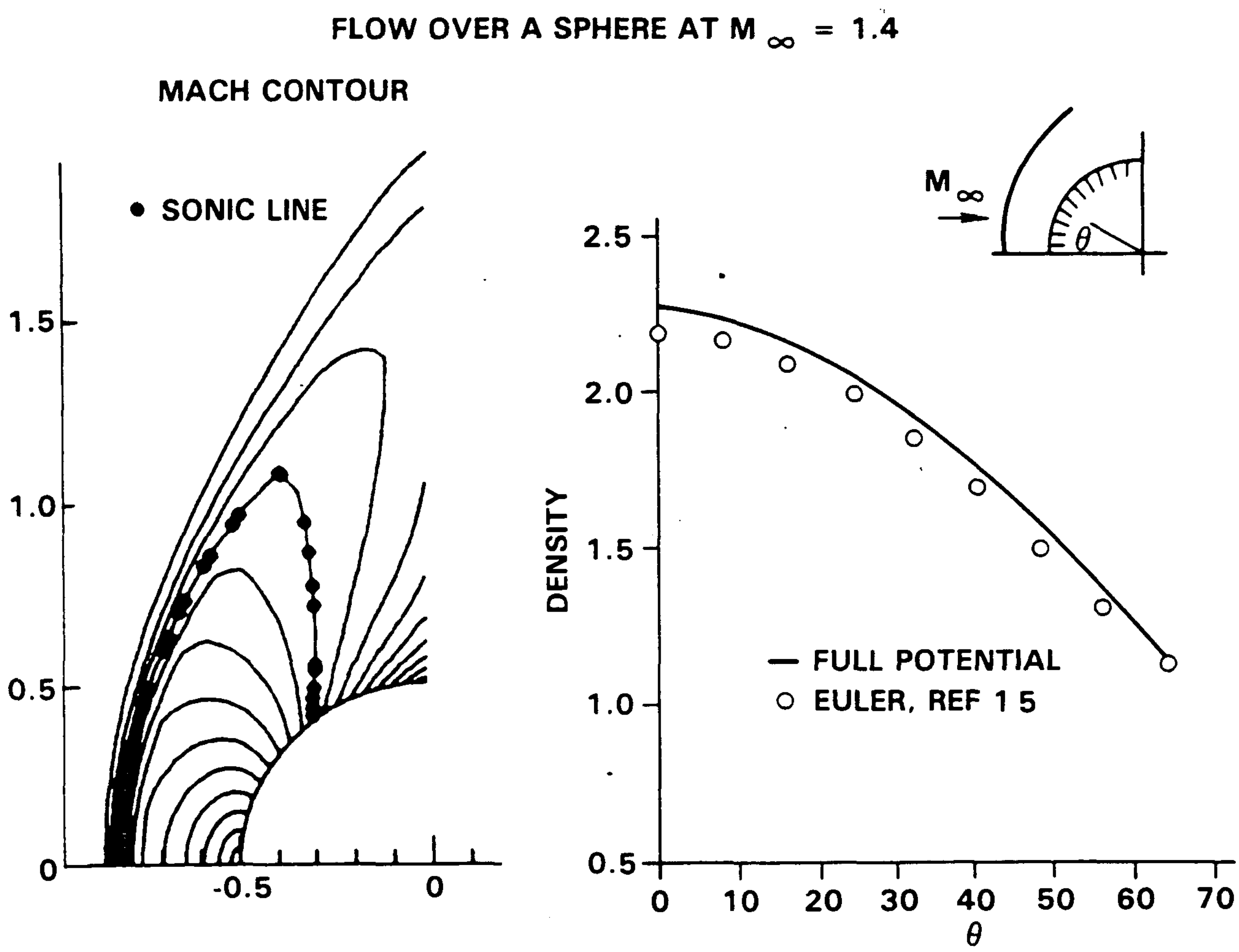

Fig. 5. Density distribution and Mach number contours for flow over a sphere at $M_\infty = 1.4$.

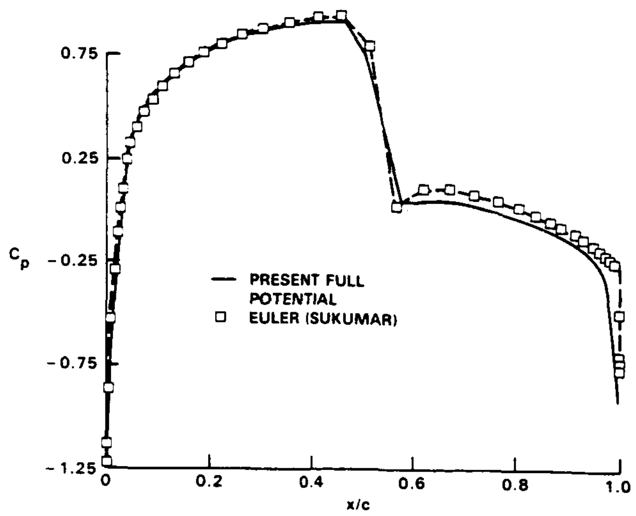

Fig. 6. Flow over NACA 0012, $M_\infty = 0.8$, $\alpha = 0°$.

8. Goorjian, P.M., "Computations of Unsteady Transonic Flow Governed by the Conservative Full Potential Equation using an Alternating Direction Implicit Algorithm," NASA CR-152274, June 1979.

9. Sankar, N.L. and Tassa, Y., "An Algorithm for Unsteady Transonic Potential Flow Past Airfoils," paper presented at the 7th International Conference on Numerical Methods in Fluid Dynamics, June 1980.

10. Steger, J. and Caradonna, F., "A Conservative Implicit Finite Difference Algorithm for the Unsteady Transonic Full Potential Equation," AIAA Paper No. 80-1368, presented at the 13th Fluid and Plasma Dynamics Conference, July 1980.

11. Malone, J.B. and Sankar, N.L., "Numerical Simulation of 2-D Unsteady Transonic Flows using the Full Potential Equation," AIAA Paper No. 83-0233.

12. Osher, S., "Scheme Design for Transonic Unsteady Aerodynamics Based on Riemann Solvers and the Entropy Condition," Transonic Unsteady Aerodynamics and Aeroelasticity Workshop, NASA-Langley Research Center, June 1983.

ORIGINAL PAGE IS
OF POOR QUALITY

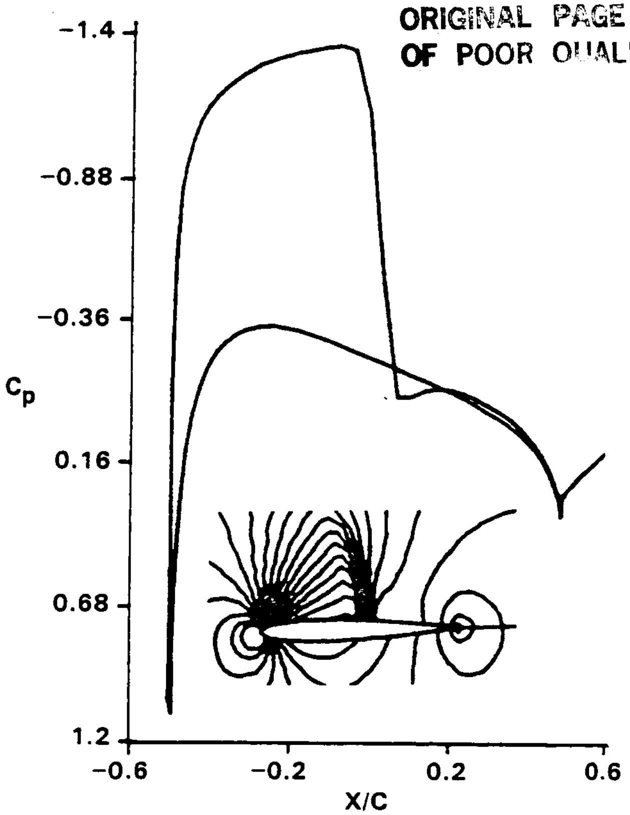

Fig. 7. Flow over NACA 0012, $M_\infty = 0.75$, $\alpha = 2°$.

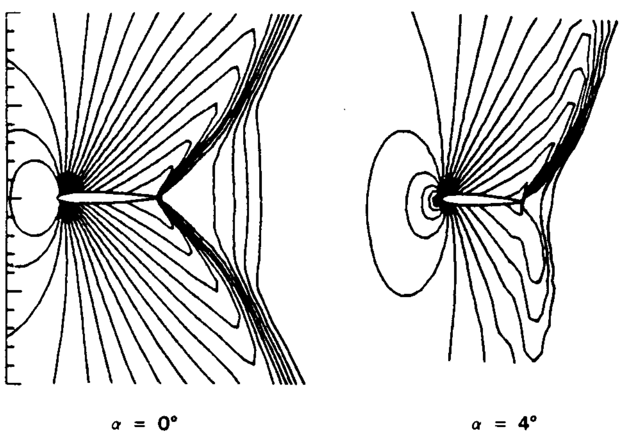

Fig. 8. Mach number contours for NACA 0012, M_∞ = 0.98.

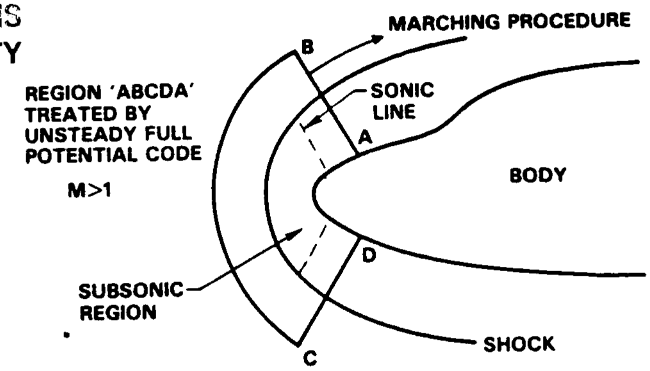

Fig.9. Blunt body starting solution for a marching code.

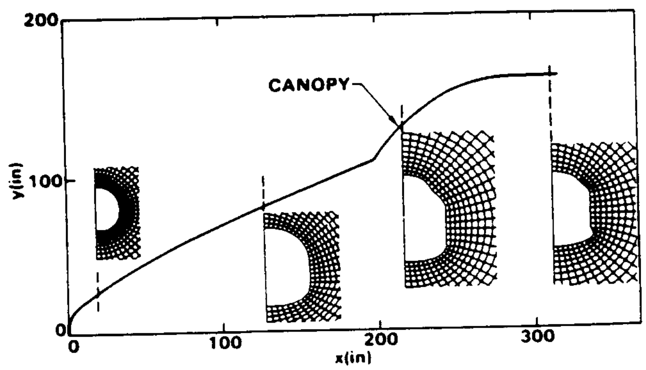

Fig. 10. Nose region geometry of Shuttle Orbiter.

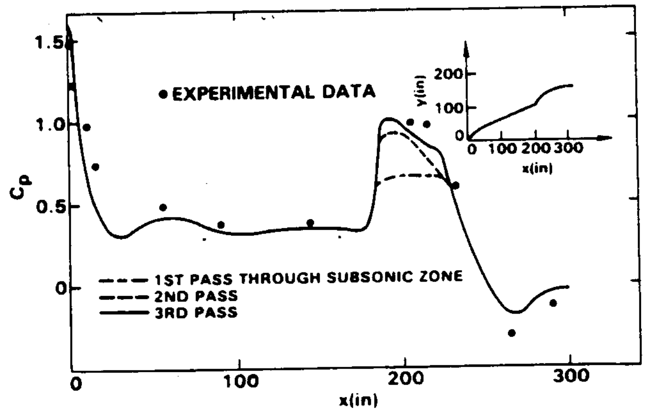

Fig. 11. Hybrid unsteady blunt body/supersonic marching calculation for the Orbiter at $M_\infty = 1.4$, $\alpha = 0°$.

13. Hafez, M., "Entropy Inequality for Transonic Flows," Transonic Unsteady Aerodynamics and Aeroelasticity Workshop, NASA-Langley Research Center, June 1983.

14. Chakravarthy, Sukumar, "Implicit Upwind Schemes without Approximate Factorization," AIAA Paper No. 84-0165.

15. Salas, M.D., "Flow Properties for a Spherical Body at Low Supersonic Speeds," Symposium on Computers in Aerodynamics, 25th Anniversary of Aerodynamics Labs, PINY, Farmingdale, NY, June 1979.

16. Szema, K.-Y. and Shankar, V., "Nonlinear Computation of Wing-Body-Vertical Tail-Wake Flows at Low Supersonic Speeds," AIAA Paper No. 84-0427.

17. South, Jr., J.C. and Brandt, A., "Application of a Multi-Level Grid Method to Transonic Flow Calculations," ICASE Report 76-8, NASA, 1976.

1. Report No. NASA CR-172507	2. Government Accession No.	3. Recipient's Catalog No.
4. Title and Subtitle NONLINEAR POTENTIAL ANALYSIS TECHNIQUES FOR SUPERSONIC AERODYNAMIC DESIGN		5. Report Date MARCH 1, 1985
		6. Performing Organization Code
7. Author(s) V. Shankar and K. Y. Szema		8. Performing Organization Report No.
		10. Work Unit No.
9. Performing Organization Name and Address Rockwell International P. O. Box 92098 Los Angeles, California 90009		11. Contract or Grant No. NAS1-15820
		13. Type of Report and Period Covered Contractor report
12. Sponsoring Agency Name and Address National Aeronautics and Space Administration Langley Research Center Hampton, Virginia 23665		14. Sponsoring Agency Code

15. Supplementary Notes

Technical monitors: Noel A. Talcott, Jr. and Kenneth M. Jones

16. Abstract

A numerical method based on the conservation form of the full potential equation has been applied to the problem of three-dimensional supersonic flows with embedded subsonic regions. The governing equation is cast in a nonorthogonal coordinate system, and the theory of characteristics is used to accurately monitor the type-dependent flow field. A conservative switching scheme is employed to transition from the supersonic marching procedure to a subsonic relaxation algorithm and vice versa. The newly developed computer program can handle arbitrary geometries with fuselage, canard, wing, flow through nacelle, vertical tail and wake components at combined angles of attack and sideslip. Results are obtained for a variety of configurations that include a Langley advanced fighter concept with fuselage centerline nacelle, Rockwell's Advanced Tactical Fighter (ATF) with wing mounted nacelles, and the Shuttle Orbiter configuration. Comparisons with available experiments were good.

17. Key Words (Suggested by Author(s)) Aerodynamic theory Potential analysis Supersonic/hypersonic	18. Distribution Statement [redacted]

19. Security Classif. (of this report) Unclassified	20. Security Classif. (of this page) Unclassified	21. No. of Pages 143	22. Price

Available: NASA's Industrial Applications Centers